Fall 2015

Shear-friction of sand-lightweight clay and slate aggregate concretes with varied reinforcement ratios

Samantha Lynn Wermager

Department:

SHEAR-FRICTION OF SAND-LIGHTWEIGHT CLAY AND SLATE AGGREGATE CONCRETES WITH VARIED REINFORCEMENT RATIOS

by

SAMANTHA LYNN WERMAGER

A THESIS

Presented to the Faculty of the Graduate School of the

MISSOURI UNIVERSITY OF SCIENCE AND TECHNOLOGY

In Partial Fulfillment of the Requirements for the Degree

MASTER OF SCIENCE

in

CIVIL ENGINEERING

2015

Approved by

Dr. Lesley Sneed, Advisor
Dr. John Myers
Dr. Mohamed ElGawady
Dr. Donald Meinheit

ABSTRACT

This thesis focuses on the structural properties of sand-lightweight aggregate concrete in terms of shear transfer strength at cold-joint interfaces. This type of interface is common for precast concrete connections which are typically designed using the shear-friction concept. This testing program was meant to expand the shear-friction database and evaluate the appropriateness of current shear-friction design provisions with respect to sand-lightweight concrete. This study builds on the work done by Shaw (2013) who studied lightweight expanded shale aggregate concrete. The current study included thirty-two push-off specimens constructed from sand-lightweight concrete with a target compressive strength of 5,000 psi. Either expanded clay or expanded slate was used as the course aggregate component, with the fine aggregate consisting of natural river sand. All specimens were cast with a construction joint (cold-joint), and the interface was either troweled smooth or roughened to a 0.25 in. amplitude. The reinforcement ratio was also varied by modifying the number of No. 3 double-legged stirrups crossing the shear plane.

The results of this thesis work have shown that shear transfer strength is higher for roughened versus smooth interface specimens, but the residual shear strength v_{ur} for roughened and smooth specimens was similar. The average ultimate shear stress $v_{u,avg}$ was generally higher for the slate aggregate specimens versus the clay aggregate specimens. The shear transfer strength v_u and residual shear strength v_{ur} increased with increasing reinforcement ratio. However, for the roughened specimens, the shear transfer strength v_u leveled off at higher reinforcement ratios. All shear transfer strengths v_u for both the roughened and smooth specimens in this study were higher than those predicted by the current ACI, PCI, and AASHTO codes/provisions. The μ_e approach from the 7th Edition of the PCI Design Handbook conservatively predicts the shear strengths of smooth specimens, even though this approach is not applicable for a smooth interface. The use of a cohesion factor c in the AASHTO shear-friction design equation was conservative for all smooth interface specimens, even though AASHTO contains a provision which sets $c = 0.0$ for vertical interface shear cracks. This project was funded by the Precast/Prestressed Concrete Institute (PCI) and the American Concrete Institute Concrete Research Council.

ACKNOWLEDGMENTS

I would like to thank Tony and Connie Wermager, for their unwavering support of my educational goals. Their encouragement gave me confidence to pursue my dreams, and I am proud to have parents that are such great people. I would also like to thank my best friend, Drew Schrader, for supporting my decision to pursue a graduate degree at Missouri S&T.

My advisor, Dr. Lesley Sneed, was also instrumental in making this project successful, and her insight and advice were always extremely helpful. She is truly an expert in her field, and it has been a pleasure to work with her. I would also like to thank my committee members for reviewing my work: Dr. John Myers, Dr. Mohamed ElGawady and Dr. Donald Meinheit.

This project would not have been possible without the sponsorship of the Precast/Prestressed Concrete Institute (PCI) and the American Concrete Institute Concrete Research Council. I am grateful for those who donated materials and provided technical assistance; the lightweight slate aggregate was donated by STALITE and the lightweight clay aggregate was donated by Big River Industries. Reinforcing steel bars used in this study were donated by Ambassador Steel Corporation and the Concrete Reinforcing Steel Institute (CRSI). I would like to gratefully acknowledge Neil Anderson of Simpson Sumphertz & Heger Inc., Roger Becker of PCI, Harry Gleich of Metromont Precast, Dr. Neil Hawkins, Dr. Donald Meinheit of Wiss, Janney, Elstner, and Dr. Larbi Sennour of Consulting Engineering Group, Inc. who served as advisors to this project.

Also, I must thank my research partner on this project, Kristian Krc, whose upbeat attitude and amazing work ethic made this project a success. Lastly, it goes without saying that assistance from fellow graduate students, professors, and department technical staff is sincerely appreciated. A special thank you goes out to John Bullock, Gary Abbott, Greg Leckrone, Brian Swift, Mike Lusher, Kerry Magner, and Dr. Dimitri Feys.

TABLE OF CONTENTS

LIST OF FIGURES

Page

LIST OF TABLES

Page

NOMENCLATURE

Symbol	Description
A_c	area of concrete shear interface, in^2
A_{cr}	area of concrete shear interface, in^2
A_{vf}	area of shear reinforcement across shear plane, in^2
c	cohesion factor
f'_c	28-day concrete compressive strength, lb/in^2
f_t	tensile strength of concrete, measured by splitting tensile strength, lb/in^2
f_y	yield stress of reinforcement, lb/in^2
K_1	fraction of concrete strength available to resist interface shear
K_2	limiting interface shear resistance, kip/in^2
P_c	permanent net compressive force normal to the shear plane; if force is tensile, $P_c = 0.0$, kip
V_n	nominal shear strength, lb
V_{ni}	nominal interface shear resistance, lb
v_n	nominal shear stress, lb/in^2
V_u	ultimate shear strength, lb
v_u	ultimate shear stress, lb/in^2
v_{ur}	residual shear stress, lb/in^2
λ	modification factor reflecting the reduced mechanical properties of lightweight concrete, relative to normalweight concrete of the same compressive strength
τ	shear stress
σ	normal stress
μ	coefficient of friction

μ_e	effective coefficient of friction
ρ	shear-friction reinforcement ratio, A_v/A_{cr}
ϕ	capacity reduction factor
ϕ	angle of internal friction
ACI	American Concrete Institute
ASCE	American Society of Civil Engineers
ASTM	American Society for Testing and Materials
DC-LVDT	direct current - linear voltage displacement transducer
PCI	Precast/Prestressed Concrete Institute

1. INTRODUCTION

1.1. PROBLEM DEFINITION

As skyscrapers are built taller and bridges span further every year, it becomes increasingly important to develop new construction materials that not only perform well, but are also economical. The use of lightweight aggregates in concrete construction projects can be beneficial because they allow a reduction in member weight for a certain geometry. This reduction in weight is particularly advantageous in multi-story concrete buildings in which the columns must support the self-weight of the floors above, in addition to various external loads. In addition, the use of precast concrete members speeds up the construction process for structures of all types. The use of lightweight concrete for precast members adds fuel cost savings when the expense of transporting these members from the production plant to the jobsite is considered.

However, the use of lightweight aggregates corresponds to a reduction in mechanical properties, which is recognized in the ACI 318 Code (2014) as well as the PCI Design Handbook 7th Edition (2014) which both require the use of a lightweight modification factor λ for certain design provisions. The use of λ is based on the idea that the tensile strength f'_t of lightweight aggregate concrete is lower than that of normalweight concrete with a similar compressive strength f'_c.

For lightweight concrete, one mechanical property needed for structural design is shear transfer strength at connections. A common method used to design reinforced concrete connections is the shear-friction concept. According to this method, shear transfer strength is a function of the interface conditions listed in Table 1.1. While extensive research has been conducted in this area using normalweight concrete, the shear-friction database does not include many lightweight specimens, especially those with a cold-joint. In 2013, Dane Shaw used cold-joint push-off specimens to study the shear-friction properties of concrete with various unit weights, compressive strengths f'_c, and interface conditions. This current project is meant to expand Shaw's work to include other lightweight aggregate types, interface types, and reinforcement ratios.

Table 1.1 Shear Interface Conditions – PCI Design Handbook 7th Edition (2011)

Case	Interface Condition
1	Concrete to concrete, cast monolithically
2	Concrete to hardened concrete, with roughened surface*
3	Concrete placed against hardened concrete not intentionally roughened
4	Concrete to steel

*Both the ACI and PCI design provisions specify an intentionally roughened surface to have an average amplitude of 0.25 in.

1.2. GOAL AND OBJECTIVES

The goal of this project was to study the effects of lightweight aggregate type, interface condition, and reinforcement ratio on the shear transfer strength of push-off specimens constructed of sand-lightweight concrete. Specific objectives were to:

a) Expand the shear-friction database to include sand-lightweight cold-joint specimens constructed with expanded slate and expanded clay coarse aggregates.
b) Evaluate the shear-friction performance of these specimens and compare results to previous data.
c) Use the results to determine the conservativeness of shear-friction design provisions from the ACI 318 Code, the PCI Design Handbook, and AASHTO LRFD Bridge Design Specifications.
d) Evaluate the apparent coefficients of friction from the specimens and compare the values to those currently used in the aforementioned design codes/specifications.

1.3. SCOPE

1.3.1. Project Scope. The scope of this entire project includes 52 push-off specimens. The laboratory work was completed by two master's students, Kristian Krc and Samantha Wermager, and portions of the data were used in separate analyses and summarized in separate theses.

The following variables were included in the test matrix:

a) The interface condition along the shear plane was either monolithic or cold-joint.
b) The interface for the monolithic specimens was either precracked or left uncracked. The cold-joint specimens had an interface that was either troweled smooth or intentionally roughened.
c) Three unit weights of concrete were studied: normalweight, sand-lightweight, and all-lightweight.
d) Three types of lightweight aggregate were used, including expanded shale, expanded slate, or expanded clay.
e) The reinforcement ratio was varied for certain specimen series. The values ranged from $\rho = 0.009$ to $\rho = 0.022$.

1.3.2. Thesis Scope. The scope of this thesis includes 32 push-off specimens, all of which were constructed from sand-lightweight concrete. Expanded slate or expanded clay was used for the course aggregate, and river sand was used for the fine aggregate. The two halves of each specimen were constructed at different times to simulate a construction joint. This casting procedure is referred to herein as 'cold-joint'. The shear interface for the specimens in this thesis were either roughened to an amplitude of 0.25 in., or troweled smooth, which represent Cases 2 and 3, respectively, from Table 1.1. Also, the amount of steel reinforcement crossing the shear plane was varied for each series. By using either 2, 3, 4, or 5 double-legged No. 3 steel reinforcing bars across the shear plane, specimens had reinforcement ratios of $\rho = 0.009$, $\rho = 0.013$, $\rho = 0.017$, or $\rho = 0.022$, respectively.

1.4. SUMMARY OF THESIS CONTENT

The problem definition, goal, objectives, and scope of this project are defined in Section 1. The background investigation including a literature review and summary of current design provisions is contained in Section 2. Section 3 describes the experimental program in terms of materials, specimen design and fabrication, test set-up, and results. Section 4 contains a discussion of the general behavior of the specimens and the observed influence of test variables. Also, Section 4 covers comparisons of the test results to current design provisions as well as previous studies of cold-joint

specimens. Finally, Section 5 contains a summary, conclusion, and recommendations for design equations as well as suggestions for future work. The database of test results used for analysis within this thesis is included in the Appendix.

2. BACKGROUND INFORMATION

2.1. INTRODUCTION

Due to the non-ductile nature of concrete, the design of connections in reinforced concrete structures is of great concern when there is little redundancy or high levels of shear forces involved. One such way to design these types of connections is by the shear-friction method which was pioneered in the 1960s by Birkeland and Birkeland (Section 2.4.2); Mast (Section 2.4.3); and Hofbeck, Ibrahim, and Mattock (Section 2.4.4). Particularly with the development and widespread use of precast reinforced concrete members, the design of connections has become increasingly complicated. Several factors must be considered including: the interface condition, the amount of reinforcement crossing the shear plane, the yield strength of the reinforcement, the compressive strength of the concrete, the density of the concrete, the presence of an externally applied tension or compression force, etc. The transfer of shear forces across an interface is discussed in Section 2.2. The development and the current (2015) shear-friction design provisions according to ACI, PCI, and AASHTO are described in Section 2.3. Previous studies concerning shear-friction are summarized in Section 2.4.

2.2. INTERFACE SHEAR-FRICTION

2.2.1. Shear-friction. The shear-friction theory was initially developed to describe the transfer of shear forces across the interface of a precast element to a cast-in-place element. It has been extended to include shear transfer across monolithic interfaces as well. One of the principal assumptions of the shear-friction theory is that a crack or discontinuous interface exists. The shear force causes the two surfaces to slip relative to each other. The mechanisms of aggregate interlock, interface shear-friction, dowel action of the reinforcement, and cohesion of the two surfaces work in unison to resist shear forces. These mechanisms are further described in Section 2.2.2.

While the shear-friction concept is applied to initially uncracked elements, initially cracked elements correspond to lower ultimate shear transfer strengths. In order to simulate the worst-case scenario, it is assumed that a crack has formed in the element in the most undesirable location. This crack could be due to temperature and/or

shrinkage cracking, accidental dropping of the specimen, unintended impact forces during transportation or placement of a precast specimen, etc. Thus, many previous studies have included both uncracked and pre-cracked monolithic specimens to compare their shear transfer strengths.

Several factors have recently been investigated for their effect on shear strength. Concretes with higher compressive strengths have the potential for higher shear capacities for normalweight concrete as noted by Mattock (2001) and Kahn and Mitchell (2002). Cyclic or sustained loading has been shown by Walraven et al. (1987) to have little effect on the shear transfer capacity; thus, it is typical for shear-friction specimens to be tested by monotonic loading. Hsu, Mau, and Chen (1987) warned of the potential influence of large amounts of steel reinforcement parallel to the shear plane on the ultimate shear strength of connections.

Several researchers (Mattock, et al. 1976; Hoff 1993; Shaw 2013) have investigated the effect on shear transfer when lightweight concrete is used. Their results reveal that the bond between the mortar and aggregate particles is stronger than the tensile strength of the aggregate alone, and cracks may propagate directly through the aggregate particles. This causes a smoother crack surface which reduces ultimate shear capacity when compared to that of normalweight concrete. Typically, in normalweight concrete the cracks propagate around the aggregate since the aggregate's tensile strength is higher than the bond between the mortar and aggregate particles (Mattock, et al. 1976). This phenomenon produces a rougher surface which aids in aggregate interlock and forces higher surface separation to occur for a given amount of slip.

Previous studies (Mattock and Hawkins 1972; Mattock, et al. 1975) have concluded that tension or compression that is externally applied normal to the shear plane can either hinder or aid, respectively, in the resistance of shear forces and must be included in shear-friction provisions.

2.2.2. Shear-friction Mechanisms. When shear forces are applied in a cracked region of concrete, slip will occur along the crack. This shear plane is likely jagged, and the two faces of concrete resist slipping through the mechanism of 'aggregate interlock.' These rough surfaces must first separate to overcome small ridges before slip can occur. Steel reinforcement normal to the shear plane is strained when there is separation of the

concrete surfaces. Tension forces are induced in the steel which in turn create equal and opposite compression forces between the concrete faces. These compression forces correspond to the 'normal' forces of the basic friction equation which is further discussed in Section 2.2.2.1. The combination of this steel clamping force and the inherent friction along the crack surface is referred to as the mechanism of interface shear-friction. The shear-friction principle is graphically demonstrated in Figure 2.1.

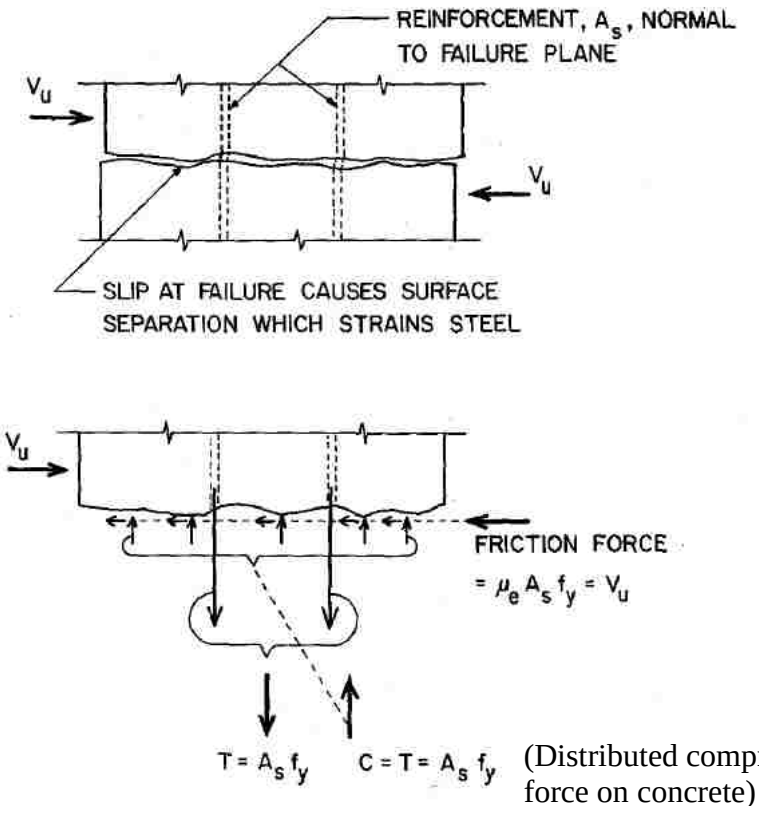

Figure 2.1. Schematic diagram of shear-friction principle (Shaikh 1978)

Another contributor to shear strength along an interface is dowel action of the steel reinforcement. Paulay et al. (1974) separated dowel action into three different mechanisms (Figure 2.2) which include flexure, shear, and kinking of the steel bar. Since

significant levels of slip and crushing of the concrete are required to engage reinforcement bars, dowel action alone cannot be relied upon as a principle shear force resistance mechanism. Large levels of slip can cause deflection issues, and large, unsightly cracks in a reinforced concrete structure are likely to be a major concern to its tenants. For typical levels of load and slip, Paulay, et al. state that only 15% of the shear-friction capacity is attributed to dowel action.

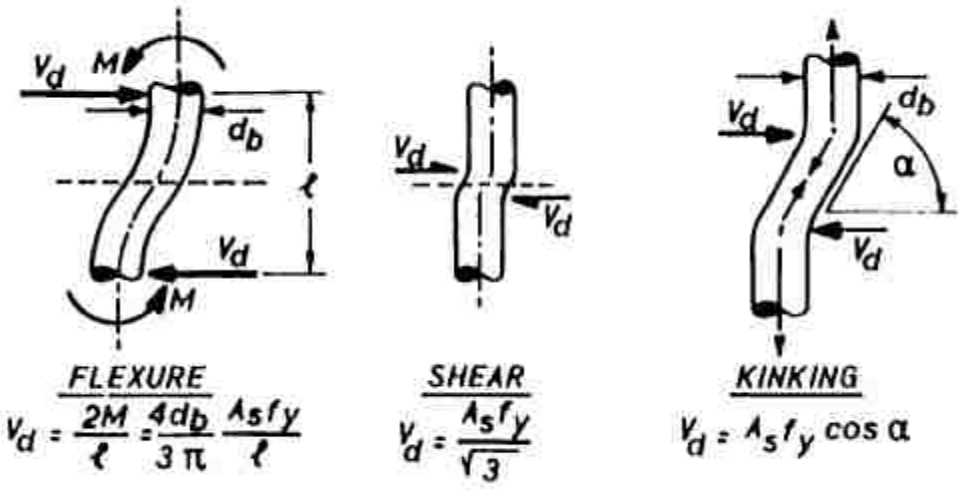

Figure 2.2. Mechanisms of dowel action (Paulay, et al. 1974)

Another component of shear-friction capacity is bond of the two opposing concrete faces, also referred to as cohesion. It has been suggested by Kahn and Mitchell (2002) that concretes with higher compressive strengths have higher shear strengths in monolithic and cold-joint specimens due to the contribution of cohesion. These researchers included a term in their proposed shear-friction equation to account for bond and asperity shear. The literature does not clearly define the term asperity shear, but the context suggests that asperity shear is the additional shear strength attributed to resistance

by the projections (asperities) on the crack interface which did not previously interact with rough areas on the opposite face as slip progresses along the shear plane.

2.2.2.1 Coefficient of friction. Harries, et al. (2012) define the shear-friction factor, μ, as the ratio of shear stress τ to the normal stress σ across the shear interface (Equation 2.1), which can be manipulated by representing the normal force as equivalent to the tensile force in the steel $A_{vf}f_s$ combined with an external clamping force P_c which may or may not be present. In this equation, V is the shear applied along the interface; A_{cv} is the area of the shear interface.

$$\mu = \frac{\tau}{\sigma} = \frac{V/A_{cv}}{\left(A_{vf}f_s + P_c\right)/A_{cv}} = \frac{V}{A_{vf}f_s + P_c} \tag{2.1}$$

The classical equation from basic physics for the force due to friction F_f (Equation 2.2) is simply the coefficient of friction μ multiplied by the normal force N. In the case of shear-friction design, this coefficient of friction does not represent the true roughness of the shear interface. Instead, researchers have modified it in the development of empirical equations. The coefficient of friction in modern design codes has become an all-inclusive parameter which also accounts for the effects of aggregate interlock and cohesion (Harries et al. 2012). These design code provisions are further discussed in Section 2.3.

$$F_f = \mu N \tag{2.2}$$

2.2.2.2 Effective coefficient of friction. In certain design provisions or equations, μ_e is used for various interface conditions. The effective coefficient of friction, μ_e, was first introduced in the 2nd edition of the PCI Handbook (1978) for use when the shear-friction concept is applied to precast concrete construction. The 7th Edition of the PCI Handbook describes μ_e as being used for conditions where load

reversal does not occur. The value of this parameter and its applicability are described in greater detail in Section 2.3.

2.3. SHEAR-FRICTION DESIGN PROVISIONS

In the fundamental equation (Equation 2.1) for the coefficient of friction μ, the term P_c accounts for an external force. It is conservative to ignore this external force if it is compressive. Yet, if an external tensile force is applied across the shear plane, extra reinforcement must be provided to account for this force, and it shall be separate from the reinforcement required by shear-friction provisions. Such a tension force may be caused by restraining the movement of members due to temperature or shrinkage expansion/ contraction. If P_c is ignored in Equation 2.1, this equation can be rearranged in terms of nominal shear strength, V_n (Equation 2.3). Here, V_u is the applied factored shear force parallel to the assumed crack, ϕ is the strength reduction factor, A_{vf} is the area of shear reinforcement, f_y is the yield strength of the reinforcement, and μ is the coefficient of friction.

$$V_n = \frac{V_u}{\phi} = A_{vf} f_y \mu \tag{2.3}$$

This fundamental equation (Equation 2.3) forms the basis of shear-friction design in the PCI Design Handbook, ACI 318 Code, and AASHTO LRFD Bridge Design Specifications. Their specific provisions are detailed in Sections 2.3.1 through 2.3.4. Within these provisions, a modification factor, λ, is used to account for the reduced tensile strength (and thus, reduced shear strength and friction capacity) of lightweight aggregate concrete (ACI 318-14 and PCI 2011). A value of $\lambda = 1.0$ corresponds to normalweight concrete, with $\lambda = 0.85$ used for sand-lightweight concrete, and $\lambda = 0.75$ for all-lightweight concrete. If lightweight concrete is used, and the splitting tensile strength f_{ct} is known, ACI and PCI design provisions allow the lightweight modification factor λ to be determined by Equation 2.4. Note that the maximum value of λ allowed by this equation is 1.0.

$$\lambda = \frac{f_{ct}}{\left(6.7\sqrt{f_c'}\right)} \leq 1.0 \tag{2.4}$$

2.3.1. PCI Design Handbook. The Precast/Prestressed Concrete Institute has been developing the body of knowledge surrounding precast and prestressed concrete since the 1950s. Shear-friction provisions have evolved over the years, and there have been some modifications in recent editions. The only change from the 5th to the 6th edition of the PCI Design Handbook was that the strength reduction factor ϕ for shear-friction design decreased from 0.85 to 0.75. Tanner (2008) explores the unique problem that this change created. The transition from the 6th to the 7th edition saw a few more changes which were also discussed by Tanner and are summarized in this section.

2.3.1.1 PCI Design Handbook 6th Edition (2004). Shear-friction provisions of the 6th Edition of the PCI Handbook require an amount of shear reinforcement normal to the crack A_{vf} as given by Equation 2.5, where, ϕ = 0.75, V_u is the applied factored shear force parallel to the assumed crack plane (lb), f_y is the yield strength of the steel reinforcement (less than or equal to 60 ksi), and μ_e according to Equation 2.6.

$$A_{vf} = \frac{V_u}{\phi f_y \mu_e} \tag{2.5}$$

$$\mu_e = \frac{1000\lambda A_{cr}\mu}{V_u} \tag{2.6}$$

A different value of μ is recommended for each of the four different crack interface conditions (Table 2.1), and is a function of the value of λ, which is a modification factor to account for the use of lightweight aggregate. Table 2.1 also shows suggested maximum values of the effective coefficient of friction μ_e and maximum values of the nominal shear strength V_n for each interface condition.

Table 2.1. Shear-friction Coefficients for PCI Design Handbook 6th Edition (2004)

Case	Crack Interface Condition	μ	Max μ_e	Max $V_u = \phi V_n$
1	Concrete to concrete, cast monolithically	1.4λ	3.4	$0.30\lambda^2 f'_c A_{cr} \leq 1000\lambda^2 A_{cr}$
2	Concrete to hardened concrete, with roughened surface	1.0λ	2.9	$0.25\lambda^2 f'_c A_{cr} \leq 1000\lambda^2 A_{cr}$
3	Concrete placed against hardened concrete not intentionally roughened	0.6λ	2.2	$0.20\lambda^2 f'_c A_{cr} \leq 800\lambda^2 A_{cr}$
4	Concrete to steel	0.7λ	2.4	$0.20\lambda^2 f'_c A_{cr} \leq 800\lambda^2 A_{cr}$

2.3.1.2 PCI Design Handbook 7th Edition (2011). The 7th Edition of the PCI Design Handbook states that the shear-friction method is applicable to reinforced concrete bearing, corbels, daps, composite sections, connections of shear walls to foundations, shear connections in precast concrete diaphragms, and other applications. From the 6th to the 7th edition, there were a few modifications. First, Table 2.2 shows that μ_e became inapplicable for the case of concrete to concrete not intentionally roughened (Case 3), as well as the case of the concrete to steel interface condition (Case 4). Instead, Equation 2.7 is used for these two cases, where μ is used in place of μ_e. For Case 1 and Case 2, Equation 2.8 is still used, with values of μ_e according to Equation 2.9. The second change in the 7th Edition is the addition of ϕ to Equation 2.9. This change was made to reflect the fact that μ_e is not a function of V_u, but rather it is a function of $V_n = V_u/\phi$. The third major change of this edition is also shown in Table 2.2, where the reduction factor λ is no longer squared in the limits for $V_{n,max}$.

$$A_{vf} = \frac{V_u}{\phi f_y \mu} \tag{2.7}$$

$$A_{vf} = \frac{V_u}{\phi f_y \mu_e} \tag{2.8}$$

$$\mu_e = \frac{\phi 1000 \lambda A_{cr} \mu}{V_u} \tag{2.9}$$

Table 2.2. Shear-friction Coefficients for PCI Design Handbook 7th Edition (2011)

Case	Crack Interface Condition	μ	Max μ_e	Max $V_u = \phi V_n$
1	Concrete to concrete, cast monolithically	1.4λ	3.4	$0.30\lambda f'_c A_{cr} \leq 1000\lambda A_{cr}$
2	Concrete to hardened concrete, with roughened surface	1.0λ	2.9	$0.25\lambda f'_c A_{cr} \leq 1000\lambda A_{cr}$
3	Concrete placed against hardened concrete not intentionally roughened	0.6λ	N/A	$0.20\lambda f'_c A_{cr} \leq 800\lambda A_{cr}$
4	Concrete to steel	0.7λ	N/A	$0.20\lambda f'_c A_{cr} \leq 800\lambda A_{cr}$

2.3.2. ACI 318 Code (2014). The current ACI (American Concrete Institute) code avoids the use of an effective coefficient of friction μ_e; instead, μ is used for all interface conditions. The nominal shear strength for the case of reinforcement perpendicular to the shear plane is given by Equation 2.10. When the shear-friction reinforcement is inclined at an angle α from the shear plane, Equation 2.11 is used. The ACI values for μ are the same as PCI 6th and 7th editions; however, the limitations on $V_{n,max}$ are slightly different (Table 2.3).

If the average splitting tensile strength of the lightweight concrete f_{ct} is known, the lightweight modification factor λ may be calculated according to Equation 2.4, which is also specified in the PCI Design Handbook. However, unlike PCI, the ACI 318 Code also allows λ to be modified based on volumetric fractions of normalweight and lightweight coarse and fine aggregates. When lightweight coarse aggregate is used with a mix of lightweight and normalweight fine aggregate, ACI 318-14 allows linear interpolation between the values of 0.75 and 0.85 based on the volumetric fraction of lightweight fine aggregate that is replaced with normalweight fine aggregate. Also, when normalweight fines are used with a blend of normalweight and lightweight coarse

aggregate, ACI 318-14 allows λ to be interpolated by volumetric fraction (with λ ranging between 0.85 and 1.0).

$$V_n = A_{vf} f_y \mu \tag{2.10}$$

$$V_n = A_{vf} f_y (\mu \sin\alpha + \cos\alpha) \tag{2.11}$$

Table 2.3. Shear-friction Coefficients for ACI 318 (2014)

Case	Crack Interface Condition	μ	$V_{n,max} = V_u/\phi$
1	Concrete to concrete, cast monolithically	1.4λ	For normalweight concrete (monolithic or roughened), $V_{n,max}$ equals least of: a) $0.2f'_c A_c$ b) $(480 + 0.08f'_c)A_c$ or c) $1600A_c$ For all other cases, $V_{n,max}$ equals lesser of: a) $0.2f'_c A_c$ or b) $800A_c$
2	Concrete to hardened concrete, with roughened surface	1.0λ	
3	Concrete placed against hardened concrete not intentionally roughened	0.6λ	
4	Concrete anchored to as-rolled structural steel by headed studs or by reinforcing bars	0.7λ	

2.3.3. AASHTO LRFD Bridge Design Specifications 7th Edition (2014).

American Association of State Highway and Transportation Officials has published a specification which contains shear-friction provisions that are slightly different than their ACI and PCI equivalents. The 7th Edition of the AASHTO LRFD Bridge Design Specifications requires the nominal shear resistance V_{ni} of the interface plane to be taken as shown in Equation 2.12. A_{cv} is defined as the area of concrete considered to be engaged in interface shear transfer (Equation 2.13), with b_{vi} and L_{vi} corresponding to the interface width and length of considered to be engaged in shear transfer. A_{vf} is the area of

interface shear reinforcement crossing the shear plane within the area A_{cv}; c and μ are cohesion and friction factors, respectively, with values specified in Table 2.4; f_y is the yield stress of the reinforcement, with a design value ≤ 60 ksi. The coefficient K_1 represents the fraction of concrete strength available to resist interface shear, and K_2 is the limiting interface shear resistance. Both of these coefficients are specified as shown in Table 2.4.

$$V_{ni} = cA_{cv} + \mu\left(A_{vf}f_y + P_c\right) \tag{2.12}$$

But, not greater than the lesser of: $K_1 f'_c A_{cv}$, or $K_2 A_{cv}$

$$A_{cv} = b_{vi}L_{vi} \tag{2.13}$$

The reinforcement parameter ρf_y is specified to be no less than 0.05. This value is found by rearranging 2.14 and recognizing that $\rho = A_{vf} / A_{cv}$. A design using an amount of steel reinforcement which satisfies Equation 2.14, must also be checked against Equation 2.16 where V_{ri} is the factored interface shear resistance (Equation 2.15), V_{ui} is the factored interface shear force due to total load based on the applicable strength and extreme event load combinations found in AASHTO LRFD Bridge Design Specifications 7th Edition, 2014. The resistance factor for shear, ϕ, is based on different concrete unit weights; ϕ = 0.9 for normalweight concrete, or ϕ = 0.7 for lightweight concrete. Note that AASHTO does not use the lightweight reduction factor λ which both ACI and PCI currently use. Instead, AASHTO has different values of ϕ, c, μ, K_1, and K_2 for normalweight versus lightweight concrete construction (Table 2.4). Also, AASHTO does not differentiate between different types of lightweight concrete, i.e. sand-lightweight and all-lightweight.

$$A_{vf} \geq \frac{0.05\ A_{cv}}{f_y} \tag{2.14}$$

$$V_{ri} = \phi V_{ni} \tag{2.15}$$

$$V_{ri} \geq V_{ui} \tag{2.16}$$

Table 2.4. AASHTO LRFD Bridge Design Specifications 7th Edition (2014) cohesion and friction factors

Concrete Density and Interface Condition*	***c*** **(ksi)**	***μ***	***K₁***	***K₂*** **(ksi)**
Cast-in-place slab on girder with roughened interface; normalweight concrete	0.28	1.0	0.3	1.8
Cast-in-place slab on girder with roughened interface; lightweight concrete	0.28	1.0	0.3	1.3
Normalweight concrete placed monolithically	0.40	1.4	0.25	1.5
Lightweight concrete placed monolithically, or lightweight cold-joint with roughened interface	0.24	1.0	0.25	1.0
Normalweight cold-joint with roughened interface	0.24	1.0	0.25	1.5
Cold-joint with interface not intentionally roughened	0.075	0.6	0.2	0.8
Concrete anchored to as-rolled structural steel by headed studs or by reinforcing bars	0.025	0.7	0.2	0.8

*Note: All concrete or steel surfaces must be clean and free of laitance; an intentionally roughened cold-joint is to be roughened to an amplitude of 0.25 in.

A very important exception to these provisions is that brackets, corbels, and ledges shall have a cohesion factor of $c = 0.0$ for all cases listed in Table 2.4. The

AASHTO commentary to this provision explains that vertical crack interfaces have unreliable cohesion and aggregate interlock properties. Therefore, the cohesion factor is conservatively set to zero for these cases. It is important to realize that the AASHTO LRFD Bridge Design Specifications are meant to be used in the "design, evaluation, and rehabilitation of bridges, and are mandated by the Federal Highway Administration for use on all bridges using federal funding." The most common shear interface in bridges is the horizontal interface between a slab and girder. Therefore, the main focus of the shear-friction provisions in this specification is horizontal shear, not vertical shear. However, the focus of this testing program is the fundamental shear-friction behavior for any general interface orientation; thus, in this study, the results of the test data will be compared both with and without the cohesion factor.

2.4. PRIOR STUDIES

The literature review contained herein summarizes the development of shear-friction theory. These previous studies have provided the framework which shaped the current shear-friction design provisions. They also provided the basis for the specimen design and testing protocol of this study.

2.4.1. Hanson, 1960. To act as a composite section, precast bridge girders overlain by a cast in-situ deck slab must be adequately connected at their interface. Hanson tested 62 push-off specimens as well as 10 larger-scale T-girders to study the transfer of horizontal shear. Concrete compressive strength varied from 3,000 to 5,000 psi. The parameters varied included roughness of interface, adhesive bond between girder and slab, the addition of keys to the interface, area of shear transfer, and reinforcement ratio.

Hanson recorded shearing stress and slip, and from the results of the push-off tests and girder specimens he concluded:

1. Concrete strength seemed to have a direct correlation to the shearing stress, although it was not an intended variable of concern in this particular investigation.
2. The shearing strength of keys cannot be added to the contribution of bond and roughness. Large values of slip are required to fully engage the keys. It is suggested that they be avoided; instead, designers should rely on bond, roughness, and stirrups for transfer of shear.

3. The results of the push-off tests seemed to be a good representation of the results of the girder tests, and thus push-off tests are a useful tool in studying horizontal shear transfer.
4. Hanson suggested values for maximum shearing stress of various interface conditions, as well as contribution of reinforcing bars on a percent reinforcement basis.

2.4.2. Birkeland and Birkeland, 1966. Several examples of rigid connection designs involving precast concrete panels, beams, and columns were developed by the authors including associated reinforcement and hardware. They also introduced the use of the shear-friction theory for connections which cannot be designed using beam shear-flexure and principal tension analyses. An example of a situation where this occurs is the plane of maximum shear at the face of a corbel. Birkeland and Birkeland stated that shear strength (capacity) V can be represented as in Equation 2.17, with tan ϕ representing the coefficient of friction between the adjoining surfaces; V_u is the total ultimate shear force (demand); A_s is the total cross-sectional area of reinforcing across the interface; f_y is the yield strength of reinforcing ($\leq$ 60 ksi); and FS is the factor of safety. The authors also provided a visual comparison of the various push-off specimen designs used in previous research, as shown in Figure 2.3.

$$V = \frac{V_u}{FS} = \frac{A_s f_y \tan \phi}{FS} \tag{2.17}$$

Where:

tan ϕ = 1.7 for monolithic concrete

tan ϕ = 1.4 for artificially roughened construction joints

tan ϕ = 0.8 to 1.0 for ordinary construction joints and concrete to steel interfaces

Birkeland and Birkeland cautioned that the shear reinforcement must be properly anchored in order to develop yield, and headed studs could be used to engage concrete. They also assumed that dowel action is negligible. They advised that the interface

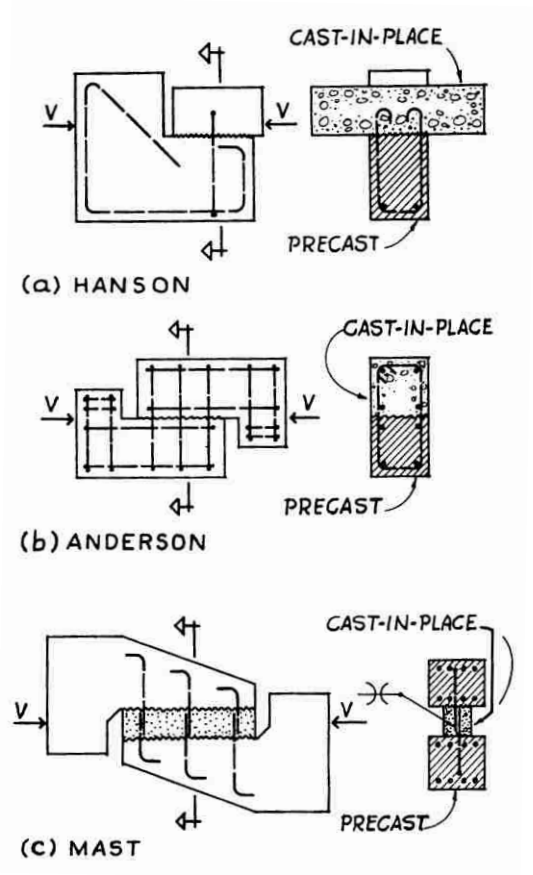

Figure 2.3. Typical push-off specimen configurations used in previous research (Birkeland and Birkeland 1966)

surface be cleared of all dirt and debris before placing the second lift of a cold-joint. Also, they cautioned designers about the decreased clamping force available when external tension loads are present. They went on to explain the limitations from previous studies by Hanson (1960) and Anderson (1960) and how they have shaped the limitations on the applicability of shear-friction theory to date. One important note is the 800 psi limit for ultimate shear stress of concrete set in place based on Mast's unpublished research. Birkeland and Birkeland suggest that this limitation is based on the result of only one specimen using poor testing methods and should be re-evaluated. They assert that if the cast-in-place concrete used in that test had been allowed to cure fully, the results would be closer to that of shear-friction theory. The authors also recognized the limitations of the shear-friction theory based on the current amount of data; for example,

only ASTM A-15, Intermediate Grade reinforcing steel had been tested at that time, with a yield strength of approximately 50 ksi. Birkeland and Birkeland gave example design calculations within their article for a knife connection as well as a bearing connection.

2.4.3. Mast, 1968. This paper summarized some of the difficulties of designing precast elements and offers examples of detailed connection designs. Mast stated that these elements must be assumed to have a pre-existing crack in order to create a conservative design. Since it is assumed that a crack exists, the provisions of the shear-friction hypothesis can be applied.

Mast warned of several limitations to this design method:

1. The shear-friction hypothesis cannot be applied in situations where slip is highly critical or where fatigue is a potential problem.
2. Reinforcement for externally applied tension across a crack must be considered separately from the tension reinforcement required by the shear-friction theory.
3. Tensile reinforcement must be properly anchored on both sides of a crack so that the full yield strength of the steel is able to develop.
4. Since all testing to date had been done using normalweight concrete, the results of this and previous studies were not recommended to be applied to lightweight concrete due to differences in the aggregate's internal structure.
5. Suggested values of tan ϕ determined from testing are summarized in Table 2.5. These values are empirical and reflect cracked specimens tested at generally low levels of stress ($\rho f_y \leq 1000$ psi).

Table 2.5. Values of tan ϕ recommended for design (Mast 1968)

Case	**Description**	**tan ϕ**
a	Concrete to concrete, rough interface	1.4
b	Concrete to steel, composite beams	1.0
c	Concrete to steel, field-welded inserts	0.7
d	Concrete to concrete, smooth interface	0.7

6. Because the angle of internal friction, ϕ, has been assumed to be unaffected by concrete strength and stress level, it is not safe to make direct correlations for test specimens of higher strength and stress levels. Further testing is needed; therefore, the author suggested limiting the reinforcement parameter, ρf_y, to 15% of the concrete compressive strength.

2.4.4. Hofbeck, Ibrahim, and Mattock, 1969. The shear-friction of normalweight concrete was studied using 36 push-off specimens which had either pre-cracked or uncracked shear interface conditions. All specimens were cast on their side to create a monolithic specimen with concrete compressive strengths f'_c ranging from approximately 2,500 to 4,500 psi. The pre-cracked condition was achieved by applying a line force along the shear plane before compression testing. This was done to simulate a crack which may form in a concrete connection before shear is applied; i.e. temperature and shrinkage cracks, or damage to a precast member during shipping or installation. The results of the study were strongly supported by the shear-friction theory. Mohr's circle was used to represent failure conditions of concrete. The Zia envelope method (Zia 1961) was applied to initially uncracked concrete specimens in order to determine their shear transfer strength.

Hofbeck, et al. found that for all levels of load, the pre-cracked specimens had an increase in slip and a reduction in ultimate shear transfer relative to uncracked specimens. Specifically, the f'_c = 4,000 psi specimens with ρf_y values of 200 to 1,000 psi had a shear strength that was 250 psi lower than that of similar uncracked specimens.
The reinforcement parameter, ρf_y, has a direct effect on the shear transfer strength. Therefore, modifying the strength, size, and spacing of steel reinforcement will change the shear transfer strength. For pre-cracked specimens, there is a definitive point in the linear regression of the shear transfer strength vs. reinforcement parameter plot in which the slope is reduced. This transition point varies for differing concrete compressive strengths, but below this point, the regression line is similar to that of concrete strengths greater than or equal to the strength being considered.

Dowel action of the reinforcing bars which cross the shear plane had minimal contribution to shear strength of the uncracked specimens, but had a significant contribution to shear strength in the pre-cracked specimens. This result was observed by

comparing pre-cracked and initially uncracked specimens to their control counterparts in which rubber sleeves had been provided around reinforcement to eliminate shear strength contributions due to dowel action. This behavior was explained by the authors as most likely being attributed to the different cracking patterns of the uncracked and pre-cracked specimens. In the initially uncracked specimens, diagonal tension cracks form, and the concrete struts in between eventually fail by crushing. This diagonal orientation of the cracks puts the reinforcement into tension, rather than direct shear. On the other hand, pre-cracking the specimens ensure that the reinforcing stirrups are perpendicular to the shear plane, and dowel action can develop since the steel bars see a more direct shearing action by both faces of concrete on opposite sides of the crack.

For pre-cracked specimens of normalweight concrete, with intermediate shear reinforcement (ASTM A432, experimental f_y = 66.1 ksi), the shear-friction theory gives a fairly conservative estimate of shear strength when a coefficient of friction between the faces of the crack of μ = 1.40 is used. This is true as long as the reinforcement parameter ρf_y is less than the smaller of $0.15f'_c$ or 600 psi. For uncracked or cold-joint specimens with a roughened interface, the Zia failure envelope provides a reasonably accurate relationship between shear transfer strength and reinforcement parameter ρf_y.

2.4.5. Mattock and Hawkins, 1972. This study investigated the shear strength of monolithic concrete connections. Variables incorporated into the test specimens included: condition of the shear plane, type of reinforcement, concrete compressive strength, and presence of direct stresses which act either parallel or perpendicular to the shear plane. Both push-off and pull-off specimens were used in this study, along with a modified push-off design as shown in Figure 2.4.

Mattock and Hawkins concluded from their data that slip will be increased and shear transfer strength will decrease if there is a pre-existing crack along the shear plane of a monolithic specimen. The researchers also discovered that if shear reinforcement strength, size, or spacing is modified among the specimens, the shear transfer strength will only be affected if the reinforcement parameter, ρf_y is changed. Note that this statement is only valid for steel yield strengths $f_y \leq 66$ ksi.

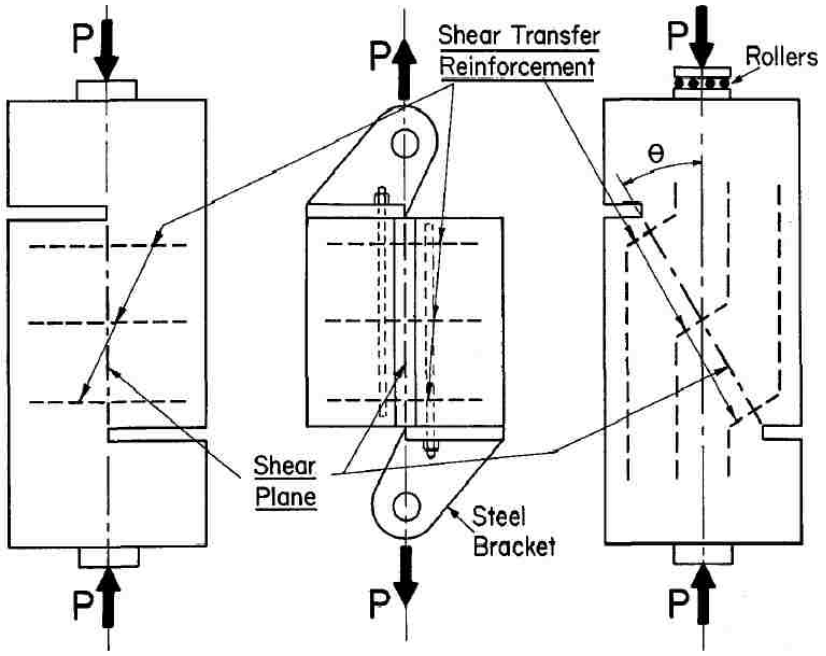

Figure 2.4. Mattock and Hawkins (1972) shear transfer study: from left to right, push-off, pull-off, and modified push-off specimens

Another key finding from this study was the effect of concrete strength on the shear strength of initially cracked specimens. As shown in Figure 2.5, specimens of 2,500 psi concrete have similar shear strengths to specimens of 4,000 psi concrete for low values of ρf_y. Then, for values of reinforcement parameter ρf_y larger than a particular value of ρf_y (about 500 psi), the shear strength is higher for concrete with a higher compressive strength f'_c.

In studying the initially uncracked pull-off specimens, it was found that direct tension stress parallel to the shear plane reduces the shear transfer strength. Yet, shear transfer strength was not reduced in specimens that were initially cracked. On the other hand, externally applied compressive stress acting perpendicular to the shear plane can be added to ρf_y in calculations of shear strength for both initially cracked and uncracked specimens. Mattock and Hawkins noticed diagonal tension cracks in their initially uncracked specimens and explained that they are due to truss action along the shear plane. After the inclined concrete 'struts' form, they eventually fail under shear and axial forces.

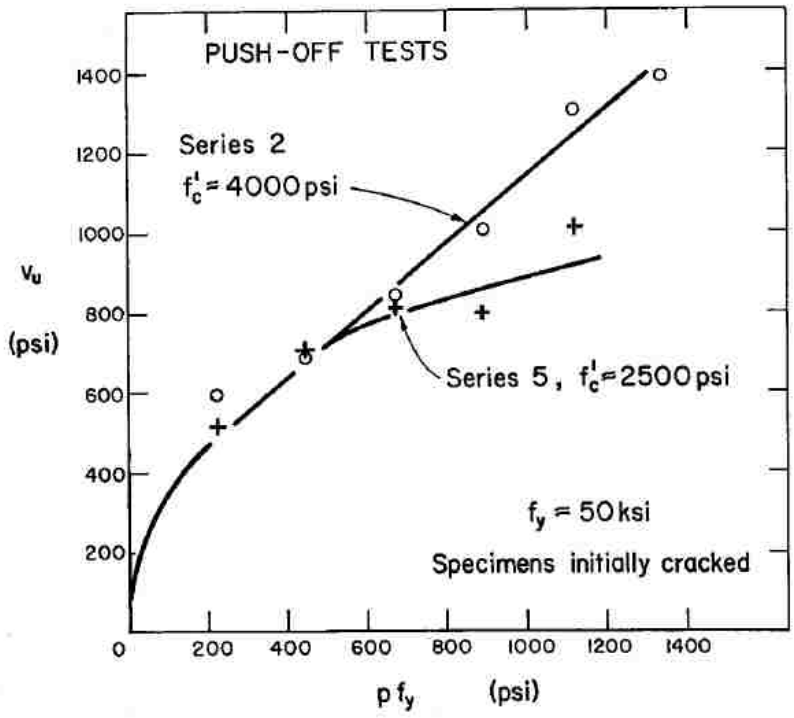

Figure 2.5. Variation in shear strength of initially uncracked specimens (Mattock and Hawkins 1972)

For initially cracked specimens, the researchers explained that the shear transfer strength is developed primarily by friction along the shear interface and dowel action of the reinforcement. In the case where there is a large amount of reinforcement or a large compressive stress perpendicular to the shear plane, the crack is essentially clamped shut. Therefore, shear transfer strength is developed as if the specimen were initially uncracked, and the diagonal tension cracking across the shear plane with eventual concrete 'strut' failure is noted.

The main conclusion of the study is that the current ACI 318 code provisions (1971) were safe, but overly conservative for higher concrete strengths and a large amount of reinforcement. In order to reflect these higher shear transfer strengths than the code-adopted value of 800 psi, Mattock and Hawkins suggested a new design equation (Equation 2.18). The term σ_{Nx} represents the externally applied direct stress across the shear plane, taken as positive for compression and negative for tension.

$$v_u = 200\ psi + 0.8\left(\rho f_y + \sigma_{Nx}\right) \quad (2.18)$$

2.4.6. Paulay, Park, and Phillips, 1974. These gentlemen tested the horizontal shear capacity of construction joints using thirty cold-joint specimens and six monolithic specimens of shear wall-footing connections (Figure 2.6). The amount of reinforcement across the shear plane was varied as well as the surface preparation of the cold-joint specimens. Joints were either steel troweled, sprayed with a chemical retarder, rough scraped, rough washed, rough chiseled, keyed, or the bond was removed through application of a varnish or wax. The concrete had a target compressive strength of f'_c = 2,500 psi, while the actual compressive strength on the test day ranged from f'_c = 2,920 to 4,350 psi. The cold-joint specimens were constructed with 9 to 25 days between each casting, and all specimens were tested at an age of 24 to 105 days. A few specimens underwent cyclic loading, and it was concluded that design interface shear capacity and slip levels can be maintained along a horizontal construction joint, even through repeated loading/unloading.

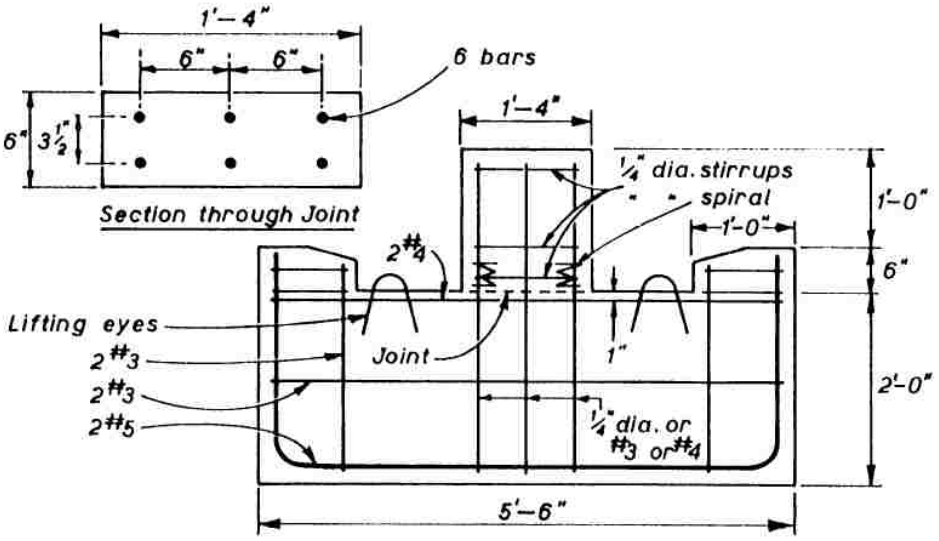

Figure 2.6. Specimen design (Paulay, Park, and Phillips 1974)

In order to differentiate between the contributions of dowel action and other shear-friction mechanisms such as bond and interface friction, bond was destroyed on several specimens with a coat of varnish or wax. It was concluded that significant dowel forces (up to 85% of the shear capacity) can be developed, but should be ignored for design purposes because a large amount of slip is created along the joint. Instead, it was estimated that only 15% of the shear capacity was supplied by dowel action at load and slip levels within the typical design range.

It was noted that the failure plane of the specimens in this study were typically not along the plane of the construction joint, except for the smooth troweled and lightly reinforced rough joints. Instead, the failure plane was about an inch below the cold-joint interface, even in the instance where the stronger concrete was located below the joint. It is assumed that this occurred due to the fresh concrete becoming non-homogeneous at the top surface once it was placed into the formwork; thus, making it weakest in the top-most layer. Since the construction joint was not deemed the weakest link in most specimens, it was concluded that adequately reinforced construction joints with a dry, clean, and roughened interface will develop horizontal interface shear strength which is greater than or equal to the surrounding shear wall structure's capacity.

2.4.7. Mattock, Johal, and Chow, 1975. Using concrete with a design strength of 4000 psi on the test day, and monolithic specimens (either pre-cracked or uncracked), shear strength of unique connections were tested by Mattock, Johal, and Chow in an effort to explore the current limitations of ACI Code and PCI Handbook design equations. Corbel type push-off specimens were used to study the effect of moment acting on a shear plane, and a sketch of the test specimen is shown in Figure 2.7. A second specimen design, as shown in Figure 2.8, was used to observe the shear strength in the presence of a tension force normal to the shear plane. In order to apply this external tension force, it was necessary to anchor ¾ in. diameter high strength bolt within the central portion of the specimen. This study also focused on the influence of spacing, location, and quantity of reinforcement on the total shear capacity of a connection. Results of the corbel-type specimens showed that the ultimate shear transfer capacity of the specimen was unaffected as long as the ultimate flexural strength was not exceeded during testing.

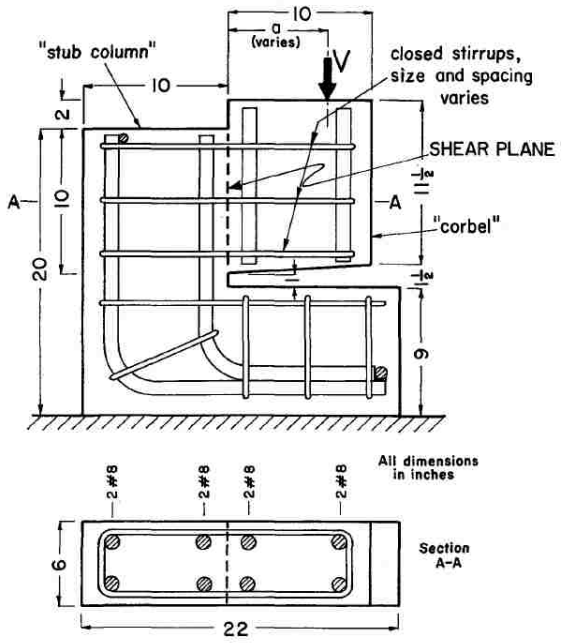

Figure 2.7. Push-off specimen design (Mattock, Johal, and Chow, 1975)

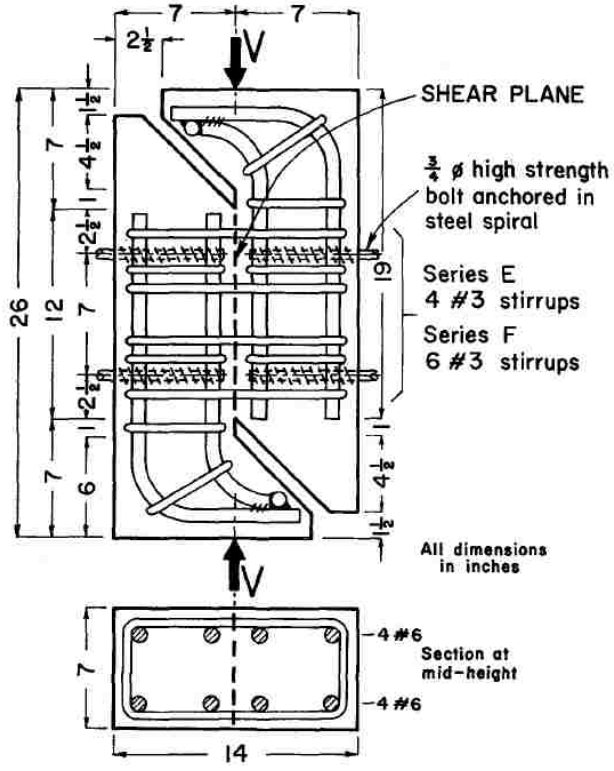

(For the application of tension across the shear plane)

Figure 2.8. Push-off specimen for testing with tension across shear plane (Mattock, Johal, and Chow, 1975)

There were several key conclusions to this study:

1. It is necessary to add the normal stress σ_{Nw} to the reinforcement parameter ρf_y when calculating shear transfer strength. This is valid for both initially cracked and initially uncracked specimens. The sign of σ_{Nw} should be positive for a compression force normal to the shear plane and negative for tension.
2. When there is tension normal to the shear plane, the amount of reinforcement required at the connection is the sum of the area of steel required for resisting shear and the area of steel required to resist the tension force.
3. If a moment is present at a reinforced concrete connection, and it is less than or equal to the flexural strength of the cracked section, then the shear capacity of the connection will not be reduced. When both moment and shear are present at a connection, the shear transfer reinforcement is most effective when located in the flexural tension zone.
4. The PCI Handbook design equation for ρf_y exceeding 600 psi is conservative for the cases of compression or tension acting normal to the shear plane, but σ_{Nw} must be added to ρf_y in the equation.
5. Equations 2.19 and 2.20 which were proposed by Birkeland (1968) and Mattock (1974), respectively, are applicable in the case of shear and compression or tension across the shear plane.

$$v_u = 33.5\sqrt{\rho f_y} \tag{2.19}$$

$$v_u = 400 + 0.8\rho f_y \tag{2.20}$$

2.4.8. Mattock, 1976. In this study, eight series of push-off specimens constructed from normalweight concrete were tested under monotonic loading along the shear plane. All nominal concrete compressive strengths f'_c at test day were 6,000 psi,

except for one series which also included 3,000 psi concrete. One series included monolithic test specimens which were pre-cracked using a line load along the shear plane before testing. All other series were of composite construction and were either pre-cracked of uncracked before testing. Also, bond was broken on several of the composite series by applying a film of soft soap and talc to the interface before casting the second half of the specimen. The composite specimens either had an interface that was troweled smooth, or roughened to a 0.25 in. amplitude.

Mattock concluded that the intentionally roughened specimens behaved similarly to monolithic pre-cracked specimens, and had shear strengths that almost reached that of the monolithic specimens. He proposed that the slight reduction in shear strength was due to the difference in the minor roughness of the crack faces in the two cases. Since the shear strengths of the smooth interface specimens were roughly half that of the roughened interface specimens, Mattock recommended deliberately roughening the interface of cold-joints. For a smooth interface, he found that dowel action was the primary mechanism of shear transfer. Mattock also made recommendations for modifications to values for the coefficient of friction μ for normalweight concrete:

a) For a roughened interface, Mattock recommended $\mu = 1.4$
b) For a smooth interface, Mattock recommended $\mu = 0.6$

Mattock also proposed modifications to ACI and PCI design equations for normalweight concrete in the form of Equation 2.21:

$$v_u = 0.8\rho f_y + 400\ psi \tag{2.21}$$

Where: $v_u \leq 0.2f'_c$ for intentionally roughened cold-joint interface, and
$v_u \leq 0.3f'_c$ for a monolithic interface with $f'_c \leq 6000$ psi

2.4.9. Mattock, Li, and Wang, 1976. Push-off tests were performed on both uncracked and pre-cracked monolithic specimens constructed from normalweight, sand-lightweight, and two types of all-lightweight concrete (rounded or angular aggregate).

Out of the ten series of specimens tested in the program, eight series contained specimens which had a design concrete compressive strength of 4,000 psi, while the last two series had f'_c = 2,500 psi and f'_c = 6,000 psi, respectively. Reinforcement ratio was also varied within each test series by including 0 – 6 stirrups across the shear plane which were all No. 3 welded closed stirrups.

Results of the study indicate:

1. For concretes of the same compressive strength, the normalweight concrete had higher shear transfer strength than lightweight in all cases.
2. Shear transfer strength is not significantly affected when rounded lightweight aggregates are used versus angular lightweight aggregates.
3. The shear-friction provisions of ACI 318-71 are not conservative for lightweight aggregate concrete, and it is suggested that the μ value should be multiplied by 0.75 for all-lightweight concrete (unit weight ≥ 92 pcf) or 0.85 for sand-lightweight concrete (unit weight ≥ 105 pcf).
4. The shear-friction provisions of the PCI Design Handbook (1971) are not conservative for lightweight concretes and should not be used.
5. The authors suggest new shear-friction design equations. For sand-lightweight concrete (unit weight ≥ 105 pcf), Equation 2.22 should be used, but shear transfer strength should not exceed $0.2f'_c$ nor 1000 psi with $\rho f_y \geq 200$ psi. For all-lightweight concrete (unit weight ≥ 92 pcf), Equation 2.23 should be used, but shear transfer strength should not exceed $0.2f'_c$ nor 800 psi with $\rho f_y \geq 200$ psi.

$$v_u = 0.8\rho f_y + 250\ psi \tag{2.22}$$

$$v_u = 0.8\rho f_y + 200\ psi \tag{2.23}$$

2.4.10. Shaihk, 1978. Shaihk summarized the current state of knowledge surrounding the shear-friction properties of normalweight and lightweight concrete. He proposed revisions to the shear-friction provisions in the PCI Manual on Design of

Connection in Precast Prestressed Concrete (1973). Previous work done by Mattock (1974), Birkeland (1969), and Raths (1977) was compared, and their proposed design equations were combined and modified. The proposed amount of reinforcement required to cross a shear plane is represented in Equation 2.24, where V_u is the ultimate shear force, f_{yv} is the specified yield strength of the shear-friction reinforcement, ϕ is the capacity reduction factor (where ϕ equals 0.85 for shear), and μ_e is the effective coefficient of friction.

$$A_{vf} = \frac{V_u}{\phi f_{yv} \mu_e} \tag{2.24}$$

Raths' expression for the effective coefficient of friction, μ_e, is one of the major proposed changes (Equation 2.25). C_s represents a constant used for the effect of concrete density, with C_s = 1.0 for normalweight, C_s = 0.85 for sand-lightweight, and C_s = 0.75 for all-lightweight concrete. The nominal shear stress (capacity of the specimen) along the interface, v_u, is the ultimate shear force, V_u, divided by the area of shear crack interface, A_{cr}.

$$\mu_e = \frac{1000\ C_s^2\ \mu}{v_u} \tag{2.25}$$

The coefficient of static friction, μ, varies according to shear interface condition, and recommended values are found in Table 2.6, along with maximum values of v_u. Mattock's suggested value for a minimum $\rho_v f_y$ = 120 psi is also included in the proposal because it corresponds to a v_u greater than or equal to the shear resistance due to the cohesion of concrete.

Table 2.6. Recommended μ and $v_{u,max}$ (Shaihk 1978)

Crack Interface Condition	Recommended μ	Maximum v_u, psi
1. Concrete to concrete, cast monolithically	1.4	$0.30 f'_c C_s^2 \leq 1200 C_s^2$
2. Concrete to hardened concrete, ¼ in. roughness	1.0	$0.25 f'_c C_s^2 \leq 1000 C_s^2$
3. Concrete to concrete, smooth interface	0.4	$0.15 f'_c C_s^2 \leq 600 C_s^2$
4. Concrete to steel	0.6	$0.20 f'_c C_s^2 \leq 800 C_s^2$

2.4.11. Hsu, Mau, and Chen, 1987. The truss-model theory was presented which is an alternative to the commonly used shear-friction theory. This theory arose from the observation that initially uncracked push-off specimens develop numerous inclined cracks along the shear plane, after which point the concrete 'struts' parallel to these cracks fail due to crushing. The theory was named for the truss-like action of the compression in the concrete struts combined with the tension in the steel reinforcement parallel to and crossing the shear plane. Data from previous studies were used to validate the accuracy of the truss model theory. The authors warned that the current ACI Building Code (ACI 318-83) shear-friction design provisions may be unconservative for connections with low amounts of transverse reinforcement.

The results of the study suggested that reinforcement parallel to and near the shear plane (transverse reinforcement) contribute to the shear strength (Figure 2.9). Specifically, when transverse steel ratios of the test specimens were reduced from 0.0587 to 0.0025, the shear strength decreased by 25%. Hsu et al. explained that since most test specimens from previous studies had large amounts of transverse reinforcement, design provisions based on these tests should not be used for cases of low amounts of transverse reinforcement; more testing would be needed to verify the shear strength of these connections.

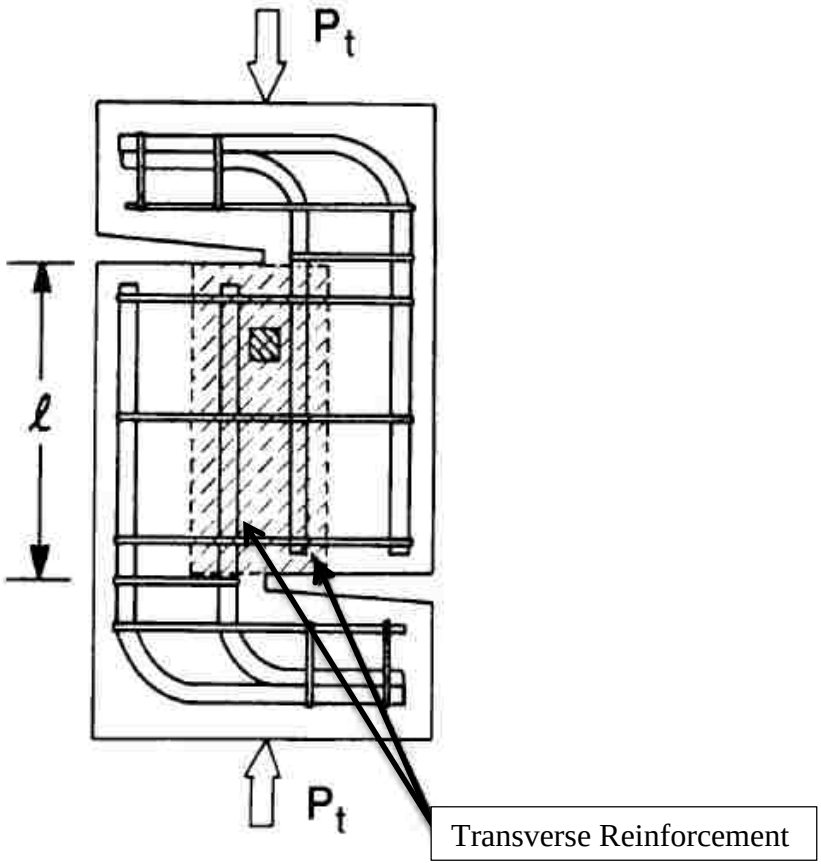

Figure 2.9. Location of transverse reinforcement (Hsu, Mau, and Chen, 1987)

2.4.12. Hoff, 1993. The aim of this study was to develop high-strength lightweight aggregate concretes suitable for use in the Arctic region. Several structural aspects of this unique concrete were studied including shear-friction capacity. Hoff constructed push-off specimens with varied reinforcement ratios and a range of concrete compressive strengths. Two types of lightweight aggregate were used: crushed or pelletized. The study showed that larger reinforcement ratios corresponded to higher shear fiction capacity. He also found that the specimens built from concrete with a higher compressive strength had higher shear-friction capacity. An interesting finding was that the maximum shear stress levels were similar in the crushed and pelletized aggregate concretes, yet the slip behavior differed for the two types of aggregates. The smoother aggregate (pelletized) experienced more abrupt slip when compared to the crushed

aggregate specimens. Hoff concluded that the shear-friction provisions of ACI 318-89 are valid for the specimens tested in this study, but a more conservative reduction factor (such as 0.75 instead of 0.85) for sand-lightweight aggregate concrete should be used in critical areas of a structure.

2.4.13. Mattock, 2001. The shear-friction properties of connections in high-strength concrete were investigated. Mattock evaluated the data from eight previous studies and concluded that shear-friction design provisions from ACI 318-99 are overly conservative when high-strength concretes are used. New shear-friction design equations were suggested by Mattock to create more economical designs.

1. For monolithic concrete and cold-joint connections with interface intentionally roughened:
   a. When $(\rho_{vf} f_y + \sigma_{Nx}) \geq K_1/1.45$

      Where: $K_1 = 0.1f'_c$, but not more than 800 psi;

$$v_n = K_1 + 0.8\left(\rho_{vf} f_y + \sigma_{Nx}\right) \ (psi) \qquad (2.26)$$

but not greater than $K_2 f'_c$ nor K_3 psi;

Where: $K_2 = 0.3$; $K_3 = 2400$ psi

   b. When $(\rho_{vf} f_y + \sigma_{Nx}) \leq K_1/1.45$

$$v_n = 2.25\left(\rho_{vf} f_y + \sigma_{Nx}\right) \ (psi) \qquad (2.27)$$

Note: For normalweight monolithic concrete, $K_1 = 0.1f'_c$ but not more than 800 psi; $K_2 = 0.3$; and $K_3 = 2400$ psi. For normalweight concrete placed against hardened normalweight concrete with the interface intentionally roughened, $K_1 = 400$ psi; $K_2 = 0.3$, where f'_c shall be taken as the lower of the compressive strengths of the two concretes; and $K_3 = 2400$ psi. For sand-lightweight concrete, $K_1 = 250$ psi; $K_2 = 0.2$; and $K_3 = 1200$ psi. For all-lightweight concrete, $K_1 = 200$ psi; $K_2 = 0.2$; and $K_3 = 1200$ psi.

2. For concrete placed against hardened concrete not intentionally roughened,

$$v_n = 0.6\lambda\rho_{vf} f_y \ (psi) \tag{2.28}$$

but not more than $0.2f'_c$ nor 800 psi

3. For concrete anchored to clean, unpainted, as-rolled structural steel by headed studs or by reinforcing bars,

$$v_n = 0.7\ \rho_{vf}\ f_y \ (psi) \tag{2.29}$$

but not more than $0.2f'_c$ nor 800 psi

2.4.14. Kahn and Mitchell, 2002. These gentlemen tested 50 push-off specimens with varying interface conditions: uncracked, pre-cracked, and cold-joint. Their aim was to either disprove or demonstrate the validity of the ACI 318-99 shear-friction equations in regards to high strength concrete. They tested concrete specimens with compressive strengths of 6,800 to 17,900 psi. The transverse shear reinforcement ratios were also varied among the specimens, between 0.37% and 1.47%. The specimens were constructed according to the design used by Hofbeck, Ibrahim, and Mattock (see Section 2.4.4), as well as Anderson (1960), in order to produce comparable results. Figure 2.10 shows a typical failed specimen. For the cold-joint specimens, the interface was neither troweled nor intentionally roughened, but it was noted that all but two specimens had a rough appearance with amplitude of about 0.25 in.

From their results, Kahn and Mitchell concluded that the ACI 318-99 code provisions were indeed applicable to concrete strengths greater than 10,000 psi. In fact, they noted that the provisions were conservative for high-strength concretes up to 18,000 psi. Therefore, they proposed a revised design equation for cold-joint and uncracked monolithic interfaces which would produce more economical designs (Equation 2.30).

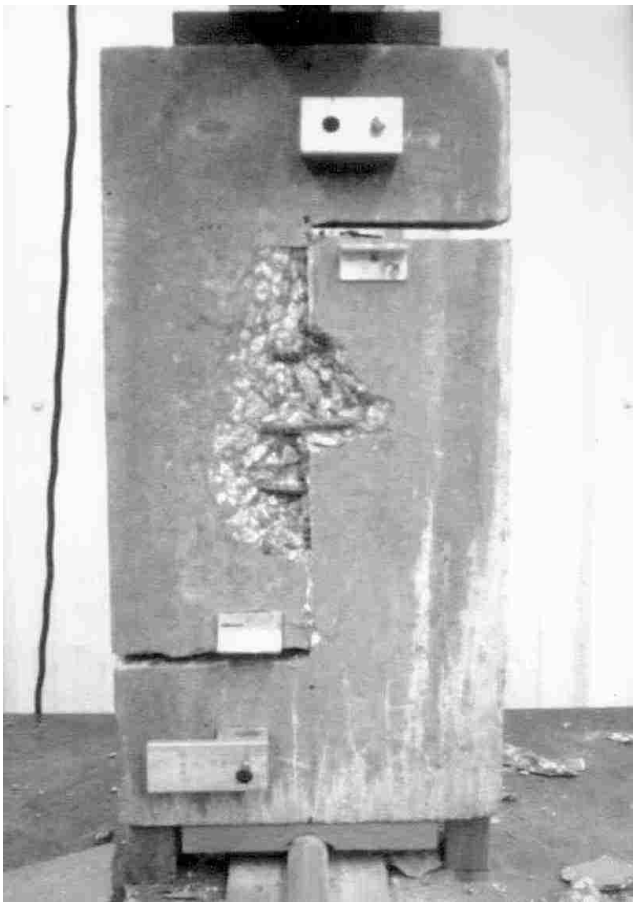

Figure 2.10. Typical failed specimen (Kahn and Mitchell 2002)

$$v_u = \frac{V_u}{A_c} = 0.05f'_c + 1.4\rho_v f_y \leq 0.2f'_c \quad (psi) \tag{2.30}$$

The first term of Equation 2.30 accounts for bond and asperity shear. Note that the coefficient of 1.4 in the second term of the equation represents the coefficient of friction typically seen in previous shear-friction design equations for monolithic concrete. Here, the authors intend for the same value of μ to be used for multiple interface conditions: monolithic, cold-joint roughened, and cold-joint smooth. The ultimate experimental shear stress (demand) in Equation 2.30 is denoted as v_u; f'_c is the

compressive strength of the concrete; ρ_v is the shear-friction reinforcement ratio; and f_y is the yield stress of the reinforcement.

Kahn and Mitchell suggested that the upper limit of 800 psi for shear strength V_u should be removed from the ACI Code for concrete strengths of 3,000 to 8,000 psi. Instead, they suggested an upper limit of 0.2 f'_c. They also concluded that residual strengths of uncracked, pre-cracked, and cold-joint specimens were similar for members of identical reinforcement ratios. In order to regulate the scatter of data, they recommend that the yield stress of the reinforcing bars f_y be limited to 60 ksi. The shear-friction strengths of all specimens, independent of interface condition, were higher than predicted by ACI 318 – 99 code provisions, using μ = 1.4 and a maximum f_y of 60 ksi. Thus, they support the idea that a coefficient of friction, μ, of 1.4 be used for a roughened cold-joint interface condition. Note that even though the smooth cold-joint interface was not the intended focus of this study, two specimens of the testing program had a smooth cold-joint interface and were also conservatively predicted by Equation 2.30.

2.4.15. Tanner, 2008. Tanner's article examined the evolution of the design equations for shear-friction in the 4th, 5th, and 6th Editions of the PCI Design Handbook and identified several key discrepancies with respect to the original test data used in their development. First, he discusses the confusion caused by researchers using V_u and V_n interchangeably as meaning shear strength. In LRFD design equations, however, the terms V_u and V_n refer to applied factored loads (demand) and strength (capacity), respectively. Also, since the ϕ factors in ultimate strength design changed from 0.85 to 0.75 for shear, the calculations of μ_e for various values of v_n produce widely varying results as seen in Figure 2.11.

Another issue noted by Tanner is the fact that μ_e should equal μ at $v_{n,max}$. He plotted the effective coefficient of friction versus nominal shear stress for each of the interface conditions according to the 6th edition of the PCI Design Handbook and found that the plots continue past the limit of v_n = 1000 psi. In fact, even at v_n = 1000 psi, the values for μ_e were unconservative. Tanner suggests replacing the $1000A_{cr}$ term with the maximum nominal shear capacity $V_{n,max}$ in the equation for μ_e. In addition, to eliminate the confusion of whether the effective coefficient of friction is a function of λ or λ^2, Tanner proposed a new equation for μ_e (Equation 2.31).

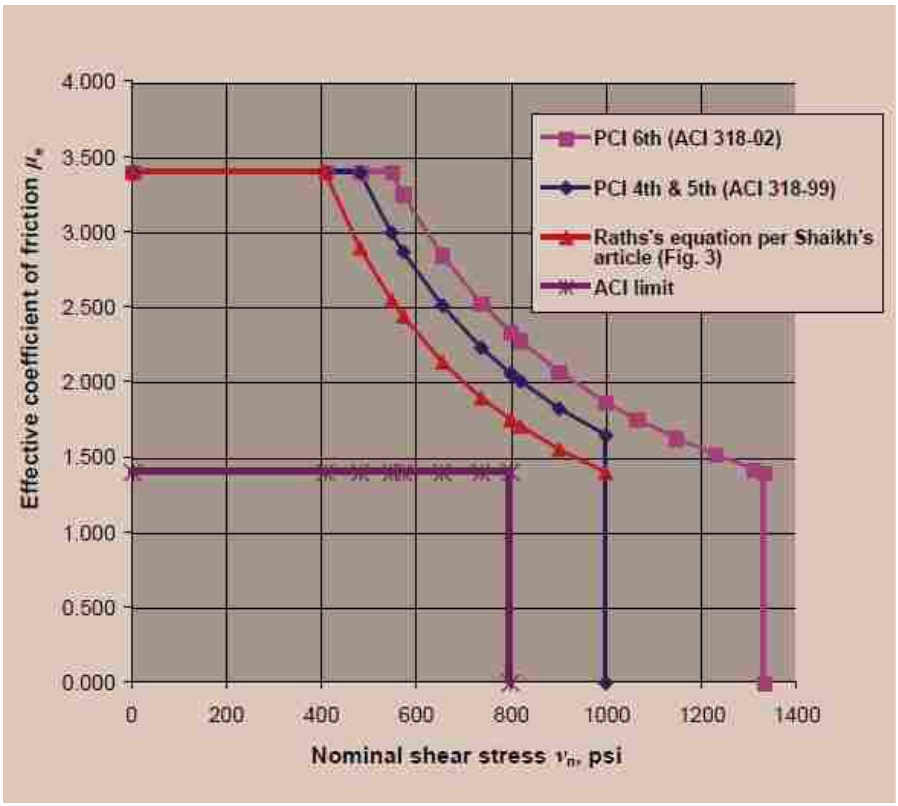

Figure 2.11. Variation in effective coefficient of friction μ_e vs. nominal shear stress v_n from four sources (Tanner 2008)

$$\mu_e = \frac{\mu V_{n,max}}{V_n} \quad or \quad \mu_e = \frac{\mu \phi V_{n,max}}{V_u} \tag{2.31}$$

Table 2.7 contains recommended values for μ (which are the same as in the PCI Design Handbook 6th and 7th Editions), maximum μ_e, and $V_{n,max}$. The values for $V_{n,max}$ were implemented in the 7th Edition of the PCI Design Handbook, yet his suggestions for the maximum values of μ_e were not included in that edition. Instead, the 7th Edition of PCI gives maximum values of μ_e for the first two interface condition cases as 3.4 and 2.9, respectively. For the third and fourth interface conditions listed in Table 2.7, the μ_e approach is not considered applicable in the 7th Edition of the PCI Design Handbook.

Table 2.7. Proposed modifications to PCI Design Handbook, 6th edition Table 4.3.6.1 (Tanner 2008)

Crack-interface condition	**Recommended μ**	**Maximum μ_e**	$V_{n,max}$
Concrete to concrete, cast monolithically	1.4λ	3.4λ	$0.30\lambda f'_c A_{cr} \leq 1000\lambda A_{cr}$
Concrete to concrete, with roughened surface	1.0λ	2.9λ	$0.25\lambda f'_c A_{cr} \leq 1000\lambda A_{cr}$
Concrete to concrete, with smooth surface	0.6λ	2.2λ	$0.20\lambda f'_c A_{cr} \leq 800\lambda A_{cr}$
Concrete to steel	0.7λ	2.4λ	$0.20\lambda f'_c A_{cr} \leq 800\lambda A_{cr}$

Note: $\lambda = 1.0$ for normalweight concrete; $\lambda = 0.85$ for sand-lightweight concrete; $\lambda = 0.75$ for all-lightweight concrete

2.4.16. Harries, Zeno, and Shahrooz, 2012. A series of cold-joint specimens with varied reinforcement ratio were constructed using either ASTM A615 (f_y = 60 ksi) reinforcing steel bars or ASTM A1035 (f_y = 100 ksi) bars. The two concrete lifts were cast 14 days apart, and their compressive strengths on the day of testing were 7120 psi and 5800 psi. Three double-legged ties crossed each shear plane and were either No. 3 or No. 4 bars, which correspond to reinforcement ratios ρ of 0.0041 and 0.0074, respectively. Interestingly, the ultimate capacity was unaffected by the grade of reinforcing. Yet, the post-peak behavior was different among the two reinforcement strengths. The specimens with the ASTM A615 bars experienced a rapid decline in post-ultimate load-carrying capacity, while the specimens with ASTM A1035 bars were able to sustain the ultimate shear load after the peak was achieved. The authors suggested that this difference in behavior may be due to the different bond characteristics of the bars.

The authors explained the three stages of shear-friction behavior, and they separate the concrete contribution to shear strength from the steel reinforcement contribution (Figure 2.12 a,b). They discovered that the steel yielding occurred well after the ultimate shear strength was achieved in the specimen with ASTM A615 bars. As shown in Figure 2.12 (a) and (b), steel yielding did not occur for the specimen with

ASTM A1035 bars, and the AASHTO specified shear capacity for this specimen according the calculation using Equation 2.32 is never reached.

$$V_{ni} = cA_{cv} + \mu\left(A_{vf}f_y + P_c\right) \tag{2.32}$$

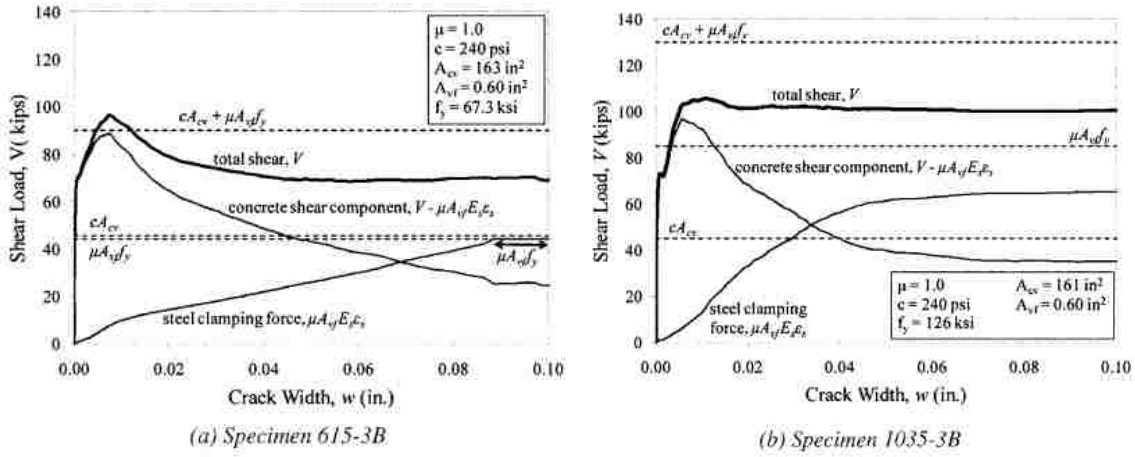

Figure 2.12. Concrete and steel components of shear resistance for (a) ASTM A615 steel reinforcing bars and (b) ASTM A1035 steel reinforcing bars (Harries, Zeno, and Shahrooz 2012)

They concluded that the current shear-friction design equations are too simplistic and do not reflect the true nature of material behavior. They stated that the ACI 318-08 and AASHTO (2007) design equations are misleading because they imply that the peak resistance to shear-friction by the concrete and steel components occurs simultaneously. Harries et al. proposed a modified form of the shear-friction equation (Equation 2.33) in which the first term represents the concrete contribution to the shear strength during the pre-cracked stage. The second term corresponds to the friction force developed by the steel reinforcement after cracking occurs. In Equation 2.33, V_{ni} represents the nominal interface shear resistance; α is a coefficient for the type of interface, with α = 0.075 for

monolithic uncracked interface, α = 0.040 for a cold-joint interface, and α = 0.0 for a monolithic pre-cracked interface; f'_c is the concrete compressive strength; A_{cv} is the area of concrete shear interface; and E_s is the modulus of elasticity of the steel reinforcement.

$$V_{ni} = \alpha A_{cv} f'_c + 0.002 A_{cv} E_s \leq 0.20 A_{cv} f'_c \quad (2.33)$$

2.4.17. Shaw, 2013. The goal of this study was to investigate the shear-friction properties of lightweight concrete with non-monolithic interface conditions. This research involved 36 cold-joint specimens of normalweight, sand-lightweight, or all-lightweight concrete. Expanded shale aggregate was used for the lightweight concretes. The interface condition was either smooth or roughened to 0.25 in. amplitude, and the target concrete compressive strengths were 5,000 psi and 8,000 psi. A constant reinforcement ratio ρ of 0.013 was used in this study.

Shaw concluded that the use of lightweight concrete did not produce shear strengths that were significantly different than the control normalweight concrete specimens. However, for a smooth interface, the shear strength did seem to be tied to concrete compressive strength. This was not true for specimens of a roughened interface. Overall, results showed that the shear transfer strength increased with higher f'_c values; yet, residual shear strength was not affected by concrete type (unit weight), concrete compressive strength, or interface condition. When comparing to PCI Design Handbook (2011) and ACI 318-11, using the μ approach, shear strengths were conservative for the lightweight specimens. Using the provisions of the 6th Edition of the PCI Design Handbook (2004), conservative values of μ_e were calculated for the sand-lightweight and all-lightweight specimens. Yet, this method was not conservative for normalweight specimens with a smooth interface and f'_c = 5,000 psi. It was also observed that the lightweight concrete modification factor λ was conservative for the lightweight shale aggregate concretes used in this study.

3. EXPERIMENTAL PROGRAM

3.1. INTRODUCTION

The objective of this experimental work is to test the shear-friction properties of sand-lightweight concrete made from clay or slate aggregate. These results are compared to current code provisions and design equations. This section describes the design and fabrication of the push-off specimens, as well as the properties of the lightweight clay and slate aggregates used. The concrete mixtures are also summarized along with the shear testing set-up. The test results of all specimens are also shown in a series of figures in terms of applied shear force, slip, dilation, and interface steel strain. The interface steel strain is defined as the strain readings from strain gages attached to the steel reinforcement bars located at the shear interface.

3.2. SPECIMEN DESIGN

Thirty-two push-off specimens were tested in this study, and all were constructed with sand-lightweight concrete. One parameter which varied was the reinforcement ratio ρ. For a shear plane area of 49.5 in^2, and either 2, 3, 4, or 5 No. 3 double-legged stirrups crossing the shear plane, associated reinforcement ratios were 0.009, 0.013, 0.017, and 0.022, respectively (Table 3.1). All specimens were named with a unique 'Specimen ID' as designated in Figure 3.1. The entire test specimen matrix is shown in Table 3.2.

Table 3.1. Stirrup Configurations and Corresponding Reinforcement Ratios

Number of Stirrups Crossing Shear Plane	Reinforcement Ratio	Number of Specimens
2	0.009	8
3	0.013	8
4	0.017	8
5	0.022	8

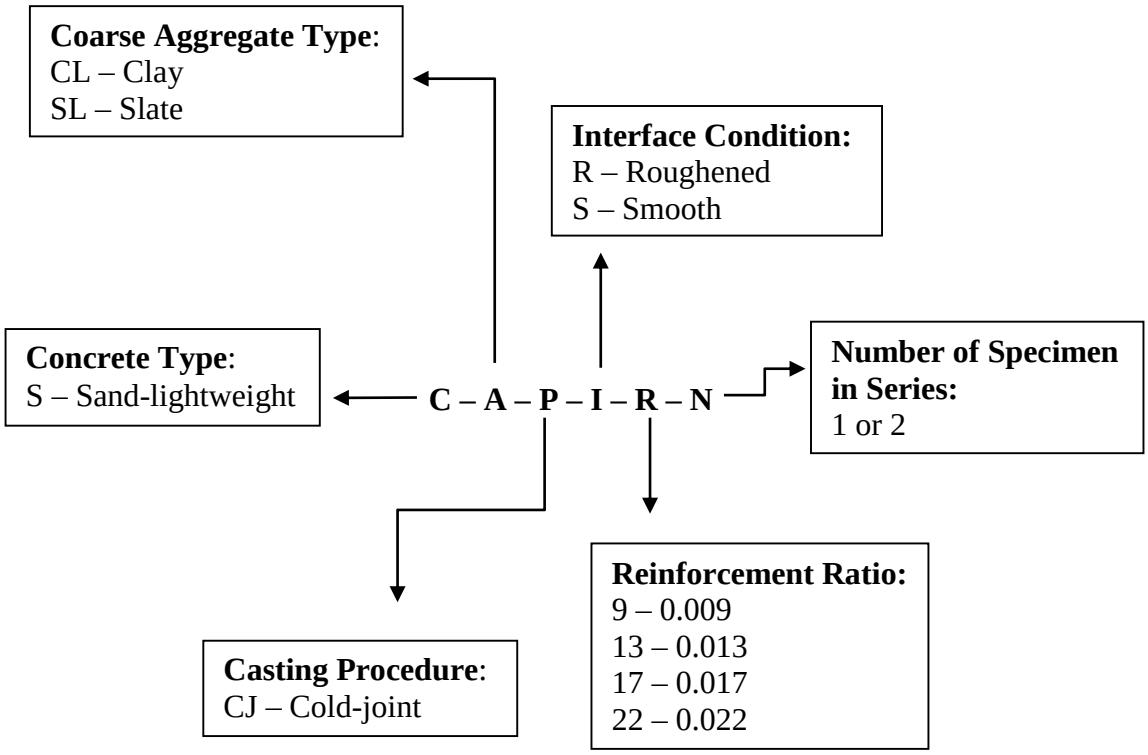

Figure 3.1. Specimen designation notation

A concrete is considered 'sand-lightweight' when normalweight sand is used for the fine aggregate, and lightweight coarse aggregate is used. Two types of lightweight aggregate were used in this study: expanded clay and expanded slate. These are further discussed in Section 3.3. All specimens of this study had a cold-joint interface that was either troweled smooth or roughened to a 0.25 in. amplitude. This process is further described in Section 3.4. The target unit weight for the sand-lightweight concrete was 115 lb/ft^3 to 120 lb/ft^3, and the target concrete compressive strength f'_c of all specimens was 5,000 psi. Actual concrete compressive strengths varied between 4550 psi and 5570 psi. This was considered acceptable since actual compressive strengths were about 500 psi from the target compressive strength. Compressive strengths for each series are summarized in Section 3.6 along with other test results.

Table 3.2. Specimen Test Matrix

Lightweight Aggregate Type	Reinforcement Ratio	Interface Condition	Specimen ID[1]
Clay	0.009	Roughened	S-CL-CJ-R-9-1
			S-CL-CJ-R-9-2
		Smooth	S-CL-CJ-S-9-1
			S-CL-CJ-S-9-2
	0.013	Roughened	S-CL-CJ-R-13-1
			S-CL-CJ-R-13-2
		Smooth	S-CL-CJ-S-13-1
			S-CL-CJ-S-13-2
	0.017	Roughened	S-CL-CJ-R-17-1
			S-CL-CJ-R-17-2
		Smooth	S-CL-CJ-S-17-1
			S-CL-CJ-S-17-2
	0.022	Roughened	S-CL-CJ-R-22-1
			S-CL-CJ-R-22-2
		Smooth	S-CL-CJ-S-22-1
			S-CL-CJ-S-22-2
Slate	0.009	Roughened	S-SL-CJ-R-9-1
			S-SL-CJ-R-9-2
		Smooth	S-SL-CJ-S-9-1
			S-SL-CJ-S-9-2
	0.013	Roughened	S-SL-CJ-R-13-1
			S-SL-CJ-R-13-2
		Smooth	S-SL-CJ-S-13-1
			S-SL-CJ-S-13-2
	0.017	Roughened	S-SL-CJ-R-17-1
			S-SL-CJ-R-17-2
		Smooth	S-SL-CJ-S-17-1
			S-SL-CJ-S-17-2
	0.022	Roughened	S-SL-CJ-R-22-1
			S-SL-CJ-R-22-2
		Smooth	S-SL-CJ-S-22-1
			S-SL-CJ-S-22-2

[1]Specimen Designation is shown in Figure 3.1

3.3. MATERIALS

The lightweight expanded clay and lightweight expanded slate aggregates used in this study are described in Section 3.3.1, and the concrete properties are in Section 3.3.2. Section 3.3.3 discusses the steel reinforcement used in the push-off specimens.

3.3.1. Aggregates. Two types of lightweight coarse aggregate, expanded clay and expanded slate, were used in conjunction with normalweight river sand to produce sand-lightweight concrete. The bulk specific gravity, density, and absorption for the clay and slate coarse aggregates are listed in Table 3.3, and samples are shown in Figure 3.2.

Table 3.3. Lightweight Clay and Slate Aggregate Material Properties

Aggregate Type	ASTM Gradation	Bulk Specific Gravity[1]	Density[2] (lb/ft^3)	Percent Absorption[3] (%)
Clay	3/8 in. x No. 8	1.302	33	19.7
Slate	3/8 in. x No. 8	1.600	52	6.0

[1]ASTM C127 / ASTM C128, Bulk Specific Gravity (SSD)
[2]ASTM C29, Loose unit weight at 6% saturation
[3]ASTM D4643, Determination of Water Content by Microwave (48 hr absorption)

Figure 3.2. Coarse aggregate samples of clay (left) and slate (right)

It is interesting to note that the extremely low density of the clay aggregate allowed it to float in water. The clay aggregate used in this study was donated by Big River Industries, Inc. and was produced at their Livingston, Alabama plant. STALITE donated the slate aggregate which came from Gold Hill, North Carolina.

3.3.1.1 Lightweight aggregate saturation. To ensure adequate internal curing of structural lightweight concrete, it is important that the lightweight aggregate has been soaked before the concrete is mixed. The internal structure of lightweight aggregate is different than normalweight aggregate in that lightweight aggregate has many more internal voids. These voids are formed when the product is processed in a rotary kiln. The excessive heat of the kiln (>2000 °F) causes certain compounds within the material to form gas bubbles. These expand the material, and the voids remain after the aggregate is cooled. These voids give the lightweight aggregate a lower density than normalweight aggregate and afford the concrete to be lighter. Yet, the presence of these voids in lightweight aggregate also means that they have a high capacity for water absorption. If dry lightweight aggregate is used in a concrete mixture, the aggregate would soak up large amounts of water and essentially 'steal' the water needed by the cement for the curing process. To avoid this problem, lightweight aggregate should be soaked in water prior to mixing the concrete. In this study, the required amount of lightweight coarse aggregate was soaked for 48 hours in the saturation tank shown in Figure 3.3. During draining of the tank, a No. 200 sieve was placed below the spout to catch any escaping fines so that they could be returned to the aggregate sample.

In order to determine the amount of water on the surface of the aggregate after draining the tank, a sample of aggregate was dried in a microwave oven to determine the moisture content according to ASTM D4643. To determine the aggregate's absorption, this process was also repeated for a separate sample of aggregate that had been brought to saturated surface dry (SSD) condition as specified in ASTM C127. The absorption was subtracted from the moisture content of the aggregate to determine the amount of water clinging to the surface of the aggregate. Then, this amount of water was subtracted from the design water for the concrete mixture. This process helped to provide an accurate measure of how much water was required for each concrete batch to ensure each mixture was consistent.

Figure 3.3. Aggregate saturation tank

3.3.1.2 Aggregate gradations. The gradations of the lightweight clay and slate aggregates provided by each manufacturer are found in Table 3.4 and Table 3.5, respectively, along with the grading requirements for 3/8 in. to No. 8 coarse aggregate as specified in ASTM C330, Standard Specification for Lightweight Aggregates for Structural Concrete. This designation of 3/8 in. to No. 8 was chosen because it aligned with the coarse aggregate gradation used in the study by Shaw (2013) which studied the shear-friction properties of concrete with lightweight shale aggregate. In Table 3.4, it is shown that the clay aggregate supplied by Big River Industries conforms to ASTM C330 in all sieve sizes except for sieve No. 4, where the percent passing slightly exceeds the specification limit. Likewise, in Table 3.5, the slate aggregate provided by STALITE also falls just outside the ASTM C330 specification limits, this time slightly lower than required. Since the clay and slate aggregate gradations were only slightly out of specification, they were considered adequate for use in this study and the gradations were not modified.

Table 3.4. Lightweight Clay Aggregate Gradation

	Sieve Designation	Percent Passing	
		Gradation	Specification[1]
3/8 in. x No. 8 Gradation	1/2 in.	100	100
	3/8 in.	99.9	80-100
	No. 4	41.8	5-40
	No. 8	7.9	0-20
	No. 16	2.0	0-10
	No. 50	1.1	---
	No. 100	0.9	---
	No. 200	0.7	0-10

[1]ASTM C330 structural concrete aggregate gradation for 3/8 in. to No. 8 Coarse Aggregate Designation

Table 3.5. Lightweight Slate Aggregate Gradation

	Sieve Designation	Percent Passing	
		Gradation	Specification[1]
3/8 in. x No. 8 Gradation	1/2 in.	100	100
	3/8 in.	98.5	80-100
	No. 4	3.6	5-40
	No. 8	1.3	0-20
	No. 16	1.3	0-10
	No. 50	0.8	---
	No. 100	0.5	---
	No. 200	0.0	0-10

[1]ASTM C330 structural concrete aggregate gradation for 3/8 in. to No. 8 Coarse Aggregate Designation

3.3.2. Concrete Mixtures. Trial batching was performed to design the clay sand-lightweight and slate sand-lightweight concrete mixtures. They were developed based on mixture designs used by Shaw (2013) and suggested mixture proportions given by STALITE, the slate aggregate supplier. These mix designs were modified in successive trial batches to create a 28-day compressive strength of f'_c = 5000 psi (± 500 psi). A rotary drum mixer with a 6 ft^3 capacity (Figure 3.4) was used for both trial batching and final specimen construction. All concrete batches consisted of Type I/II concrete, lightweight coarse aggregate, normalweight fine aggregate (natural river sand), and water. No mixture additives such as high range water reducers were used in this testing program. The final concrete mixture proportions which were used to construct the specimens are shown in Table 3.6. Values for unit weight determined in accordance with ASTM C138 for the sand-lightweight concrete batches were 105 lb/ft^3 for the clay, and 117 lb/ft^3 for the slate (Table 3.7). Values for air content and slump of the fresh concrete are also listed in Table 3.7, with the corresponding testing equipment shown in Figure 3.5. The volumetric method was used for the determination of air content (ASTM C173), and slump was determined using a slump cone (ASTM C143). All concrete batching and specimen construction was performed in the Concrete Materials Laboratory in Butler-Carlton Hall at Missouri University of Science and Technology.

Figure 3.4. Rotary drum concrete mixer

Table 3.6. Concrete Mixture Proportions

Concrete Type	Mixture Design Quantities (lbs/yd^3)				
	Coarse Aggregate	Fine Aggregate	Water	Cement[1]	w/c
Clay Sand-Lightweight	692	1251	263	612	0.43
Slate Sand-Lightweight	975	1125	265	530	0.50

[1]Type I/II

Table 3.7. Plastic Concrete Properties

Concrete Type	Density (lb/ft^3)	Air (%)	Slump (in.)
Clay Sand-Lightweight	105	2.5	1.25
Slate Sand-Lightweight	117	1.5	2.00

Figure 3.5. Air content testing equipment (left) and slump testing equipment (right)

All casting was done according to ASTM C31 specifications. Material test cylinders as well as test specimens were removed from molds or formwork within 24 hours, then stored in a moist-cure room for 28 days at which point they were tested. The 200-kip Tinius Olsen load frame in the Load Frame Laboratory, also in Butler-Carlton Hall, was used for all cylinder testing and also the testing of the push-off specimens. Concrete cylinders (4 in. by 8 in.) were tested according to ASTM C1231 for compressive strength (Figure 3.6). Steel retaining rings and neoprene pads were used to confine the ends of the cylinders. Load was applied at a rate of 500 lbs/sec until failure. Splitting tensile tests were also performed on the concrete cylinders in accordance with ASTM C496, and modulus of elasticity was determined in accordance with ASTM C469. The test set-up for determining these two properties is shown in Figure 3.7 and Figure 3.8, respectively.

Figure 3.6. Compressive strength test set-up

Figure 3.7. Splitting tensile test specimen

Figure 3.8. Modulus of elasticity test set-up

Both the clay sand-lightweight and the slate sand-lightweight concretes were designed with a target compressive strength f'_c = 5,000 psi. Actual compressive strengths on test day ranged from 4,550 psi to 5,570 psi (Table 3.8). Since three compressive strength tests were performed for each batch of concrete, the standard deviation of the three values is also shown in parenthesis below each f'_c value in that particular column. Other hardened concrete properties shown in Table 3.8 include the splitting tensile strength f'_t and modulus of elasticity E of each batch of test specimens. All specimens were constructed in sets of four, so that for each reinforcement ratio within each aggregate type, all came from the same batch of concrete.

Table 3.8. Hardened Concrete Properties

Concrete Type	**Associated Reinforcement Ratio of Test Batch**	**Target f'_c (psi)**	**f'_c at Test Day (w/ std. deviation) (psi)**	**Splitting Tensile Strength (psi)**	**Modulus of Elasticity (ksi)**
Clay Sand-Lightweight	0.009	5000	4770 (32)	$340 = 4.9\sqrt{f'c}$	2500
	0.013		4640 (118)	$360 = 5.3\sqrt{f'c}$	2650
	0.017		4550 (129)	$410 = 6.1\sqrt{f'c}$	2600
	0.022		4790 (50)	$485 = 7.0\sqrt{f'c}$	2700
Slate Sand-Lightweight	0.009		5380 (367)	$595 = 8.1\sqrt{f'c}$	3300
	0.013		5570 (781)	$570 = 7.6\sqrt{f'c}$	3500
	0.017		4950 (127)	$670 = 9.5\sqrt{f'c}$	3050
	0.022		5000 (359)	$445 = 6.3\sqrt{f'c}$	3450

3.3.3. Reinforcing Steel Bars. No. 3 and No. 5 deformed steel reinforcing bars were used to construct the reinforcement cages for the specimens in this study. All bars were ASTM A615 Grade 60, supplied by Ambassador Steel Corporation. According to the mill certificates, the No. 3 bars had a yield strength f_y = 74,880 psi and an ultimate tensile strength f_u = 108,640 psi; while the No. 5 bars had f_y = 65,820 psi and f_u = 102,870 psi. Tension tests on samples of the bars were performed as a part of this study to verify their yield strength according to the procedure outlined in ASTM A370. Strain gages were applied directly to a sanded portion at the longitudinal center of the bar. A sample plot of the load versus strain gage reading is shown in Figure 3.9 for each of the bar sizes.

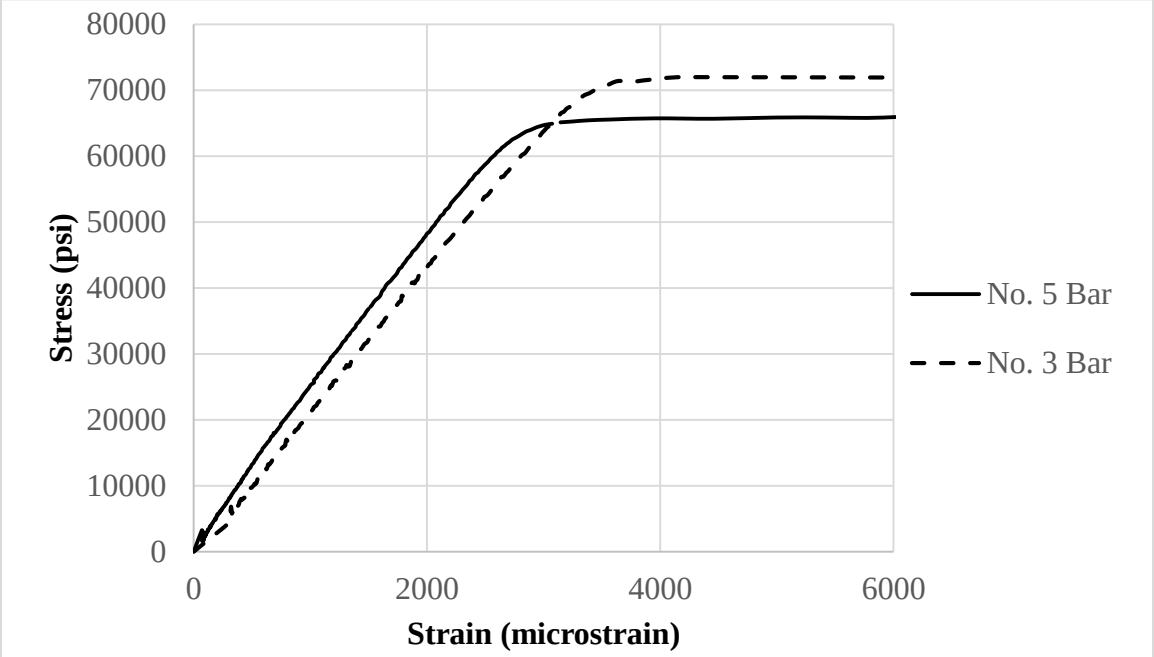

Figure 3.9. Typical stress vs. strain for reinforcing steel bar tensile coupon tests; Specimen 60-5-2 and Specimen 60-3-3 shown

An extensometer with an 8 in. gage length was used to verify the strain gage results up to the point of yielding of the specimen. Results of the tensile tests are summarized in Table 3.9. Note that an error with the computer occurred during the

testing of the first No. 3 bar, and values of the yield stress and modulus of elasticity were unable to be obtained for this specimen. The average yield stress for the No. 5 and No. 3 bars were 70,700 psi and 72,190 psi, respectively. These are both greater than the nominal grade of the steel (60 ksi). The average ultimate stress of the No. 5 and No. 3 bars were 102,390 psi and 101,055 psi, respectively. The average modulus of elasticity for the No. 5 and No. 3 bars were 28,110,000 psi and 30,253,000 psi, respectively.

Table 3.9. Reinforcing Steel Bar Properties

Specimen ID[1]	**Bar Size**	**Yield Stress (psi)**	**Ultimate Stress (psi)**	**Modulus of Elasticity (psi)**
60-5-1	No. 5	70,700	102,750	27,437,000
60-5-2	No. 5	70,470	102,555	28,021,000
60-5-3	No. 5	70,915	101,870	28,871,000
AVERAGE		70,695	102,390	28,110,000
60-3-1	No. 3	N/A	100,870	N/A
60-3-2	No. 3	72,200	101,110	32,040,000
60-3-3	No. 3	72,165	100,995	28,466,000
AVERAGE		72,185	101,055	30,253,000

[1]Specimen ID notation; first indicates reinforcement grade, second indicates bar size, and third indicates specimen number

3.4. SPECIMEN FABRICATION

All specimens in this study were fabricated in the High Bay Laboratory of Butler-Carlton Hall at Missouri University of Science and Technology. The 32 specimens included in the scope of this thesis were constructed in the winter and spring of 2015. Section 3.4.1 discusses the preparation of the reinforcing bar cages. Formwork assembly

is covered in Section 3.4.2. Concrete placement and shear interface preparation is described in Section 3.4.3. Lastly, Section 3.4.4 discusses the concrete curing process.

3.4.1. Reinforcing Steel Bar Cage Preparation. Each reinforcing cage was constructed of ASTM A615 Grade 60 steel, as described in Section 3.3.3. In order to achieve four different reinforcement ratios among the test specimens, four different reinforcing cage configurations were used (Figure 3.10). These were based on Shaw's design for a cage with $\rho = 0.013$ which is shown in Figure 3.11. The bars were bent in the High Bay Laboratory and consisted of No. 3 closed tied stirrups as well as L-shapes bent from No. 5 bars. The No. 3 stirrups which served as the shear reinforcement were distributed evenly across the shear plane. As shown in Figure 3.11, the shear plane measured 11 in. x 4.5 in. to equal a total shear plane area of 49.5 in^2. Either two, three, four, or five stirrups were used as shear reinforcement to create reinforcement ratios of 0.009, 0.013, 0.017, or 0.022, respectively. No. 3 bars were also used in the flanges to confine the L-shapes and to provide extra reinforcement of the flanges.

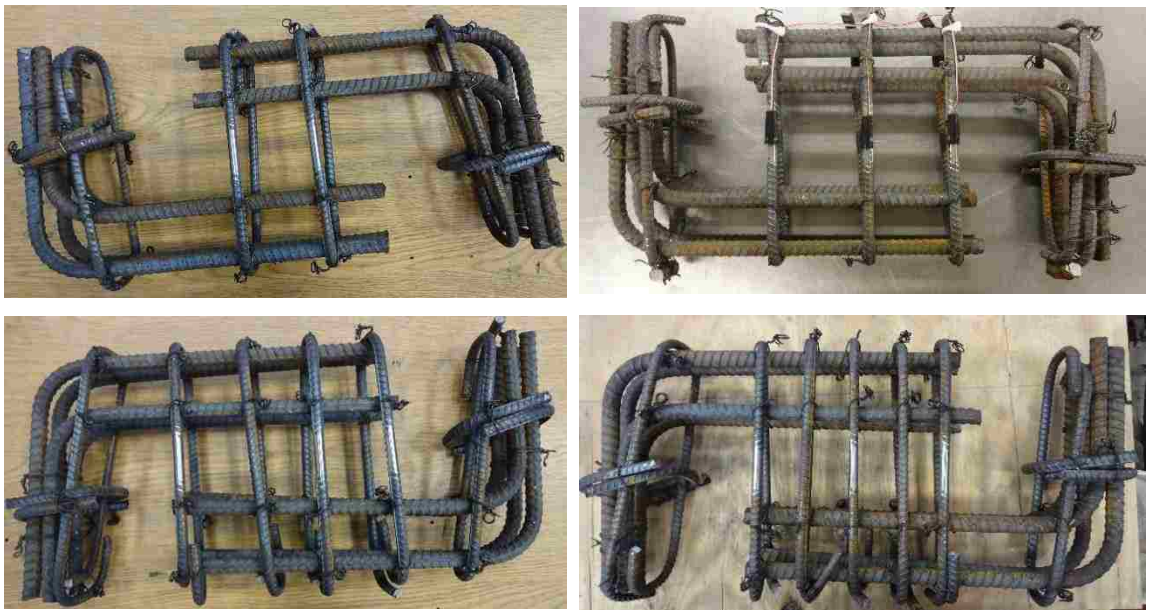

Figure 3.10. Reinforcement cages of each reinforcement ratio

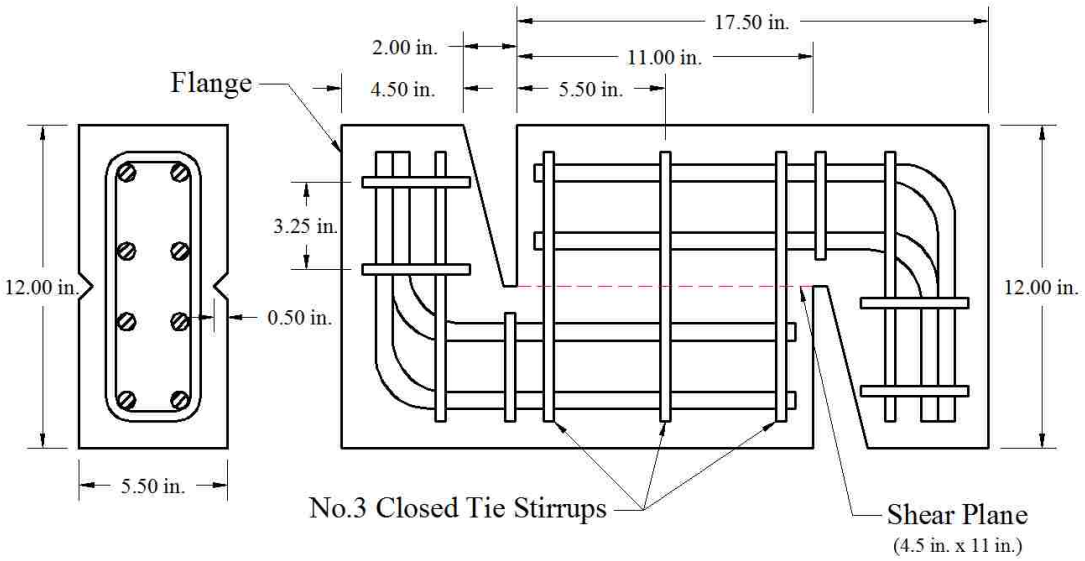

Figure 3.11. Reinforcing steel bar cage detail for ρ = 0.013, to the nearest ¼ in., by Krc (2015)

Each reinforcing cage had three strain gages applied to the No. 3 stirrups at the location where they cross the shear plane (at approximately the center of the stirrup in terms of its height). Thus, each of these locations on the cages needed to be prepared before strain gage application. This was done by using an electric belt sander to grind down the ribs of the steel bar and then polish the surface to a smooth, mirror-like condition. Sander belts of No. 80, No. 340, and No. 400 grit were used in succession to create the condition shown in Figure 3.12. Care was taken to ensure that the bars were sanded a minimal amount in order to retain as much of the cross-sectional area as possible. It is important to leave a majority of the bar's cross-section intact, so that the bar's behavior is not affected by a reduced cross-sectional area. After the bars were sanded, the polished surface was cleaned with an acid solution, then a neutralizing base solution. This cleaning process was done to ensure an adequate bond between the bar and the strain gage. Refer to Section 3.5.4.2 for further information on strain gage application and position.

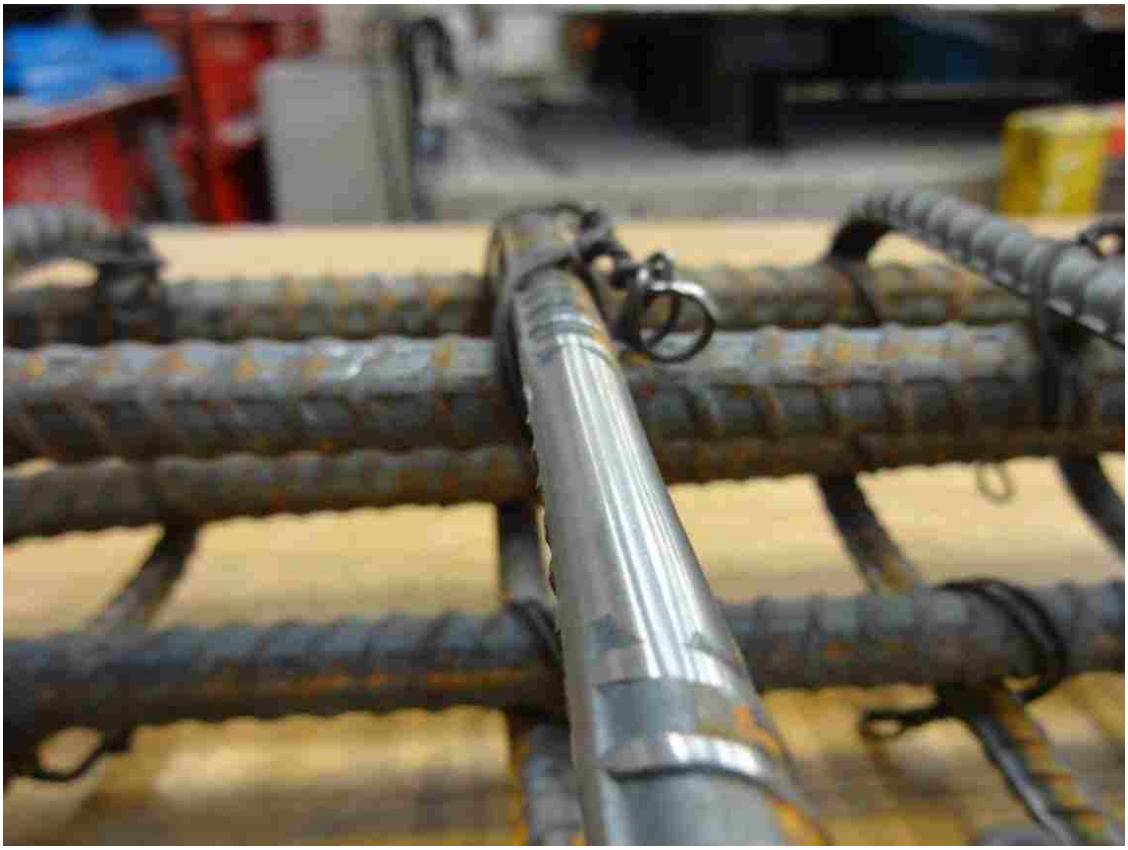

Figure 3.12. Reinforcing bar prepared for strain gage application

3.4.2. Formwork and Assembly. Specimens in this study were cast in sets of four using the formwork shown in Figure 3.13. The total outside dimensions of the finished specimens measured 12 in. x 24 in. x 5.5 in. Custom formwork was built from 2 in. by 6 in. lumber, 0.75 in. plywood, and 0.5 in. wood chamfers. The completed formwork was coated with water-sealer to enhance the durability of the formwork through multiple castings. The cavities included in the specimen design were created by using 0.25 in. thick welded steel triangle inserts. The lower steel insert was bolted through the bottom of the formwork, and the top steel insert was held in place by a steel rod which was anchored through holes in the sides of the wood formwork. It was important to secure these two pieces to the formwork to ensure they did not shift during placement and vibration of the concrete. The formwork was able to be partially disassembled for the first concrete placing, to allow the shear plane to be exposed for

surface preparation between castings. Nuts, washers, and bolts were the selected fasteners for the formwork so that it could be easily disassembled during the removal of the specimens.

In an effort to control the failure mode of the specimens, the cross-sectional area was reduced at the shear plane to create a weak point. This was achieved by stapling wood chamfers to the formwork at the intended shear plane. A concrete cover of 0.5 in. was designed for this portion of the specimen, and a cover of 0.75 was used for all other edges. Two cavities were designed in the specimen to allow both sides of the shear plane the freedom to slip past each other. This specimen design is identical to that used by Shaw (2013), with the exception of the modification in the number of stirrups crossing the shear plane.

Figure 3.13. Formwork partially assembled for first half of cold-joint specimen

3.4.3. Concrete Placement and Shear Interface Preparation. Prior to placement of the concrete, the forms were oiled to ensure easy removal of the specimens after initial curing. The forms were partially assembled as in Figure 3.14, with the reinforcement cages placed inside. Chairs were attached to the bottom of the reinforcement cage, and the top of the cage was also tied to bolts at the top of the

formwork with steel wire to help keep the cage centered during placement of the concrete. As previously stated, all specimens of this study had a cold-joint interface condition. To achieve this, the first half of the specimen (one 'L-shape') was allowed to cure for a minimum of 8 hours before the second half of the specimen was added. This is consistent with the procedure followed by Shaw (2013). To assist in consolidating the concrete within the formwork and cylinders, a shake-table was used to vibrate the concrete. This device is shown in the foreground of Figure 3.14.

Figure 3.14. Completed first lift of cold-joint specimens

Immediately after filling the first half of the formwork, the interface of each specimen was troweled smooth with a narrow paint scraper. A typical smooth interface

specimen is shown in Figure 3.15. About three hours later, the shear plane interfaces for the roughened specimens were prepared with a special instrument shown in Figure 3.16. The edge of this instrument was marked up to ¼ in. with a dark marker to act as a guide for the depth of roughness. The average amplitude of interface roughness was ¼ in. which was verified by a digital caliper. This measurement device as well as the groove patterning is shown in Figure 3.17. The amplitude of ¼ in. is specified in both ACI 318-14 and the PCI Design Handbook, 7th Edition (2014) for specimens with an 'intentionally roughened' interface. The grooves were carved about 1 in. apart from each other in a pattern perpendicular to the direction of slip when the specimens are loaded in compression.

Figure 3.15. Typical smooth interface specimen

Figure 3.16. Instrument used for roughening of concrete interface

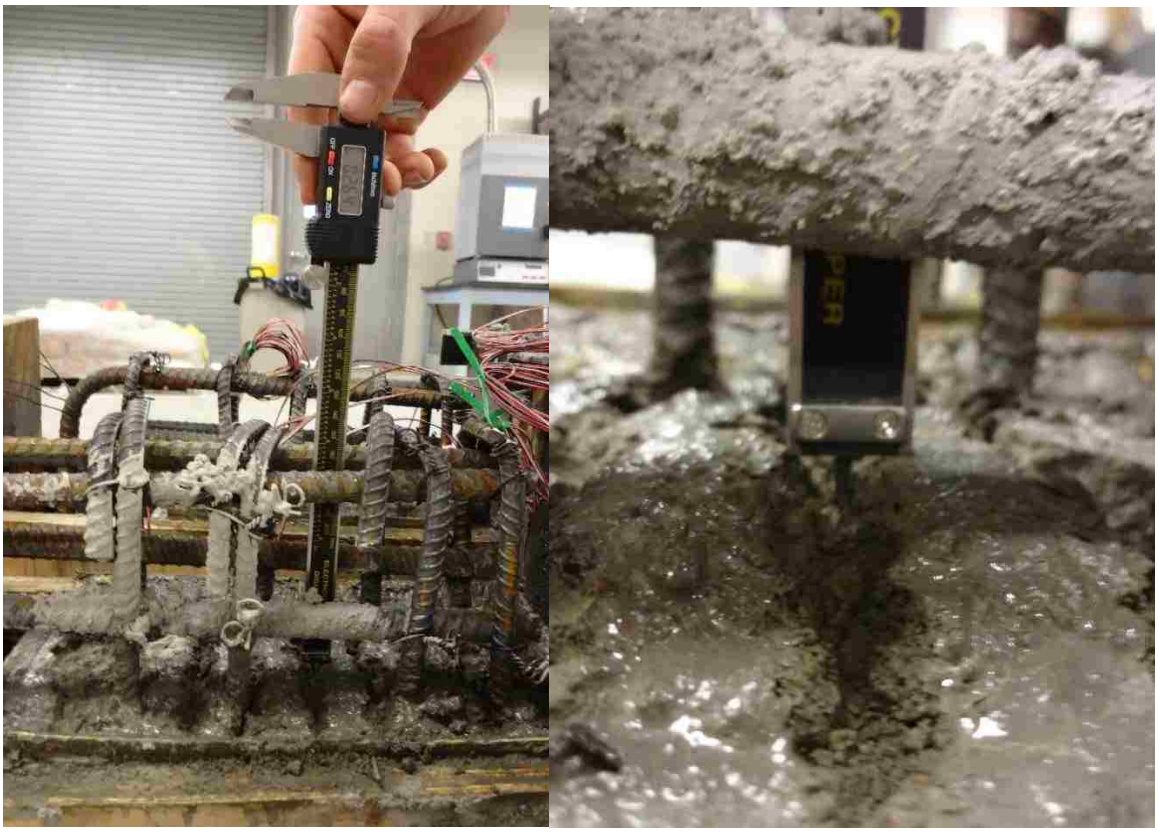

Figure 3.17. Groove pattern and measurement of roughness amplitude per digital caliper

3.4.4. Concrete Curing. All specimens and cylinders were cured on the floor of the laboratory under a sheet of plastic for 24 hours before the forms were removed. After demolding, the shear specimens and cylinders were labeled and stored in the Moist-Cure Room in the Concrete Laboratory of Butler-Carlton Hall at Missouri University of Science and Technology. This room maintains a constant environment of 70°F and 100% humidity which aids in the curing process of the concrete. The specimens and cylinders remained in the moist-cure room for the full 28-day period prior to testing. Concrete placement and test dates are summarized in Table 3.10.

Table 3.10. Specimen Casting and Test Dates

Specimen Series	Concrete Placement Date	Test Date	Age at Test Date (days)
S-CL-CJ-9	4/1/15	4/29/15	28
S-CL-CJ-13	4/8/15	5/6/15	28
S-CL-CJ-17	4/15/15	5/13/15	28
S-CL-CJ-22	4/24/15	5/22/15	28
S-SL-CJ-9	3/2/15	3/30/15	28
S-SL-CJ-13	1/30/15	2/27/15	28
S-SL-CJ-17	3/9/15	4/6/15	28
S-SL-CJ-22	2/11/15	3/11/15	28

3.5. TEST SETUP

The test set-up used by Shaw (2013) was closely followed in order to mitigate variability among the test results from this study for clay and slate sand-lightweight concretes and Shaw's results for shale sand-lightweight concrete. Support conditions are described in Section 3.5.1; loading protocol is included in Section 3.5.2; flange confinement is described in Section 3.5.3; and data acquisition and instrumentation are listed in Section 3.5.4.

3.5.1. Support Conditions. The use of a pin-roller support condition in trial specimens tested by Shaw (2013) caused several issues during testing of specimens with a roughened cold-joint interface. First, the higher shear capacity of these specimens caused the flanges to fail before shear failure occurred. It was noted that after flexural cracking occurred, the specimens translated laterally, which caused uneven loading at the points of bearing on the top and bottom of the specimen. Also, as the specimen rotated, the loading became eccentric to the shear plane. Since there was minimal lateral translation prior to the initiation of flexural cracking, the roller system was deemed unnecessary for the experiment. Thus, the lateral roller system was removed for the testing of Shaw's specimens, even though a similar roller set-up was used for previous studies by Hofbeck et al. (1969) and others.

In this study, the lateral roller system was not utilized. The bottom surface of each specimen was in direct bearing on the bottom platen of the test machine while the top surface of the specimen was considered to be pin supported due to the rotating hemispherical head of the testing machine. The base and top surfaces of the specimen were covered with a 0.25 in. thick sheet of neoprene to aid in the distribution of load.

3.5.2. Loading Protocol. A Tinius Olsen Load Frame in the Load Frame Laboratory of Missouri University of Science and Technology with a 200-kip capacity was used to test the shear specimens in this study. A preload of approximately 200 lbs was applied to each specimen; then, load was applied so that displacement of the upper head relative to the load frame table occurred at a constant rate of 0.015 in. per minute. Testing was stopped when either a slip of 0.3 in. was reached, or the applied load had fallen to 60% of the peak applied load, whichever occurred first.

3.5.3. Flange Prestressing/Confinement Systems. Prestressing/confinement systems developed by Shaw (2013) were used in this study and applied to all specimens. Their purpose was to both confine the flanges and apply a compressive stress on them in order to prevent flexural failure of the flanges before the specimen had failed in shear along the shear plane. Two sets of prestressing/confinement systems were used: primary and secondary. As shown in Figure 3.18, the primary prestressing system consisted of the 1 in. thick plates parallel to the shear plane (to the right and left in the photo). These are applied to both the top and bottom flanges. The steel plates were connected by

horizontal all-thread rods (at the front and back of the specimen) on which the nut was tightened to 50 lb-ft by a torque wrench. Applying pressure to the flange provided active confinement which counteracted the tension forces that developed in the flange and would otherwise cause it to fail in flexure. Neoprene pads approximately 0.75 in. thick were positioned between the specimen and the primary prestressing plates to evenly distribute the pressure.

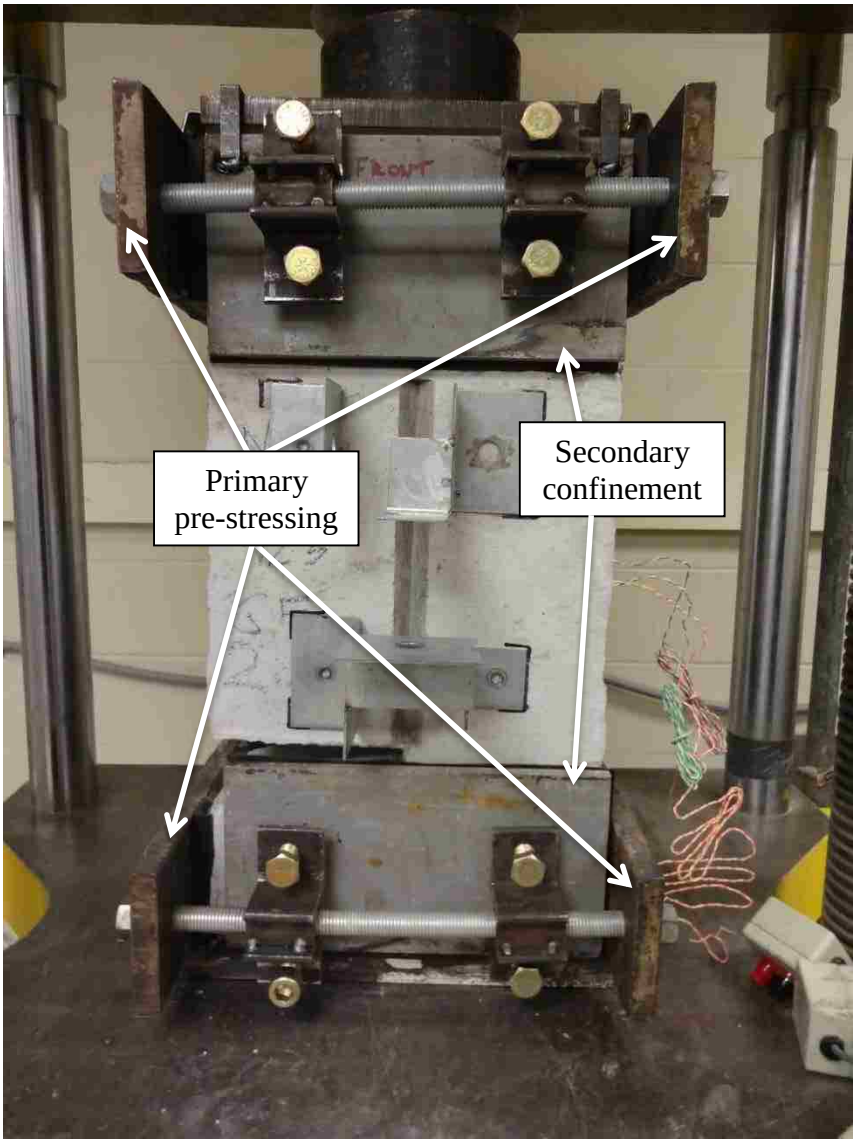

Figure 3.18. Primary pre-stressing and secondary flange confinement

The secondary confinement system consisted of a set of plates on the front and back of the specimen (Figure 3.18) which were perpendicular to the primary prestressing. Instead of being tightened to a specified torque, these plates (at the top and bottom of the specimen) confined the flanges when the bolts at the front face were fastened to snug-tight position. This in turn tightened the back plates as well, since an angle shape welded to the primary prestressing plate holds the back plate against the specimen. Thin neoprene pads were aligned beneath the secondary confinement plates before mounting them. This secondary system did not provide active confinement; rather, it prevented spalling of the concrete cover on the flanges.

3.5.4. Data Acquisition and Instrumentation. Several types of data were recorded in this experimental program. The test set-up and data acquisition system are shown in Figure 3.19.

Figure 3.19. Test setup and data acquisition system

For each specimen, three uniaxial strain gages adhered to separate reinforcing bars were used to record the strain in the interface steel. Six direct current-linear variable differential transducers (DC-LVDTs) were applied to the front and rear faces of the specimen to measure displacement. These nine load channels were recorded at a rate of 1 sample per second by the gray box data acquisition device (to the far right of Figure 3.19). Load and global displacement were also reported by the Tinius Olsen load frame (shown to the far left of Figure 3.19). The application and purpose of the DC-LVDTs and the strain gages are further described in Section 3.5.4.1 and 3.5.4.2, respectively.

3.5.4.1 Direct current-LVDTs. Six direct current-linear variable differential transducers (DC-LVDTs) were attached to each specimen, three on the front face and the other three mirrored on the back face (Figure 3.20).

Figure 3.20. LVDT configuration to measure slip and dilation

The horizontal DC-LVDTs (four total) were used to measure dilation (crack separation) of the shear interface. The other two DC-LVDTs were placed vertically to measure the slip along the interface. The LVDTs have a precision of 1 μ-in. Since these sensitive devices only have a capacity for measuring displacement +/- 0.5 in., it was important to zero their readings before beginning each test. The brackets used to hold the DC-LVDTs in place were made from aluminum angles and were applied to the face of the specimen using slow-setting hot glue. Care was taken to make sure they were square with the shear plane. A bubble level was used to mark a horizontal line on the specimen before gluing the brackets. After testing was complete, the brackets were easily pulled off the specimens for reuse.

3.5.4.2 Strain gages. Vishay Micro-Measurements CEA-06-125UN-120 uniaxial electronic resistance strain gages were used to measure the strain in the steel stirrups crossing the shear plane (three gages per specimen). They were also used to measure strain for the tensile tests of the reinforcing bars as described in Section 3.3.3. The strain gages were installed on the outside face of bar at mid-height of the stirrup to mitigate bending effects. Once the reinforcing cages had been sanded as discussed in Section 3.4.1, care was taken to clean the polished surface per the instructions provided by Vishay. The stain gages were adhered to the surface of the bar at the intended location of the shear plane of the specimen. Wires were soldered to the tabs of the strain gage, and a protective black coating (Barrier E) was applied over the strain gages (Figure 3.21). This coating provided protection against moisture infiltration and impact during concrete placement and interface preparation. Gages were tested after application and replaced if they were not functioning. Several were damaged during placement of the concrete, but at least two were functioning per specimen during testing.

Power input for several of the tests had been mistakenly set to alternating current (AC) instead of direct current (DC) which caused large amounts of noise in the strain data for those specimens. Yet, the overall trend in the strain data was visible, and the noise was able to be removed by writing a function in Microsoft Excel. It should be noted that this revised (corrected) data was used in place of the original data for all affected specimens when test results figures were created for Section 3.6.

Figure 3.21. Strain gages and protective coating applied to reinforcement

3.6. TEST RESULTS

The test results for this experimental program are presented in this section, with important values shown in Table 3.11. The Specimen ID follows the naming convention which is shown in Section 3.2. The compressive strength f'_c at test day has been rounded to the nearest 10 psi. Other important data include: the peak applied load (ultimate shear force) V_u, slip at peak load, dilation at peak load, and residual load (residual shear force) V_{ur}. In Table 3.11, v_u and v_{ur} are the ultimate shear stress and residual shear stress, respectively. They were calculated by dividing the respective shear force by the area of the shear plane (49.5 in^2). A typical specimen failed by shear along the intended shear plane is shown in Figure 3.22.

Figure 3.22. Typical specimen failed in shear along the intended shear plane

Residual load represents a transition point where the effects of dowel action contribute significantly to the shear resistance (Shaw 2013). Shaw chose to define residual load as the value of load at a slip of 0.15 in. Other researchers have arbitrarily chosen to record residual load at other values of slip. For example, Kahn and Mitchell (2002) chose a slip of 0.2 in. The residual load represents the constant value of load which is achieved during testing while slip continues to increase. In the load vs. slip curves of Figures 3.30, 3.35, 3.41, 3.46, 3.51, 3.56, 3.62, and 3.70 it is shown that the residual shear force for most specimens is fairly constant for values of slip from 0.1 in. to 0.2 in. Thus, the residual shear force could be recorded anywhere in this range. For the current study, a slip of 0.15 in. was chosen to be consistent with Shaw (2013).

Table 3.11. Summary of Testing Results

Specimen ID	f'_c at test day (psi)	V_u (lbs)	v_u[1] (psi)	$v_{u,\,avg}$ (psi)	Slip at V_u (in.)	Dilation at V_u (in.)	V_{ur}[2] (lbs)	v_{ur}[1] (psi)	$v_{ur,\,avg}$ (psi)	$\left(\frac{v_u}{v_{ur}}\right)_{avg}$ (psi)
S-CL-CJ-R-9-1	4770	37060	749	808	0.012	0.007	ND	ND	ND	ND
S-CL-CJ-R-9-2		42910	867		0.008	0.005	ND	ND		
S-CL-CJ-S-9-1		31920	645	706	0.012	0.005	23610	477	519	1.36
S-CL-CJ-S-9-2		37960	767		0.009	0.005	27730	560		
S-CL-CJ-R-13-1	4640	50790	1026	987	0.007	0.006	31310	633	651	1.51
S-CL-CJ-R-13-2		46890	947		0.015	0.005	33180	670		
S-CL-CJ-S-13-1		41010	828	823	0.015	0.006	31030	627	600	1.37
S-CL-CJ-S-13-2		40470	818		0.018	0.007	28400	574		
S-CL-CJ-R-17-1	4550	51240	1035	1090	0.004	0.004	37420	756	751	1.45
S-CL-CJ-R-17-2		56660	1145		0.009	0.005	36920	746		
S-CL-CJ-S-17-1		43140	872	930	0.012	0.005	ND	ND	667	1.39
S-CL-CJ-S-17-2		48930	988		0.013	0.006	33040	667		
S-CL-CJ-R-22-1	4790	56720	1146	1111	0.008	0.003	ND	ND	670	1.66
S-CL-CJ-R-22-2		53230	1075		0.017	0.006	33250	672		
S-CL-CJ-S-22-1		52400	1059	1061	0.01	0.004	40300	814	815	1.30
S-CL-CJ-S-22-2		52590	1062		0.005	0.003	ND	ND		
S-SL-CJ-R-9-1	5380	49340	997	1008	0.009	0.007	30560	617	617	1.63
S-SL-CJ-R-9-2		50480	1020		0.007	0.006	ND	ND		
S-SL-CJ-S-9-1		26950	544	601	0.021	0.007	23040	465	529	1.14
S-SL-CJ-S-9-2		32500	657		0.012	0.006	29300	592		
S-SL-CJ-R-13-1	5570	63170	1276	1238	0.013	0.008	ND	ND	735	1.69
S-SL-CJ-R-13-2		59370	1199		0.013	0.009	36360	735		
S-SL-CJ-S-13-1		39490	798	892	0.017	0.007	30510	616	700	1.27
S-SL-CJ-S-13-2		48770	985		0.016	0.008	38770	783		
S-SL-CJ-R-17-1	4950	62380	1260	1288	0.012	0.008	ND	ND	ND	ND
S-SL-CJ-R-17-2		65150	1316		0.009	0.007	ND	ND		
S-SL-CJ-S-17-1		47640	962	957	0.018	0.007	ND	ND	694	1.38
S-SL-CJ-S-17-2		47120	952		0.019	0.007	34330	694		
S-SL-CJ-R-22-1	5000	64460	1302	1233	0.011	0.006	39640	801	801	1.54
S-SL-CJ-R-22-2		57590	1163		0.006	0.007	ND	ND		
S-SL-CJ-S-22-1		49810	1006	1074	0.018	0.006	32600	659	694	1.55
S-SL-CJ-S-22-2		56530	1142		0.016	0.006	36130	730		

[1]Shear stresses v_u and v_{ur} are defined as the applied shear load divided by the area of the shear plane, 49.5 in^2.

[2]Residual load, V_{ur}, is defined as the load at 0.15 in. of slip. Some values for V_{ur} and v_{ur} are denoted as ND (no data) because the slip did not reach a value of 0.15 in. before the test was concluded.

Each series of data is plotted in figures which show the following relationships: applied shear force vs. slip, applied shear force vs. interface dilation, applied shear force vs. interface steel strain, slip vs. interface dilation, and slip vs. interface steel strain. Reported slip is the average of values from the front and back faces of the specimen. Interface dilation has been averaged among four locations across the specimen's shear plane: the top and bottom of the front face as well as the top and bottom of the back face. For several specimens, the adhesive failed on the brackets which held the LVDTs (Figure 3.23). In these cases, the slip or dilation readings from those particular LVDTs were excluded from the reported averages.

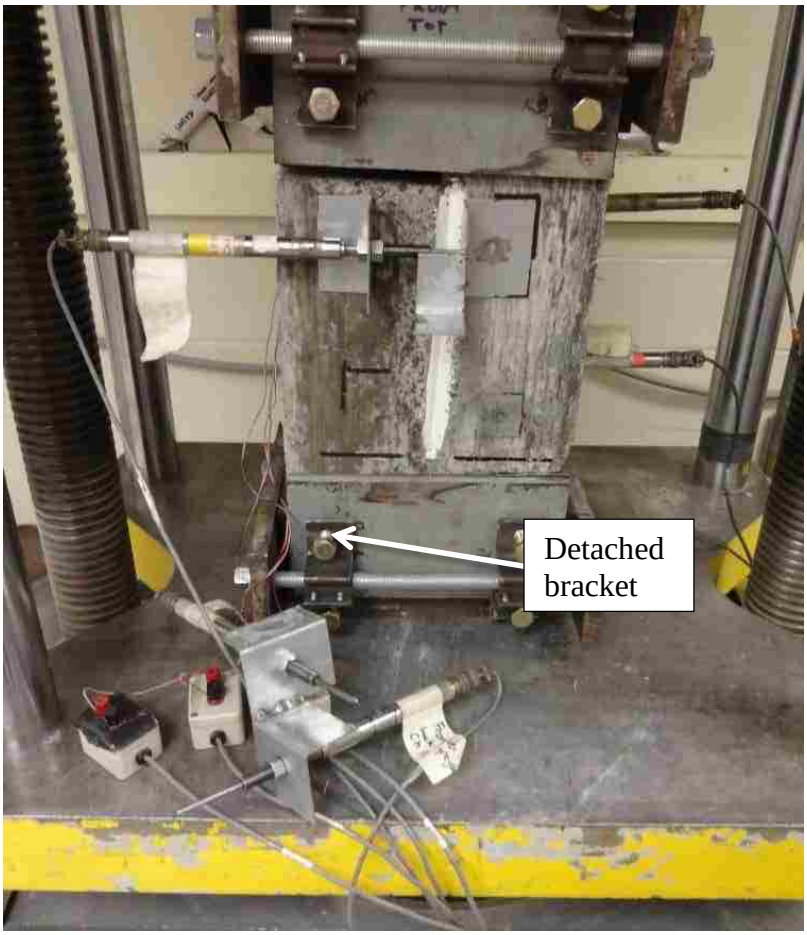

Figure 3.23. Failed adhesion of LVDT bracket

Interface steel strain data from one functioning gage per specimen was plotted to provide a representation of the strain behavior. Strain measurements can be highly variable and highly localized, even if the gages are working properly, and cracks at discrete locations cause localized fluctuations in strain. Therefore, even when all three strain gages on a specimen were functioning properly, only one gage per specimen was shown in the figures in Section 3.6. Several gages became damaged or detached from the steel bars during testing as shown in Figure 3.24; therefore, the last part of some sets of strain data was removed for clarity. Analysis and discussion of the data contained in this section as well as comparison to previous studies is presented in Chapter 4.

Figure 3.24. Typical damage to strain gage at conclusion of testing

3.6.1. Splitting Failure. As shown in the 'Failure Mode' column of Figure 3.11, six specimens of this testing program experienced loss of bond of the steel reinforcing bars to the surrounding concrete which led to eventual failure due to splitting of the

concrete. These specimens either underwent splitting failure before the specimens experienced a failure along the shear plane, or a shear crack never appeared. Thus, the principal failure mode for specimens S-CL-CJ-R-17-1, S-CL-CJ-R-17-2, S-CL-CJ-R-22-1, S-CL-CJ-R-22-2, S-CL-CJ-S-22-1, and S-CL-CJ-S-22-2 was splitting failure.

The behavior of these six sand-lightweight clay specimens can be described in terms of adhesion, bearing, and friction forces along the No. 5 steel reinforcing bars (L-shaped bars in Figure 3.11). As shown in Figure 3.25, adhesion of the concrete to the steel bar was lost when the bar slipped due to the tension forces on it. Yet, this slip was resisted by friction along the barrel and ribs of the reinforcing bar as well as bearing forces on the face of each rib on the bar. Hoop tensile stresses formed in the surrounding concrete as a result of the wedging action of the steel reinforcing bar ribs on the concrete. If the concrete cover is not thick enough, or if there is no or minimal transverse reinforcement (stirrups) to confine the reinforcing bars which are under tension, then a crack may form as a result of the hoop stresses in the concrete (Figure 3.26, left). These splitting cracks may extend between the reinforcing bars if they are closely spaced, and may also extend through the concrete cover if it is insufficiently thick (Figure 3.26, right). If anchorage to the concrete is adequate, the stress in the reinforcement may become high enough to yield and even strain harden the bar (ACI 408R-03).

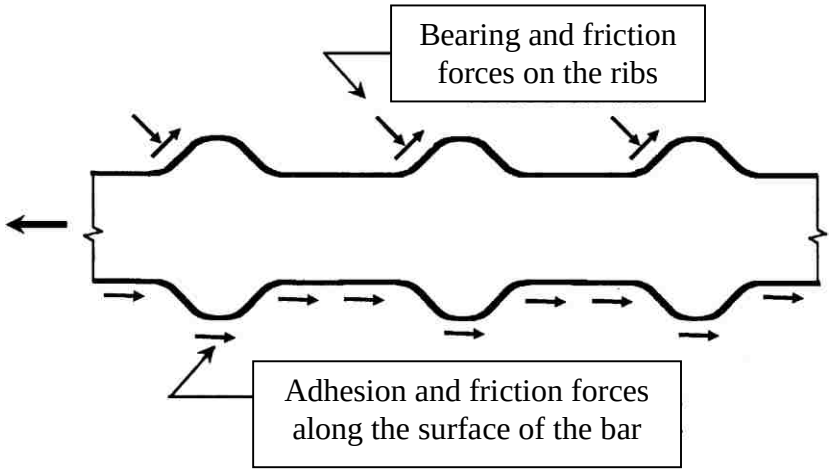

Figure 3.25. Bond-force transfer mechanisms (ACI 408R-03)

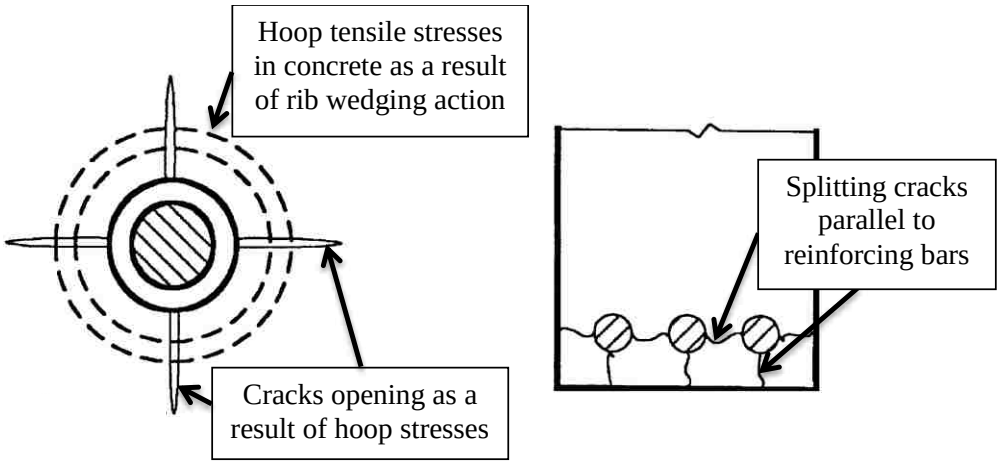

Figure 3.26. Tensile stress field/cracks in concrete surrounding a reinforcing bar (left) and splitting cracks in end view of concrete member (right) (ACI 408R-03)

To investigate the failure mode of the six specimens in question, the slip, dilation, and interface steel strain were plotted versus time, with the peak applied shear force plotted as a straight vertical line (Figure 3.27). An example of a specimen with a shear failure along the intended shear plane is plotted on the left side of Figure 3.27, and an example of a splitting failure is shown in the right side. As shown in Figure 3.27 (left), the sharp increase in both slip and dilation is associated with the peak applied shear force. This indicates that this specimen failed in shear along the intended shear plane. On the contrary, Figure 3.27 (right), shows the sharp upward spike in both slip and dilation occurring well after the onset of the peak applied shear force. This suggests that the failure mode was something other than failure of the shear plane.

Observations of cracking patterns and the dilation of such cracks suggest that concrete splitting failure was indeed the mode of failure of these six specimens. As shown in Figure 3.28 (left), large cracks propagated on the side faces of these specimens which were oriented parallel to the No. 5 bars of the steel reinforcing cage (vertical crack). Figure 3.28 (right) shows more splitting cracks on the top face of the specimen and also demonstrates that several specimens exhibited flexural cracks on the front or back face near the base of the flange. However, flexure of the flange was not the failure mode of these specimens. Instead, the flexural cracks indicate that the tensile strength of

the concrete was exceeded and the tension forces were then carried entirely by the steel reinforcing bars (the No. 5 L-shaped bars). If the failure mode had been flexure of the flange, the specimens would have exhibited crushing of the concrete in the compression region of the flange (adjacent to the cavity), and/or the No. 5 flexural reinforcement bars could have possibly fractured. Neither of these behaviors were observed.

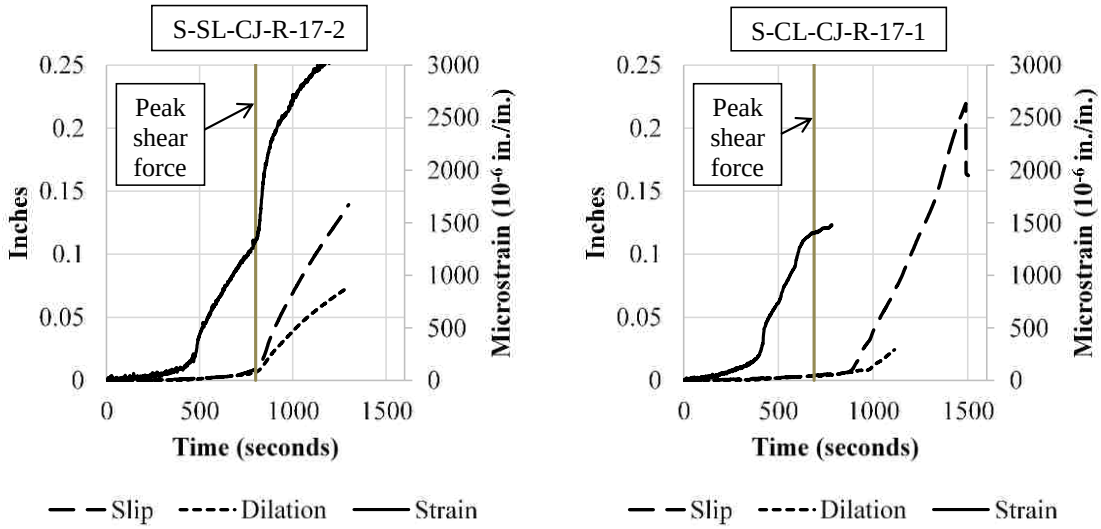

Figure 3.27. Real time plots of slip, dilation, and strain for a specimen which failed in shear along the intended shear plane (left); and a specimen with a splitting failure (right)

It is important to note that all the specimens in this study were of comparable compressive strength (about 5000 psi). If these failures were due to flexure, similar specimens made from slate aggregate would most likely have exhibited the same behavior since flexural strength is a function of compressive strength of the concrete. Also, note that there are a few horizontal cracks on this specimen which look as though they may be flexural cracks; yet, when Figure 3.28 (left) is compared with Figure 3.29, it becomes apparent that these cracks line up with the stirrups of the steel reinforcement cage. Therefore, the horizontal cracks on the side face of this specimen are most likely splitting cracks which follow the horizontal reinforcement bars, rather than flexural

cracks. Also worth noting is that the peak applied shear force of the clay specimens was not significantly higher than similar slate specimens in this study. Therefore, it is not likely that the clay specimens would fail in flexure under similar applied loads as underwent by the slate specimens. As a comparison, Kahn and Mitchell (2002) used a similar size test specimen for high strength concrete, with much higher applied forces, without failing the flanges. The more reasonable explanation is that the low tensile strength of this concrete was not adequate to restrain the bars as they were being stressed, and concrete splitting occurred, which destroyed the cover and therefore did not allow the bars to bond to the concrete to carry the required forces. Figure 3.29 also reinforces the splitting failure hypothesis because once all of the loose concrete is removed from the tested specimen, it is confirmed that the cracking extended to the surface of the flexural reinforcement, which is an indication of concrete splitting failure.

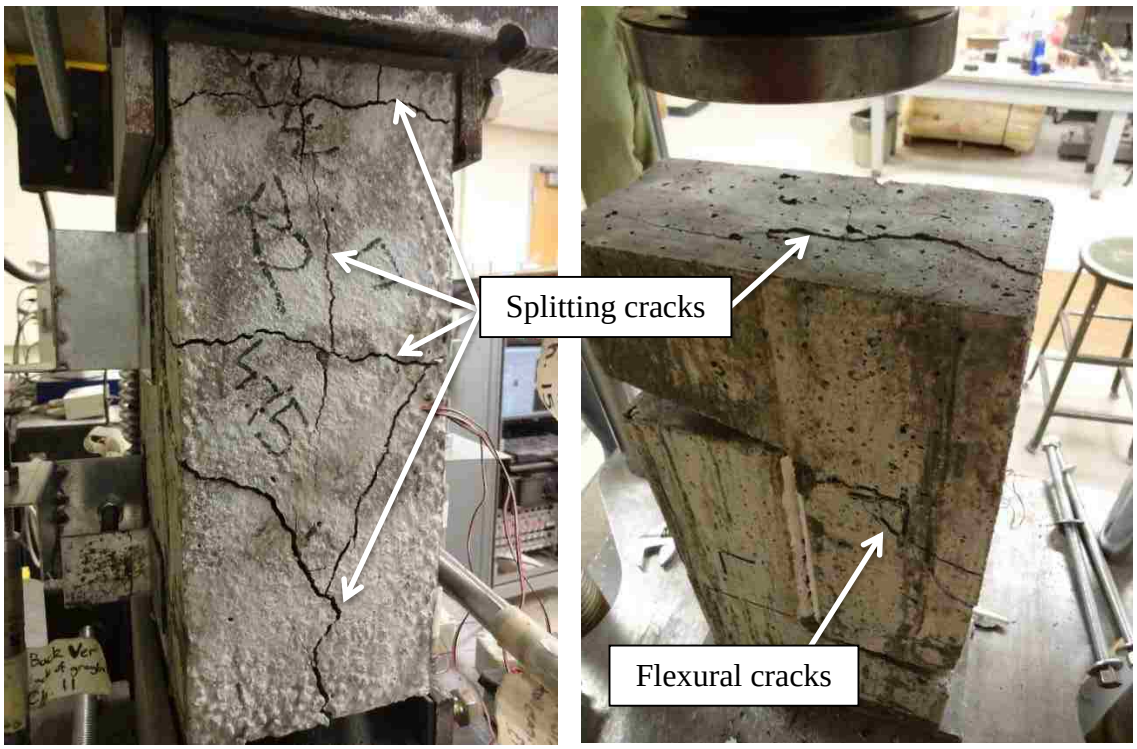

Figure 3.28. Typical cracking due to splitting failure: side face (left) and top/back face (right); specimen S-CL-CJ-R-17-2 shown

Figure 3.29. Specimen S-CL-CJ-R-17-2 with loose concrete removed, confirming that cracks extend to surface of longitudinal reinforcement bar (splitting failure)

In this study, out of the six specimens which had a splitting failure, two of them had interface steel strain readings which exceeded the yield strain (S-CL-CJ-R-17-2 and S-CL-CJ-R-22-2). This suggests that after splitting failure occurred, the shear interface failed as the testing machine continued its displacement. In the other four specimens with a splitting failure, the interface steel strain reading never reached the yield strain value. This suggests that either there was no failure of the interface shear plane, or the strain gage quit working or was damaged before it reached the yield strain value. Yet, the instrumentation readings implied increasing slip and dilation. After examination of the failed specimen, it was discovered that the slip/dilation readings were not measuring the

response of the shear interface, but rather a ‘panel’ of concrete cover on the specimen’s front face, between the flanges and to the left or right of the shear plane delaminating (not shear failure of the shear interface). It appeared to be similar to failure of the shear plane, but when that ‘panel’ was removed after testing, no shear plane crack was visible underneath. So, the slip and dilation readings are misleading in that it seems a shear plane crack propagated through the whole thickness of the specimen, when it did not.

Potential contributors to the low bond strength (and eventual splitting failure of these specimens) include: the possible presence of small internal shrinkage cracks, small concrete cover, close reinforcing bar spacing, inadequate transverse reinforcement (stirrups), the use of a weak coarse aggregate, inadequate consolidation, etc. However, the most critical contributors for this type of failure are the tensile strength and fracture energy of the sand-lightweight clay-aggregate concrete. Fracture energy is defined by ACI 408R-03 as the capacity of concrete to dissipate energy as a crack opens.

For this study, the splitting tensile strength of the clay and slate specimens on test day averaged 399 psi and 570 psi, respectively. These values support the assumption that the splitting failures of the six clay specimens were due to the lower tensile strength of the clay sand-lightweight concrete as compared to similar slate specimens. Interestingly, the shale sand-lightweight specimens with a nominal compressive strength of 5,000 psi (4,600 psi actual on test day) tested by Shaw (2013) had a reported splitting tensile strength of 320 psi, which is actually a lower value than the clay. The Shaw specimens had the same design, but did not exhibit any signs of splitting failure. Yet, it is important to note that the shale sand-lightweight specimens tested by Shaw (2013) had a reinforcement ratio of $\rho = 0.013$, whereas the clay sand-lightweight specimens from this study, which failed due to splitting, had higher reinforcement ratios ($\rho = 0.017$ and $\rho = 0.022$).

Several other testing programs have studied the bond strength of lightweight concrete versus normalweight concrete of similar compressive strength. A few studies indicated that the bond strengths were similar for both types of concrete. Yet, Baldwin (1965) concluded that the use of lightweight aggregate concrete can reduce bond strength to only 65% of that of normalweight concrete (through the use of pullout tests). Another study involving pullout tests by Robins and Standish (1982) had similar findings, but

bond strength was only 10 to 15% higher for normalweight concrete versus lightweight concrete. These two studies support the hypothesis that the six 'splitting failure' specimens from this testing program failed due to loss of bond of the reinforcing bars to the surrounding concrete, because of the low tensile strength of the clay sand-lightweight concrete.

3.6.2. Sand-lightweight Clay Specimens. This section presents information regarding the sand-lightweight clay specimens tested in this program. As discussed previously in Sections 3.6.1, the sand-lightweight clay specimens with $\rho = 0.017$ and a roughened interface (two specimens), as well as all four of the sand-lightweight clay specimens with $\rho = 0.022$ failed due to splitting of the concrete.

3.6.2.1 Specimens with reinforcement ratio of 0.009. Testing of the sand-lightweight clay specimens with a reinforcement ratio of 0.009 occurred on 04/29/15. The results are summarized in Figure 3.30 through Figure 3.34. All specimens failed along the shear plane as expected.

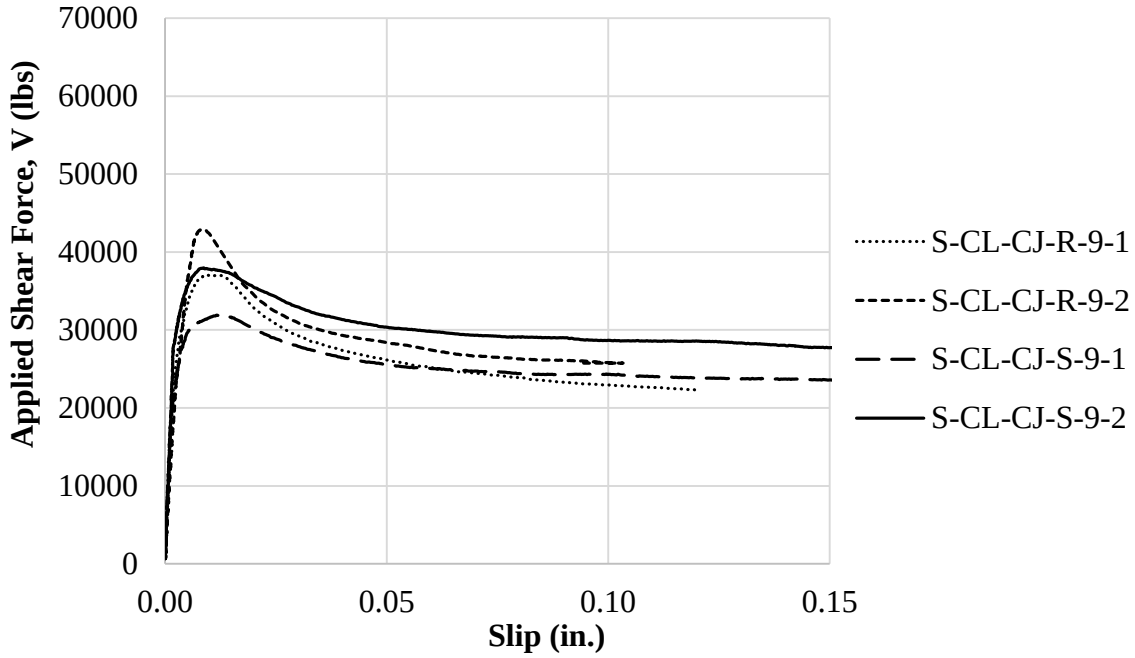

Figure 3.30. Applied shear force vs. slip relations for sand-lightweight clay specimens; with $\rho = 0.009$

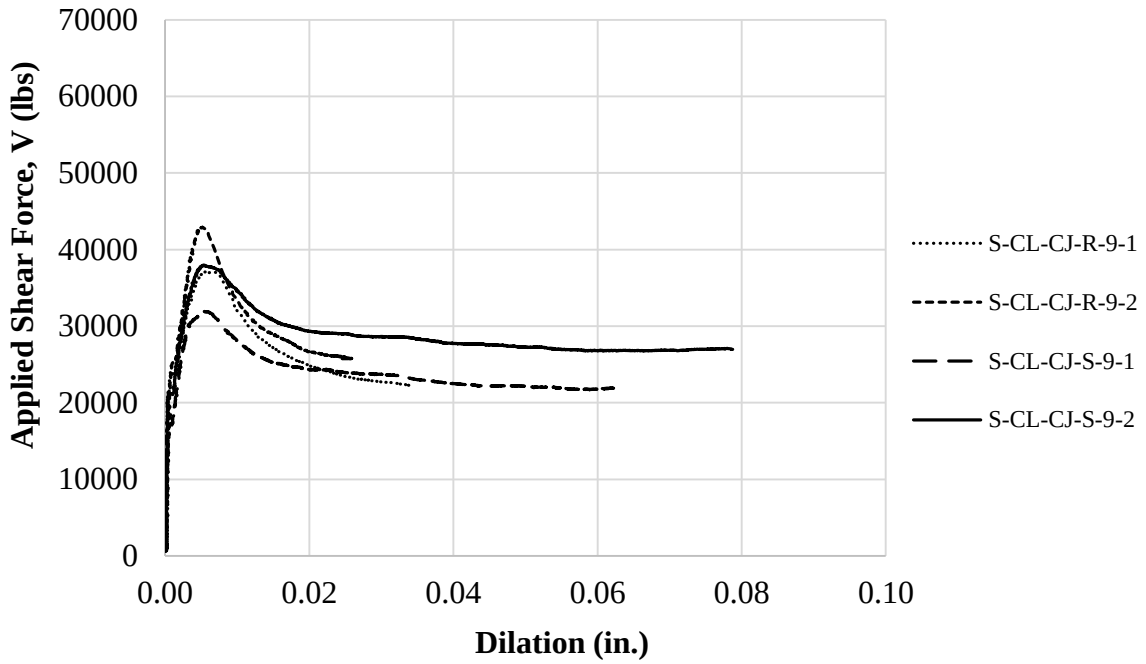

Figure 3.31. Applied shear force vs. interface dilation relations for sand-lightweight clay specimens; ρ = 0.009

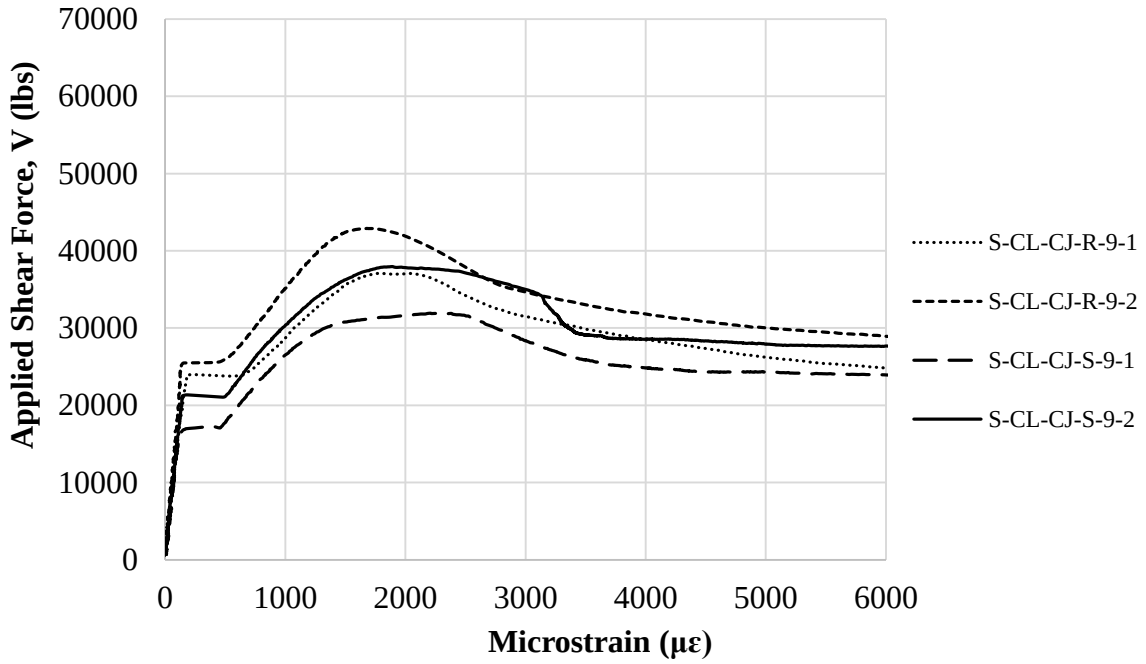

Figure 3.32. Applied shear force vs. interface steel strain for sand-lightweight clay specimens; ρ = 0.009

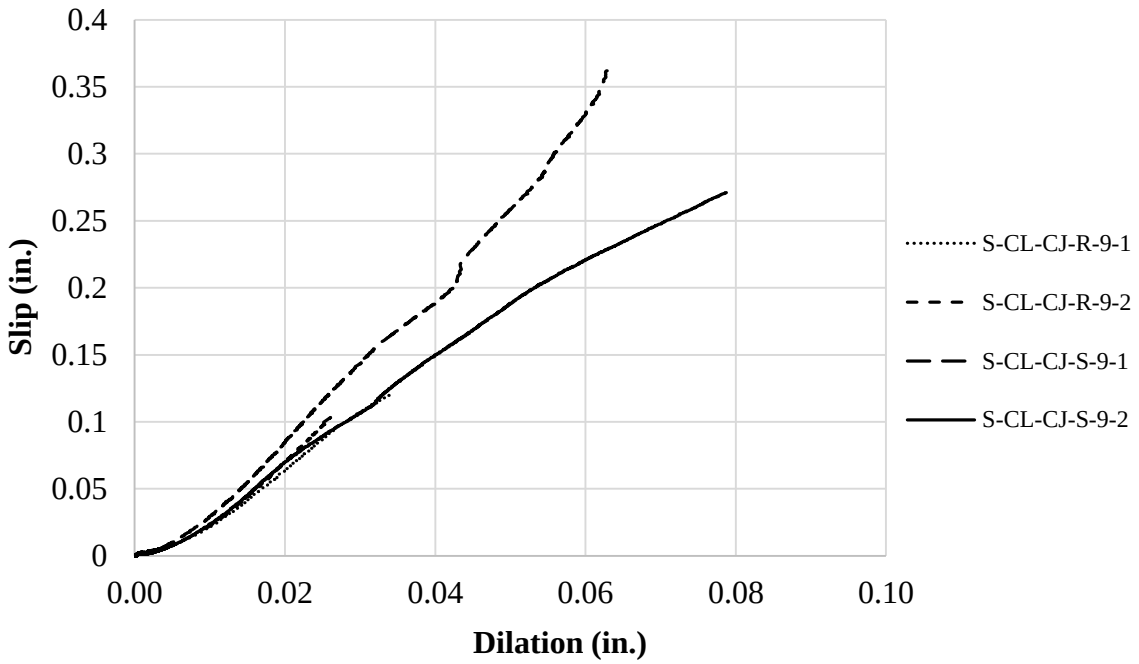

Figure 3.33. Slip vs. dilation for sand-lightweight clay specimens; ρ = 0.009

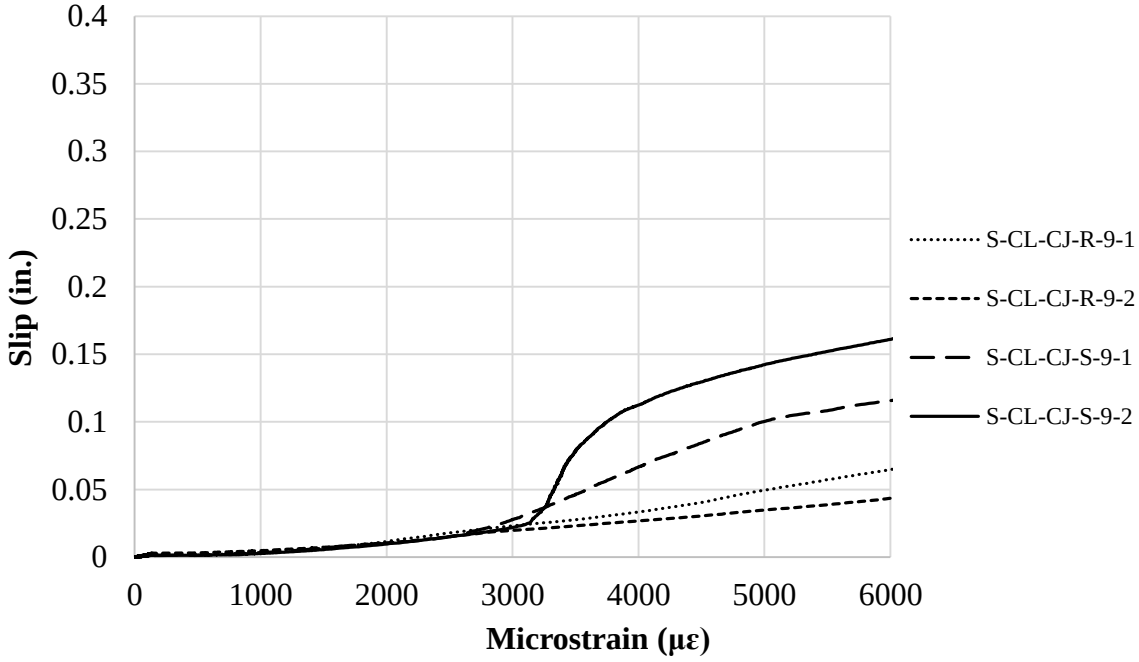

Figure 3.34. Slip vs. interface steel strain for sand-lightweight clay specimens; ρ = 0.009

3.6.2.2 Specimens with reinforcement ratio of 0.013. Testing of the sand-lightweight clay specimens with a reinforcement ratio of 0.013 occurred on 05/06/15. The results are summarized in Figure 3.35 through Figure 3.39.

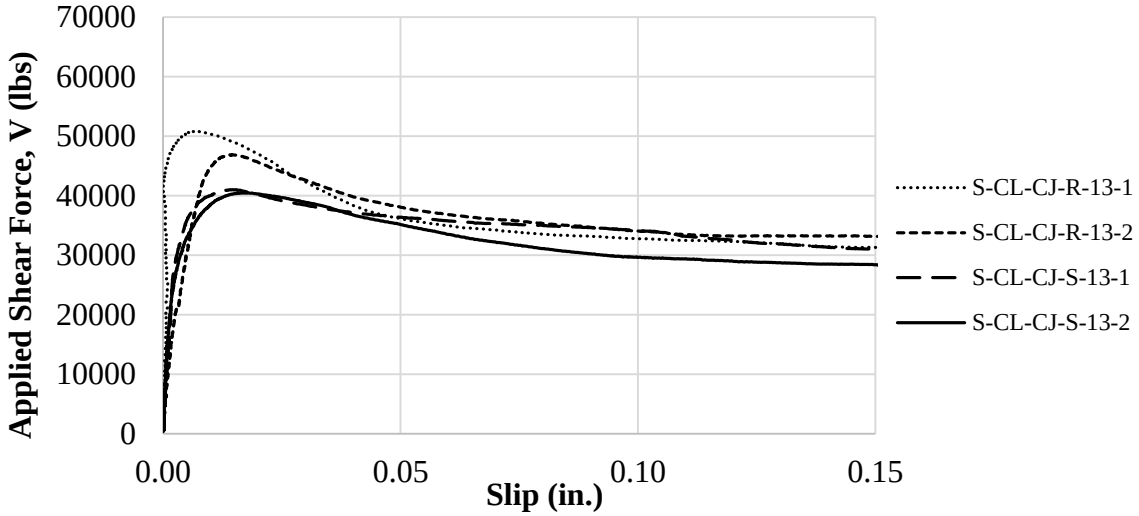

Figure 3.35. Applied shear force vs. slip relations for sand-lightweight clay specimens; with ρ = 0.013

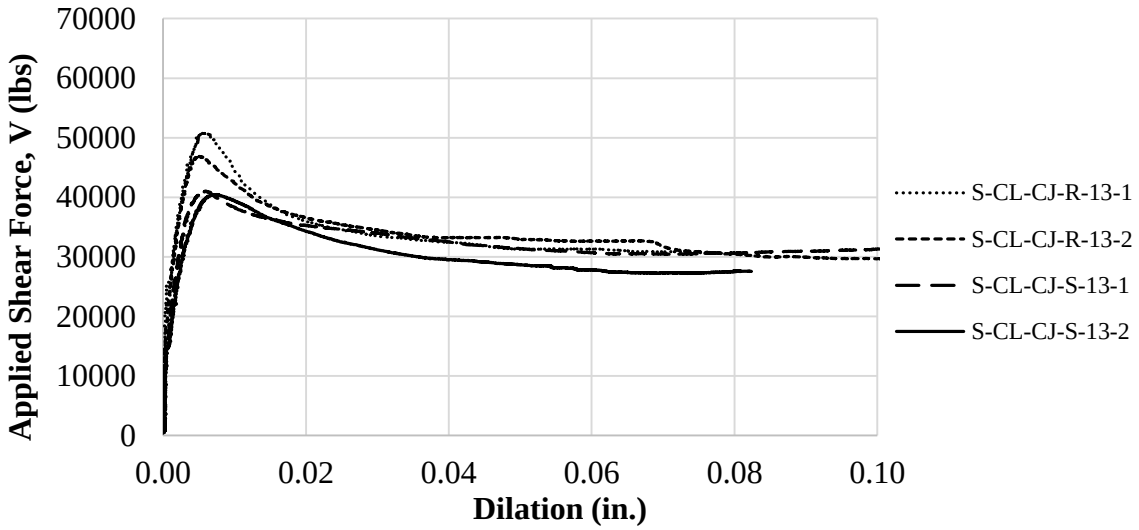

Figure 3.36. Applied shear force vs. interface dilation relations for sand-lightweight clay specimens; ρ = 0.013

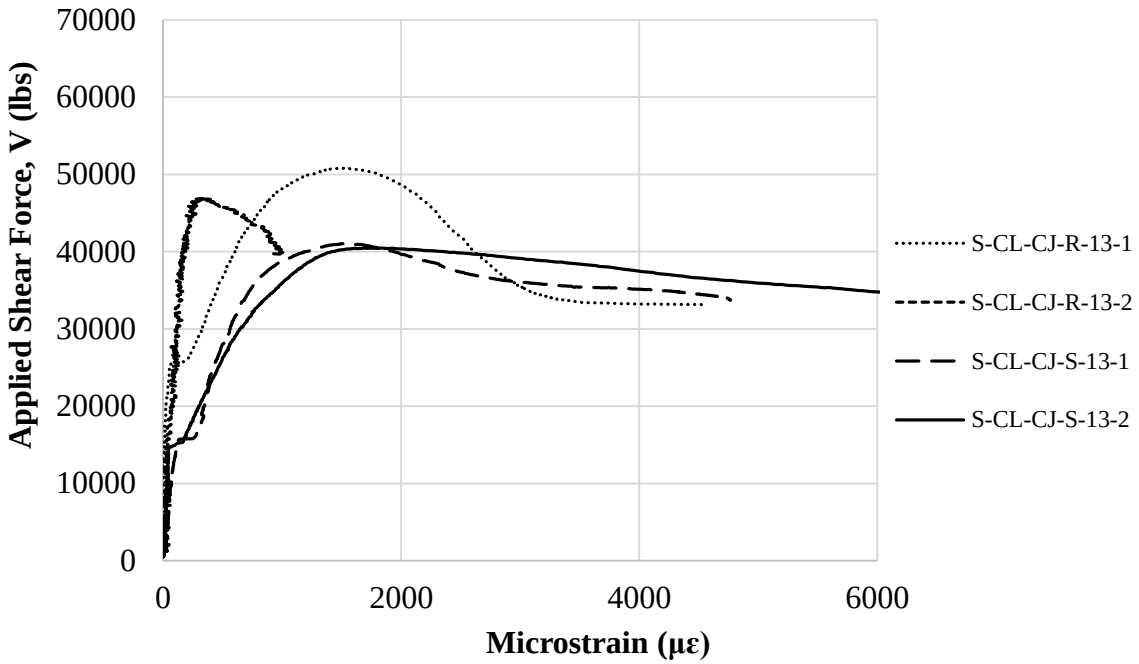

Figure 3.37. Applied shear force vs. interface steel strain for sand-lightweight clay specimens; $\rho = 0.013$

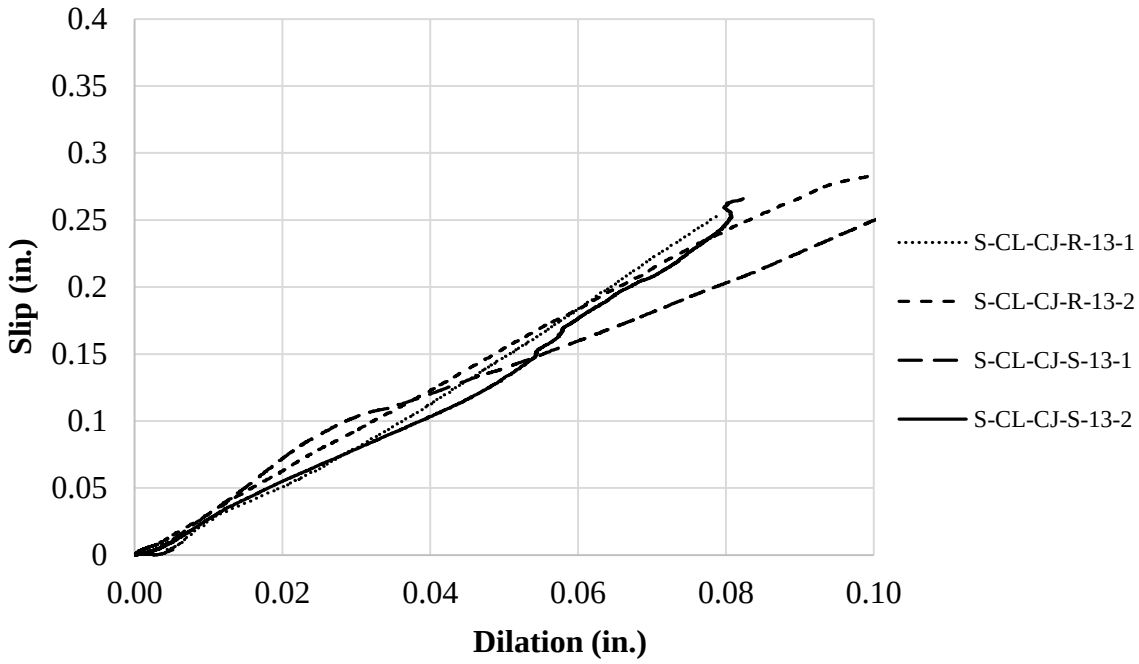

Figure 3.38. Slip vs. dilation for sand-lightweight clay specimens; $\rho = 0.013$

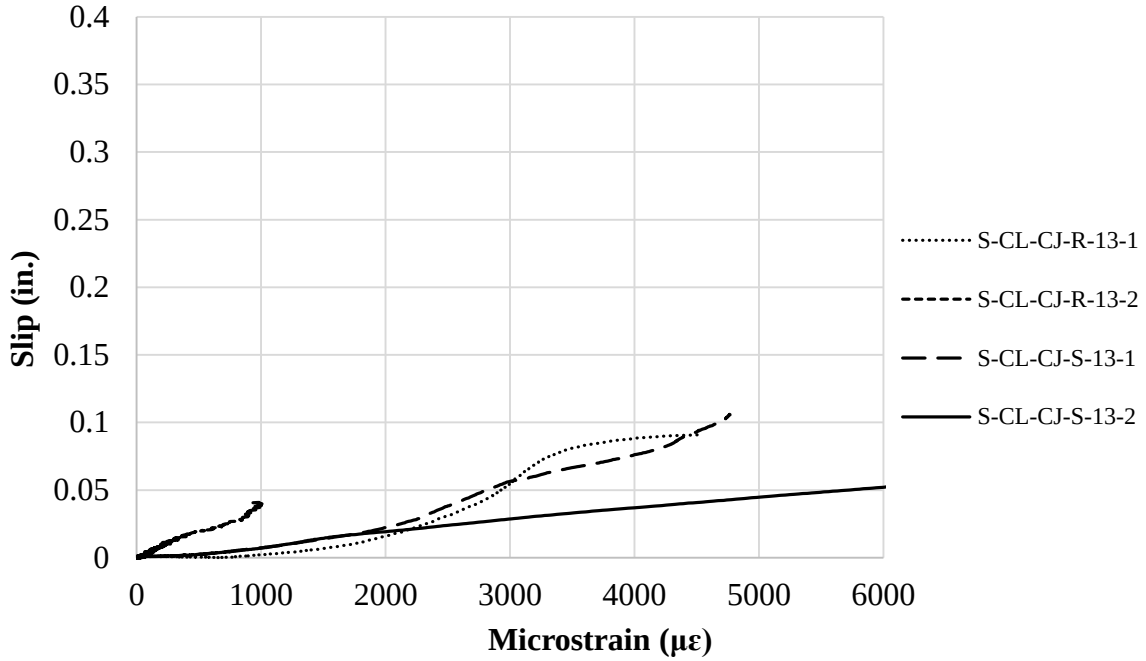

Figure 3.39. Slip vs. interface steel strain for sand-lightweight clay specimens; ρ = 0.013

3.6.2.3 Specimens with reinforcement ratio of 0.017. The sand-lightweight clay specimens with a reinforcement ratio of 0.017 were tested on 05/13/15. The results are shown in Figure 3.41 through Figure 3.45. As previously mentioned in Section 3.6.1, two of the specimens of this series failed due to splitting rather than shear. These were specimens S-CL-CJ-R-17-1 and S-CL-CJ-R-17-2, both of which had a roughened interface. With such a weak aggregate and high reinforcement ratio across the shear plane, the concrete experienced a tensile failure before shear failure could occur along the intended shear plane. It is worth noting that the S-CL-CJ-17 series had the lowest compressive strength on test day of any other series in this study at f'_c = 4,550 psi. Furthermore, this series had the third lowest splitting tensile strength of all the series of the study, having f'_t = 410 psi.

Values were recorded for slip and dilation, but they are not likely valid since they were caused by the front 'panel' of concrete spalling off as the flange flexed. When this section of spalled concrete was removed after testing concluded, it was found that the ‘panel’ only extended to the outer edge of the shear reinforcement and a shear crack

could not be seen underneath it (Figure 3.40). Therefore, a true shear crack did not form for these two specimens and their load, slip, dilation, and strain data are not truly representative of the shear strength of the specimens. However, it is implied that the true shear strength of these specimens is at least as high as the peak applied shear force from Figures 3.41 through 3.45. It is also important to note that the interface reinforcing steel did not reach yield strain for specimen S-CL-CJ-R-17-1. The maximum steel strain for this specimen was less than the yield strain of 2,400 $\mu\varepsilon$. Note that the yield strain was defined as 2,400 $\mu\varepsilon$ because this value equals the average yield strain f_y of the No. 3 bars in the coupon tests described in Section 3.3.3 divided by the average modulus of elasticity E from these same coupon tests.

Figure 3.40. Specimen S-CL-CJ-R-17-2 with spalled concrete removed and no shear failure visible

Also worth noting, the shear force vs. interface steel strain graph (Figure 3.43) shows roughened specimen behavior much different than smooth interface. The roughened specimens did not have a parabolic peak behavior like the smooth specimens did. This behavior is due to the splitting failure of the roughened specimens of this series. In addition, Specimen S-CL-CJ-R-17-1 did not exhibit a peak in applied shear force. Another interesting observation is in Figure 3.45, the plot of slip vs. interface steel strain. Specimen S-CL-CJ-S-17-1 shows that after the peak applied load (associated with failure) occurs, the slip continues to increase, whereas the axial strain in the bar remains constant. However, the slip vs. interface dilation curve (Figure 3.44) shows the crack continuing to widen as slip increases. This could be due to the bar kinking. The bar has been strained, and at this point it is simply rotating. This explains the increases in slip and dilation without an increase in interface steel strain. Another logical explanation is that the strain gage became unattached from the bar, but not damaged to the point where it was unable to take readings.

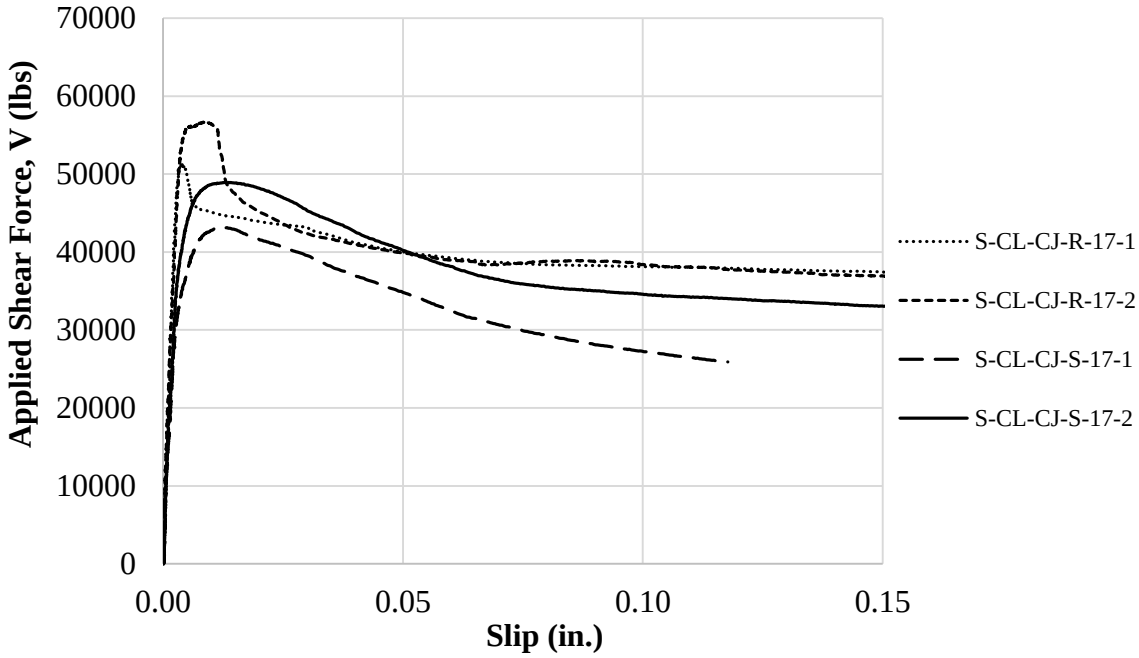

Figure 3.41. Applied shear force vs. slip relations for sand-lightweight clay specimens; with $\rho = 0.017$

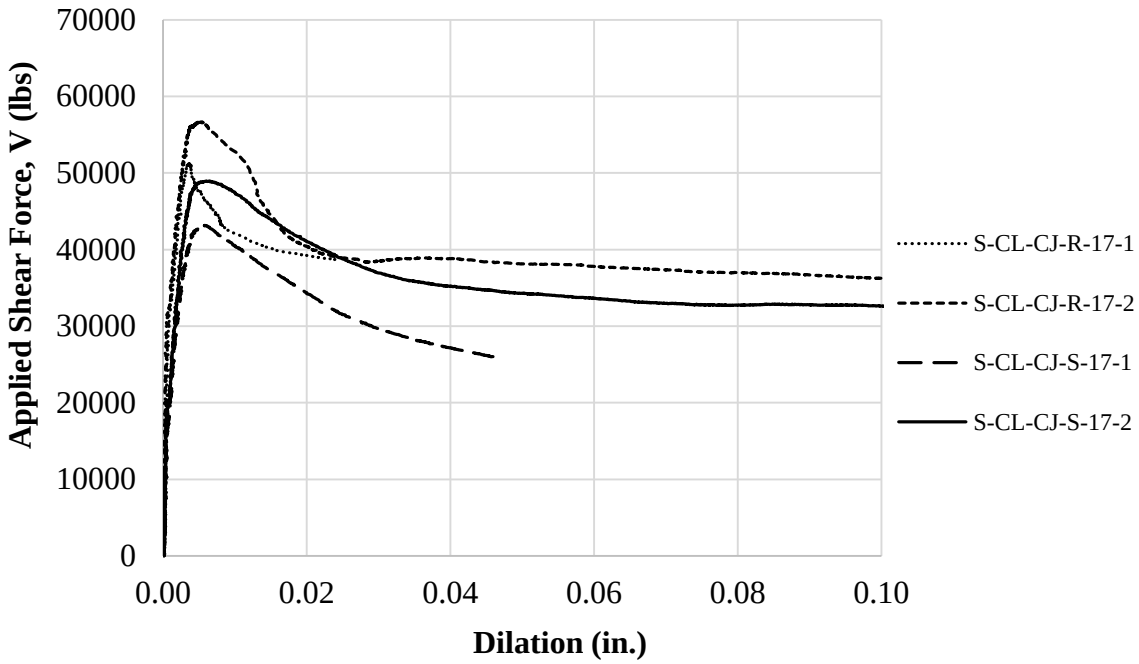

Figure 3.42. Applied shear force vs. interface dilation relations for sand-lightweight clay specimens; ρ = 0.017

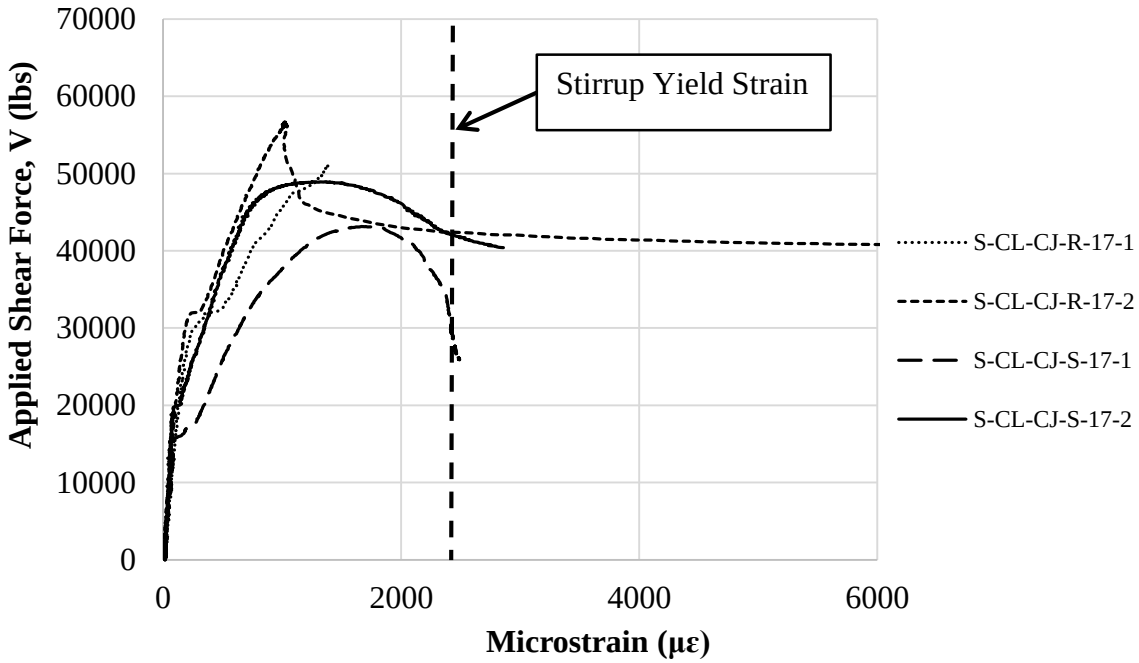

Figure 3.43. Applied shear force vs. interface steel strain for sand-lightweight clay specimens; ρ = 0.017

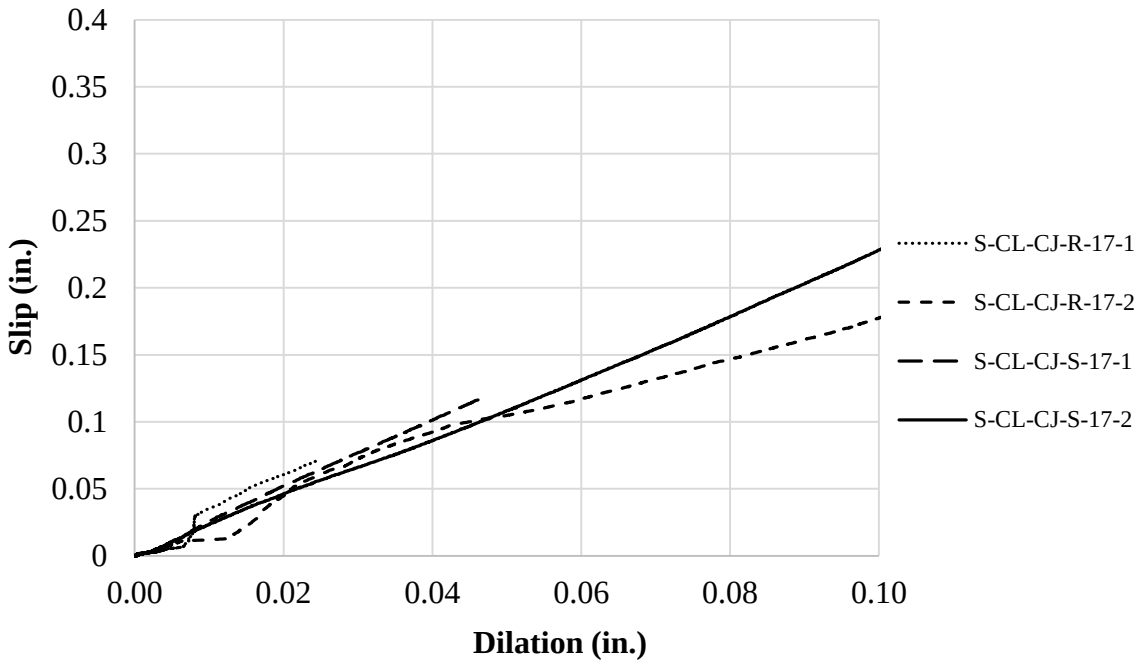

Figure 3.44. Slip vs. dilation for sand-lightweight clay specimens; ρ = 0.017

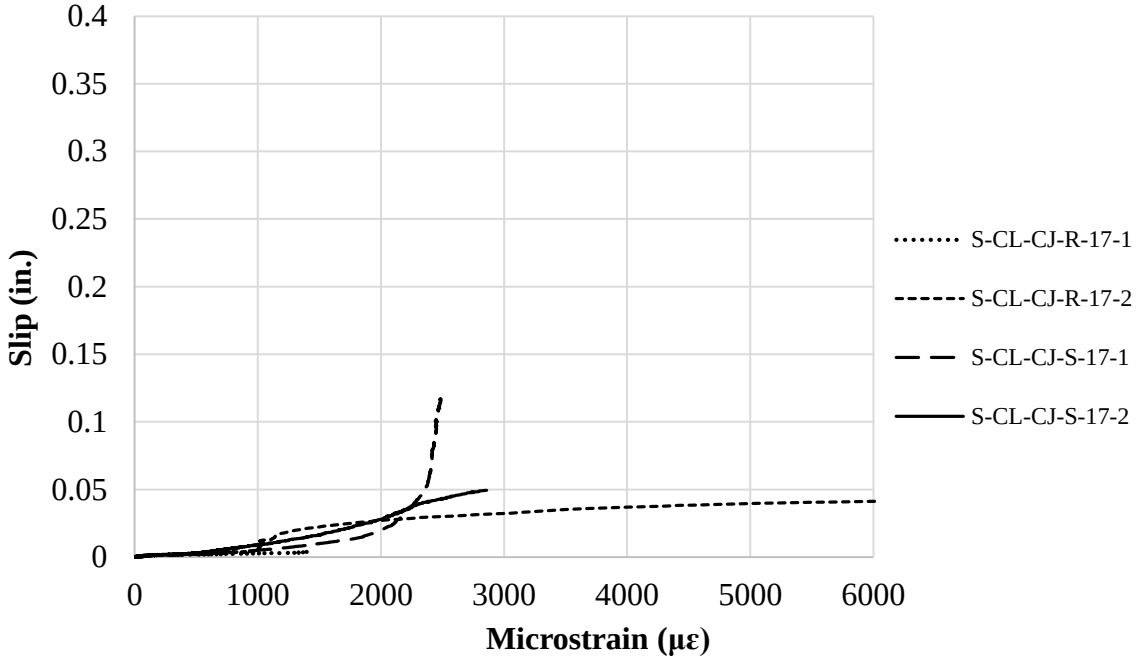

Figure 3.45. Slip vs. interface steel strain for sand-lightweight clay specimens; ρ = 0.017

3.6.2.4 Specimens with reinforcement ratio of 0.022. Testing of the sand-lightweight clay specimens with a reinforcement ratio ρ of 0.022 was done on 05/22/15. The results are shown in Figure 3.46 through Figure 3.50, and as previously discussed, all four specimens of this series failed due to concrete splitting rather than shear.

In the plot of applied shear vs. interface shear strain, Figure 3.48, it can be seen that all specimens of this series except S-CL-CJ-R-22-2 failed to reach steel yield strain in the reinforcement stirrups. This means that the level of strain for those shear stirrups stayed below 2,400 $\mu\varepsilon$ and that for this specimen geometry. If there had been more cover on the bars (or no splitting failure), the bars may have been able to yield. Yet, there is no way to determine this other than by redesigning the specimens and re-testing them. A standard cover of ¾ in. was used for the specimens in this study. Doubling the cover to 1.5 in. would possibly prevent this splitting failure issue from occurring.

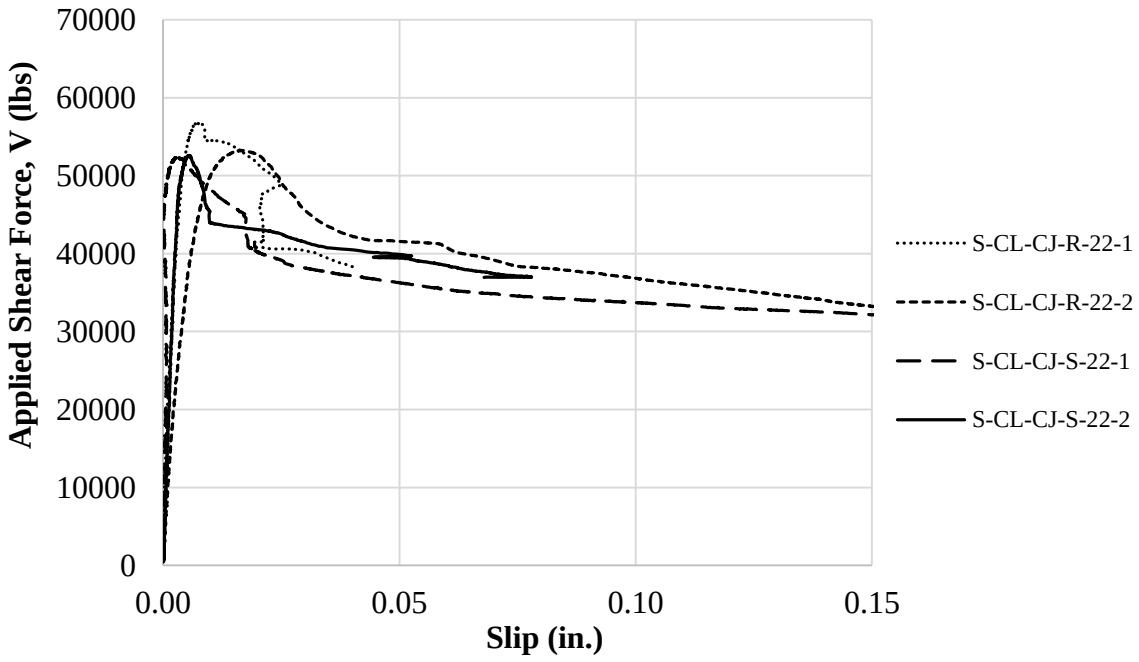

Figure 3.46. Applied shear force vs. slip relations for sand-lightweight clay specimens; with ρ = 0.022

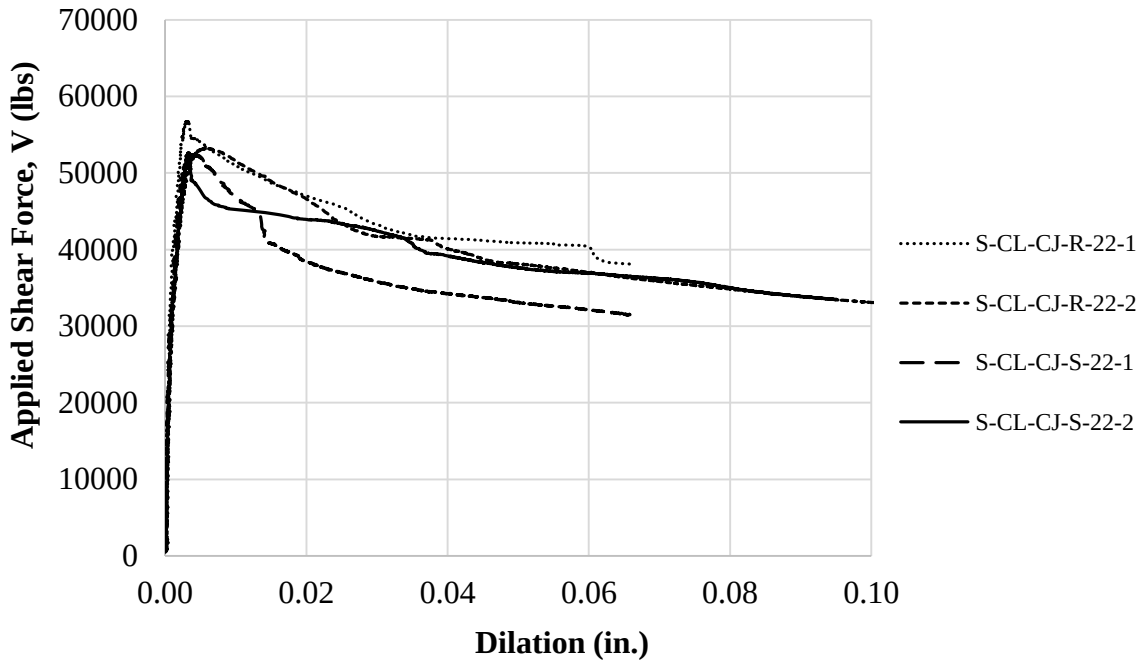

Figure 3.47. Applied shear force vs. interface dilation relations for sand-lightweight clay specimens; ρ = 0.022

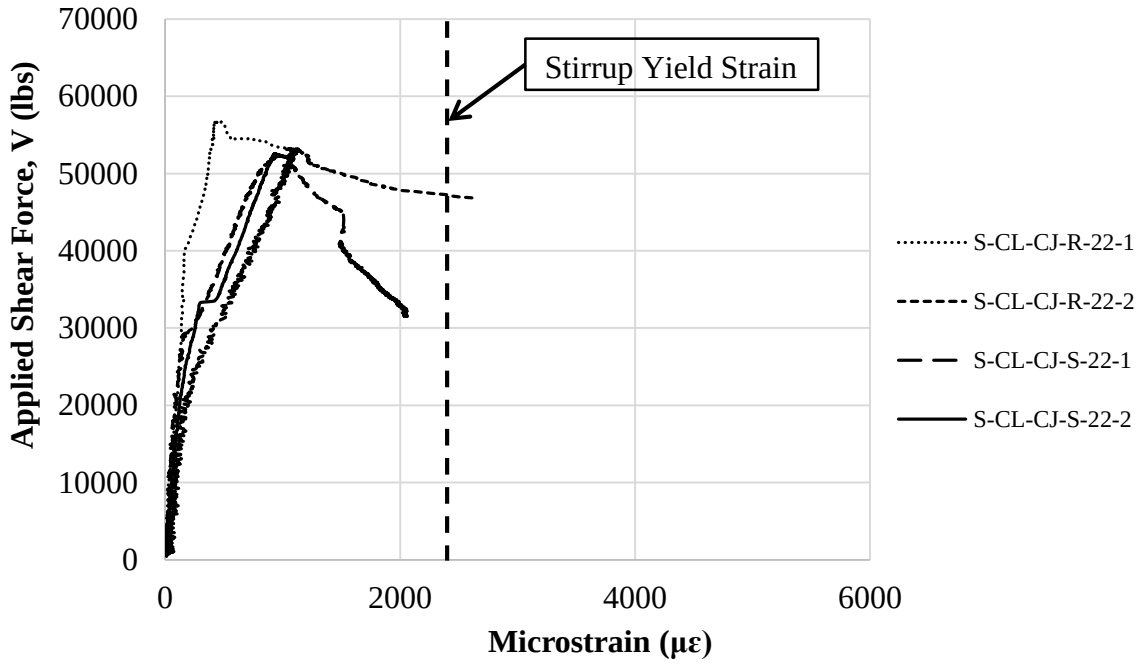

Figure 3.48. Applied shear force vs. interface steel strain for sand-lightweight clay specimens; ρ = 0.022

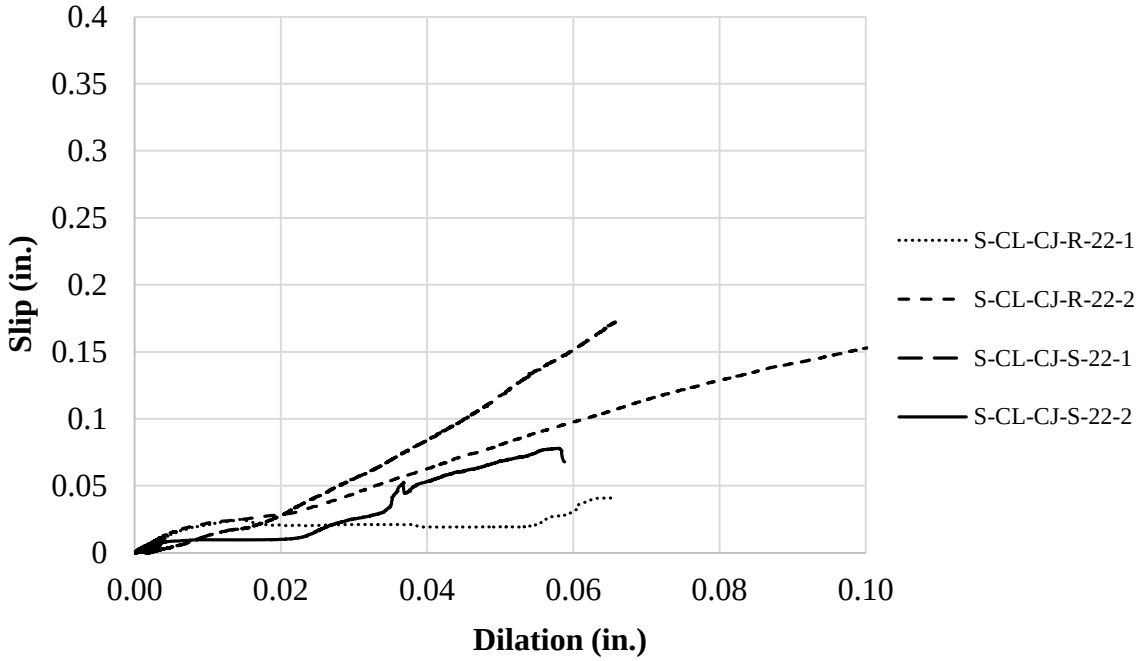

Figure 3.49. Slip vs. dilation for sand-lightweight clay specimens; ρ = 0.022

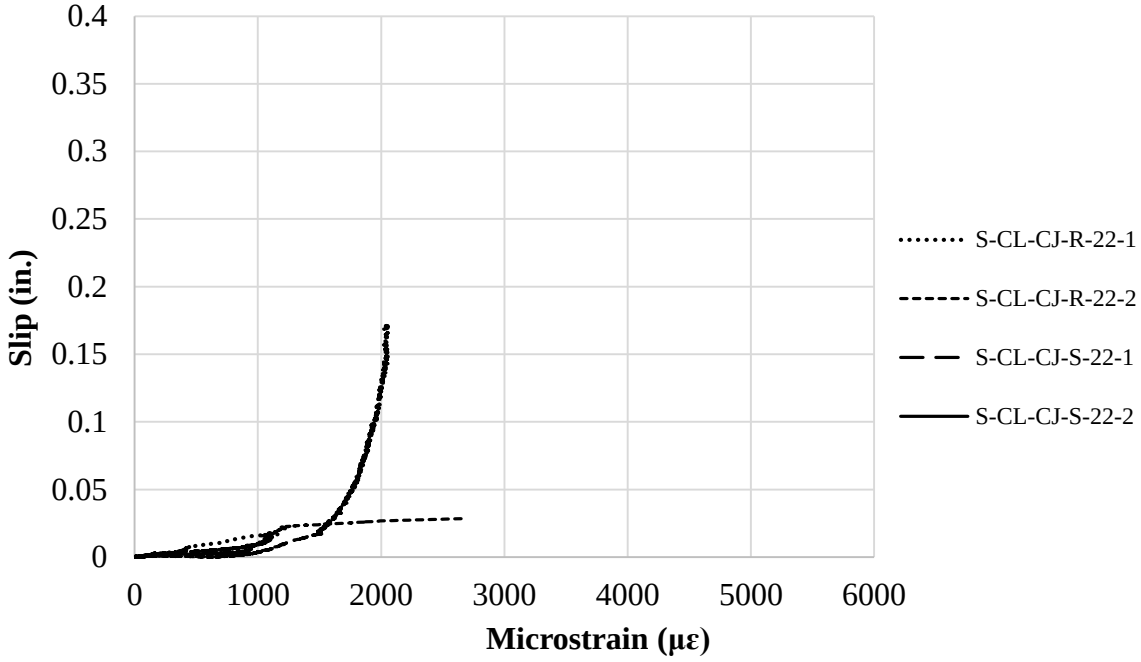

Figure 3.50. Slip vs. interface steel strain for sand-lightweight clay specimens; ρ = 0.022

3.6.3. Sand-lightweight Slate Specimens. This section presents the results of the sand-lightweight slate specimens tested in this program. As previously discussed, none of the sand-lightweight slate specimens failed due to concrete splitting.

3.6.3.1 Specimens with reinforcement ratio of 0.009. The sand-lightweight slate specimens with the lowest reinforcement ratio (ρ = 0.009) were tested on 03/30/2015. Their results are plotted in Figure 3.51 through Figure 3.55. All specimens failed in shear along the intended shear plane. Another interesting observation is in Figure 3.55, the plot of slip vs. interface steel strain. For specimen S-SL-CJ-S-9-1 the figure shows that after the peak applied load (associated with failure) occurs, the slip continues to increase, whereas the axial strain in the bar remains constant. However, the slip vs. interface dilation curve (Figure 3.54) shows the crack continuing to widen as slip increases. This could be due to the bar kinking as discussed in Section 3.6.2.3.

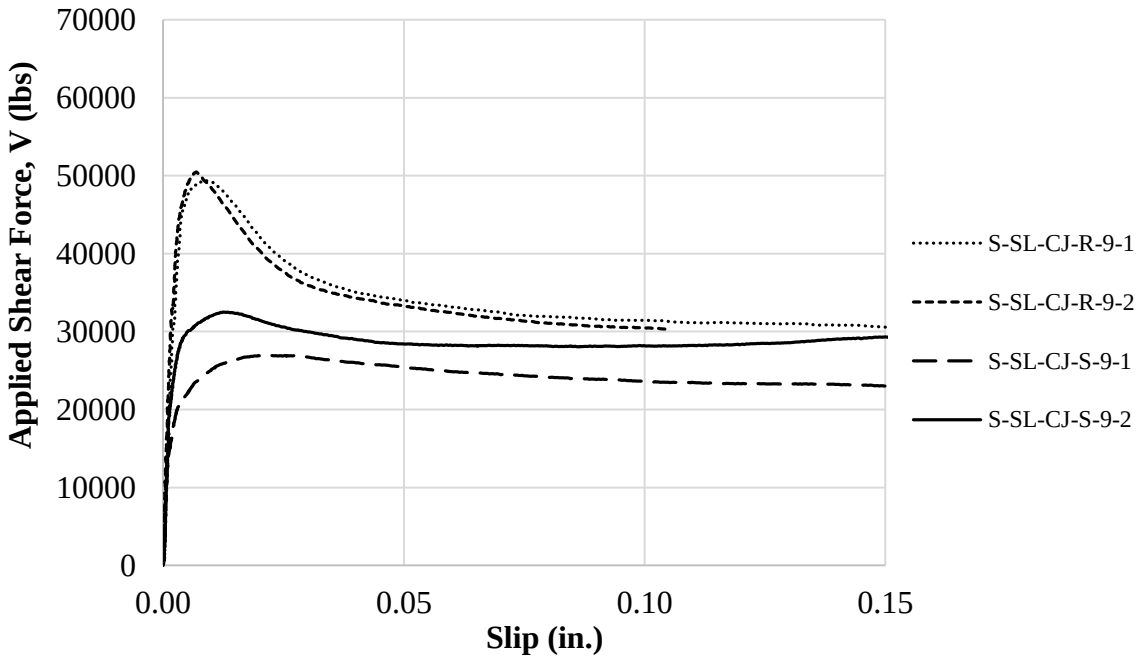

Figure 3.51. Applied shear force vs. slip relations for sand-lightweight slate specimens; with ρ = 0.009

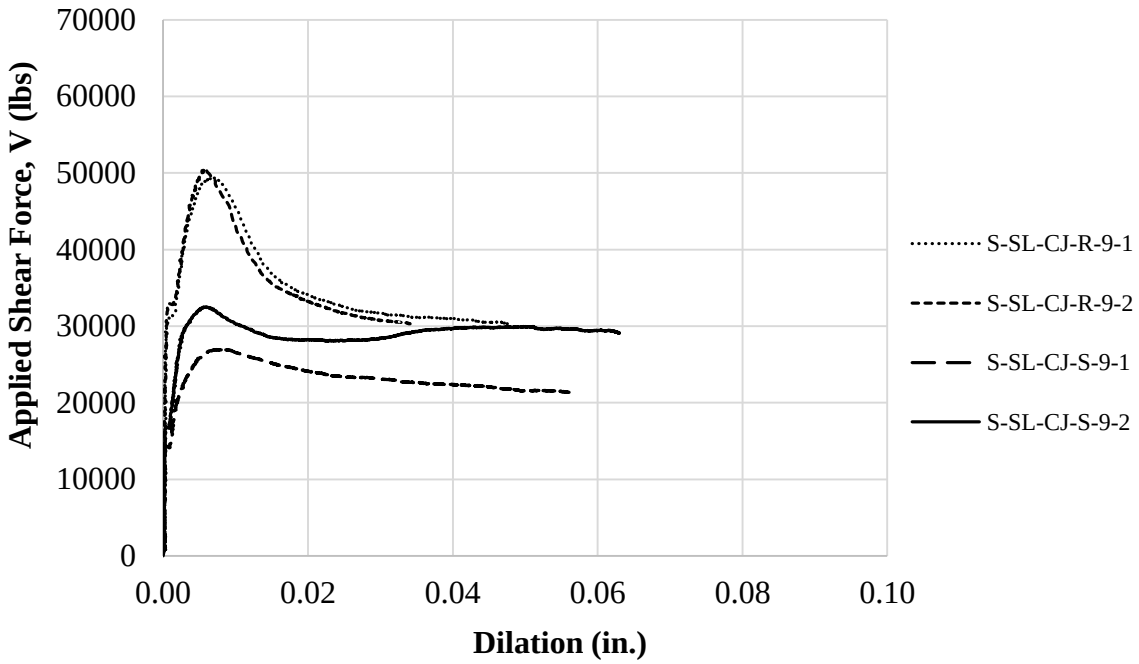

Figure 3.52. Applied shear force vs. interface dilation relations for sand-lightweight slate specimens; ρ = 0.009

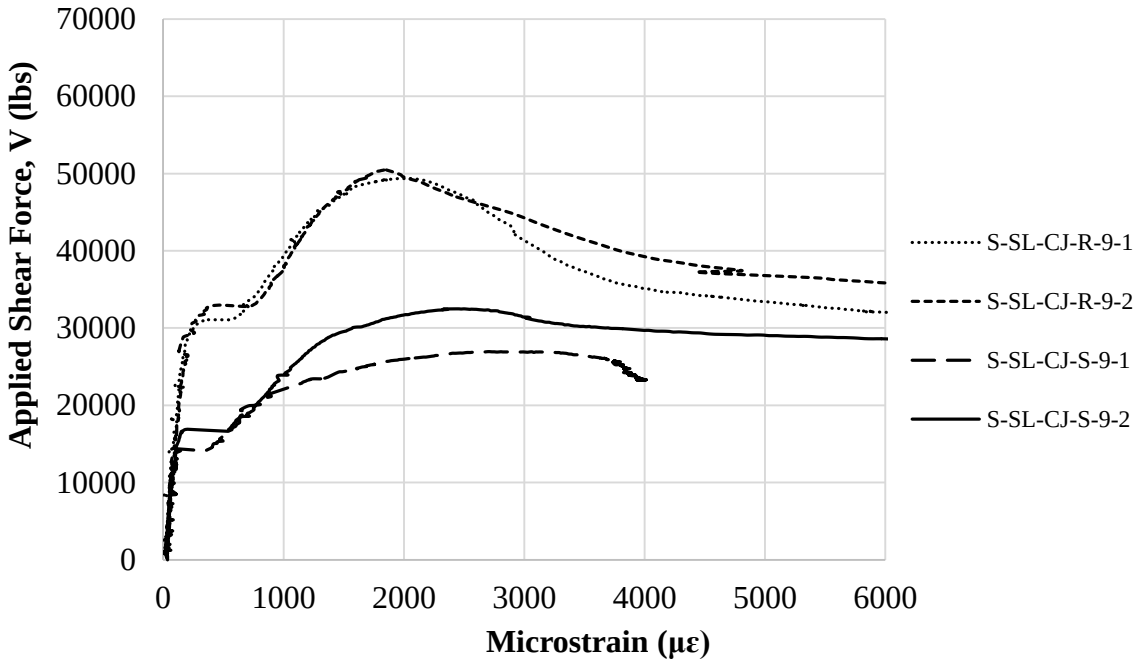

Figure 3.53. Applied shear force vs. interface steel strain for sand-lightweight slate specimens; ρ = 0.009

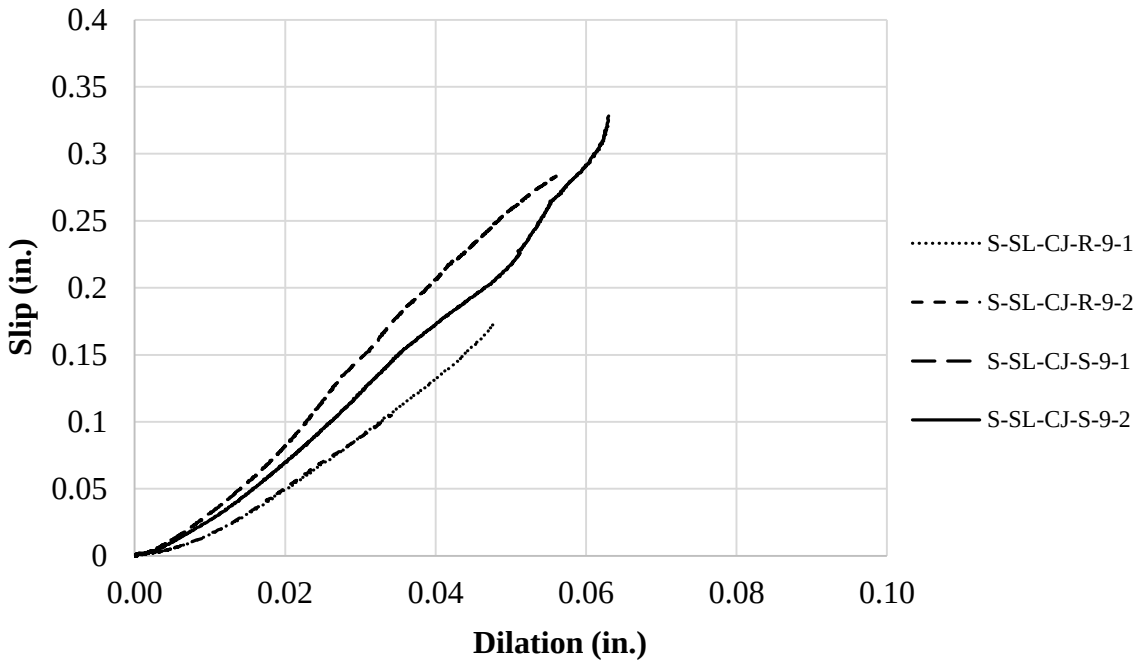

Figure 3.54. Slip vs. dilation for sand-lightweight slate specimens; ρ = 0.009

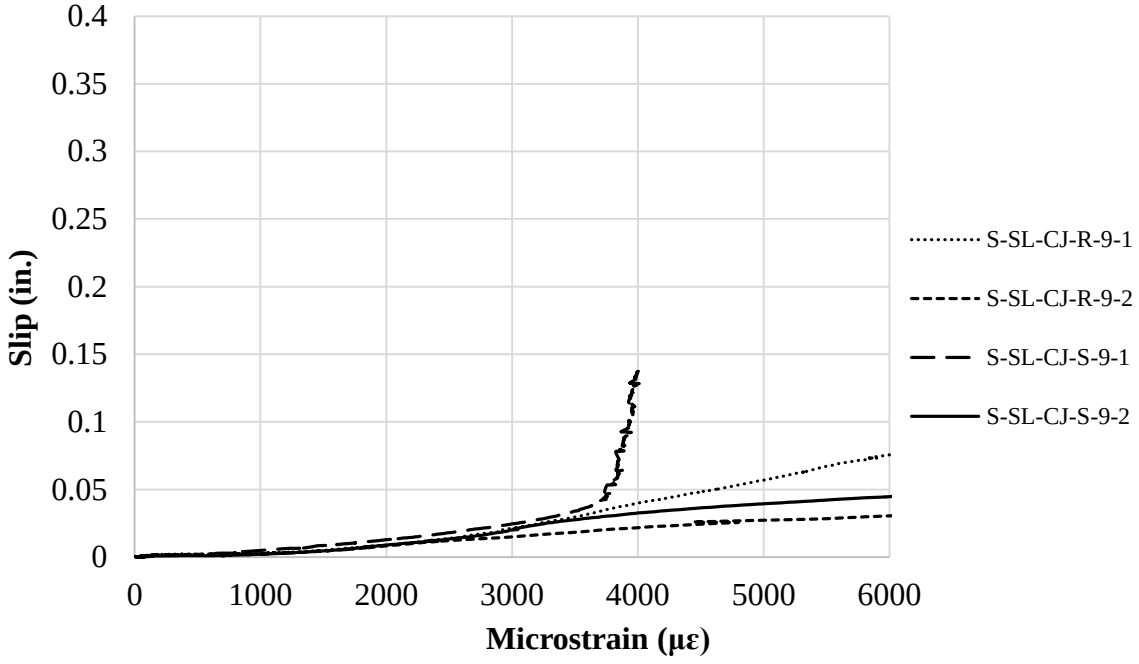

Figure 3.55. Slip vs. interface steel strain for sand-lightweight slate specimens; ρ = 0.009

3.6.3.2 Specimens with reinforcement ratio of 0.013. The slate sand-lightweight specimens with reinforcement ratio of 0.013 are presented in this section. Important recorded data are plotted in Figure 3.56 through Figure 3.60.

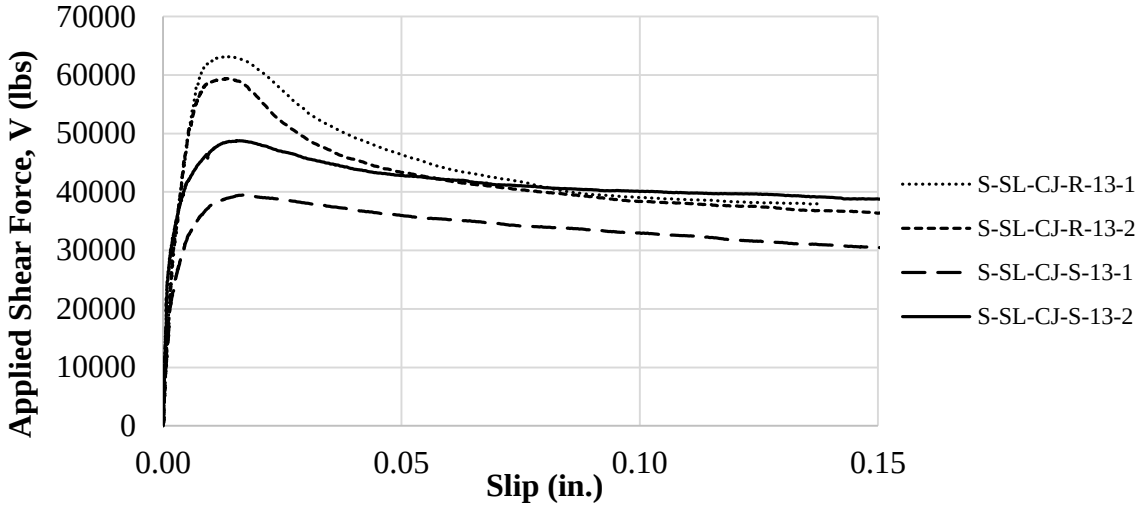

Figure 3.56. Applied shear force vs. slip relations for sand-lightweight slate specimens; with ρ = 0.013

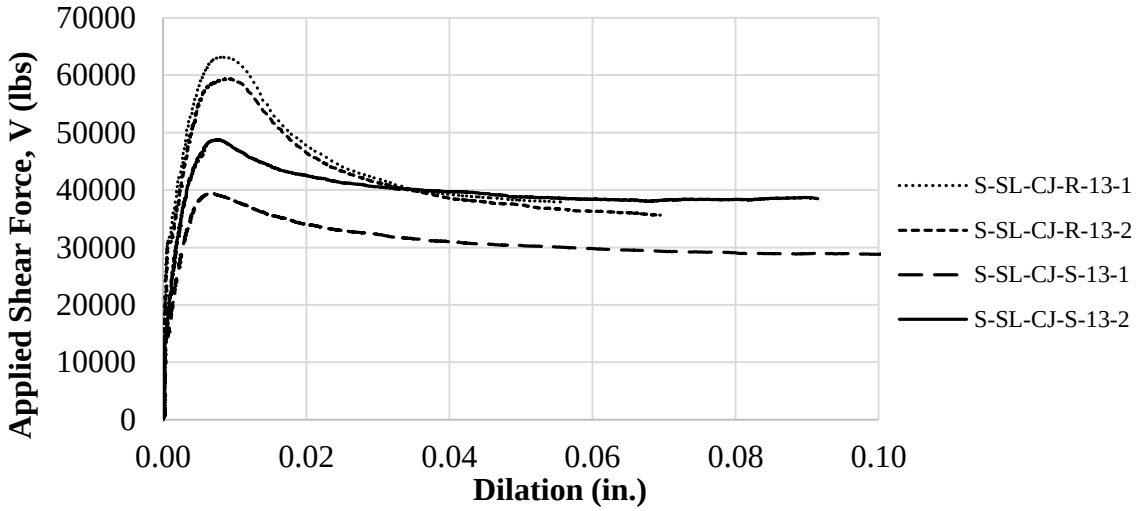

Figure 3.57. Applied shear force vs. interface dilation relations for sand-lightweight slate specimens; ρ = 0.013

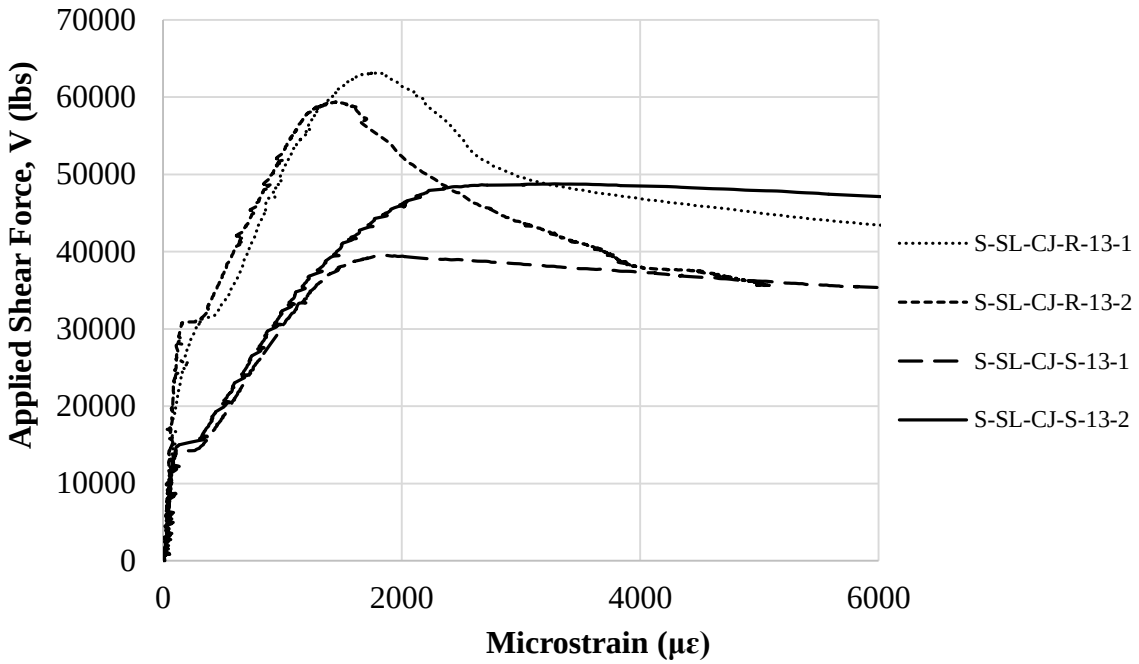

Figure 3.58. Applied shear force vs. interface steel strain for sand-lightweight slate specimens; ρ = 0.013

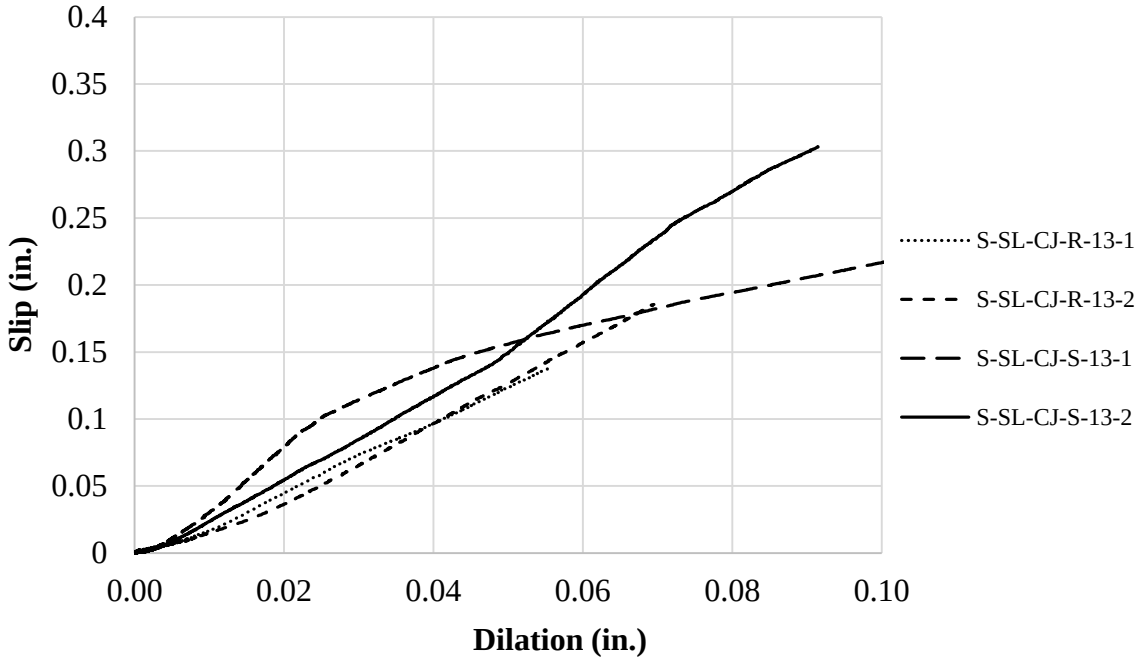

Figure 3.59. Slip vs. dilation for sand-lightweight slate specimens; ρ = 0.013

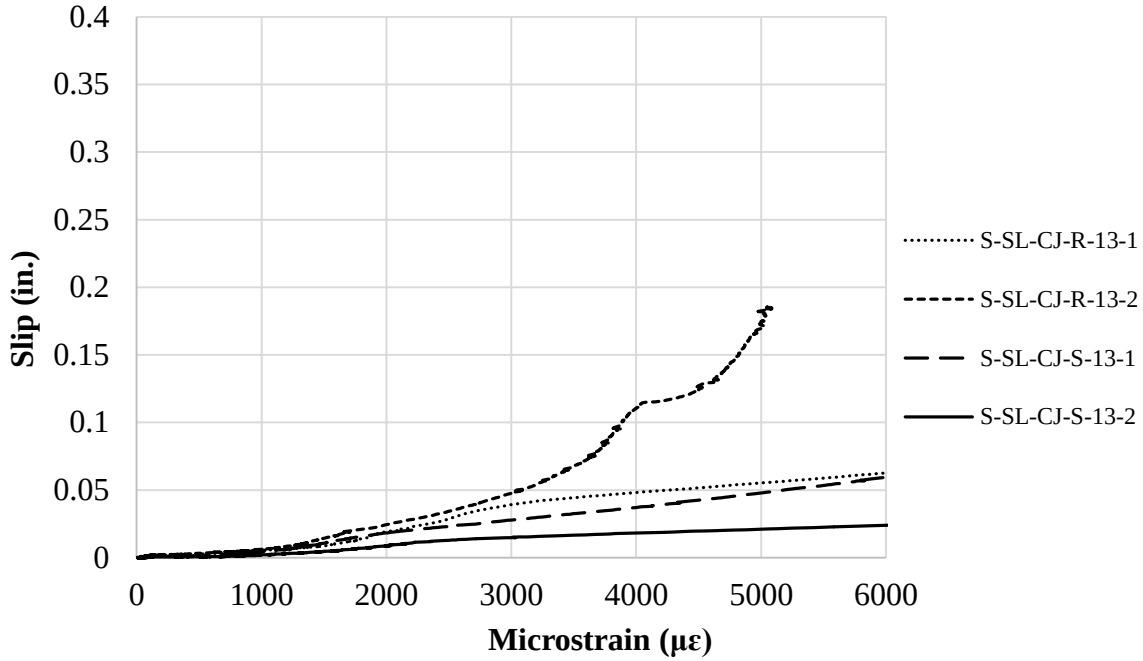

Figure 3.60. Slip vs. interface steel strain for sand-lightweight slate specimens; ρ = 0.013

3.6.3.3 Specimens with reinforcement ratio of 0.017. Testing of slate sand-lightweight specimens with reinforcement ratio of 0.017 was performed on 04/06/2015. Results are shown in Figure 3.62 through Figure 3.66. The only unexpected failure was that of specimen S-SL-CJ-S-17-1. The shear crack did not form at the intended shear plane. Instead, it was about a half inch offset from the vertical centerline of the specimen as shown in Figure 3.61. This behavior implies that the bond of one side of the cold-joint interface to the other was very good. Even though the shear plane has a smaller cross-section than the adjacent body of the specimen, as well as a construction joint which was troweled smooth, the crack did not form along the shear plane. In this figure you can also see minor honeycombing of the concrete in the top flange. This occurs when there is inadequate consolidation of the concrete during casting. To avoid honeycombing in other specimens, the construction method was modified. The concrete was vibrated for longer periods of time during specimen construction, especially in the flanges. The concrete was added to the forms in thinner layers and vibrated before the addition of the next layer. Another interesting behavior is observed in Figure 3.66, which shows slip vs.

strain, after the peak load (associated with failure), the slip continues to increase for Specimen S-CL-CJ-R-17-2, whereas the axial strain in the bar remains relatively constant for that specimen. However, the slip-dilation curve (Figure 3.65) shows the crack continuing to widen as slip increases. This could be due to the bar kinking as discussed in Sections 3.6.2.3 and 3.6.3.2.

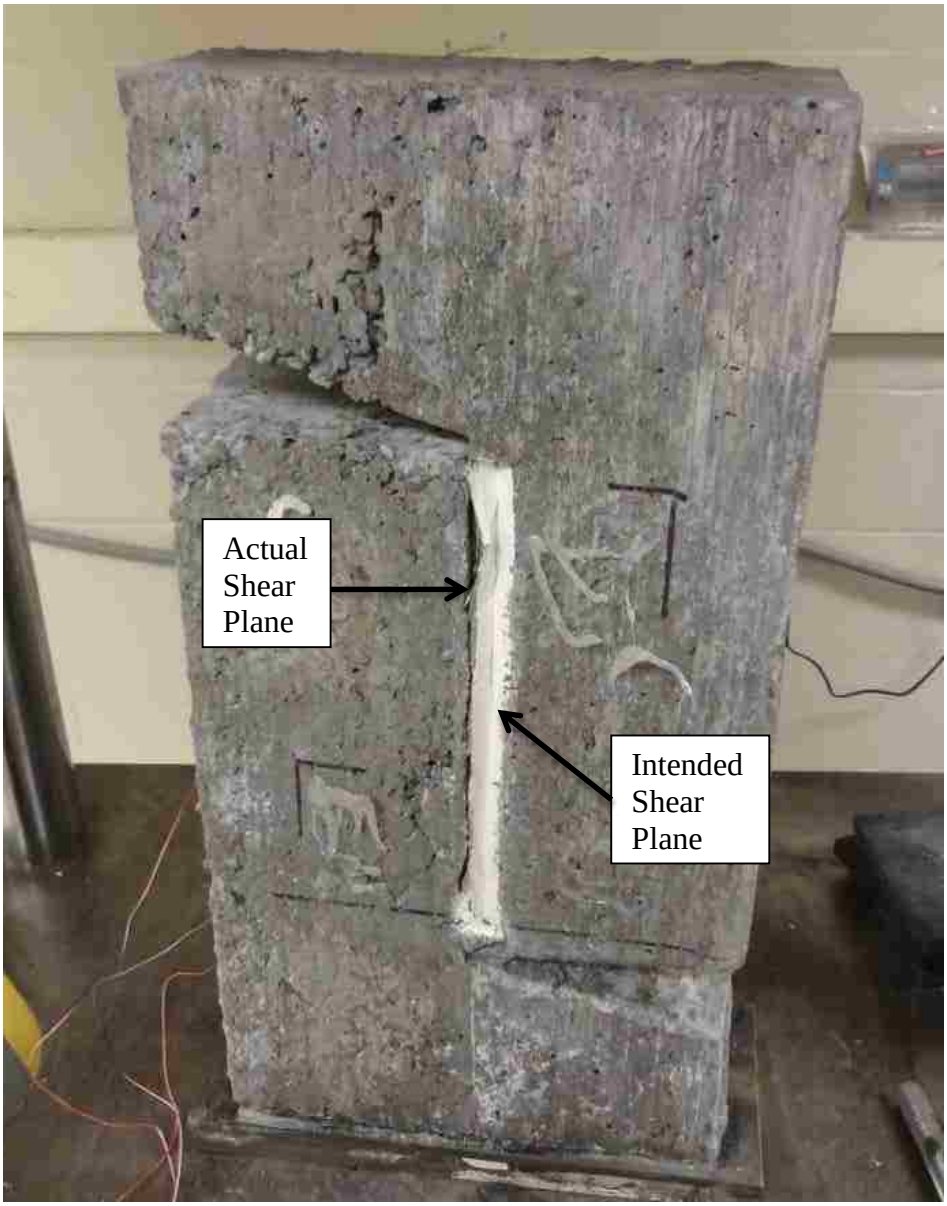

Figure 3.61. Shear plane crack of specimen S-SL-CJ-S-17-1

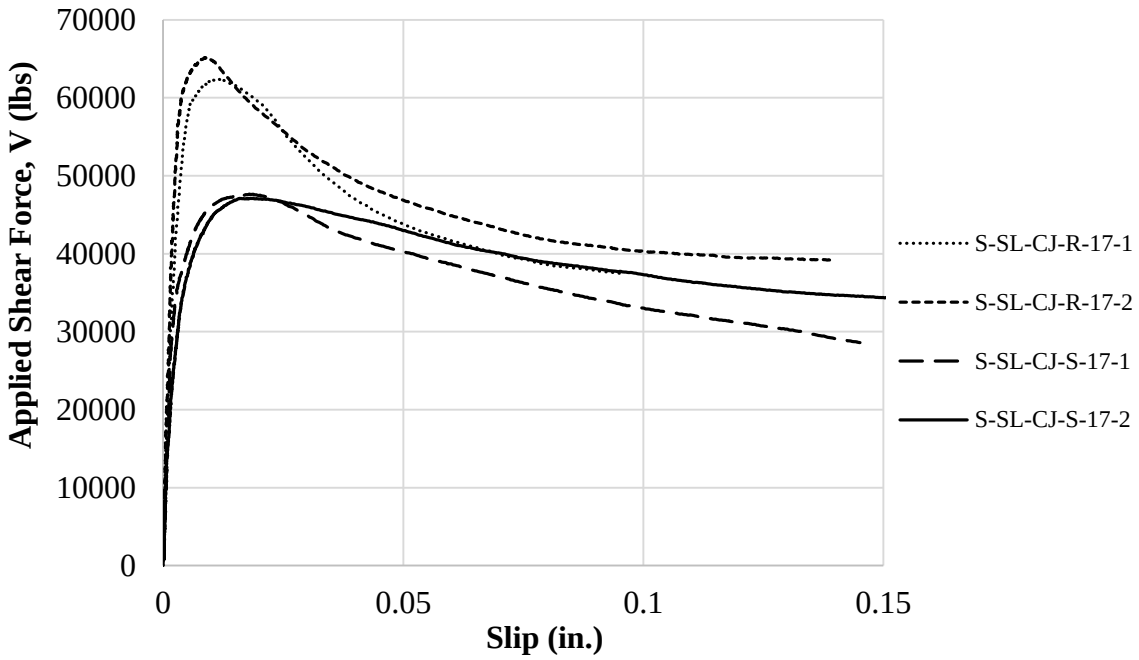

Figure 3.62. Applied shear force vs. slip relations for sand-lightweight slate specimens; with $\rho = 0.017$

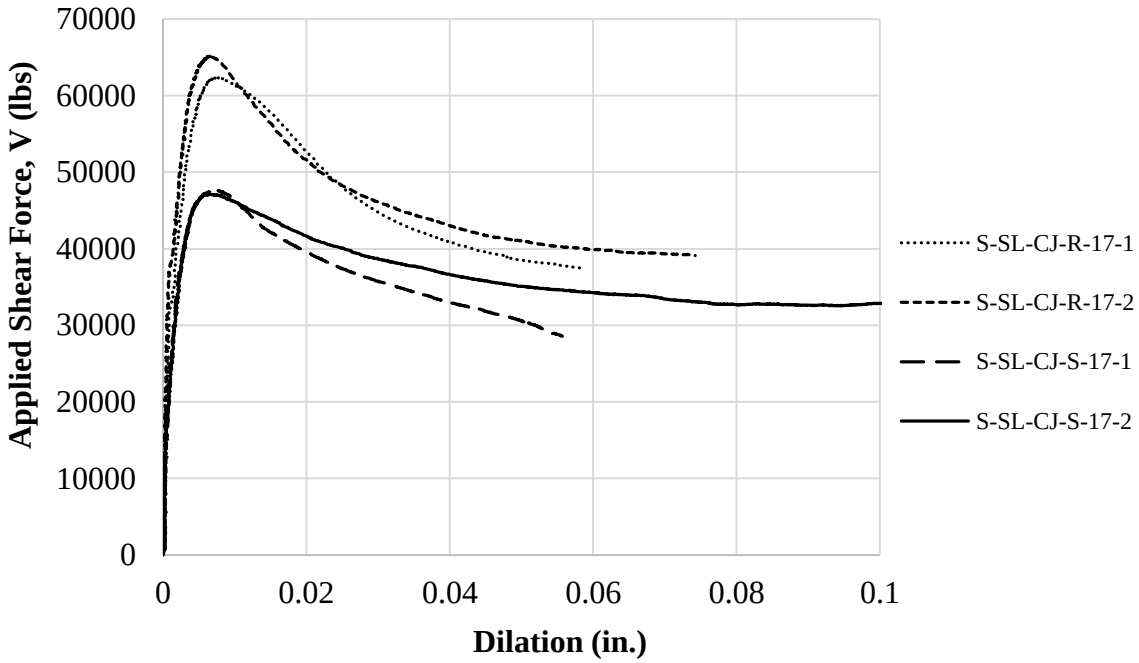

Figure 3.63. Applied shear force vs. interface dilation relations for sand-lightweight slate specimens; $\rho = 0.017$

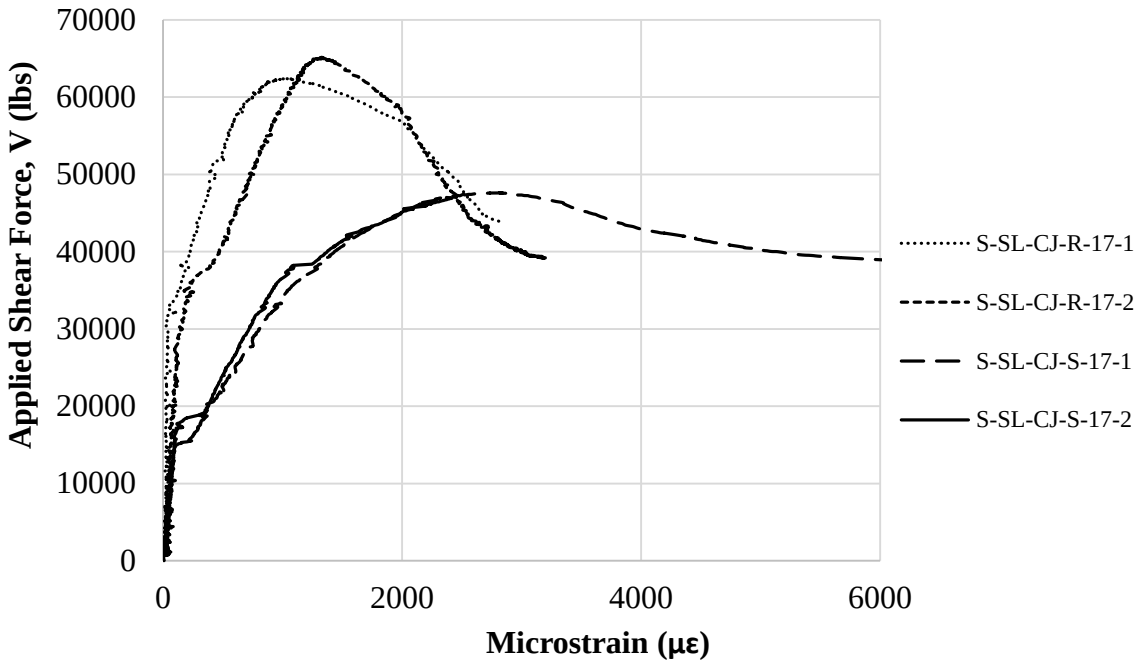

Figure 3.64. Applied shear force vs. interface steel strain for sand-lightweight slate specimens; ρ = 0.017

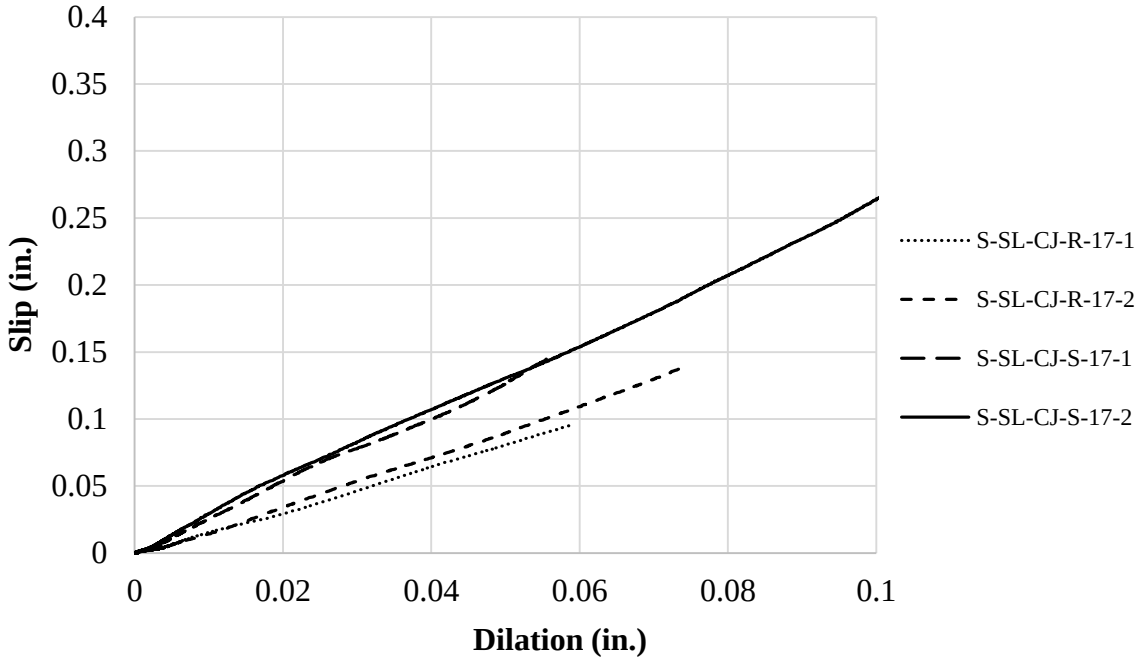

Figure 3.65. Slip vs. dilation for sand-lightweight slate specimens; ρ = 0.017

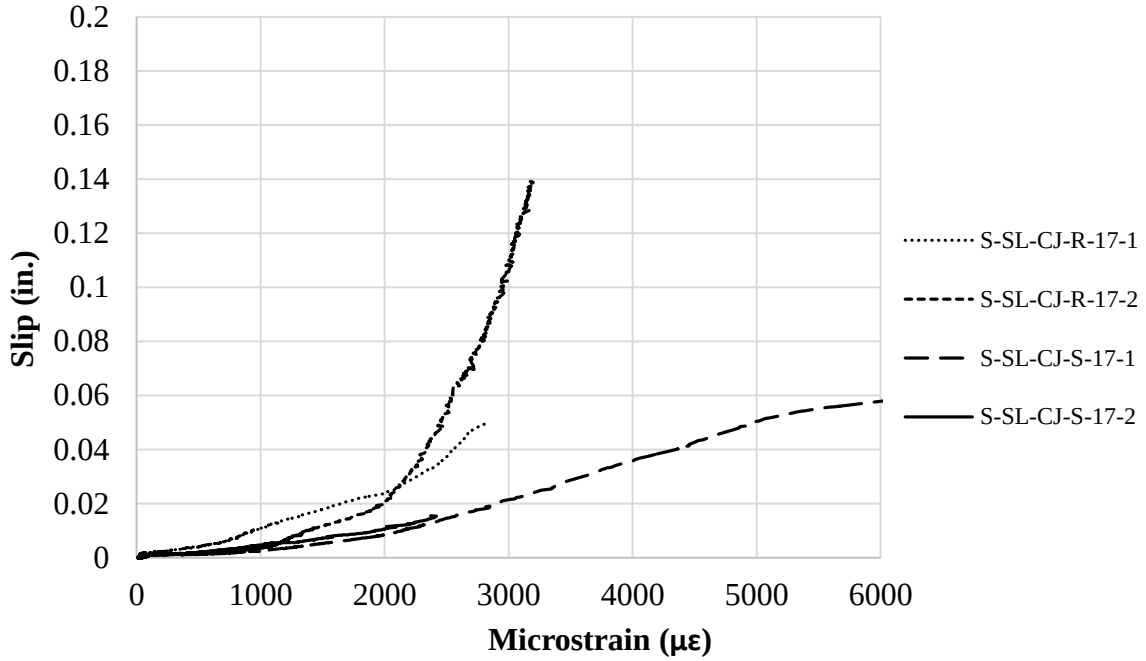

Figure 3.66. Slip vs. interface steel strain for sand-lightweight slate specimens; ρ = 0.017

3.6.3.4 Specimens with reinforcement ratio of 0.022. The sand-lightweight slate specimens with the highest reinforcement ratio (0.022) were tested on 03/11/2015. The behaviors of these specimens are plotted in Figure 3.70 through Figure 3.74. Splitting cracks on the side face and flexural cracks on the back face were observed in the roughened specimens of this series (Figure 3.67). This behavior was similar to that of the sand-lightweight clay specimens that had splitting failures, with an important exception: when the outer layer of cracked concrete was removed from the slate specimens after testing, a definite shear crack along the shear plane was visible (Figure 3.68). This suggests that shear along the shear plane was the principle failure mode. Further investigation of the real-time plots in Figure 3.69 show that these two roughened specimens behaved similar to other specimens which failed along the shear plane (Figure 3.27 left, shown in Section 3.6.1) in that the sharp spikes in slip and dilation correspond to the peak applied shear force. This supports the idea that the failure mode of the roughened specimens of this series was indeed shear along the shear plane.

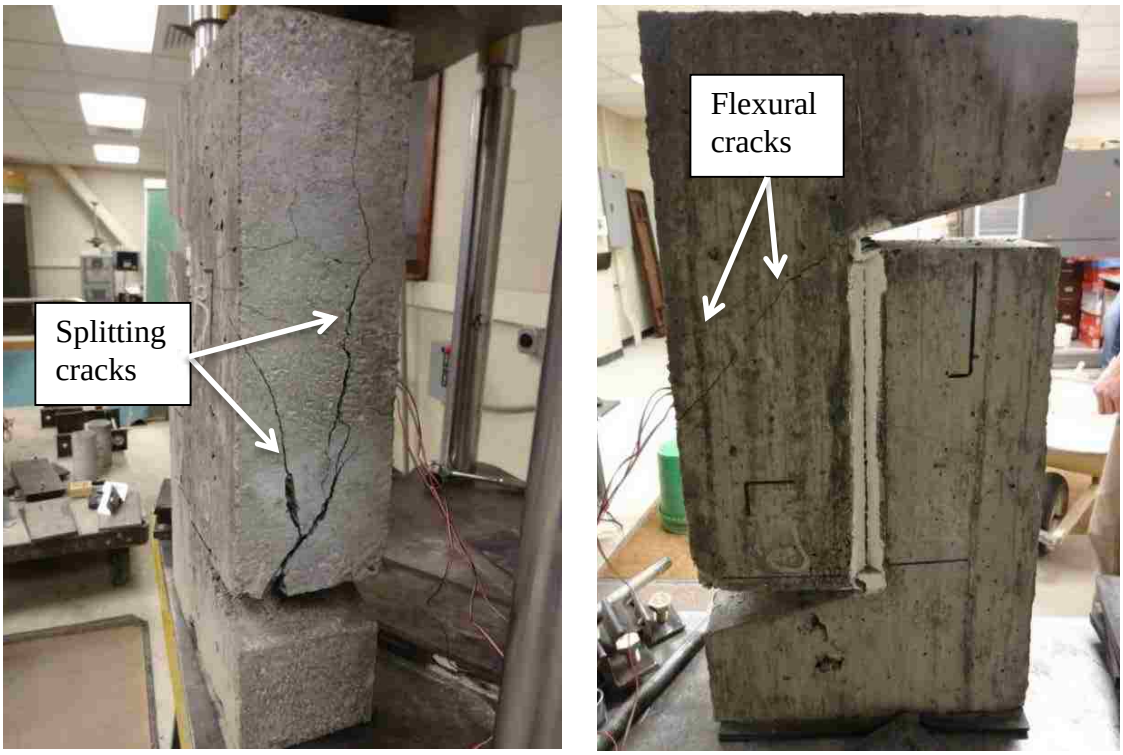

Figure 3.67. Specimen S-SL-CJ-R-22-1 shown; splitting cracks on side face (left), and flexural cracks on back face (right)

Another interesting behavior is observed in Figure 3.74, which shows slip vs. strain. After the peak load (associated with failure), the slip continues to increase for Specimen S-CL-CJ-R-22-2, whereas the axial strain in the bar remains relatively constant for that specimen. However, the slip-dilation curve (Figure 3.73) shows the crack continuing to widen as slip increases. This behavior is similar to Specimen S-CL-CJ-R-17-2 of Section 3.6.3.3 and could be due to the bar kinking. Also, it is worth noting that the interface steel strain did not exceed the steel yield strain for specimen S-SL-CJ-R-22-1 (Figure 3.72). Analysis of the raw strain data indicates that the strain gages were damaged prior to reaching the level of strain associated with yield and no further values were able to be recorded past that point. Thus, it is not known if the bars did actually reach yield strain since all three strain gages were damaged early in the test.

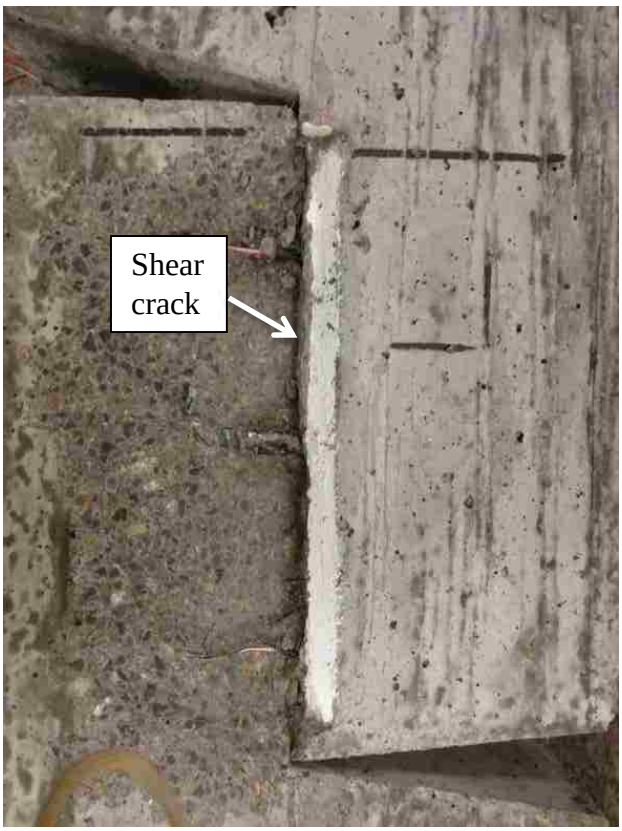

Figure 3.68. Specimen S-SL-CJ-R-22-1 with spalled concrete removed and shear plane exposed

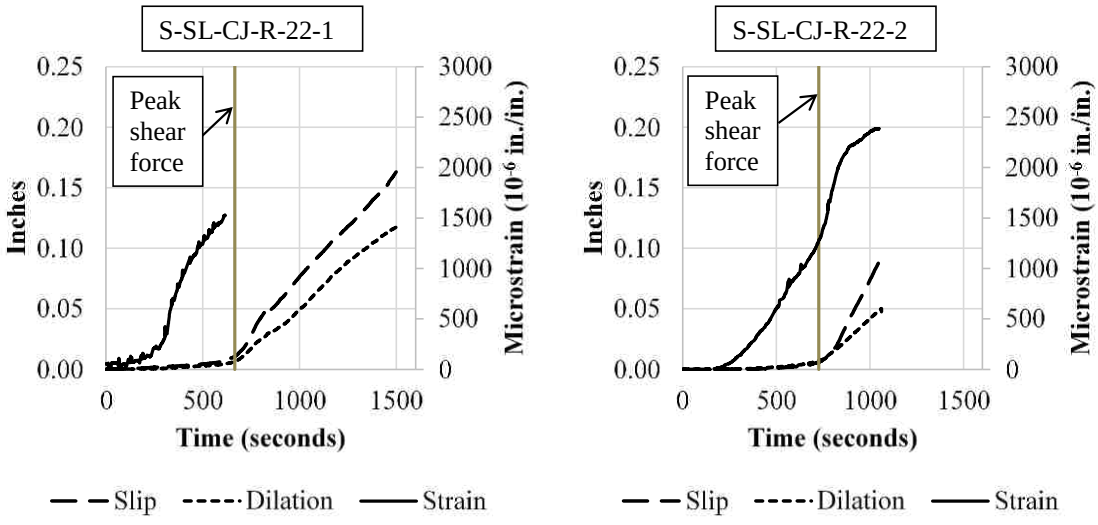

Figure 3.69. Real time plots of slip, dilation, and strain for a Specimen S-SL-CJ-R-22-1 (left); and Specimen S-SL-CJ-R-22-1 (right); which both failed due to shear

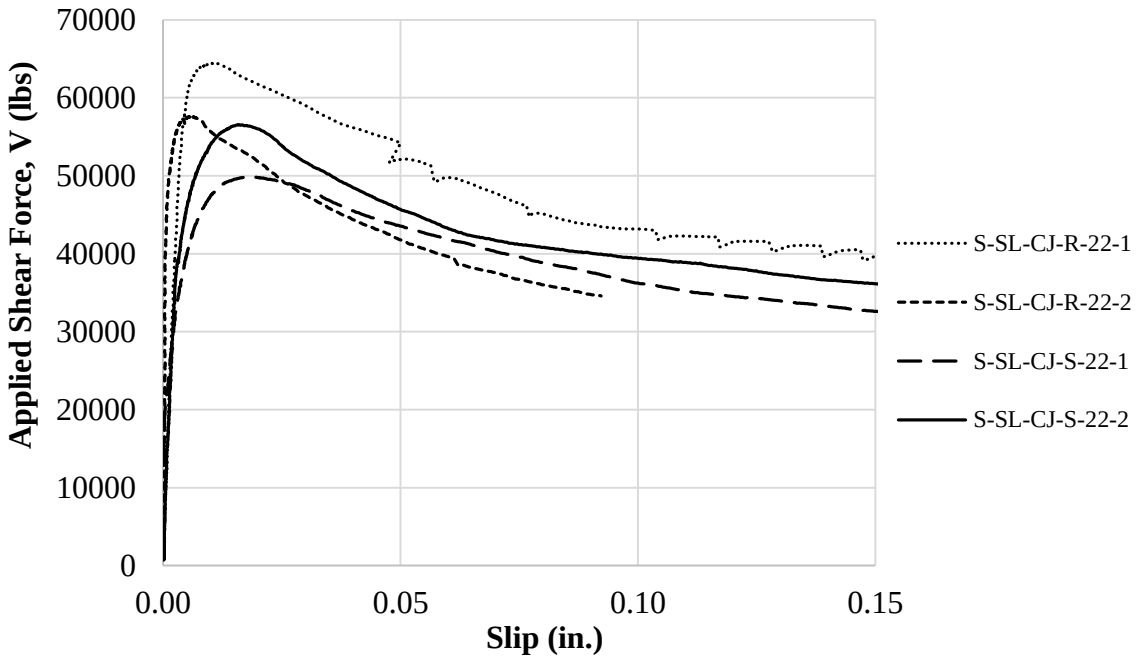

Figure 3.70. Applied shear force vs. slip relations for sand-lightweight slate specimens; with ρ = 0.022

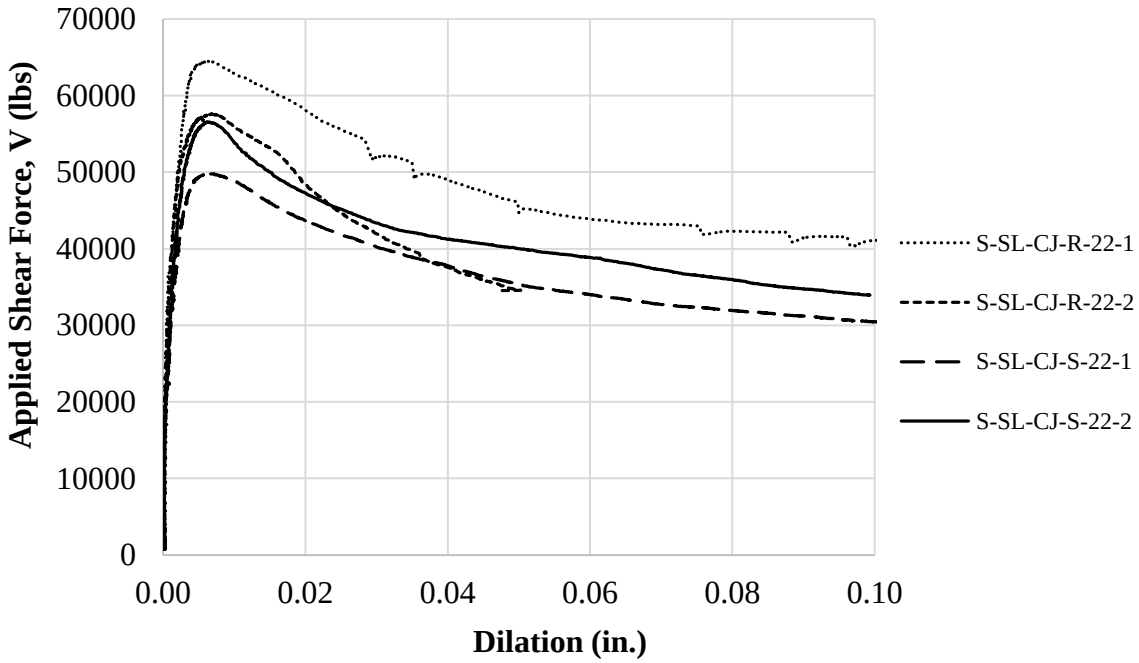

Figure 3.71. Applied shear force vs. interface dilation relations for sand-lightweight slate specimens; ρ = 0.022

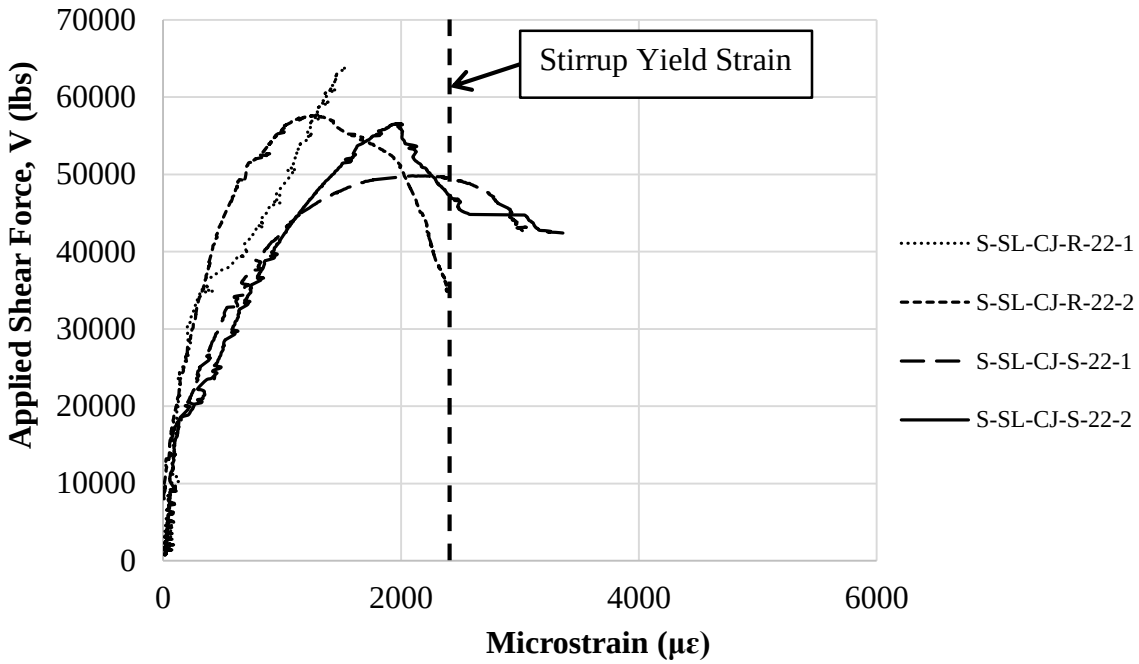

Figure 3.72. Applied shear force vs. interface steel strain for sand-lightweight slate specimens; $\rho = 0.022$

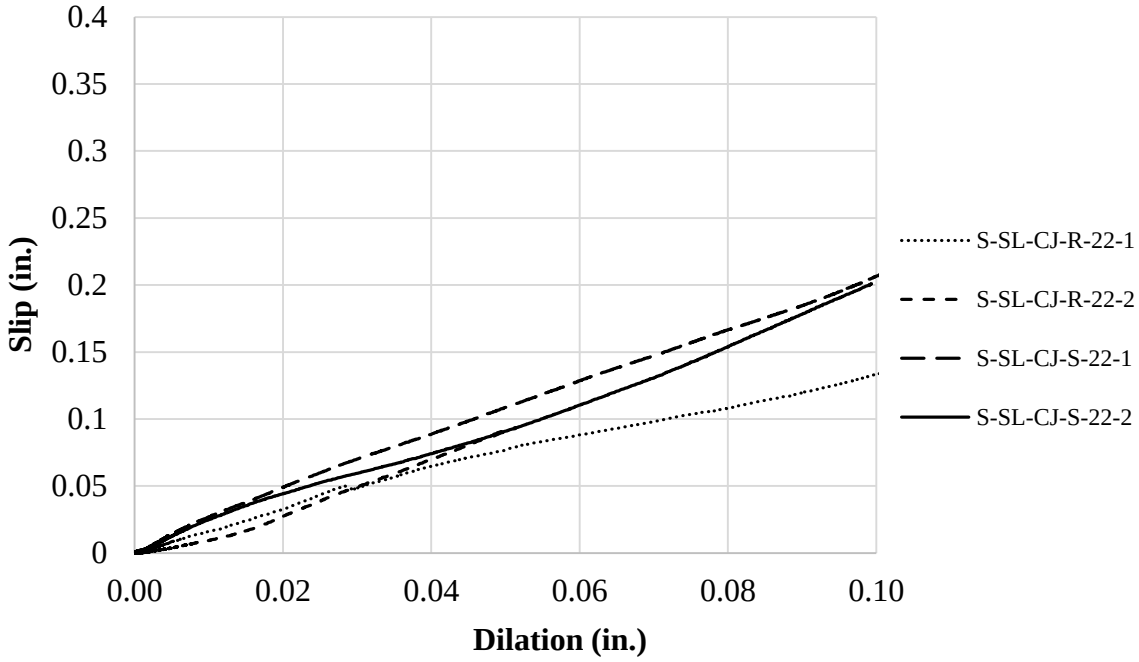

Figure 3.73. Slip vs. dilation for sand-lightweight slate specimens; $\rho = 0.022$

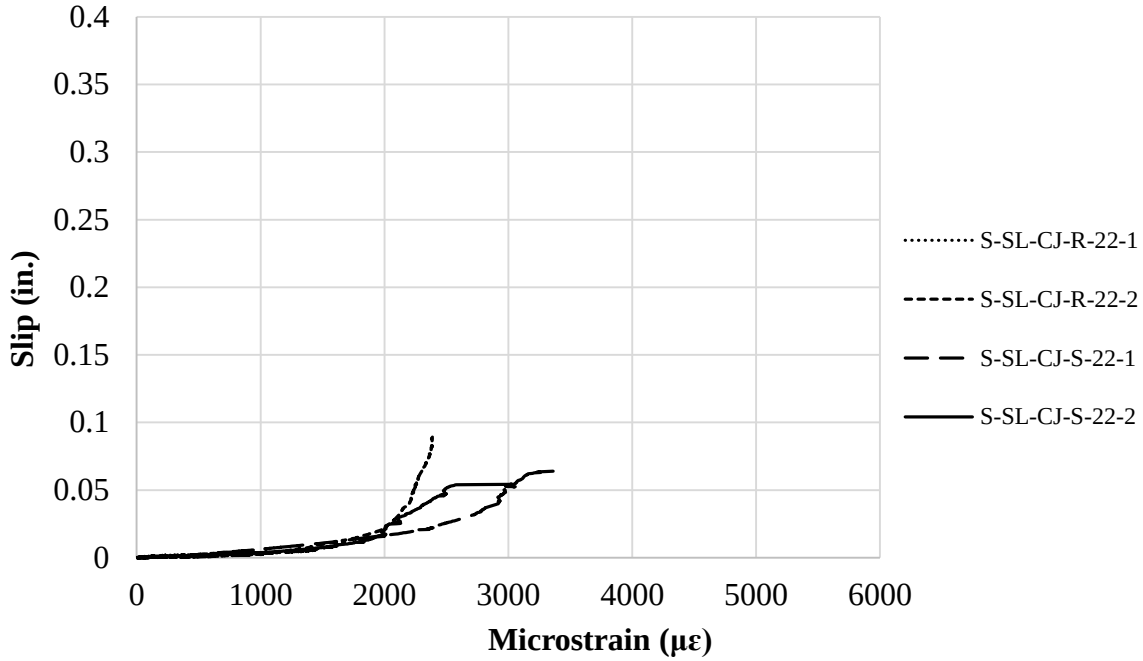

Figure 3.74. Slip vs. interface steel strain for sand-lightweight slate specimens; ρ = 0.022

4. ANALYSIS AND DISCUSSION

4.1. INTRODUCTION

This section contains the analysis and discussion of the results presented in Section 3.6. The general behavior of the specimens in terms of cracking, applied shear force vs. slip relations, and applied shear force vs. interface strain relations are discussed in Section 4.2. The influence of aggregate type, interface condition, and reinforcement ratio on the test results is summarized in Section 4.3. A comparison of shear strengths predicted by current design provisions to the results of this study is presented in Section 4.4. Section 4.5 contains an assessment of the test data in relation to the previous studies which are summarized in Section 2.4.

4.2. GENERAL BEHAVIOR

4.2.1. Cracking. The cracking behavior of specimens with lower reinforcement ratios (ρ = 0.009 and ρ = 0.013) differed from that of the specimens with higher reinforcement ratios (ρ = 0.017 and ρ = 0.022). As shown in Figure 4.1, most of the specimens with lower reinforcement ratios had clearly defined cracks along the shear plane with smaller flexural cracks horizontally across the front face of the specimen and small splitting cracks inside the cavity beneath the top flange. The flexural and splitting cracks are not associated with the shear failure, and the applied shear force, slip, strain, and dilation responses as well as the real-time plots from Section 3.6 indicate that these specimens failed predominately due to shear along the intended shear plane, not flexure or splitting. Specimens with higher reinforcement ratios had more splitting and flexural cracks that were significantly wider than those of the specimens with smaller reinforcement ratios, but most of these specimens still failed in shear (Figure 4.2). As previously discussed in full detail in Section 3.6.1, it was determined that Specimens S-CL-CJ-R-17-1, S-CL-CJ-R-17-2, S-CL-CJ-R-22-1, S-CL-CJ-R-22-2, S-CL-CJ-S-22-1, and S-CL-CJ-S-22-2 failed due to splitting of the concrete. This cracking pattern is shown in Figure 4.3.

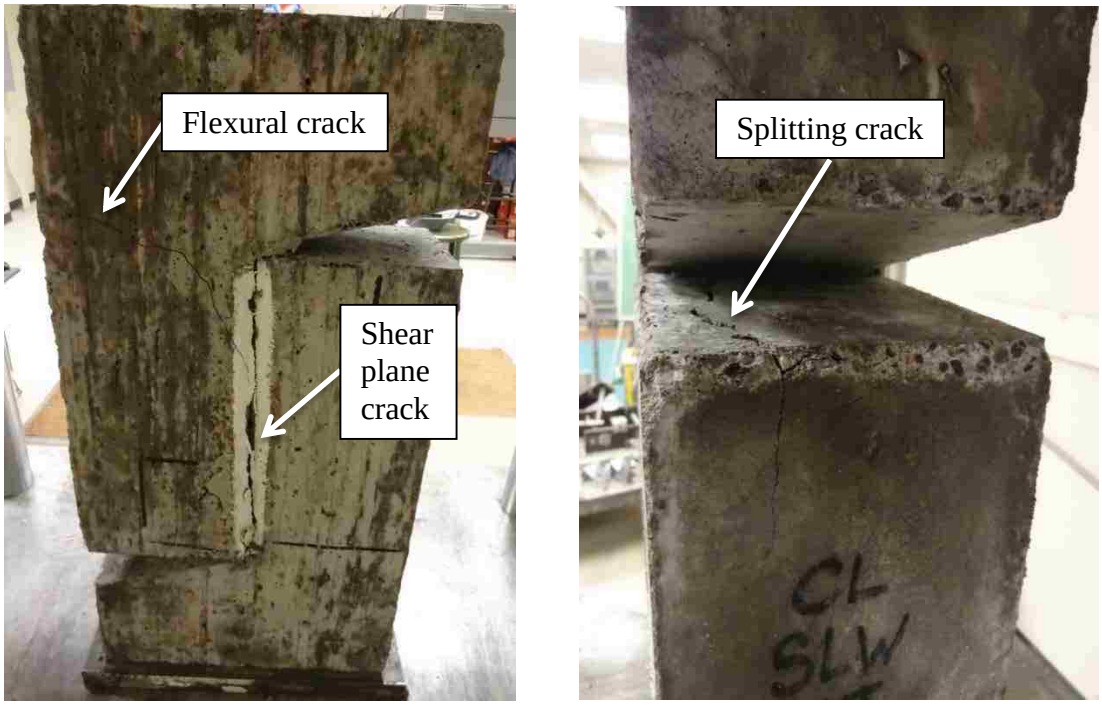

Figure 4.1. Typical cracking of specimens with lower reinforcement ratios; Specimens S-CL-CJ-R-13-2 (left) and S-CL-CJ-S-13-2 (right) shown

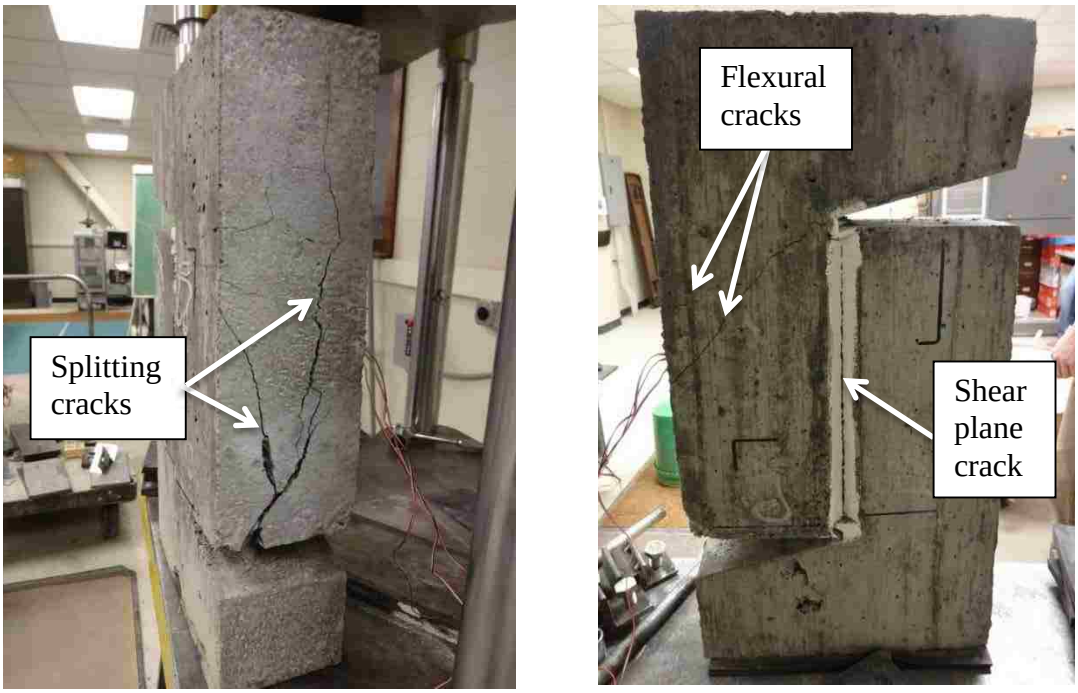

Figure 4.2. Typical cracking of specimens with higher reinforcement ratio that failed in shear along the shear plane; specimen S-SL-CJ-R-22-1 shown

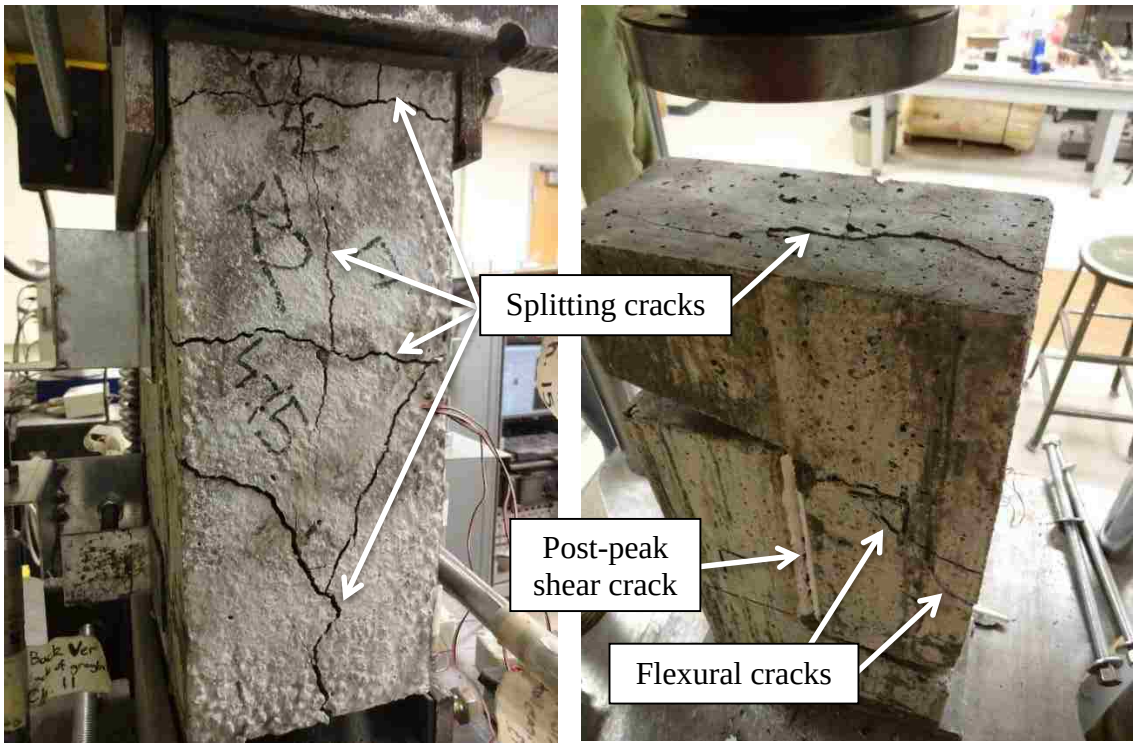

Figure 4.3. Typical cracking due to concrete splitting failure: side face (left) and top/back face (right); specimen S-CL-CJ-R-17-2 shown

Previous studies discuss diagonal tension cracks forming across the shear plane at angles between 15 to 50 degrees, and ranging from 1 to 3 in. long. The reinforcement ratio used in these studies ranged from ρ = 0.003 to ρ = 0.019 (Mattock and Hawkins 1972), or ρ = 0.000 to ρ = 0.026 (Mattock et al. 1976), or ρ = 0.004 to ρ = 0.015 (Kahn and Mitchell 2002). A vertical crack eventually formed along the shear plane which connected these diagonal cracks. This behavior was noted by Mattock and Hawkins (1972) as well as Mattock et al. (1976) for uncracked monolithic specimens. Kahn and Mitchell (2002) also described this behavior occurring for both uncracked monolithic and cold-joint specimens. These diagonal tension cracks were not observed for any specimens in this testing program.

The roughened and smooth specimens had similar values of dilation at the peak applied load (Table 4.2), but the cracks along the shear plane of the roughened specimens appeared jagged when compared to smooth interface specimens at the conclusion of

testing (Figure 4.4). Spalling of concrete cover occurred for some specimens, particularly for those which failed due to concrete splitting. In some instances, this spalling caused detachment of the aluminum brackets which held the LVDTs.

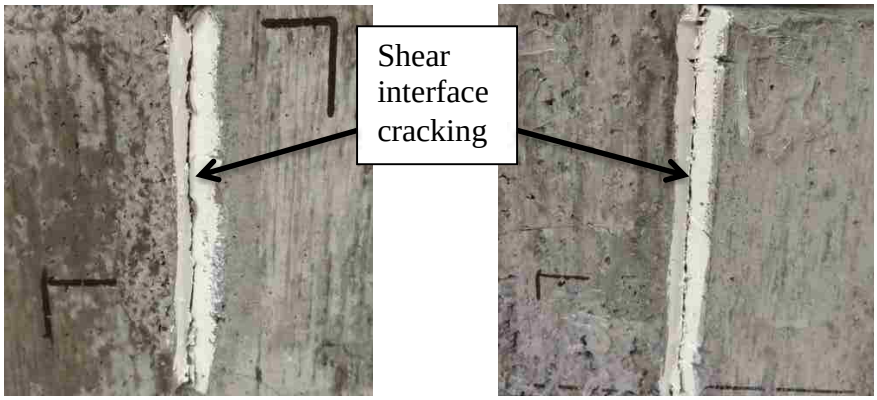

Figure 4.4. Typical shear cracks of specimens with roughened (left) and smooth interfaces (right); specimens S-CL-CJ-R-13-1 (left) and S-SL-CJ-S-22-S (right) shown

4.2.2. Applied Shear Force – Slip Relations. Figures 3.30, 3.35, 3.41, 3.46, 3.51, 3.56, 3.62, and 3.70 show the applied shear force vs. slip relations for the sand-lightweight clay and sand-lightweight slate specimens tested in this study. These figures follow a general trend of an elastic region, then a softening behavior up to a peak in applied shear force, followed by a gentle decline in applied shear force until it levels off to a constant value in which slip continues to increase. The elastic region is linear, and its slope seems to be unaffected by shear plane interface condition. The peak applied shear force, however, tends to be higher for specimens with a roughened interface as compared to specimens of similar aggregate type and reinforcement ratio having a smooth interface. The peak applied shear force occurred at levels of slip ranging from 0.004 in. to 0.021 in. After the peak shear force is achieved, the roughened specimens also have a steeper drop-off in applied shear force as compared to smooth specimens. This quasi-brittle behavior was also noted in Shaw (2013). As a general trend, the

roughened specimens had similar residual shear strengths V_{ur} to the specimens with a smooth interface. Further discussion of the influence of shear plane interface condition is presented in Section 4.3.2.

4.2.3. Applied Shear Force – Interface Steel Strain Relations. The applied shear force vs. interface steel strain plots are presented in Figures 3.32, 3.37, 3.43, 3.48, 3.53, 3.58, 3.64, and 3.72. As previously noted, each of these plots represents the data from one strain gage, even if all three gages from a specimen were in working order. This ensured that multiple yield plateaus were not exhibited on a single graph as would occur if all three stain gage readings had been averaged. In order to determine the applied shear stress at which cracking occurred in each specimen, graphs were made of applied shear stress v versus interface steel strain. Applied shear stress is the applied shear force divided by area of shear plane ($v = V/A_{cr}$). These graphs reveal a plateau which corresponds to the initiation of shear plane cracking and contribution of concrete cohesion as shown in Figure 4.5. For specimens that failed in shear along the shear plane, this first cracking stress v_{cr} occurred at values between 305 psi and 390 psi for smooth interface specimens, and values between 495 psi and 680 psi for specimens with a roughened interface. Table 4.1 and Figure 4.6 show these values averaged for each series $v_{cr,avg}$, including those specimens which failed due to splitting. Each series shown in Figure 4.6 has higher $v_{cr,avg}$ values for roughened interface specimens versus smooth interface specimens of the same aggregate type and reinforcement ratio.

It is worth noting in Table 4.1 and Figure 4.6 that the specimens with concrete splitting failures had some of the highest values of average interface cracking stresses v_{cr}. Since these values represent cracking of the interface rather than cracking in other areas of the specimen, it is possible that the first cracks to form on these specimens were splitting cracks. Since the splitting cracks were perpendicular to the strain gages, the initiation of splitting cracks was not able to be monitored. Furthermore, as testing continued, shear cracks most likely formed on the intended shear plane at higher levels of applied shear force than would normally occur if the specimen were free of splitting cracks. Thus, the shear cracks were incorrectly recorded as being the initial cracks on these specimens.

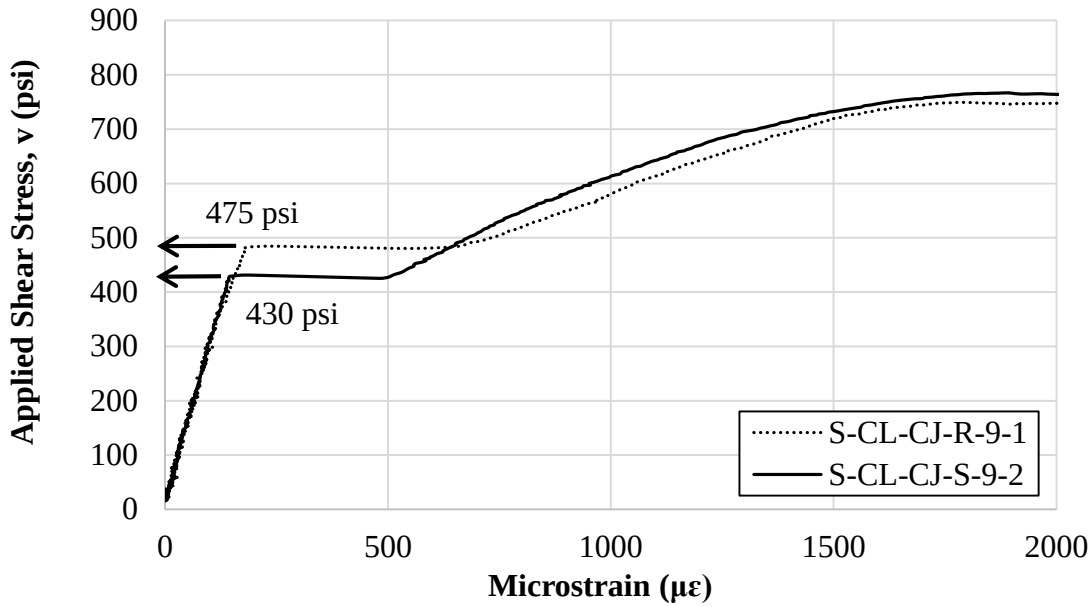

Figure 4.5. Typical shear stress-interface reinforcement strain plots for the determination of interface cracking stress (Specimens S-CL-CJ-R-9-1 and S-CL-CJ-S-9-2 shown)

Table 4.1. Average Interface Cracking Stress $v_{cr,avg}$ for All Series

Aggregate Type	Reinforcement Ratio	Interface Condition	$v_{cr,avg}$ (Cohesion)	Ratio R / S
Clay	0.009	Rough	495	1.28
		Smooth	388	
	0.013	Rough	500	1.57
		Smooth	318	
	0.017	Rough	645*	1.73
		Smooth	373	
	0.022	Rough	715*	1.15
		Smooth	623*	
Slate	0.009	Rough	645	2.06
		Smooth	313	
	0.013	Rough	625	2.06
		Smooth	303	
	0.017	Rough	680	2.01
		Smooth	338	
	0.022	Rough	560	1.44
		Smooth	388	

*Specimens in this series failed predominantly due to concrete splitting

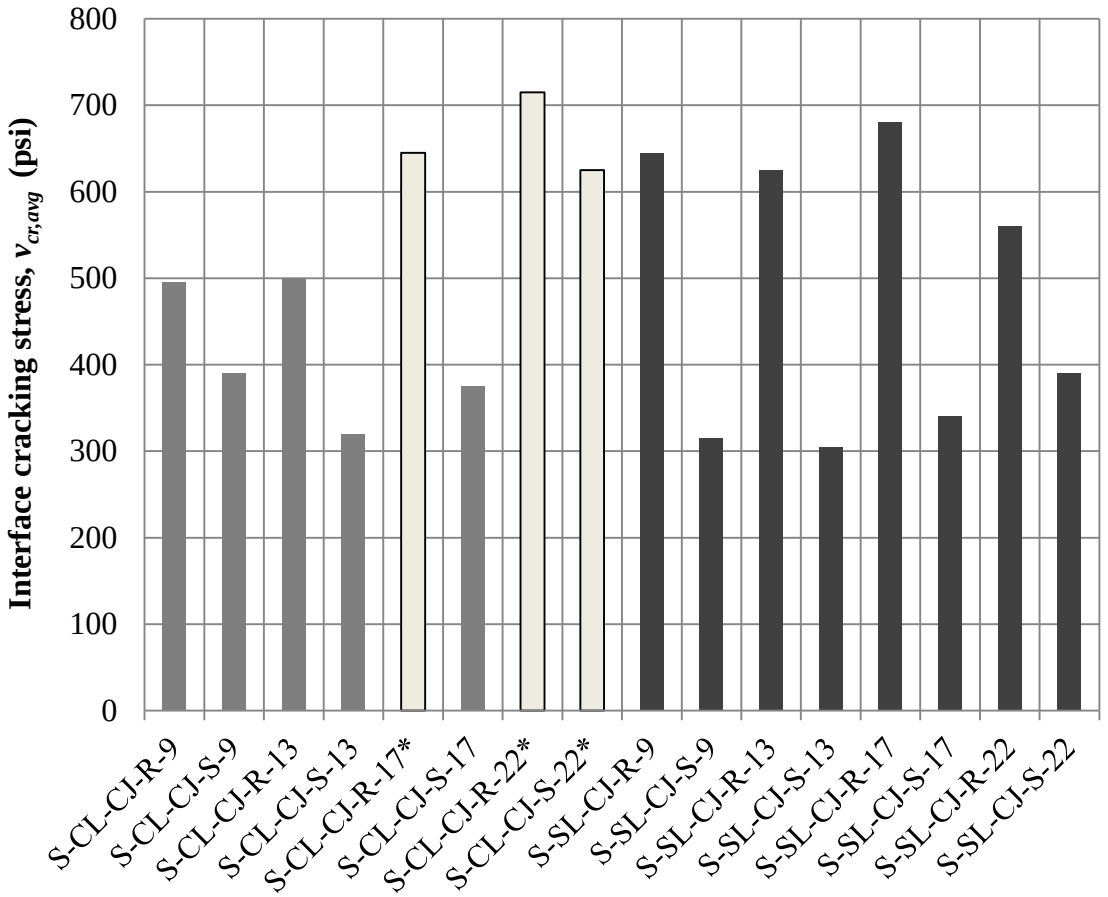

*Specimens in this series failed predominantly due to concrete splitting

Figure 4.6. Average interface cracking stress, $v_{cr,avg}$ for all series

4.3. INFLUENCE OF TEST VARIABLES

This section presents an analysis of the data presented in Section 3.6 in terms of the variables of this testing program. Section 4.3.1 discusses the effect of aggregate type on the shear transfer strength v_u of the specimens. Section 4.3.2 covers the effect of shear interface condition on shear transfer strength. Lastly, Section 4.3.3 analyzes of the effect of varying the reinforcement ratio ρ. The test results contained in Table 4.2 are the basis of this analysis.

Table 4.2. Summary of Testing Results

Specimen ID	f'_c at test day (psi)	V_u (lbs)	v_u[1] (psi)	$v_{u,\,avg}$ (psi)	Slip at V_u (in.)	Dilation at V_u (in.)	V_{ur}[2] (lbs)	v_{ur}[1] (psi)	$v_{ur,\,avg}$ (psi)	$\left(\frac{v_u}{v_{ur}}\right)_{avg}$ (psi)
S-CL-CJ-R-9-1	4770	37060	749	808	0.012	0.007	ND	ND	ND	ND
S-CL-CJ-R-9-2		42910	867		0.008	0.005	ND	ND		
S-CL-CJ-S-9-1		31920	645	706	0.012	0.005	23610	477	519	1.36
S-CL-CJ-S-9-2		37960	767		0.009	0.005	27730	560		
S-CL-CJ-R-13-1	4640	50790	1026	987	0.007	0.006	31310	633	651	1.51
S-CL-CJ-R-13-2		46890	947		0.015	0.005	33180	670		
S-CL-CJ-S-13-1		41010	828	823	0.015	0.006	31030	627	600	1.37
S-CL-CJ-S-13-2		40470	818		0.018	0.007	28400	574		
S-CL-CJ-R-17-1	4550	51240	1035	1090	0.004	0.004	37420	756	751	1.45
S-CL-CJ-R-17-2		56660	1145		0.009	0.005	36920	746		
S-CL-CJ-S-17-1		43140	872	930	0.012	0.005	ND	ND	667	1.39
S-CL-CJ-S-17-2		48930	988		0.013	0.006	33040	667		
S-CL-CJ-R-22-1	4790	56720	1146	1111	0.008	0.003	ND	ND	670	1.66
S-CL-CJ-R-22-2		53230	1075		0.017	0.006	33250	672		
S-CL-CJ-S-22-1		52400	1059	1061	0.01	0.004	40300	814	815	1.30
S-CL-CJ-S-22-2		52590	1062		0.005	0.003	ND	ND		
S-SL-CJ-R-9-1	5380	49340	997	1008	0.009	0.007	30560	617	617	1.63
S-SL-CJ-R-9-2		50480	1020		0.007	0.006	ND	ND		
S-SL-CJ-S-9-1		26950	544	601	0.021	0.007	23040	465	529	1.14
S-SL-CJ-S-9-2		32500	657		0.012	0.006	29300	592		
S-SL-CJ-R-13-1	5570	63170	1276	1238	0.013	0.008	ND	ND	735	1.69
S-SL-CJ-R-13-2		59370	1199		0.013	0.009	36360	735		
S-SL-CJ-S-13-1		39490	798	892	0.017	0.007	30510	616	700	1.27
S-SL-CJ-S-13-2		48770	985		0.016	0.008	38770	783		
S-SL-CJ-R-17-1	4950	62380	1260	1288	0.012	0.008	ND	ND	ND	ND
S-SL-CJ-R-17-2		65150	1316		0.009	0.007	ND	ND		
S-SL-CJ-S-17-1		47640	962	957	0.018	0.007	ND	ND	694	1.38
S-SL-CJ-S-17-2		47120	952		0.019	0.007	34330	694		
S-SL-CJ-R-22-1	5000	64460	1302	1233	0.011	0.006	39640	801	801	1.54
S-SL-CJ-R-22-2		57590	1163		0.006	0.007	ND	ND		
S-SL-CJ-S-22-1		49810	1006	1074	0.018	0.006	32600	659	694	1.55
S-SL-CJ-S-22-2		56530	1142		0.016	0.006	36130	730		

[1]Shear stresses v_u and v_{ur} are defined as the applied shear load divided by the area of the shear plane, 49.5 in^2.

[2]Residual load, V_{ur}, is defined as the load at 0.15 in. of slip. Some values for V_{ur} and v_{ur} are denoted as ND (no data) because the slip did not reach a value of 0.15 in. before the test was concluded.

Values reported for each specimen in Table 4.2 include: compressive strength at test day f'_c, peak (ultimate) applied shear force V_u, slip and dilation at V_u, and residual shear force V_{ur} (which is the applied shear force at a value of 0.15 in. of slip). Peak (ultimate) applied shear stress v_u and residual shear stress v_{ur} are also included in Table 4.2 and were calculated by dividing the respective shear force by the area of the shear interface A_{cr}. To help enable the comparisons, the average values in each series for v_u, v_{ur}, and the ratio v_u/v_{ur} are also reported.

4.3.1. Effect of Lightweight Aggregate Type. This testing program included two types of lightweight aggregate: expanded clay, and expanded shale. Properties of these two aggregates were discussed in Section 3.3.1. This section addresses the effect of aggregate type on the shear strength of the specimens in this study. To isolate this parameter, specimens with the same interface condition and reinforcement ratio were compared. Figures 4.7 through 4.14 show the applied shear force versus slip relations of similar slate and clay specimens.

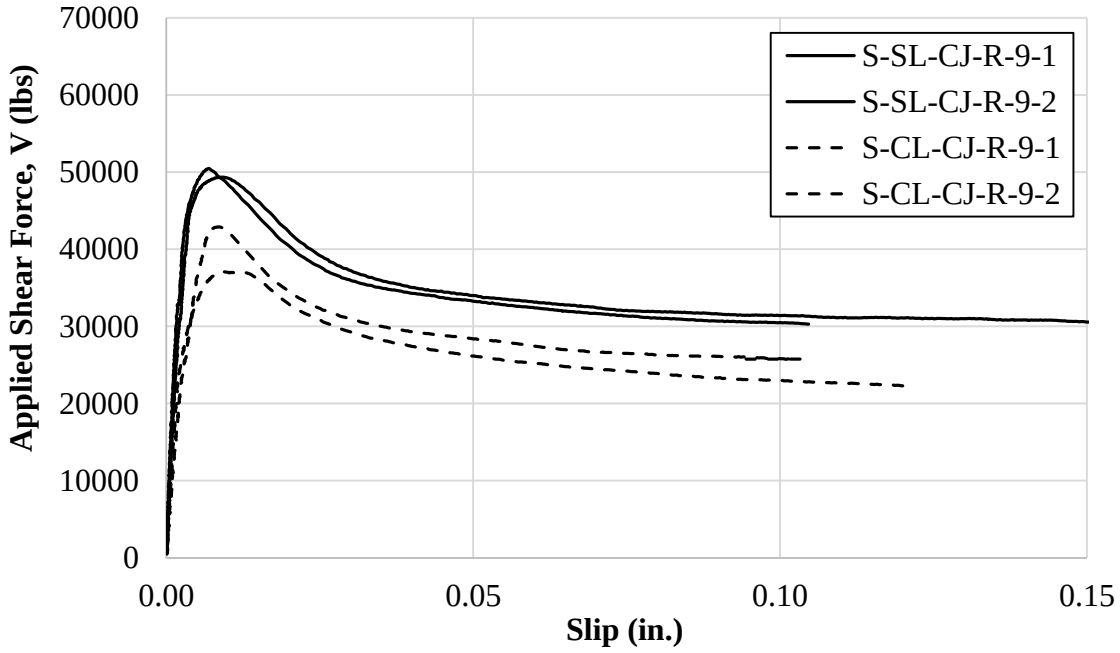

Figure 4.7. Effect of lightweight aggregate type for roughened specimens with ρ = 0.009

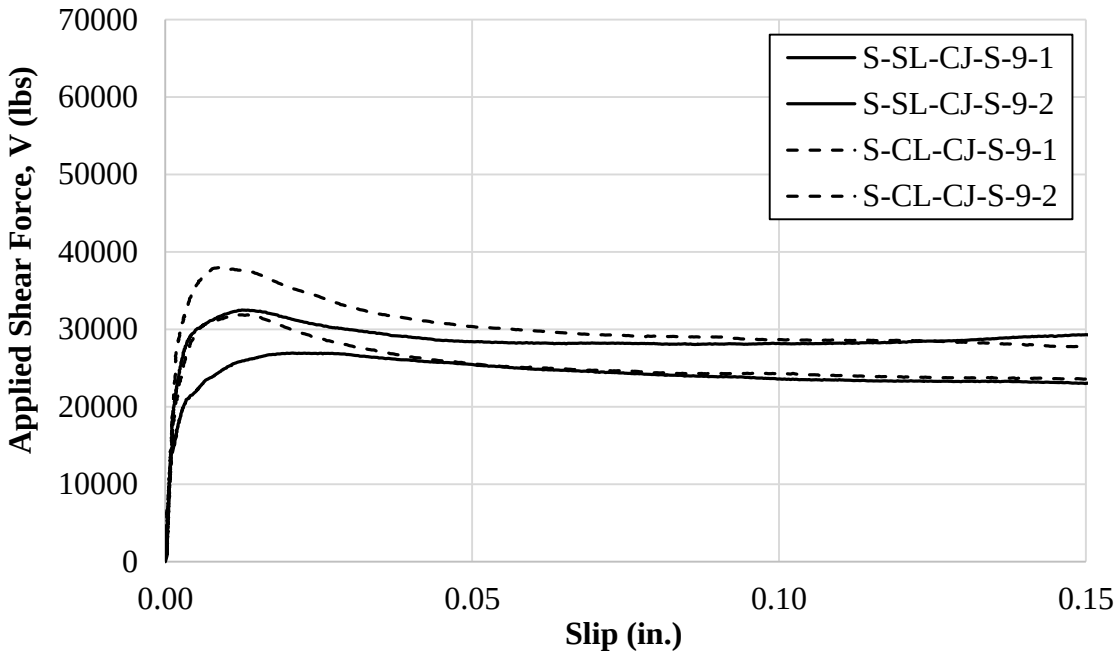

Figure 4.8. Effect of lightweight aggregate type for smooth specimens with ρ = 0.009

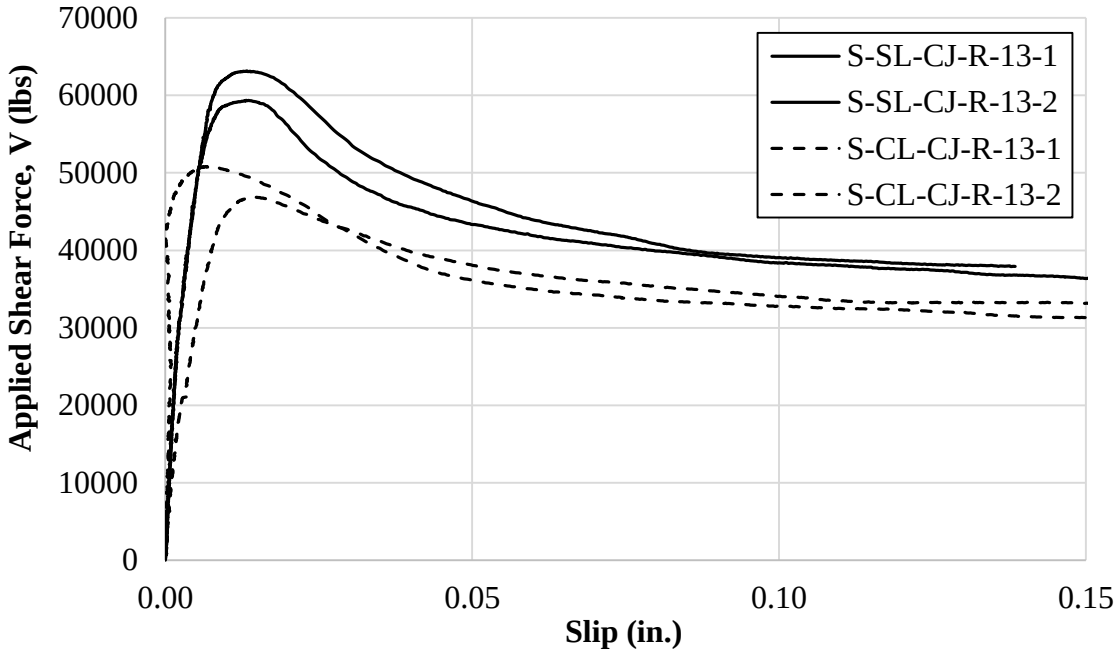

Figure 4.9. Effect of lightweight aggregate type for roughened specimens with ρ = 0.013

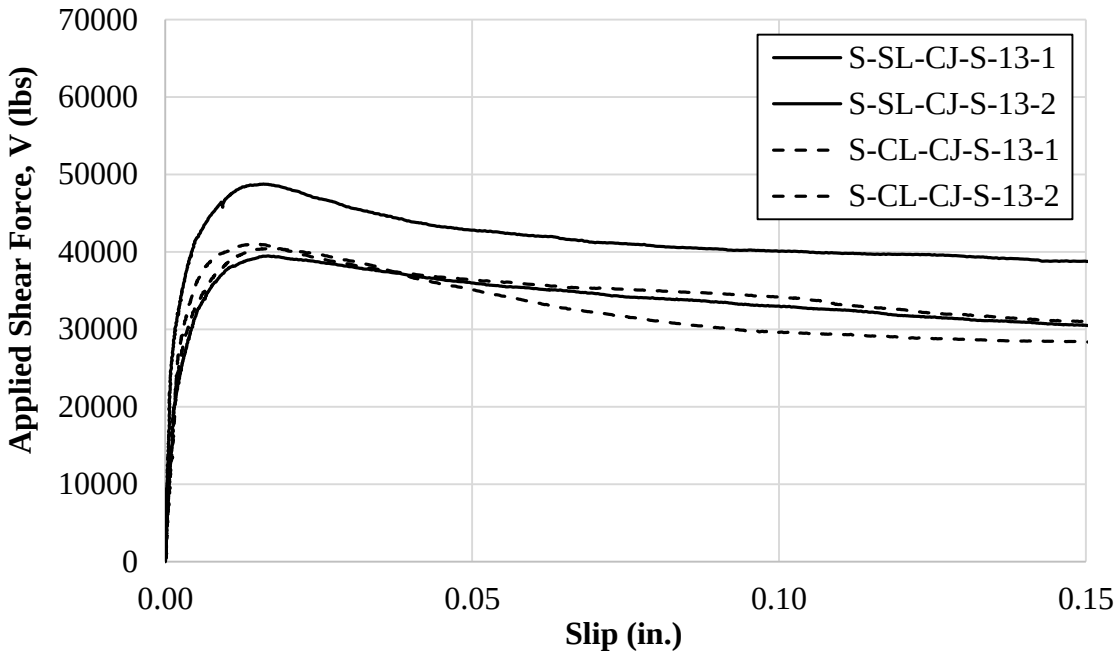

Figure 4.10. Effect of lightweight aggregate type for smooth specimens with ρ = 0.013

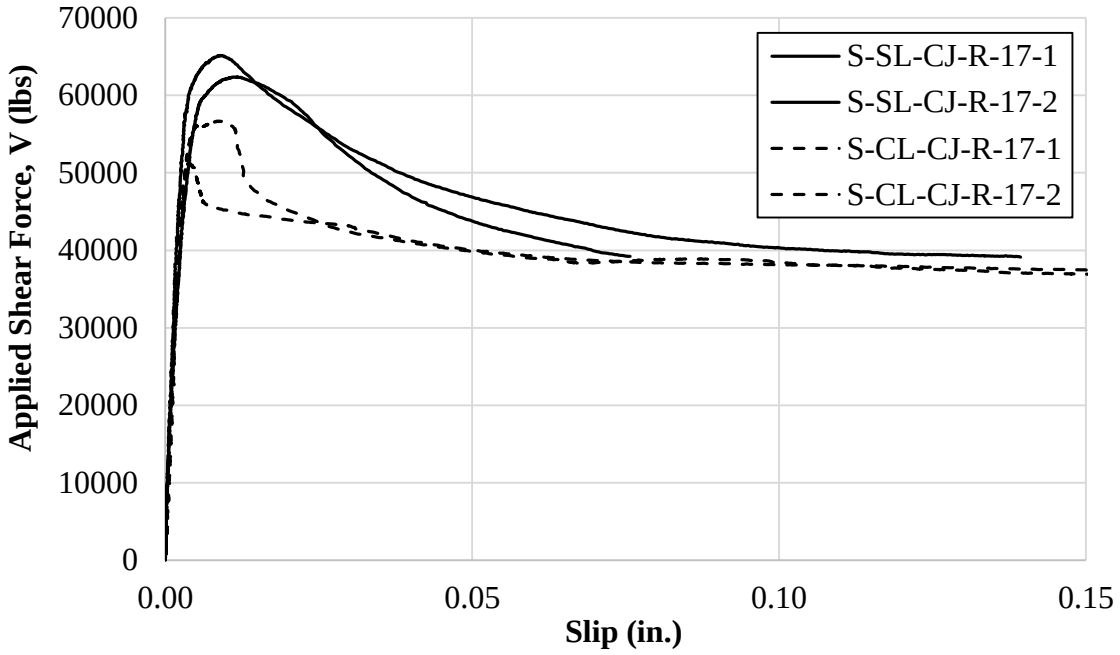

Figure 4.11. Effect of lightweight aggregate type for roughened specimens with ρ = 0.017

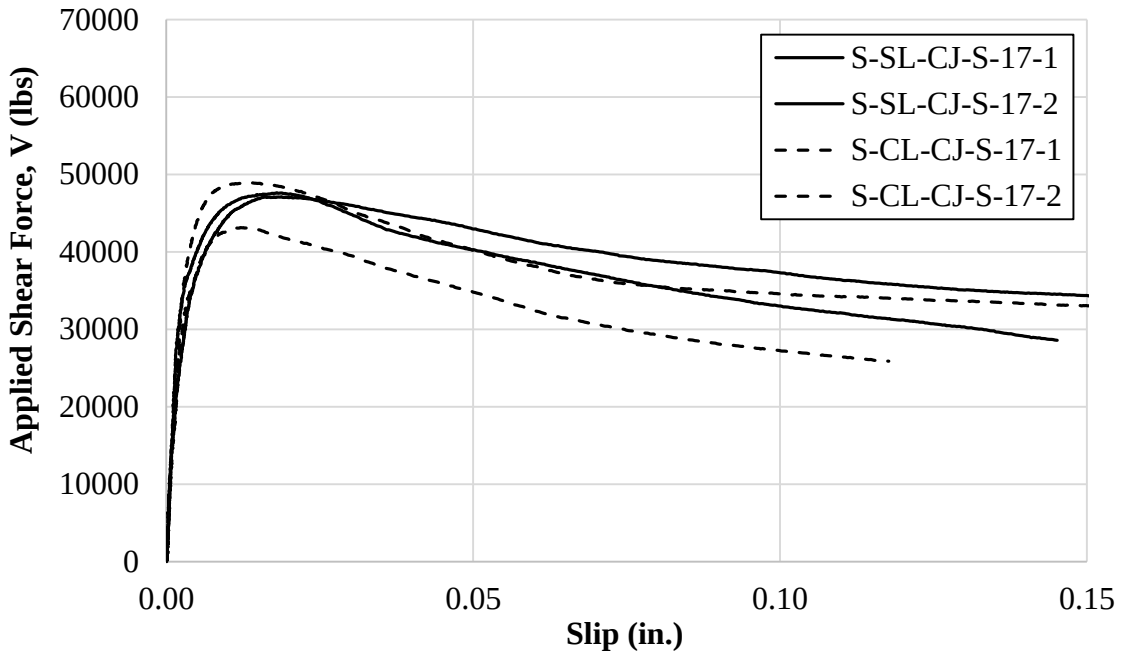

Figure 4.12. Effect of lightweight aggregate type for smooth specimens with ρ = 0.017

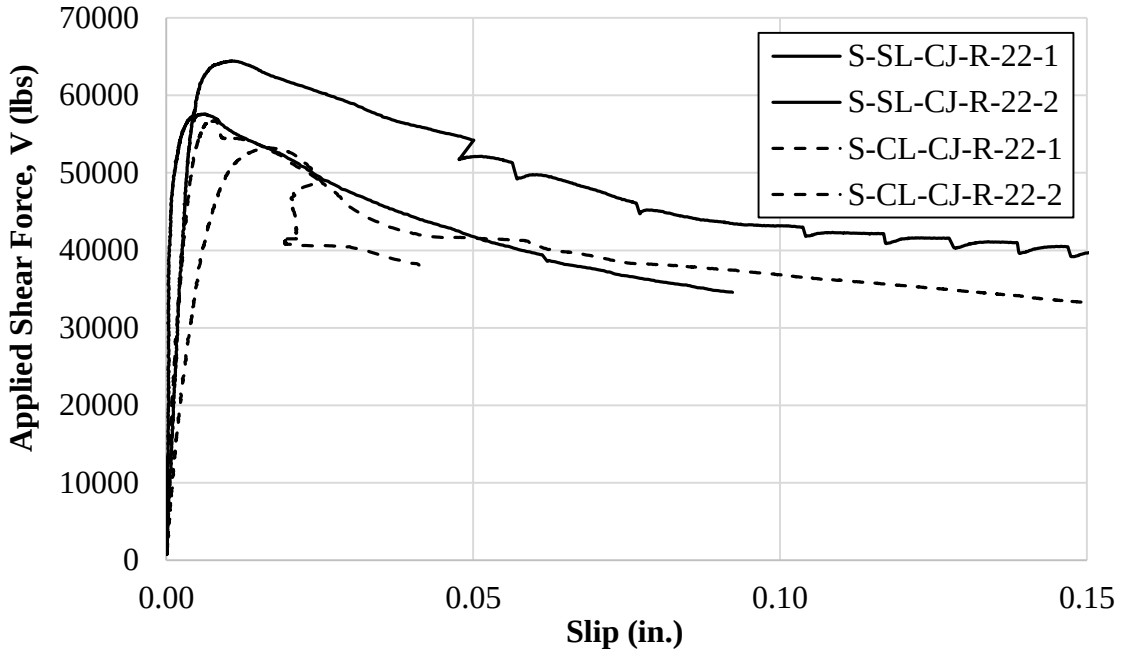

Figure 4.13. Effect of lightweight aggregate type for roughened specimens with ρ = 0.022

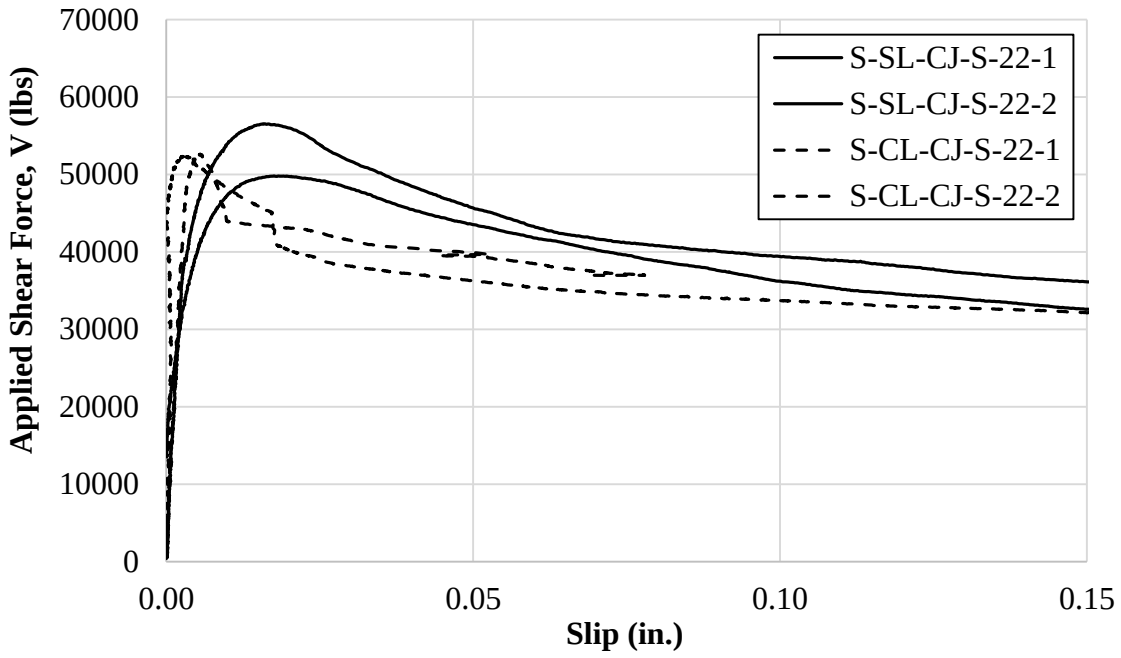

Figure 4.14. Effect of lightweight aggregate type for smooth specimens with ρ = 0.022

Table 4.3 shows the average ultimate shear stress $v_{u,avg}$ for each series of this study. Interestingly, the average shear transfer strength of all clay specimens with a smooth interface (880 psi) is nearly equal to the average shear transfer strength of all slate specimens with a smooth interface (881 psi). This suggests that shear transfer strength of specimens with a smooth interface is not affected by aggregate type. This idea is supported by Table 4.4, which shows shale sand-lightweight data from Shaw (2013) compared with the data from this study for specimens of ρ = 0.013, with nominal compressive strengths of 5,000 psi and cold-joint construction with a smooth interface. Among the three aggregate types listed in this table, the range of shear strength is not significant: v_u = 757 psi to 892 psi. Table 4.4 also suggests that for specimens with a smooth interface, increases in shear strength have a direct correlation to increases in compressive strength and splitting tensile strength.

On the other hand, slate sand-lightweight specimens with a roughened interface show a greater increase in average shear strength as compared to similar clay specimens (Table 4.3). Interestingly, in Table 4.4, the average shear strength of the shale specimens

from Shaw (2013) was not the lowest of the three aggregate types when a roughened interface was considered. Instead, the clay sand-lightweight specimens had the lowest average shear strength. This suggests that shear strength did not have a direct correlation to compressive strength and splitting tensile strength for the roughened specimens, as it did with the smooth specimens. A possible reason for this is that the increased roughness of the interface created a higher level of friction (as compared to the smooth specimens) which outweighed the influence of the compressive strength and tensile strength of the concrete.

Table 4.3. Average Ultimate Shear Stress $v_{u,avg}$ for Each Specimen Series

Reinforcement Ratio	**Smooth Interface**				**Roughened Interface**			
	Clay (psi)	Slate (psi)	% Diff	Slate/Clay % Increase	Clay (psi)	Slate (psi)	% Diff	Slate/Clay % Increase
0.009	706	601	16	-15	808	1008	22	25
0.013	823	892	8	8	987	1238	23	25
0.017	930	957	3	3	1090*	1288	17	18
0.022	1061	1074*	1	1	1111*	1233	10	11
Average	880	881			999	1192		

*Specimens in this series failed predominantly due to concrete splitting

Also worth noting in Table 4.3 is that the percent increase in shear strength of the slate over the clay reduces as reinforcement ratio increases (with the exception of the clay and slate specimens with a smooth interface and $\rho = 0.009$). For example, the roughened specimens with $\rho = 0.009$ had a percent increase in shear strength of 25% for slate compared to clay aggregate, while the percent increase was only 11% for roughened specimens with $\rho = 0.022$. This result suggests that shear strength relies more heavily on the amount of shear reinforcement than aggregate type as reinforcement ratio increases.

Figure 4.15 shows a bar graph of the average ultimate shear stress $v_{u,avg}$ for all series. As a general trend, the average ultimate shear stress for the slate aggregate

specimens was higher than that of the clay aggregate specimens with a similar interface condition and reinforcement ratio, especially for the roughened interface specimens.

Table 4.4. Mechanical Properties for Various Sand-Lightweight Aggregate Concretes with $\rho = 0.013$

		Current Study[1]		Shaw, 2013[1]
		Slate SLW	**Clay SLW**	**Shale SLW**
Shear Strength $v_{u,avg}$ (psi)	**Smooth Interface**	892	823	757
	Rough Interface	1248	987	1117
Compressive Strength f'$_c$ (psi)		5570	4640	4550
Splitting Tensile Strength f$_t$ (psi)		570	360	320

[1]Specimens summarized in this table each had $\rho = 0.013$, had nominal compressive strengths of 5,000 psi, were constructed from sand-lightweight concrete, and were of cold-joint construction.

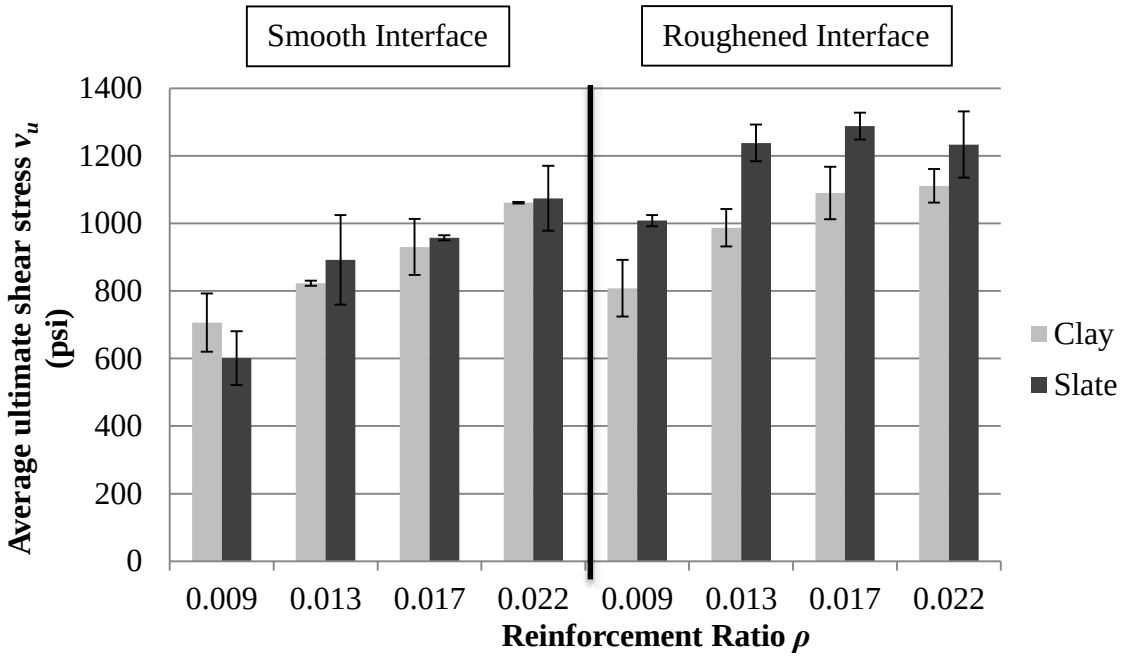

Figure 4.15. Effect of lightweight aggregate type on the average ultimate shear stress for each specimen series

However, there is one outlier in Figure 4.15; the S-CL-CJ-S-9 series had a higher average ultimate shear stress $v_{u,avg}$ than the S-SL-CJ-S-9 series. Even though the S-CL-CJ-S-9 series had a lower compressive strength (f'_c = 4,770 psi) than the S-SL-CJ-S-9 series (f'_c = 5,380 psi), the clay specimens still outperformed the similar slate specimens in terms of ultimate shear stress for ρ = 0.009. The S-CL-CJ-S-9 series also had a lower splitting tensile strength (f_t = 340 psi) than the S-SL-CJ-S-9 series (f_t = 595 psi). Therefore, the cause of this outlier is unknown. Figure 4.15 also shows the standard deviation of each specimen series in the form of error bars.

4.3.2. Effect of Interface Condition. All specimens in this thesis work were cast with a cold-joint along the shear plane. The shear plane interface was prepared in two ways; it was either troweled smooth, or intentionally roughened to a 0.25 in. amplitude. This section discusses the effect of interface condition on the shear transfer strength of specimens in this study. To isolate this parameter, specimens with the same aggregate type and reinforcement ratio were compared. Figures 4.16 through 4.23 are similar to those in Section 3.6, with the format changed for consistency with the rest of Section 4.3. Since all four specimens shown in the applied shear force vs. slip figures were constructed from the same batch of concrete, they each have the same concrete compressive strength f'_c. Therefore, it is not necessary to normalize the shear force.

In Figures 4.16 through 4.23 it is apparent that the average peak shear force of the roughened specimens of each series is higher than the corresponding smooth interface specimens with a similar aggregate type and reinforcement ratio. This is caused by the reduced aggregate interlock capacity of the smooth interface specimens. The initial slope of the applied shear force versus slip relations are the same for both smooth and roughened specimens because they have a similar concrete cohesion at the interface. Yet, as discussed in Section 4.2.3, the cracking stress v_{cr} of the smooth specimens is much lower than that of the roughened specimens. The reduction in aggregate interlock for the smooth specimens versus the roughened specimens causes the smooth specimens to crack at lower applied loads. Once the bond of the interface is lost, the smooth specimens must rely on dowel action and clamping force since aggregate interlock has been drastically decreased. This explains the lower shear strengths of the smooth specimens as compared to the roughened specimens and also their different applied shear force versus slip

behaviors. As shown in Figures 4.16 through 4.23, the roughened specimens behave in a more quasi-brittle manner than the smooth specimens. The residual shear force V_{ur} of the smooth specimens are very close to that of their peak shear force, whereas the applied shear force drops off sharply after the peak is achieved for the roughened specimens. Yet, these figures reveal that the values for residual shear force are very similar among roughened and smooth specimens of the same aggregate type and reinforcement ratio.

The average ultimate shear capacities are summarized in Table 4.5. The percent increase in average ultimate shear capacity from smooth interface specimens to roughened specimens for each aggregate type/reinforcement ratio range from 5% to 68% (including average shear capacities for specimens which failed due to concrete splitting). Overall, these percent increases are higher for the slate specimens than the corresponding clay specimens. Also, as discussed in Section 4.3.1, the difference in shear transfer strengths between specimens with a smooth versus a rough interface diminishes as reinforcement ratio increases. This trend is also shown in Table 4.5.

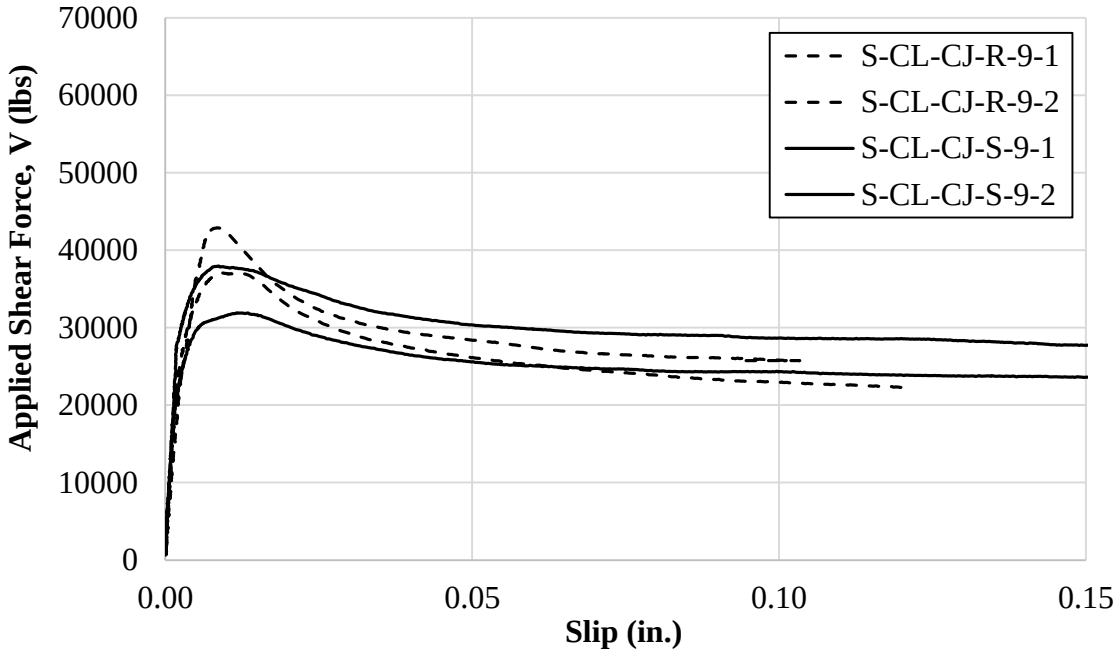

Figure 4.16. Effect of interface condition for clay specimens with ρ = 0.009

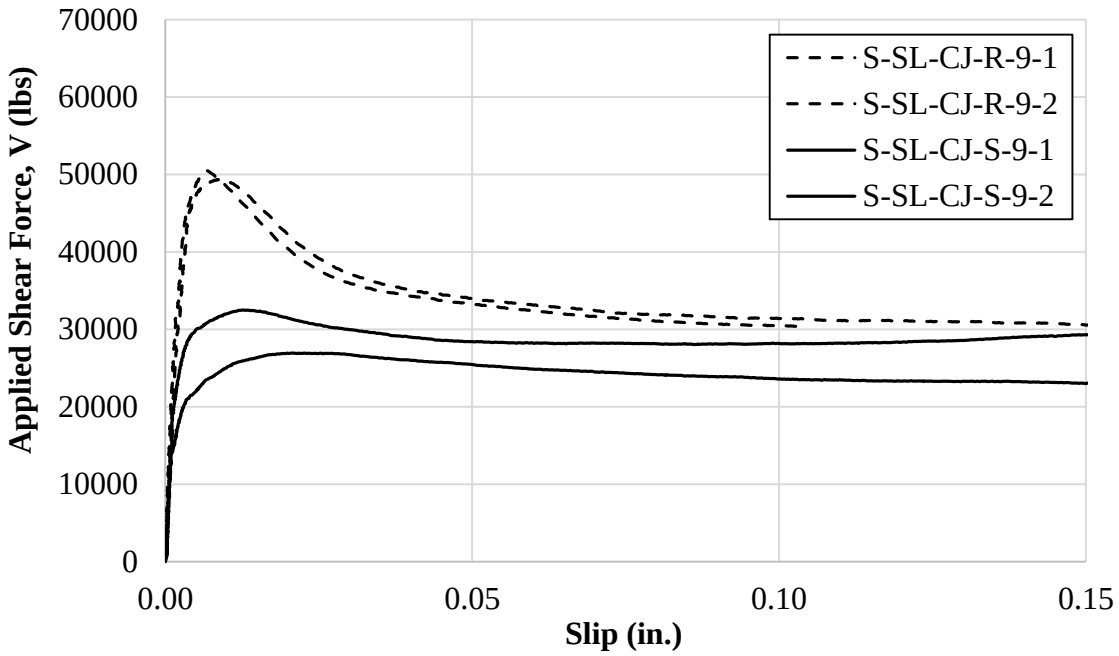

Figure 4.17. Effect of interface condition for slate specimens with ρ = 0.009

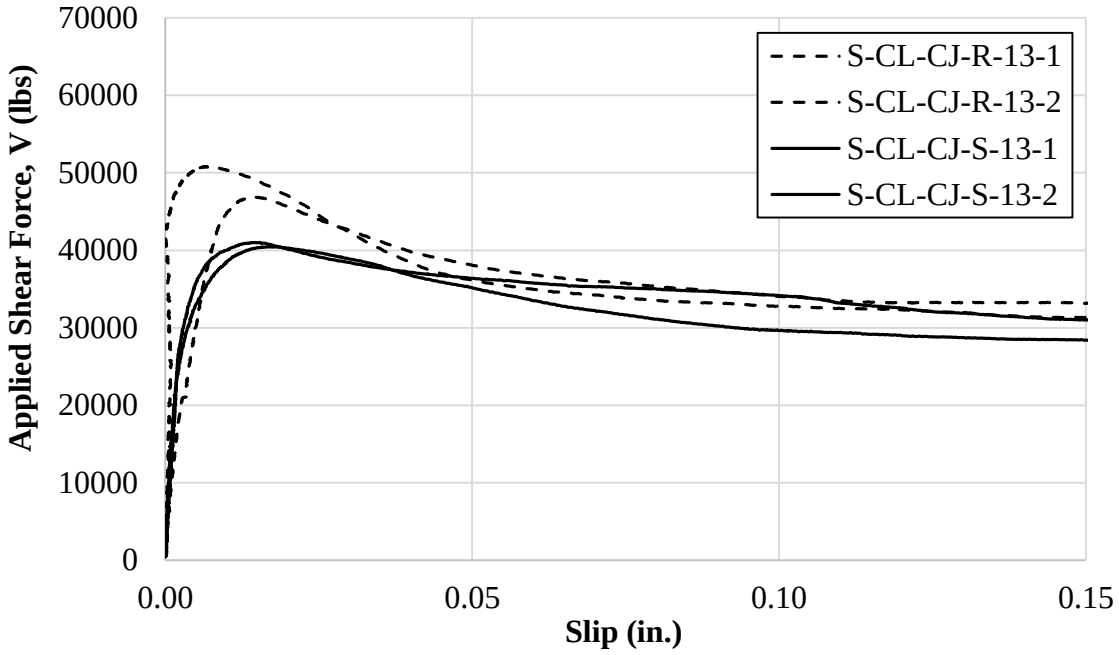

Figure 4.18. Effect of interface condition for clay specimens with ρ = 0.013

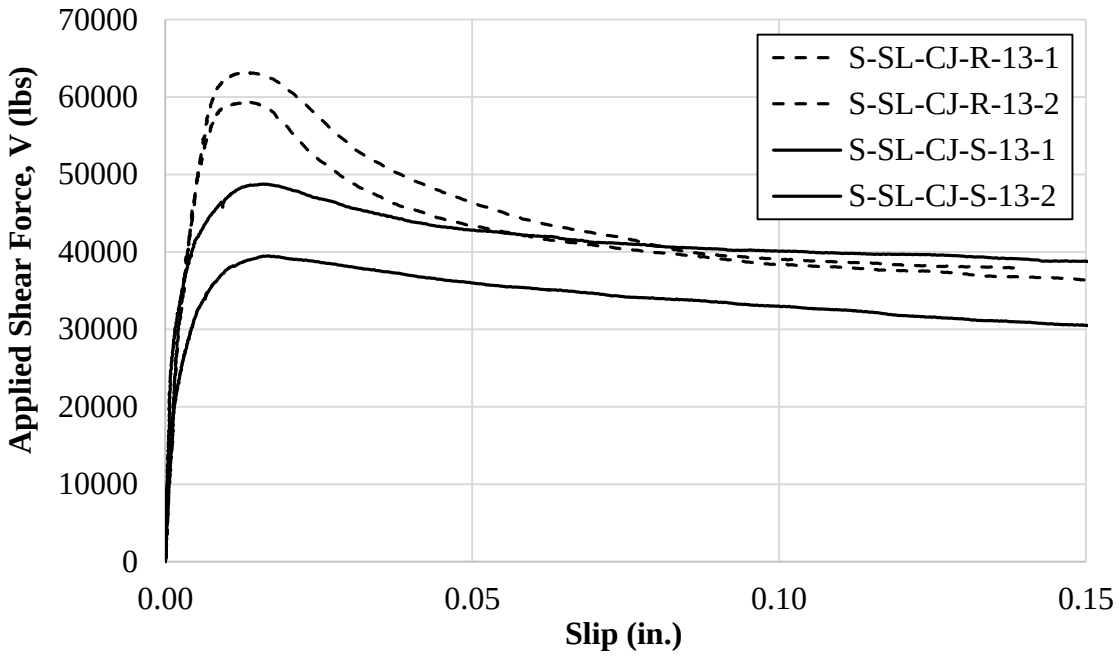

Figure 4.19. Effect of interface condition for slate specimens with ρ = 0.013

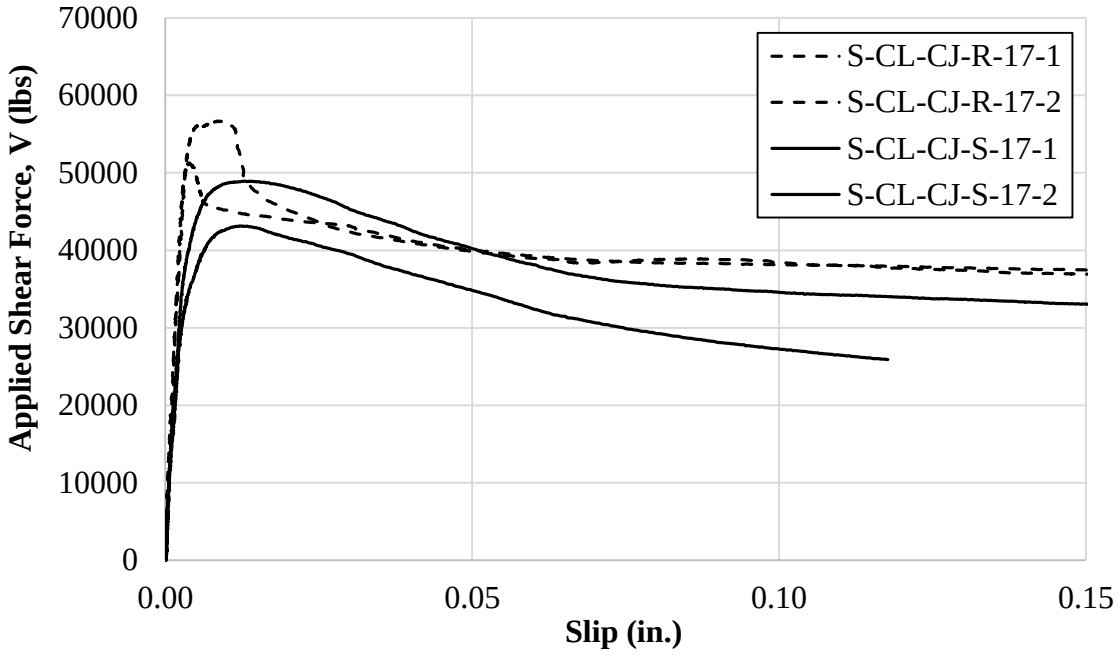

Figure 4.20. Effect of interface condition for clay specimens with ρ = 0.017

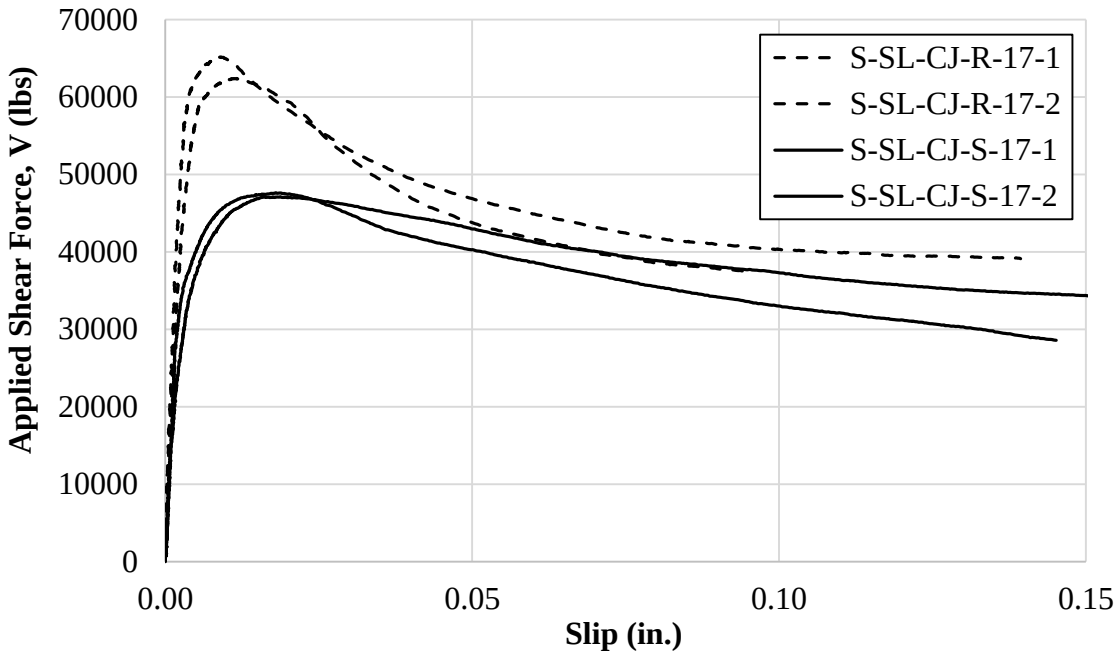

Figure 4.21. Effect of interface condition for slate specimens with ρ = 0.017

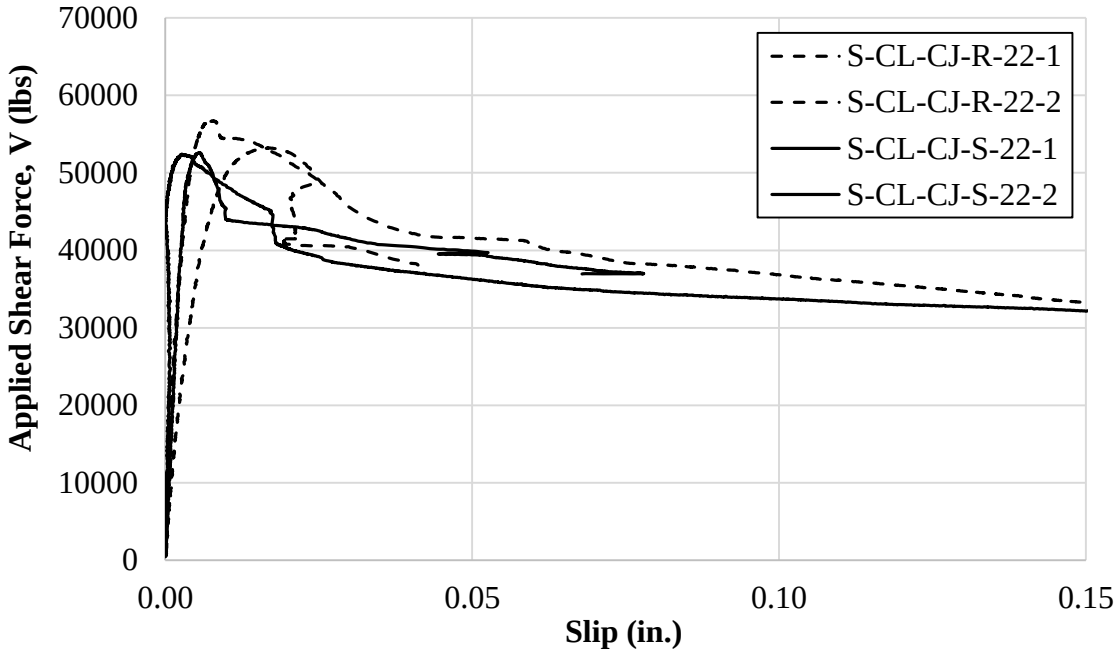

Figure 4.22. Effect of interface condition for clay specimens with ρ = 0.022

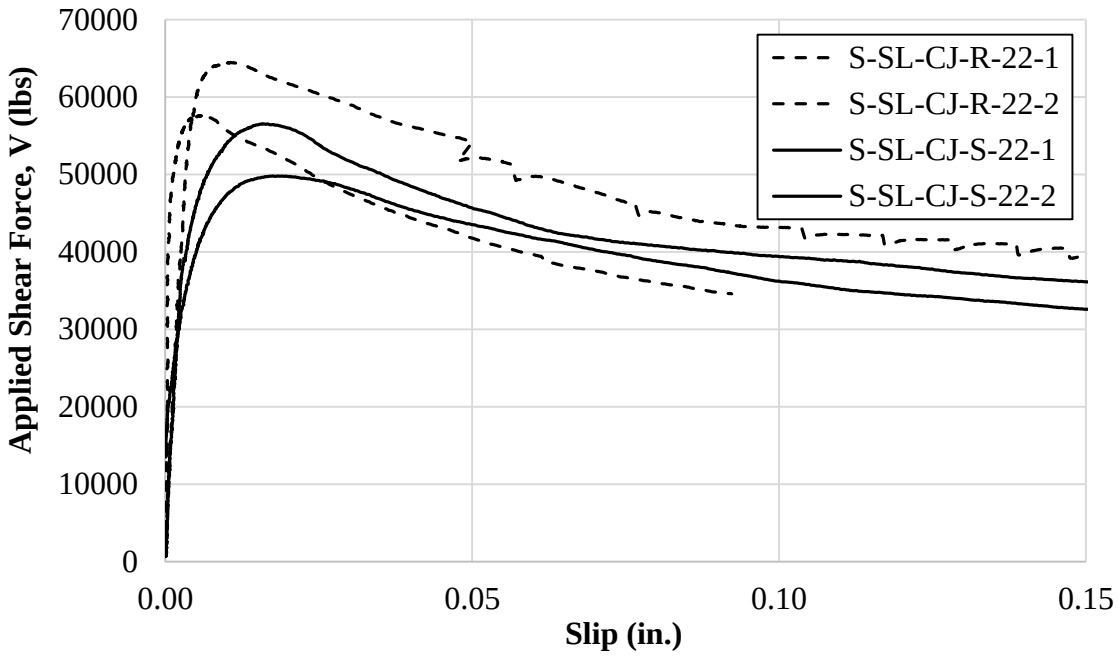

Figure 4.23. Effect of interface condition for slate specimens with ρ = 0.022

Table 4.5. Effect of Interface Preparation on the Average Ultimate Shear Capacity, $V_{u,avg}$

Specimen Series	**Average Ultimate Shear Capacity $V_{u,avg}$ (psi)**		
	Smooth Interface	**Roughened Interface**	**Ratio R/S**
CL-9	706	808	1.14
CL-13	823	987	1.20
CL-17	930	1090*	1.17
CL-22	1061*	1111*	1.05
SL-9	601	1008	1.68
SL-13	892	1238	1.39
SL-17	957	1288	1.35
SL-22	1074	1233	1.15

*Specimens in this series failed predominantly due to concrete splitting

4.3.3. Effect of Reinforcement Ratio. Within this study, four reinforcement ratios ρ were tested: 0.009, 0.013, 0.017, and 0.022. This corresponds to the use of 2, 3, 4, or 5 double-legged No. 3 stirrups across the shear plane, which had an area of A_{cr} = 49.5 in^2. This section summarizes the effect of varied reinforcement ratios on shear transfer strength of the specimens in this study. To isolate this parameter, specimens with the same aggregate type and interface condition were compared.

Figures 4.24 through 4.27 compare the shear transfer strength v_u of the specimens in this study according to their respective reinforcement ratios ρ. Figure 4.24 shows the ultimate shear stress (not normalized) versus reinforcement ratio for each specimen. Figure 4.25 shows the average ultimate shear stress (not normalized) for each series versus reinforcement ratio. Trendlines are also plotted in Figure 4.25 for each aggregate type and interface condition. All trendlines in this section are in the form of a power function because that is the empirical model which best fit the data. The R^2 (coefficient of determination) value for each trendline is also shown on in Figure 4.25. Each roughened interface series has a dashed trendline, and each smooth interface series has a smooth trendline. An increasing trend in shear transfer strength is shown in Figure 4.25 as reinforcement ratio increases. This holds true for all aggregate types and interface conditions. All specimens in this study had a nominal compressive strength of f'_c = 5,000 psi, but actual compressive strengths on test day ranged from 4,550 psi to 5,570 psi. To make the results more comparable, Figure 4.26 shows normalized shear strength v_u / f'_c versus reinforcement ratio for all specimens. Figure 4.27 contains the average normalized ultimate shear stress for each series versus reinforcement ratio, with associated trendlines. Again, the trendlines indicate that normalized shear stress increases with increasing reinforcement ratio. Interestingly, when the shear strength is normalized by compressive strength, the average shear strength of the smooth clay specimens are all higher than the smooth slate specimens which contradicts previous trends (Figure 4.27).

Residual shear stress v_{ur} was also analyzed in Figures 4.28 through 4.31 in a similar manner. Residual shear stress is defined in this thesis as the stress corresponding to a slip of 0.15 in. This value represents the stage of testing well after the peak shear force has occurred, during which the shear stress has essentially leveled off and the

interface maintains the transfer of the applied load. This data could potentially be valuable in the study of the post-peak residual capacity of a connection. It is included here for completeness. Note that this value of slip is arbitrary, and simply represents a point in the applied shear force versus slip plot where applied shear force has leveled off as slip continues to increase. Other researchers have chosen to record residual shear strength at other values of slip; for example, Kahn and Mitchell (2002) recorded v_{ur} at a slip of 0.2 in. Figure 4.28 shows a plot of the residual shear stress v_{ur} (not normalized) versus reinforcement ratio. The average values of the residual shear stress (not normalized) for each series are plotted versus reinforcement ratio in Figure 4.29, along with associated trendlines. Figure 4.30 shows the normalized (by concrete compressive strength) residual shear stress versus reinforcement ratio for each specimen. Lastly, Figure 4.31 shows the average values of the normalized residual shear stress for each series plotted versus reinforcement ratio, with associated trendlines.

As previously discussed, all specimens in this program were tested under displacement control until one of the following conditions occurred: a target slip of 0.3 in. was reached, or the applied load dropped to 60% of the peak capacity. In several instances, the applied load dropped to 60% of the peak capacity before the slip reached 0.15 in. This occurred for the following specimens: S-CL-CJ-R-9-1, S-CL-CJ-R-9-2, S-CL-CJ-S-17-1, S-SL-CJ-R-9-2, S-SL-CJ-R-13-1, S-SL-CJ-R-17-1, S-SL-CJ-R-17-2, and S-SL-CJ-S-17-1. For these eight specimens, the residual shear stress was estimated as the applied shear stress at the last recorded value of slip, which happened to lie between 0.10 in. and 0.14 in. This was considered to be a valid range of slip for recording v_{ur} because it represents the initiation of the plateau in which applied shear stress remains constant as slip continues to increase. For two specimens, S-CL-CJ-R-22-1 and S-SL-CJ-R-22-2, the residual shear stress was not recorded due to the low levels of final recorded slip (0.08 in. or less). Thus, the values for average v_{ur} in Figures 4.29 and 4.31 for the S-CL-CJ-R-22 and S-SL-CJ-R-22 do not represent averages; they represent the only recorded value for each respective series. The trendlines in Figure 4.29 and Figure 4.31 indicate that overall, an increase in residual shear strength is associated with an increase in reinforcement ratio.

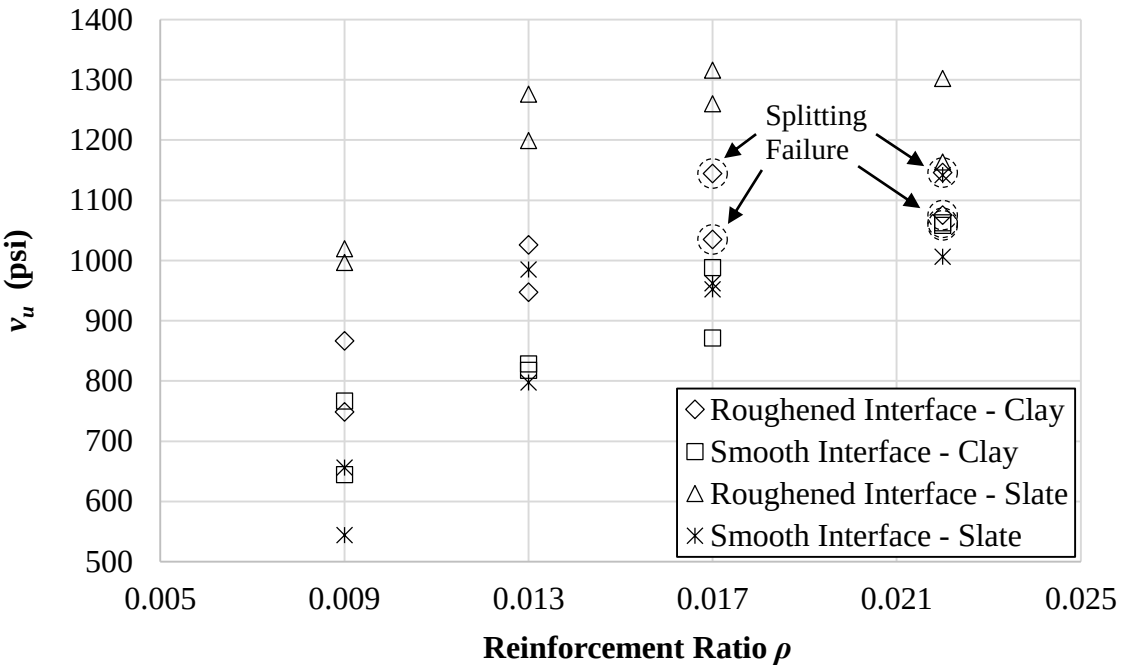

Figure 4.24. Shear strength v_u versus reinforcement ratio ρ for all specimens

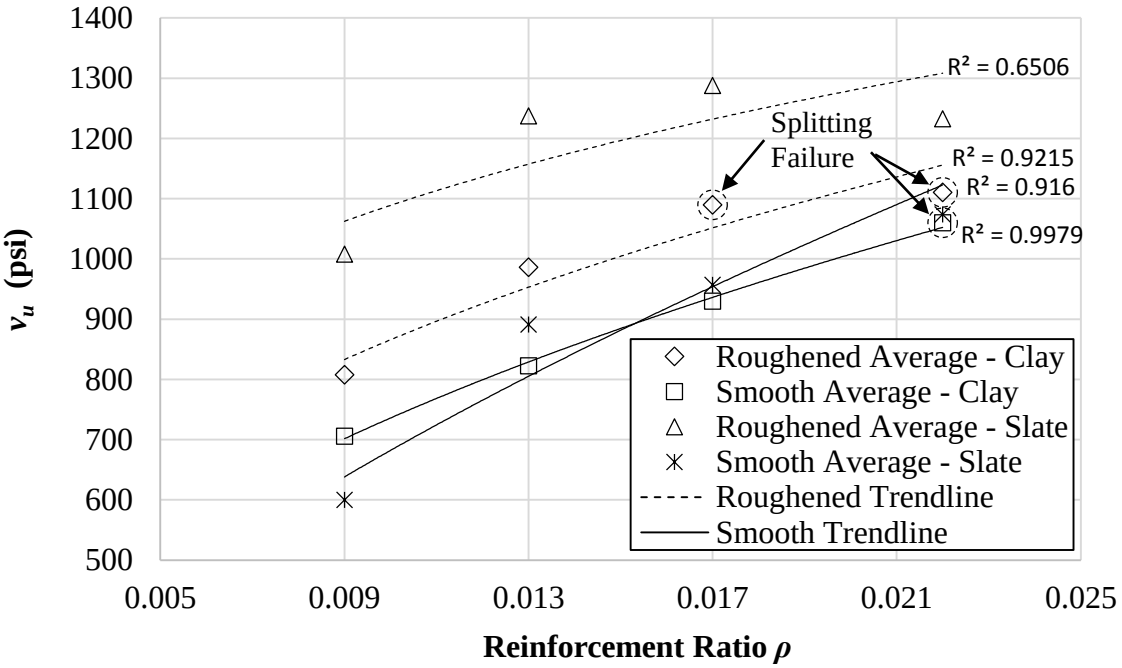

Figure 4.25. Average shear strength v_u versus reinforcement ratio ρ for each series

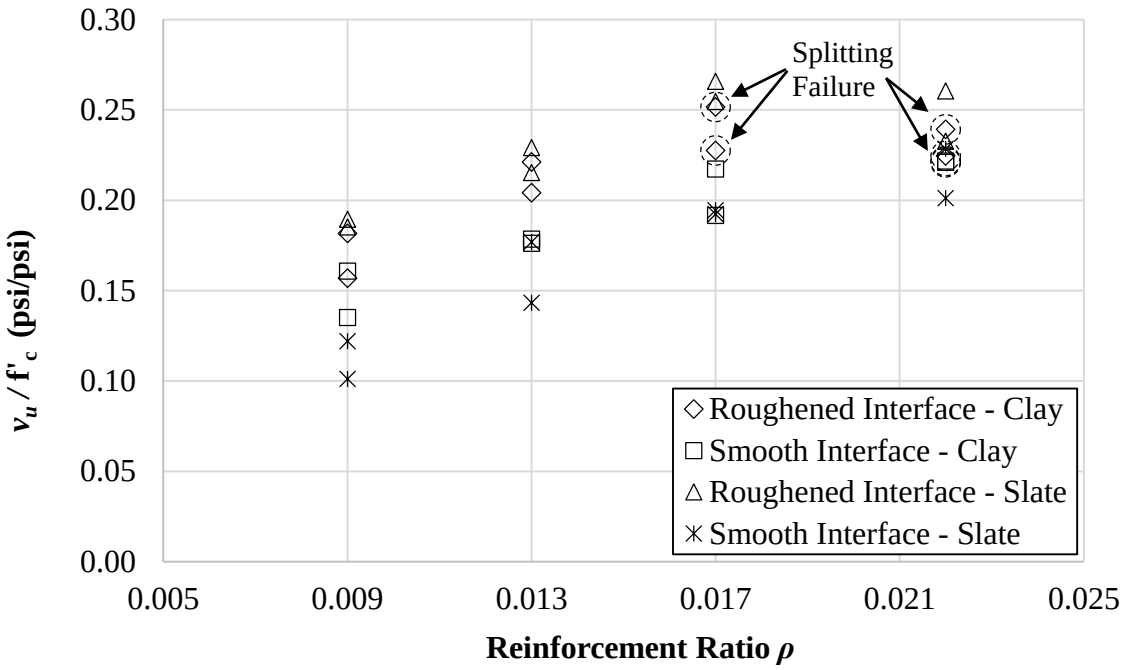

Figure 4.26. Normalized shear strength v_u / f'_c versus reinforcement ratio ρ for all specimens

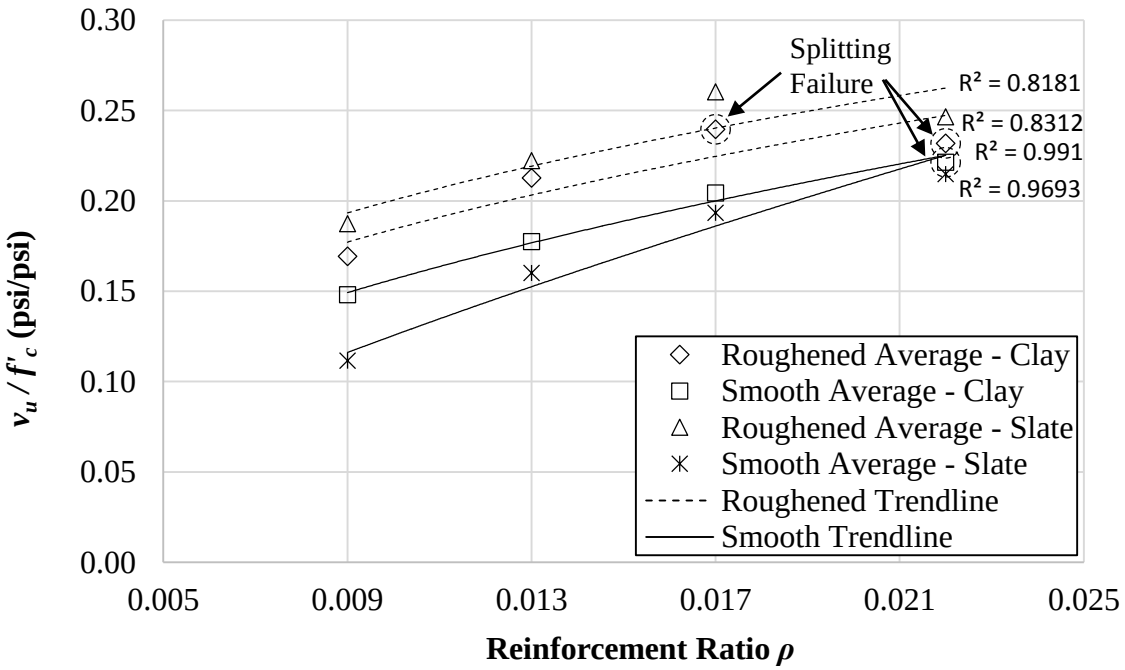

Figure 4.27. Normalized average shear strength v_u / f'_c versus reinforcement ratio ρ for each series

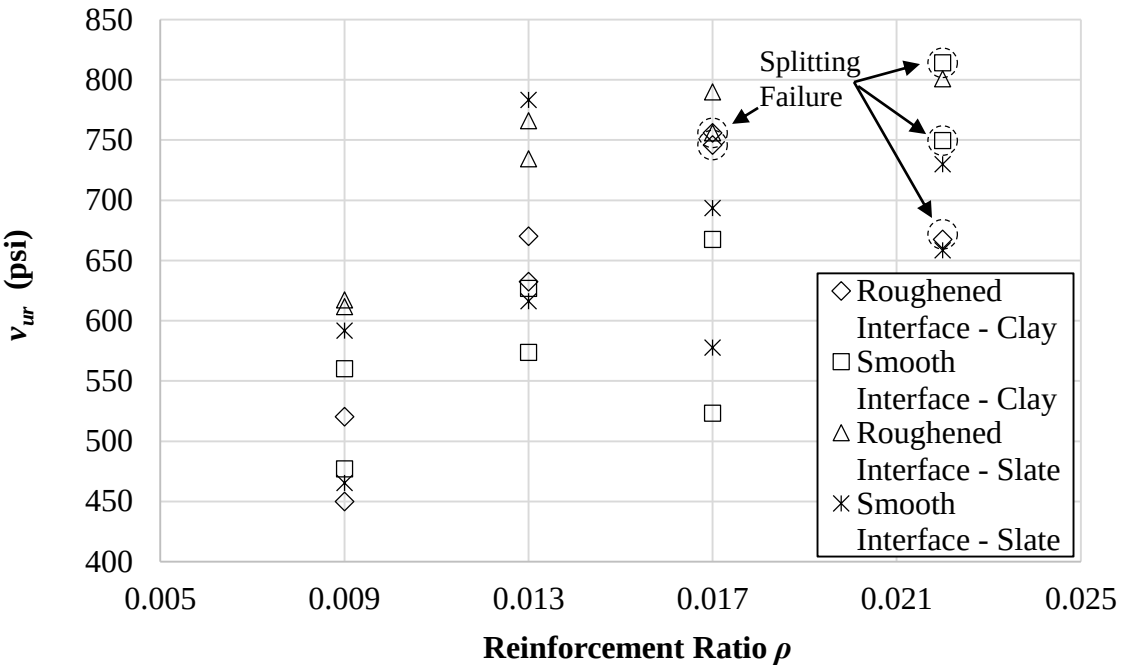

Figure 4.28. Residual shear strength v_{ur} versus reinforcement ratio ρ for all specimens

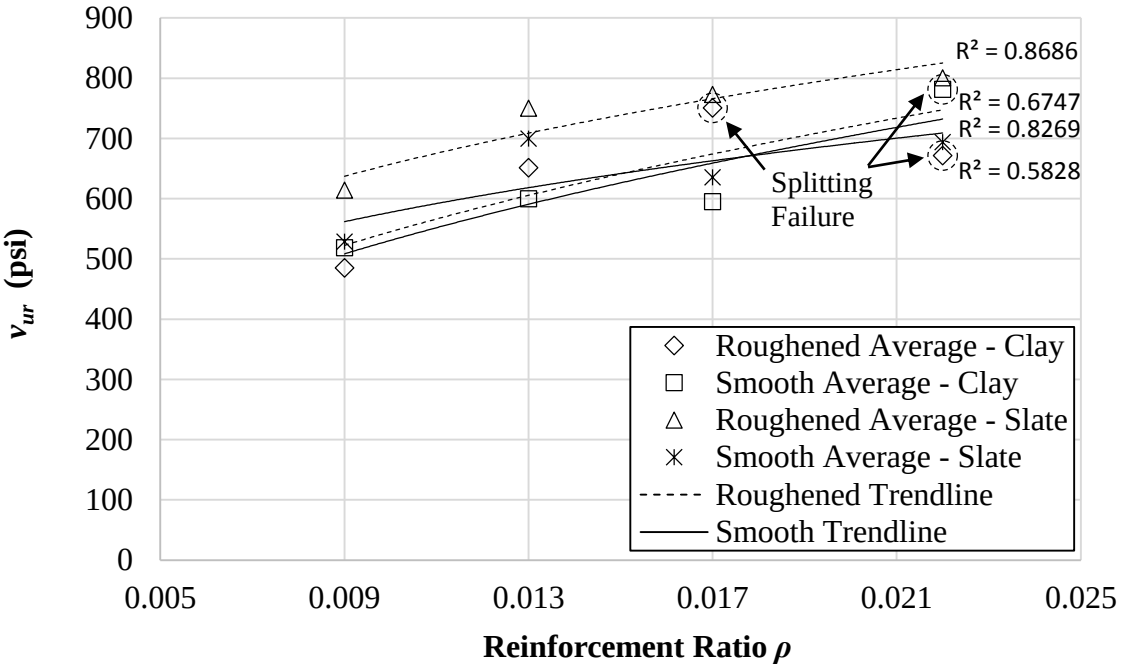

Figure 4.29. Average residual shear strength v_{ur} versus reinforcement ratio ρ for each series

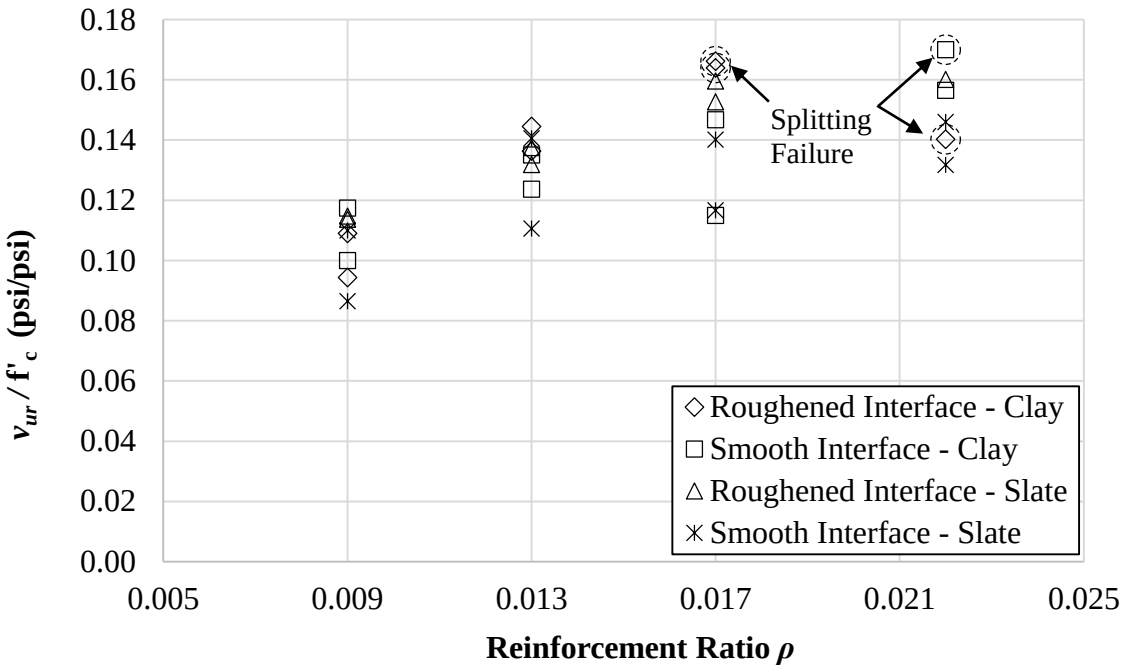

Figure 4.30. Normalized residual shear strength v_{ur} / f'_c versus reinforcement ratio ρ for all specimens

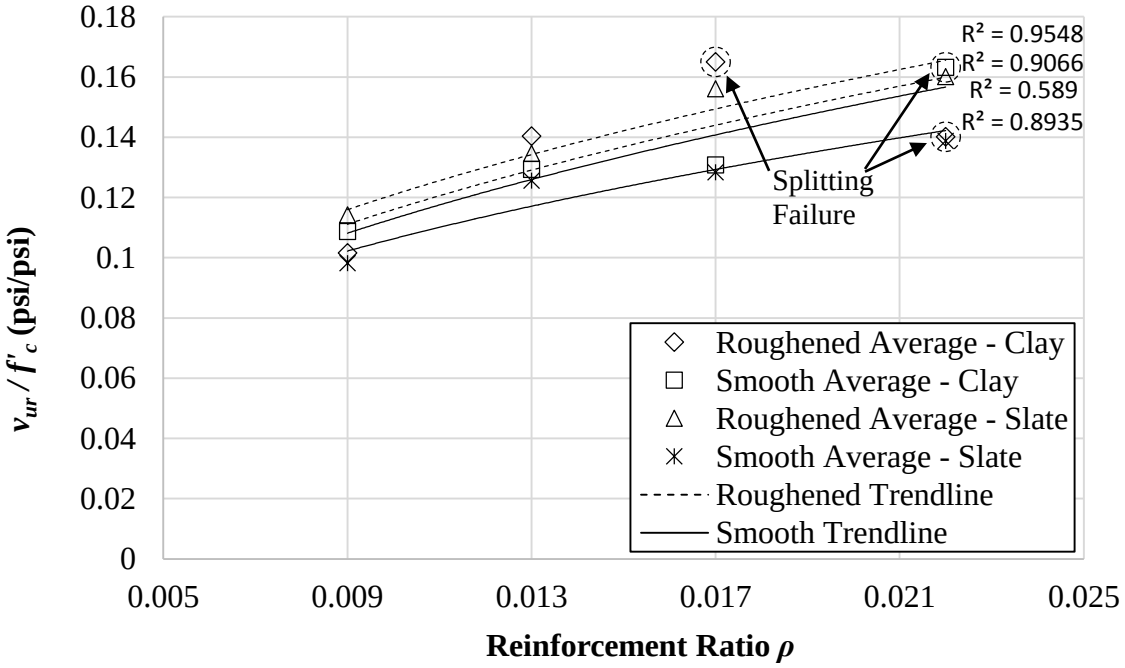

Figure 4.31. Normalized average residual shear strength v_{ur} / f'_c versus reinforcement ratio ρ for each series

4.4. COMPARISON TO DESIGN PROVISIONS

This section contains an assessment of how well the results of this study correlate to current shear-friction design provisions. Section 4.4.1 summarizes the equations and limits used for this analysis which come from the 6th and 7th Editions of the PCI Design Handbook, the ACI 318-14 Code, and the 7th Edition of AASHTO LRFD Bridge Design Specifications. In Section 4.4.2, results of the specimens in this study are compared to design provisions in terms of nominal shear strength V_n (or $v_n = V_n/A_{cr}$), or nominal interface shear resistance V_{ni} (or $v_{ni} = V_{ni}/A_{cr}$). Section 4.4.3 contains a comparison of the test results to design provisions in terms of the effective coefficient of friction μ_e.

4.4.1. Shear-friction Design Provisions. This section describes the equations and limits used in the comparison of test results to current shear-friction design provisions. Specifically, the codes/specifications which are addressed include: the 6th and 7th Editions of the PCI Design Handbook (2004 and 2011), the ACI 318-14 Code, and the 7th Edition of AASHTO LRFD Bridge Design Specifications (2014). The shear-friction provisions of these codes/specifications are thoroughly described in Section 2.3. Tables 4.6 through 4.9 describe the code/specification limits for V_u (or V_n or V_{ni}), as well as recommended values for μ, μ_e, λ, and other shear-friction coefficients.

Table 4.6. Limits for Applied Shear of Shear-friction Elements

Case	PCI 6th Ed. Max $V_u = \phi V_n$	PCI 7th Ed. Max $V_u = \phi V_n$	ACI 318-14[1] Max $V_n = V_u/\phi$	AASHTO 5th Ed. Max $V_{ni} = V_{ri}/\phi$
1	$0.30\lambda^2 f'_c A_{cr} \leq 1000\lambda^2 A_{cr}$	$0.30\lambda f'_c A_{cr} \leq 1000\lambda A_{cr}$	For lightweight concretes, V_n shall not exceed the smaller of: $0.2 f'_c A_c$ or $800 A_c$	V_{ni} shall not exceed the smaller of: $K_1 f'_c A_{cv}$ or $K_2 A_{cv}$
2	$0.25\lambda^2 f'_c A_{cr} \leq 1000\lambda^2 A_{cr}$	$0.25\lambda f'_c A_{cr} \leq 1000\lambda A_{cr}$		
3	$0.20\lambda^2 f'_c A_{cr} \leq 800\lambda^2 A_{cr}$	$0.20\lambda f'_c A_{cr} \leq 800\lambda A_{cr}$		
4	$0.20\lambda^2 f'_c A_{cr} \leq 800\lambda^2 A_{cr}$	$0.20\lambda f'_c A_{cr} \leq 800\lambda A_{cr}$		

[1] For normalweight concrete with a monolithic or roughened interface, ACI 318-14 specifies different limits than shown for Cases 1 and 2, but these cases are not included in this testing program; therefore, their limits for V_n are omitted from Table 4.6.

Table 4.7. PCI and ACI Recommended Values for μ and λ with Respect to Concrete Type and Crack Interface Condition

Factor	Normalweight		Sand-lightweight		All-Lightweight	
	Smooth	Rough	Smooth	Rough	Smooth	Rough
μ	0.60	1.00	0.51	0.85	0.45	0.75
λ	1.00	1.00	0.85	0.85	0.75	0.75

Table 4.8. PCI (2011) and ACI (2014) Shear-friction Design Coefficients

		PCI 6th Edition		PCI 7th Edition		ACI 318-14
Case	Crack Interface Condition	μ	Max μ_e	μ	Max μ_e	μ
1	Concrete to concrete, cast monolithically	1.4λ	3.4	1.4λ	3.4	1.4λ
2	Concrete to hardened concrete, with roughened surface	1.0λ	2.9	1.0λ	2.9	1.0λ
3	Concrete placed against hardened concrete not intentionally roughened	0.6λ	2.2	0.6λ	N/A	0.6λ
4	Concrete to steel	0.7λ	2.4	0.7λ	N/A	0.7λ

Table 4.9. AASHTO (2014) Shear-friction Design Coefficients

Concrete Density and Interface Condition*	c (ksi)	μ	K_1	K_2 (ksi)
Cast-in-place slab on girder with roughened interface; normalweight concrete	0.28	1.0	0.3	1.8
Cast-in-place slab on girder with roughened interface; lightweight concrete	0.28	1.0	0.3	1.3
Normalweight concrete placed monolithically	0.40	1.4	0.25	1.5
Lightweight concrete placed monolithically, or lightweight cold-joint with roughened interface	0.24	1.0	0.25	1.0
Normalweight cold-joint with roughened interface	0.24	1.0	0.25	1.5
Cold-joint with interface not intentionally roughened	0.075	0.6	0.2	0.8
Concrete anchored to as-rolled structural steel by headed studs or by reinforcing bars	0.025	0.7	0.2	0.8

4.4.1.1 PCI Design Handbook 6th Edition (2004). Equations from the 6th Edition of the PCI Design Handbook for the required amount of shear reinforcement perpendicular to the shear plane A_{vf} and effective coefficient of friction μ_e are shown in Equations 4.1 and 4.2, respectively. These equations are fully defined in Section 2.3.1.1, and apply to all four cases of interface conditions which are listed in Table 4.8.

$$A_{vf} = \frac{V_u}{\phi f_y \mu_e} \tag{4.1}$$

$$\mu_e = \frac{1000 \lambda A_{cr} \mu}{V_u} \tag{4.2}$$

To make the comparisons to test results easier, these two equations can be rearranged in terms of nominal shear stress and reinforcement ratio. When the term V_n is substituted for V_u/ϕ, and V_n/A_{cr} is then replaced with v_n, Equations 4.1 and 4.2 can be rearranged and combined to become Equation 4.3:

$$v_n = 31.62 \sqrt{\frac{\rho \, f_y \, \lambda \, \mu}{\phi}} \tag{4.3}$$

Using the relations $V_n=V_u/\phi$, $v_n=V_n/A_{cr}$, and $\rho=A_{vf}/A_{cr}$, Equation 4.1 can be rewritten in terms of μ_e as shown in Equation 4.4:

$$\mu_e = \frac{v_n}{\rho \, f_y} \tag{4.4}$$

The provisions of the 6th Edition of the PCI Design Handbook restrict the design value of f_y to a maximum of 60 ksi as discussed in Section 2.3.1.1. Maximum values for V_u are listed in Table 4.6 for all interface conditions, Cases 1-4; values for μ and $\mu_{e,max}$ are listed in Table 4.8; and corresponding values for μ and λ are summarized in Table 4.7 for all concrete types and interface conditions.

4.4.1.2 PCI Design Handbook 7th Edition (2011). The 7th Edition of the PCI Design Handbook contains a major change from the previous edition in that μ_e is no longer considered applicable for crack interface condition Cases 3 and 4: smooth interface and concrete to steel, respectively. Instead, shear-friction design for these two cases is governed by Equation 4.5, as explained in Section 2.3.1.2.

$$A_{vf} = \frac{V_u}{\phi f_y \mu} \tag{4.5}$$

When the term V_n is substituted for V_u/ϕ, and V_n/A_{cr} is then replaced with v_n, with ρ used in place of A_{vf}/A_{cr}, Equation 4.5 can be rearranged as shown in Equation 4.6: Equation 4.6 can also be expressed in terms of μ as shown in Equation 4.7:

$$v_n = \rho f_y \mu \tag{4.6}$$

$$\mu = \frac{v_n}{\rho\, f_y} \tag{4.7}$$

For cases where load reversal does not occur, and the interface is either monolithic or roughened (Cases 1 or 2), Equation 4.8 may be used to design the amount

of reinforcement crossing the shear plane perpendicularly. Note that this is the same as Equation 4.1 from the 6th Edition of the PCI Design Handbook.

$$A_{vf} = \frac{V_u}{\phi f_y \mu_e} \tag{4.8}$$

The value for μ_e in Equation 4.8 is computed using Equation 4.9. Equation 4.9 is similar to Equation 4.2 from the 6th Edition of the PCI Design Handbook. The only difference is the addition of ϕ in the numerator.

$$\mu_e = \frac{\phi 1000 \lambda A_{cr} \mu}{V_u} \tag{4.9}$$

When the term V_n is substituted for V_u/ϕ, and V_n/A_{cr} is then replaced with v_n, with ρ used in place of A_{vf}/A_{cr}, Equations 4.8 and 4.9 can be rearranged and combined as shown in Equation 4.10.

$$v_n = 31.62 \sqrt{\rho f_y \lambda \mu} \tag{4.10}$$

Also, as done before, Equation 4.8 can be solved for μ_e as shown in Equation 4.11.

$$\mu_e = \frac{v_n}{\rho f_y} \tag{4.11}$$

The provisions of the 7th Edition of the PCI Design Handbook restrict the design value of f_y to a maximum of 60 ksi as discussed in Section 2.3.1.2. Maximum values for V_u are listed in Table 4.6 for all interface conditions, Cases 1-4; values for μ and $\mu_{e,max}$ are listed in Table 4.8; and corresponding values for μ and λ are summarized in Table 4.7 for all concrete types and interface conditions.

4.4.1.3 ACI 318-14. The design equations in ACI 318-14 do not include an effective coefficient of friction. Rather, a similar shear-friction design approach is used as for the smooth interface and concrete to steel conditions in the 7th Edition of the PCI Handbook. The nominal shear strength V_n is calculated according to Equation 4.12:

$$V_n = \mu A_v f_y \tag{4.12}$$

When the term V_n/A_{cr} is replaced with v_n, with ρ used in place of A_{vf}/A_{cr}, Equation 4.12 can be rearranged as shown in Equation 4.13:

$$v_n = \rho f_y \mu \tag{4.13}$$

Equation 4.13 can also be expressed in terms of μ as shown in Equation 4.14:

$$\mu = \frac{v_n}{\rho f_y} \tag{4.14}$$

The provisions of ACI 318-14 restrict the design value of f_y to a maximum of 60 ksi as discussed in Section 2.3.2. Maximum values for V_n are listed in Table 4.6 for all interface conditions, Cases 1-4; values for μ are listed in Table 4.8; and corresponding

values for μ and λ are summarized in Table 4.7 for all concrete types and interface conditions.

4.4.1.4 AASHTO LRFD Bridge Design Specifications. The AASHTO Specifications (7th Edition) regarding shear-friction are quite different than the previously discussed codes. First, sand-lightweight concrete is not distinguished from all-lightweight concrete. They are both considered together as lightweight concrete; therefore, the lightweight correction factor λ is not used in the AASHTO Specification. The friction factor μ is used, but the values for lightweight concrete with smooth (μ = 0.6) and roughened interfaces (μ = 1.0) are different from the ACI and PCI codes, since they do not include the lightweight correction factor λ. Values for μ and several other coefficients are listed in Table 4.9: c is the cohesion factor; K_1 represents the fraction of concrete strength available to resist interface shear; and K_2 is the limiting interface shear resistance. The nominal shear resistance V_{ni} of the interface plane is defined in Equation 4.15, with all coefficients and variables defined as in Section 2.3.3.

$$V_{ni} = cA_{cv} + \mu\left(A_{vf}f_y + P_c\right) \tag{4.15}$$

A very important provision in the AASHTO LRFD Bridge Design Specifications is that brackets, corbels, and ledges shall have a cohesion factor of c = 0.0 for all cases listed in Table 4.9. The commentary to AASHTO Section 5.8.4.3 states that this provision is necessary due to the unreliable cohesion and aggregate interlock properties of vertical cracks. Therefore, the cohesion factor is conservatively set to zero for these cases. In order to study the validity of this provision, Equation 4.15 will be used for two conditions: with the cohesion factor considered as 0.0 and also for the cohesion factor considered to be the value given in Table 4.9.

Since this testing program aims to study the fundamental shear-friction properties for all general interfaces, the first method of analysis will require that the cohesion factor c be set to zero in the shear-friction design equation. This means that the first term of Equation 4.15 is effectively eliminated. P_c may also be eliminated from Equation 4.15

since none of the specimens in this study had an externally applied compressive force across the shear plane. Therefore, these considerations condense Equation 4.15 into the form shown in Equation 4.16, recognizing that the nominal interface shear stress (same as nominal shear stress in ACI and PCI) $v_{ni} = V_{ni}/A_{cv}$, and $\rho = A_{vf}/A_{cr}$. Note that the AASHTO Specifications limit the reinforcement parameter ρf_y to values greater than or equal to 0.05.

$$v_{ni} = \rho f_y \mu \tag{4.16}$$

Rewriting Equation 4.16 in term of μ gives Equation 4.17:

$$\mu = \frac{v_{ni}}{\rho f_y} \tag{4.17}$$

As discussed above, the second method of comparing the test data from this study to AASHTO specifications is to use Equation 4.15 with the cohesion factors from Table 4.9 included. This will either reinforce or contradict the validity of the AASHTO provision which considers the cohesion factor c to be equal to 0.0 in the shear-friction equation for the case of a vertical crack. Again, it is appropriate to eliminate P_c from Equation 4.15 since none of the specimens in this study had an externally applied compressive force across the shear plane. Recognizing that $v_{ni} = V_{ni}/A_{cv}$, and $\rho = A_{vf}/A_{cr}$, Equation 4.15 can be rearranged into the form shown in Equation 4.18.

$$v_{ni} = c + \rho f_y \mu \tag{4.18}$$

Rewriting Equation 4.18 in term of μ gives Equation 4.19:

$$\mu = \frac{v_{ni} - c}{\rho f_y} \tag{4.19}$$

Equations 4.16 and 4.17 are the same as those in ACI and PCI design provisions with the nominal shear stress given a slightly different title (nominal interface shear stress). The AASHTO LRFD Bridge Design Specifications restrict the design value of f_y to a maximum of 60 ksi as discussed in Section 2.3.3. Maximum values for V_{ni} are listed in Table 4.6 for all interface conditions, Cases 1-4, and values for c, μ, K_1 and K_2 are listed in Table 4.9.

4.4.2. Shear Strength. This section compares the values of peak shear stress v_u (or v_{ui}) for the specimens tested in this study versus the current design codes and specifications discussed in Section 4.4.1. These include the 7th Edition (most current) of the PCI Design Handbook (2011), ACI 318-14, and the AASHTO LRFD Bridge Design Specifications (2014). Note that for this comparison analysis, v_u can be used interchangeably with v_n since ϕ =1.0. It is acceptable to set the resistance factor ϕ equal to 1.0 since all dimensions and material properties are known. This allows a direct comparison of calculated capacities from the code/specification to actual capacities of tested specimens.

The four design approaches used in this analysis are summarized in Table 4.10, along with the calculated shear strength limits for smooth and roughened interface conditions. In this section, both the 'μ' method and the 'μ_e' method of determining shear strength v_n were used. For Figures 4.32 and 4.33, Equation 4.13 is plotted and shown as the ACI 318-14 Code equation. Note that this follows the 'μ' approach and is also the same as Equation 4.6 from the 7th Edition of the PCI Design Handbook and is applicable to all crack interface conditions. For the PCI Design Handbook shear-friction capacity equation shown in Figures 4.32 and 4.33, the 'μ_e' approach is followed, and v_n is plotted according to Equation 4.10. As previously discussed, a major change from the 6th to the

7th Edition of the PCI Design Handbook was that the use of the μ_e method is no longer considered applicable for a smooth interface condition (Case 3). For comparison purposes, the μ_e method is also used for smooth interface specimens to determine how well it correlates with the experimental data from this study. Note that the equations and limits for the PCI comparison are exclusively from the 7th Edition. The AASHTO shear-friction equations shown in Figures 4.32 and 4.33 are Equations 4.16 and 4.18, which correspond to the cohesion factor being set to either zero or set to the values from Table 4.9, respectively. The shear-friction coefficients for roughened and smooth interface conditions are found in Table 4.9 as the fourth and sixth cases, respectively.

Table 4.10. Shear Strength Limits for Each Shear-friction Design Approach for $f'_c \geq 5000$ psi

Design Approach	**Equation No.**	**Equation Description**	**Smooth Interface Limit (psi)**	**Roughened Interface Limit (psi)**
PCI 7th Ed. "μ_e approach"*	4.10	$v_n = 31.62\sqrt{\rho f_y \lambda \mu}$	680	850
ACI 318-14 "μ approach"	4.13	$v_n = \rho f_y \mu$	800	800
AASHTO 7th Ed. (w/o cohesion)	4.16	$v_{ni} = \rho f_y \mu$	800	1000
AASHTO 7th Ed. (w/ cohesion)	4.18	$v_{ni} = \mathrm{c} + \rho f_y \mu$	800	1000

*Note: This approach is not applicable in the 7th Edition of the PCI Design Handbook for the smooth interface condition, but is used here for the purpose of this section.

Most of the roughened specimens from this study had shear strengths which were higher than those predicted by current design provisions from ACI, PCI, and AASHTO (Figure 4.32). The only unconservative values for the AASHTO approach in the roughened analysis came from clay specimens with ρf_y less than about 1000 psi. Several of these specimens failed to meet the AASHTO 7th Edition design equation which

included the cohesion factor *c* (Equation 4.18). For specimens with a roughened interface (Figure 4.32), the shear-friction design equations are more conservative for the shear strengths of the slate specimens than the clay specimens. The data from this study supports ignoring the cohesion factor *c* from Equation 4.15 for specimens with a roughened interface. Overall, the predicted shear strengths from the AASHTO specifications had the closest correlation to the test data for the roughened specimens.

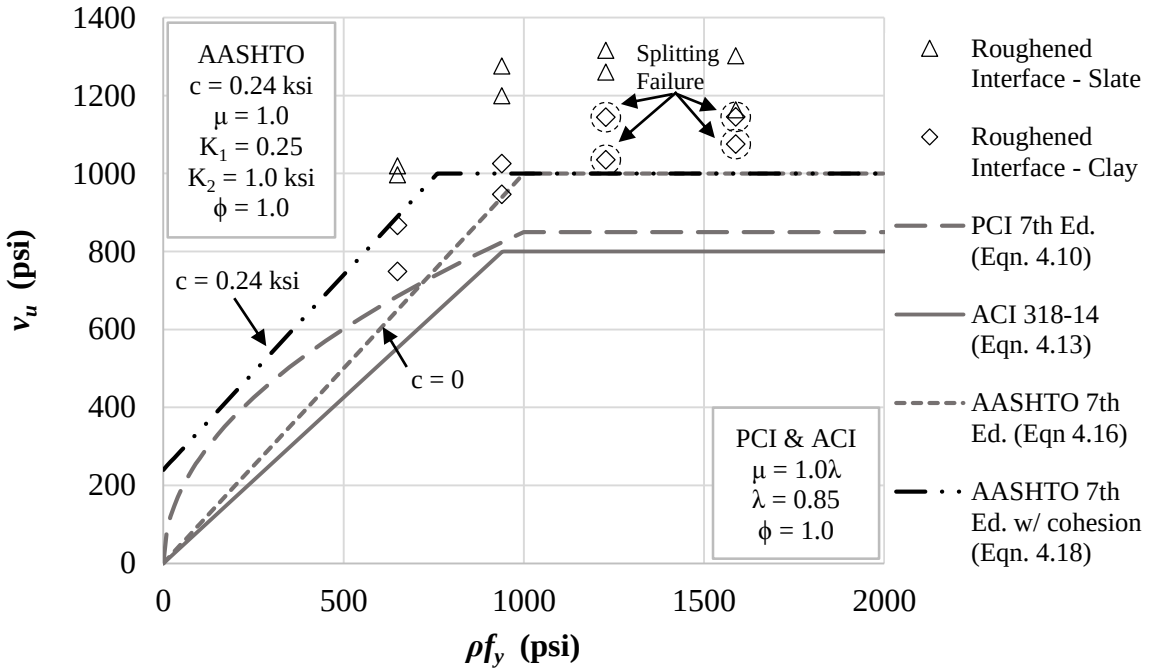

Figure 4.32. Comparison of shear strength v_u (or v_{ui}) with Equations 4.10, 4.13, 4.16, and 4.18 for slate and clay aggregate sand-lightweight specimens with a roughened interface

As shown in Figure 4.33, all shear strengths from the smooth interface test specimens in this study were higher than the predicted shear strengths from the current ACI, PCI, and AASHTO codes/specifications. For values of ρf_y less than about 900 psi, the μ_e approach of Equation 4.10 (PCI 7th Ed.) had the best correlation with the test data for the smooth specimens of this testing program. At higher values of ρf_y (greater than

about 900 psi), Equation 4.18 from AASHTO had the closest correlation to the smooth interface test data. For specimens with a smooth interface (Figure 4.33), the shear-friction design equations are equally conservative for the shear strengths of the slate specimens and the clay specimens. Since the shear strength of all of the smooth interface specimens exceeded Equation 4.18, the results indicate that the cohesion factor c can be used for smooth interface specimens.

The shear strengths of the smooth interface test specimens all exceed the shear strengths predicted by Equation 4.10 from the 7th Edition of the PCI Design Handbook (Figure 4.33). Therefore, these results support the use of the μ_e approach for specimens with a non-monolithic smooth interface condition (Case 3) in the PCI Design Handbook. Also, as ρf_y increases, Equation 4.10 becomes more conservative for specimens with both rough and smooth interface conditions. This suggests that the limit on $\underline{v_{n,max}}$ in the 7th Edition of the PCI Design Handbook could be increased. This would also make the PCI limits more consistent with ACI and AASHTO.

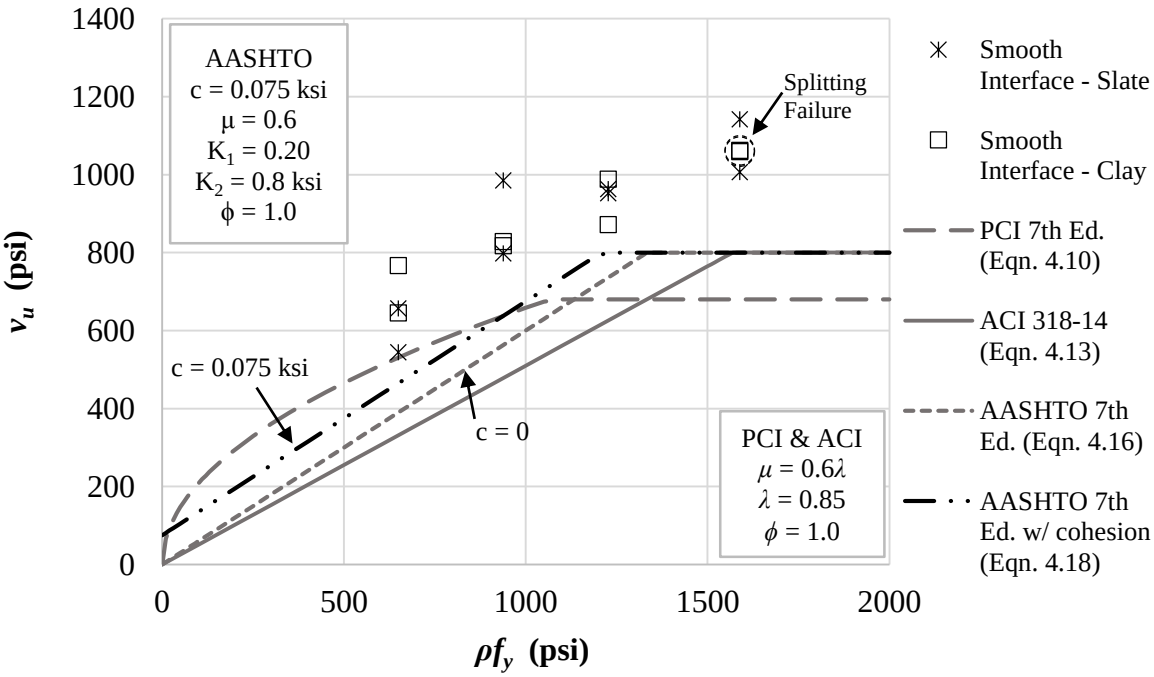

Figure 4.33. Comparison of shear strength v_u with Equations 4.10, 4.13, 4.16, and 4.18 for slate and clay aggregate sand-lightweight specimens with a smooth interface

4.4.3. Effective Coefficient of Friction, μ_e. This section compares the results of this experimental study to the values of the effective coefficient of friction μ_e from the 6th and 7th Editions of the PCI Design Handbook. As shown in Table 4.8, the maximum recommended value of μ_e for a roughened interface condition is 2.9 in both the 6th and 7th Editions of the PCI Design Handbook. For the case of a smooth interface, the 6th Edition uses a maximum value of $\mu_e = 2.2$; yet, for the 7th Edition of the PCI Design Handbook, the μ_e approach is not applicable. In this section, all equations and limits for shear strength from the PCI Design Handbook are in reference to the 7th Edition, yet the value for μ_e of a smooth interface is taken from the 6th Edition for comparison purposes.

Figures 4.34 and 4.35 show the effective coefficient of friction μ_e versus nominal shear strength for specimens with a roughened or smooth interface condition, respectively. The effective coefficient of friction μ_e was computed for each specimen using Equation 4.11 from the 7th Edition of the PCI Design Handbook with the measured shear strength (which is the same equation as Equation 4.4 from PCI 6th Edition). The average tested yield strength of the No. 3 stirrups (f_y = 72,185 psi) was used in Equation 4.11 for f_y.

The predicted values of μ_e are plotted as a solid line in Figures 4.34 and 4.35. This line comes from Equation 4.9 of the 7th Edition of the PCI Design Handbook, which is similar to Equation 4.2 of the 6th Edition, except the strength reduction factor ϕ is added to the numerator. Since all specimen dimensions and material properties are known in this testing program, it is permitted to take $\phi = 1.0$; therefore, these two equations for μ_e produce the same values. The maximum values of shear strength are the PCI 7th Edition limits listed in Table 4.6. These values are computed as 850 psi and 680 psi for the roughened and smooth interface specimens of this study, respectively. As previously discussed, the maximum values for μ_e of roughened and smooth interface specimens were taken as 2.9 and 2.2 for this comparison.

All experimental data points plotted above or to the right of Equation 4.9 in Figures 4.34 and 4.35, which indicates the PCI 7th Edition equation and limits for μ_e and v_n are conservative for all specimens in this study. As a general trend, Equation 4.9 is more conservative for the slate aggregate specimens than the clay aggregate specimens of a similar reinforcement ratio and interface condition.

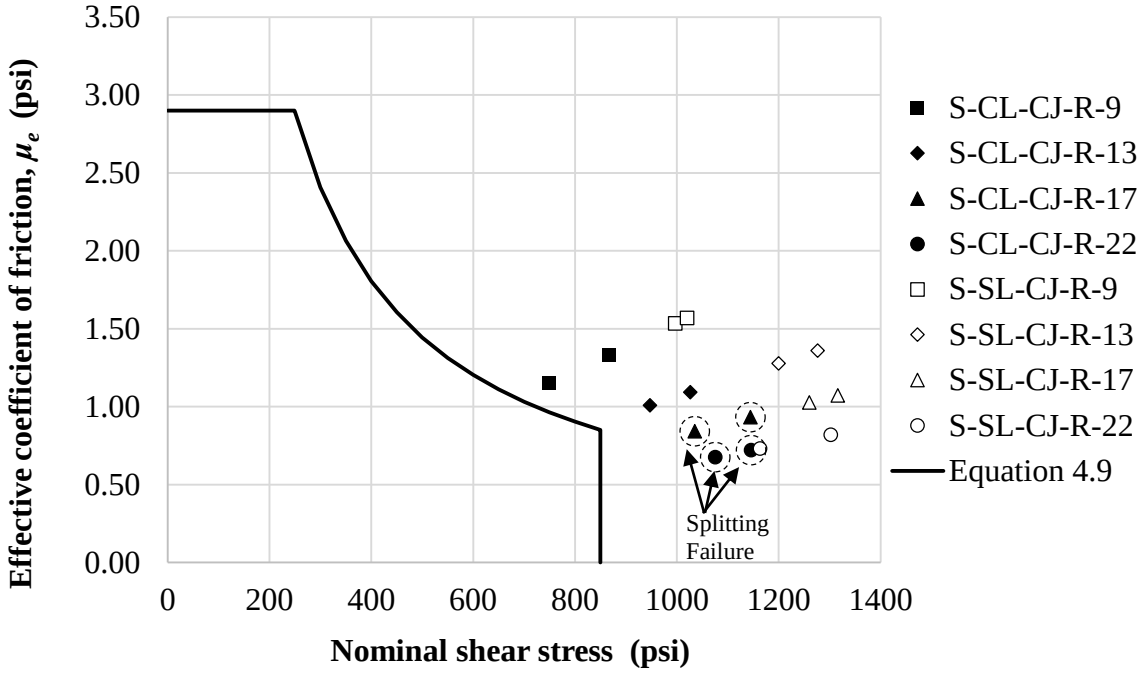

Figure 4.34. Evaluation of the effective coefficient of friction for sand-lightweight concrete with a roughened interface

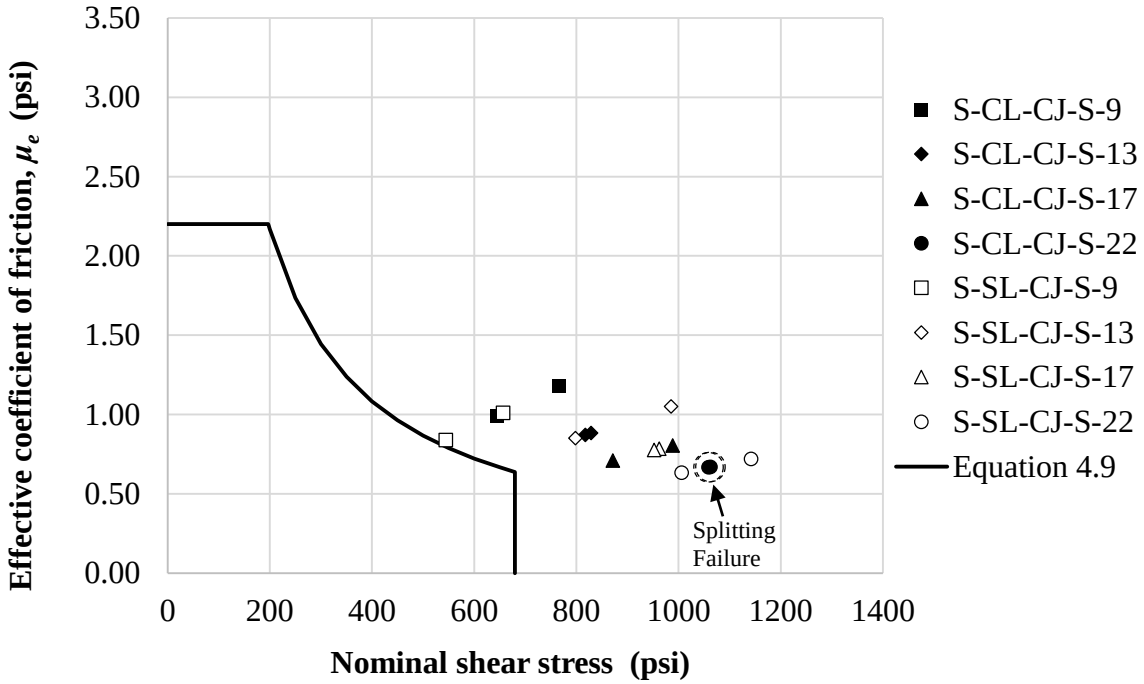

Figure 4.35. Evaluation of the effective coefficient of friction for sand-lightweight concrete with a smooth interface

One outlier in Figure 4.35 is the clay data point which lies closer to Equation 4.9 than the corresponding slate specimen with ρ = 0.009 and a smooth interface. This outlier was discussed in 4.3.1 in the discussion of the effect of lightweight aggregate type. Also worth noting in Figures 4.34 and 4.35 is that Equation 4.9 is slightly more conservative for specimens with a roughened interface than specimens with a smooth interface.

Figures 4.36 and 4.37 are similar to Figures 4.34 and 4.35, except the explicit value of the lightweight modification factor is removed from Equation 4.9. The value of λ which is included in the friction factor μ was not changed in Figures 4.36 and 4.37. As shown in these two figures, removing the explicit instance of λ from Equation 4.9 reveals a good correlation for the slate sand-lightweight and clay sand-lightweight specimens included in this study. However, there was one outlier in Figure 4.37 which produced an unconservative result using this method (S-SL-CJ-S-9-1).

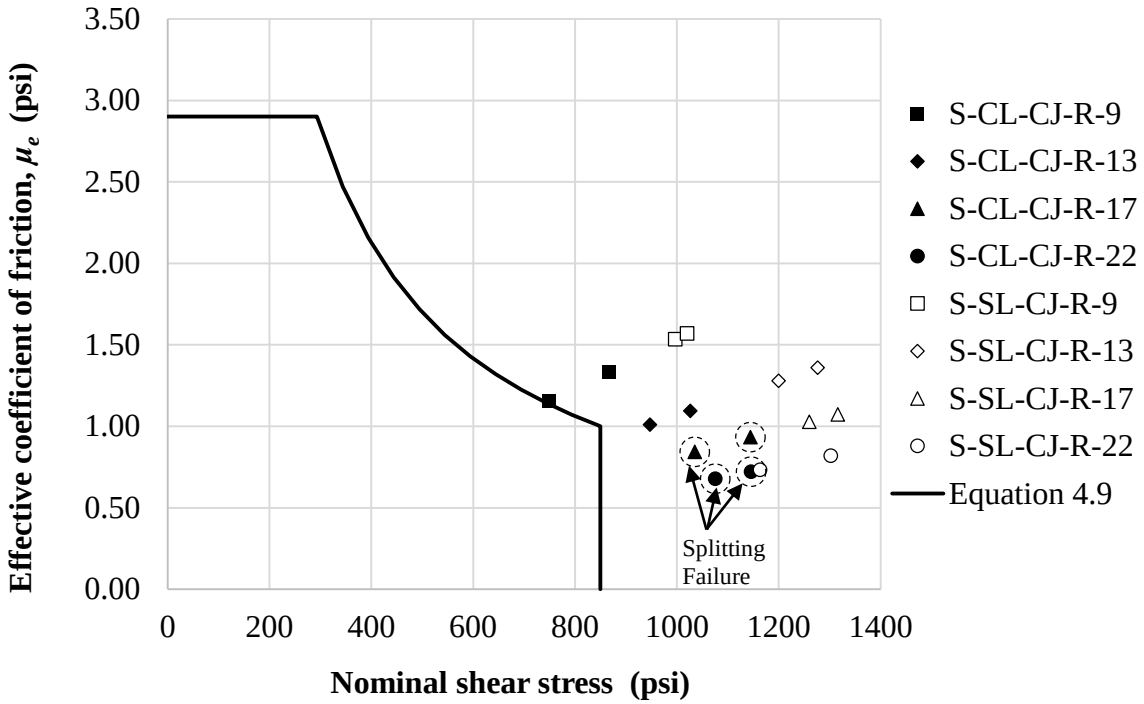

Figure 4.36. Evaluation of the effective coefficient of friction for sand-lightweight concrete with a roughened interface with explicit λ term removed from Equation 4.9

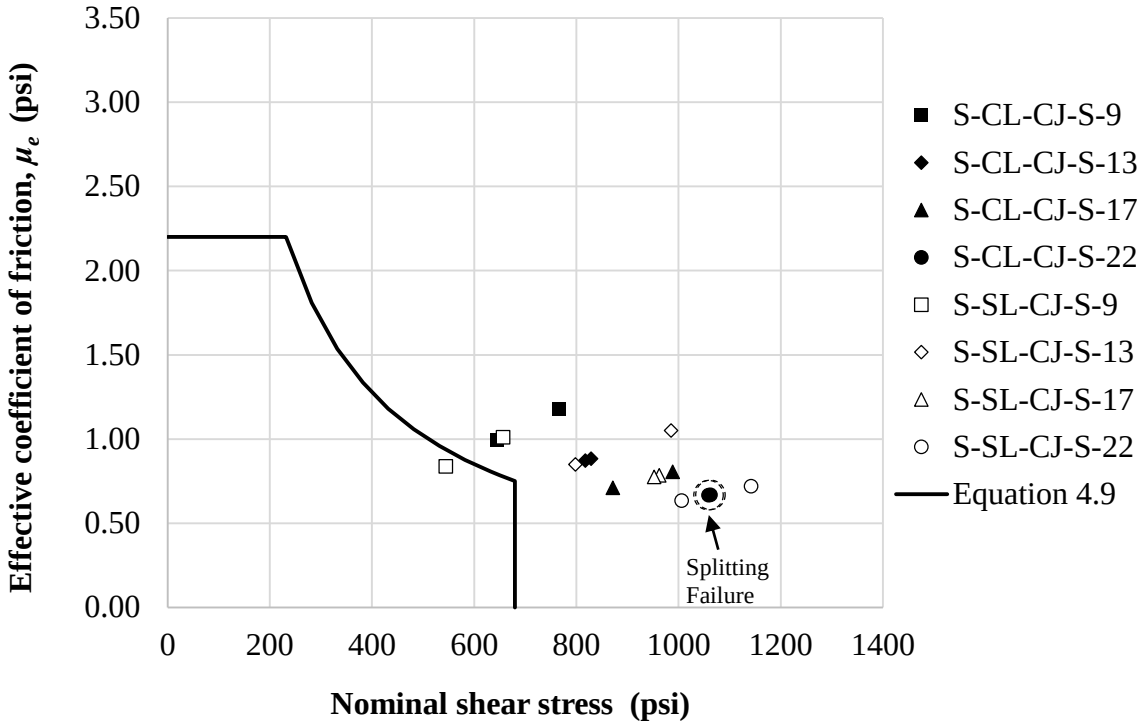

Figure 4.37. Evaluation of the effective coefficient of friction for sand-lightweight concrete with a smooth interface with explicit λ term removed from Equation 4.9

The lightweight modification factor λ is meant to account for a reduction in mechanical properties relative to normalweight concrete when lightweight aggregate is used in concrete. Since λ appears twice in Equation 4.9, once explicitly and again in the definition for μ, there are significant reductions in μ_e values for lightweight concrete as noted by Tanner (2008). In previous work by Shaw (2013), a similar study of μ_e showed that removing the two instances of λ (essentially λ^2) from Equation 4.9 produced a good correlation for normalweight, sand-lightweight (shale), and all-lightweight (shale) specimens with a similar compressive strength as the specimens in this study ($f'_c \approx 5{,}000$ psi). Figures 4.36 and 4.37 show that removing only the explicit value of λ from Equation 4.9 provides a good correlation to the slate sand-lightweight and clay sand-lightweight concretes used in this study.

4.5. COMPARISON TO PREVIOUS STUDIES

Several previous studies involved cold-joint specimens with smooth and rough interfaces. These include: Shaw (2013), Harries et al. (2012), Kahn and Mitchell (2002), Mattock (1976), and Paulay et al. (1974). Several all-lightweight slate and clay specimens from the concurrent study by Krc (2015) are also included in the analysis contained in this section. The specimens from these studies were constructed of normalweight concrete (NWC), sand-lightweight concrete (SLW), or all-lightweight concrete (ALW). In this section, the results from these studies are summarized in terms of specimens with a roughened interface (Figure 4.38) or a smooth interface (Figure 4.39). The data are plotted in terms of peak shear stress v_u versus reinforcement parameter ρf_y. For Figures 4.38 and 4.39, actual steel reinforcement yield strengths f_y were used. Further details of the results from these specific studies are tabulated in the Appendix of this thesis.

It should be noted that most of the compressive strengths of the specimens shown in Figures 4.38 and 4.39 range from about 3,000 psi to about 6,000 psi. As shown in the figure legends, several series from Shaw 2013 had a target compressive strength of 8,000 psi. Also, Kahn and Mitchell studied the shear-friction properties of high-strength concrete; thus, the specimens from that study had compressive strengths of about 12,000 psi to 15,000 psi. In addition, Kahn and Mitchell did not intentionally roughen their specimens, but the shear interface surfaces appeared rough, with an average amplitude of about 0.25 in. This was true for all specimens except two, which appeared smooth due to the use of a high-slump concrete mixture, even though they were not troweled smooth. For comparison purposes, the specimens from Kahn and Mitchell's study were considered roughened or smooth in Figures 4.38 and 4.39 based on these descriptions of their appearances, even though none of them were 'intentionally roughened.' In addition, the specimens from Mattock (1976) were pre-cracked before loading as is sometimes done in the testing of monolithic specimens. Yet, these specimens were included in this analysis since they were constructed with a cold-joint at the shear interface. Also worth noting is that the specimens' shear interfaces were intentionally roughened through several methods in the study by Paulay et al. (1974), but actual amplitudes for some specimens reached as high as 0.75 in. and others may have been below 0.25 in.

As shown in both Figures 4.38 and 4.39, the shear strength v_u shows an increasing trend as the reinforcement parameter ρf_y increases. Another interesting observation is that v_u is higher for specimens with a higher concrete compressive strength f'_c when compared to specimens with a similar reinforcement parameter ρf_y. This trend is true for both interface conditions shown, but it is more apparent for specimens of a roughened interface. In general, shear strengths are higher for roughened interface specimens (Figure 4.38) than smooth interface specimens (Figure 4.39) of the same value of ρf_y.

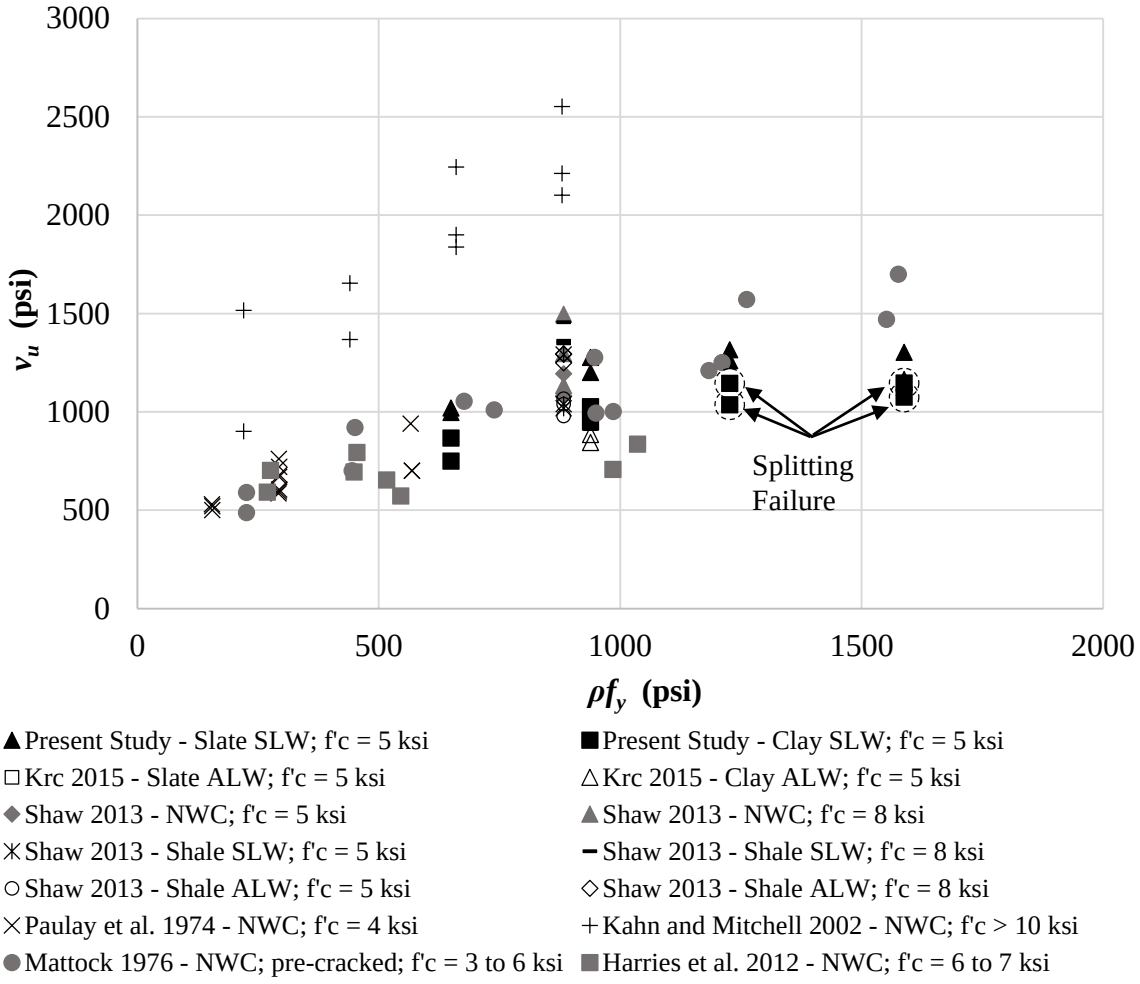

Figure 4.38. Comparison of shear strength v_u for cold-joint specimens with a roughened interface (normalweight, sand-lightweight, and all-lightweight concrete specimens included)

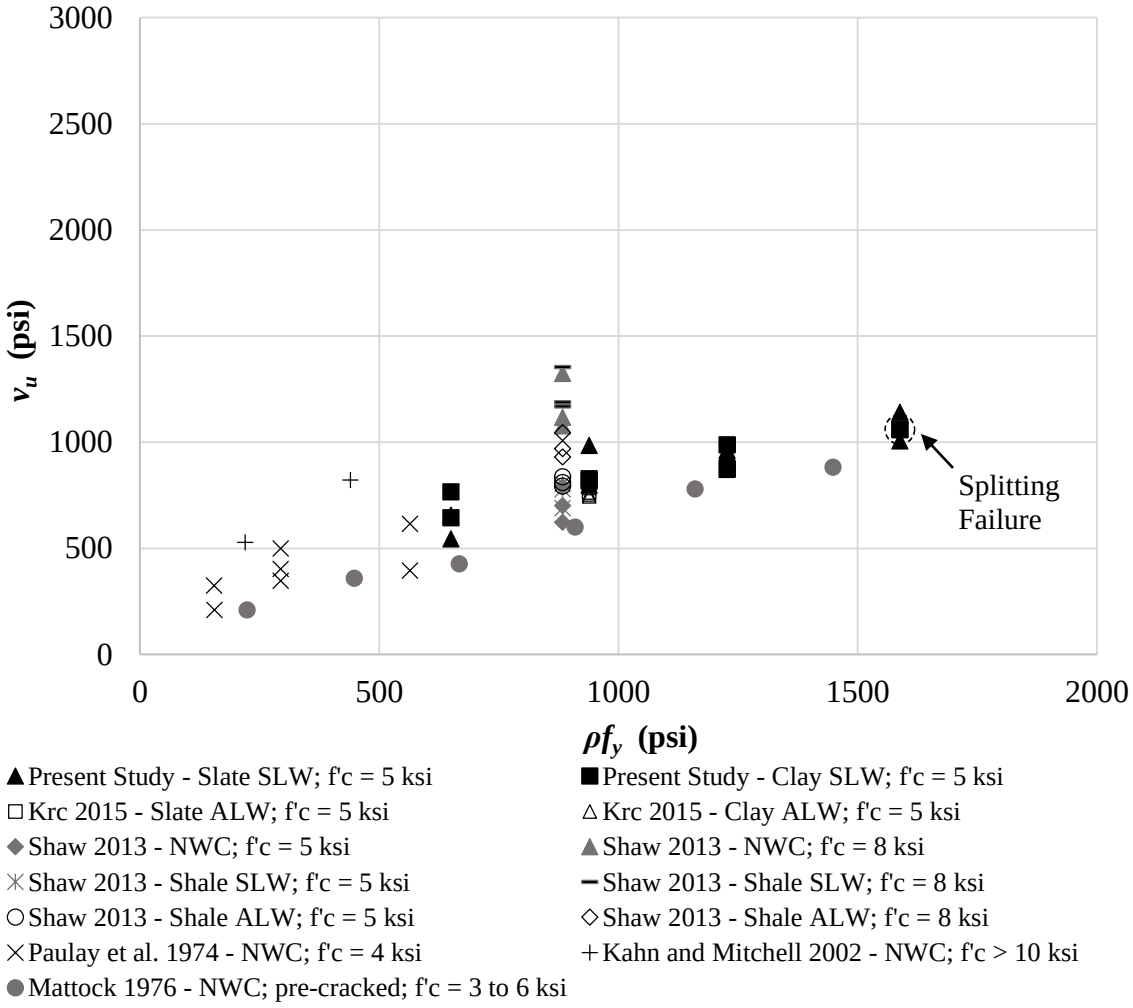

Figure 4.39. Comparison of shear strength v_u for cold-joint specimens with a smooth interface (normalweight, sand-lightweight, and all-lightweight concrete specimens included)

The higher shear strength values for concretes with higher concrete compressive strengths suggests that shear-friction design equations or limits for shear strength should include f'_c as proposed by Kahn and Mitchell (2002) and Harries et al. (2012). Also, as shown in Figures 4.38 and 4.39, Kahn and Mitchell's (2002) specimens had reinforcement parameters ρf_y below 900 psi. It would be interesting to see the behavior of specimens with f'_c > 10,000 psi that have reinforcement parameters ρf_y in the 1,000 psi to 1,600 psi range. Adding this data to Figures 4.38 and 4.39 would provide a better understanding of the behavior of specimens with high reinforcement parameters (ρf_y >

1,000 psi). For the roughened interface specimens (Figure 4.38), especially from this study, the shear strengths v_u seemed to level off at higher levels of ρf_y. Yet, this behavior was not observed for Mattock's (2002) normalweight specimens which seemed to increase linearly for all values of ρf_y. Therefore, it would be interesting to see which pattern the normalweight specimens from Kahn and Mitchell's study would follow if their testing program were extended to values of ρf_y up to 1,600 psi.

Also, it would be useful to test specimens of ρf_y greater than that which is shown on Figures 4.38 and 4.39 (ρf_y > 1,600 psi). This would reveal whether shear strength v_u increases indefinitely with increasing ρf_y, or if there is a maximum value of shear strength which can be achieved.

Section 4.4 compared the results of this study to the current shear-friction design provisions of the ACI, PCI, and AASHTO codes/specifications. This comparison showed that the predicted shear strengths from the AASHTO provisions had the closest correlation to the test data for both the roughened and smooth interface conditions. Thus, it is worthwhile to also compare the AASHTO shear-friction design provisions to other data sets from previous studies of cold-joint specimens. Shear-friction design equations proposed by Mattock (2001) are in a similar form as the AASHTO shear-friction equation. Therefore, to determine how the Mattock equations fit the data as compared to AASTHO, both sets of equations were plotted in Figures 4.40 through 4.43. As described in detail in Section 2.4.13, Mattock proposed the following design equations and limits:

1. For monolithic concrete and cold-joint connections with interface intentionally roughened:
   a. When $(\rho_{vf} f_y + \sigma_{Nx}) \geq K_1/1.45$

      Where: $K_1 = 0.1f'_c$, but not more than 800 psi;

$$v_n = K_1 + 0.8\left(\rho_{vf} f_y + \sigma_{Nx}\right) \ (psi) \qquad (4.20)$$

but not greater than $K_2 f'_c$ nor K_3 psi;

Where: $K_2 = 0.3$; $K_3 = 2400$ psi

b. When $(\rho_{vf} f_y + \sigma_{Nx}) \leq K_1/1.45$

$$v_n = 2.25(\rho_{vf} f_y + \sigma_{Nx}) \ (psi) \tag{4.21}$$

Note: For normalweight monolithic concrete, $K_1 = 0.1f'_c$ but not more than 800 psi; $K_2 = 0.3$; and $K_3 = 2400$ psi. For normalweight concrete placed against hardened normalweight concrete with the interface intentionally roughened, $K_1 = 400$ psi; $K_2 = 0.3$, where f'_c shall be taken as the lower of the compressive strengths of the two concretes; and $K_3 = 2400$ psi. For sand-lightweight concrete, $K_1 = 250$ psi; $K_2 = 0.2$; and $K_3 = 1200$ psi. For all-lightweight concrete, $K_1 = 200$ psi; $K_2 = 0.2$; and $K_3 = 1200$ psi.

2. For concrete placed against hardened concrete not intentionally roughened,

$$v_n = 0.6\lambda\rho_{vf} f_y \ (psi) \tag{4.22}$$

but not more than $0.2f'_c$ nor 800 psi

Due to the different limits on shear strength for normalweight, sand-lightweight, and all-lightweight concrete with a roughened interface, it was necessary to break up the data in Figure 4.38 according to unit weight. The resulting plots for the roughened interface specimens are shown in Figures 4.40, 4.41, and 4.42. Since there were six different compressive strengths for the normalweight test data, there were many different shear strength limits for both the AASHTO equation and the Mattock equation. These are summarized in Table 4.11. For the smooth specimens, it was also necessary to break up the data according to unit weight due to the inclusion of the lightweight modification factor λ in the Mattock proposed equation. Therefore, the smooth interface specimens are shown in Figures 4.43, 4.44, and 4.45 which correspond to sand-lightweight, all-lightweight, and normalweight specimens, respectively.

As was done in Section 4.4, the AASHTO predicted shear strengths in Figures 4.40 through 4.43 are shown in two different forms: Equations 4.16 and 4.18, which correspond to the cohesion factor being set to either zero or set to the values from Table 4.9. As discussed previously, this was done to validate the AASHTO provision which requires the cohesion factor *c* to be set to zero for the case of brackets, corbels, and ledges. This provision is in place due to the unreliable cohesion and aggregate interlock properties of a vertical crack interface.

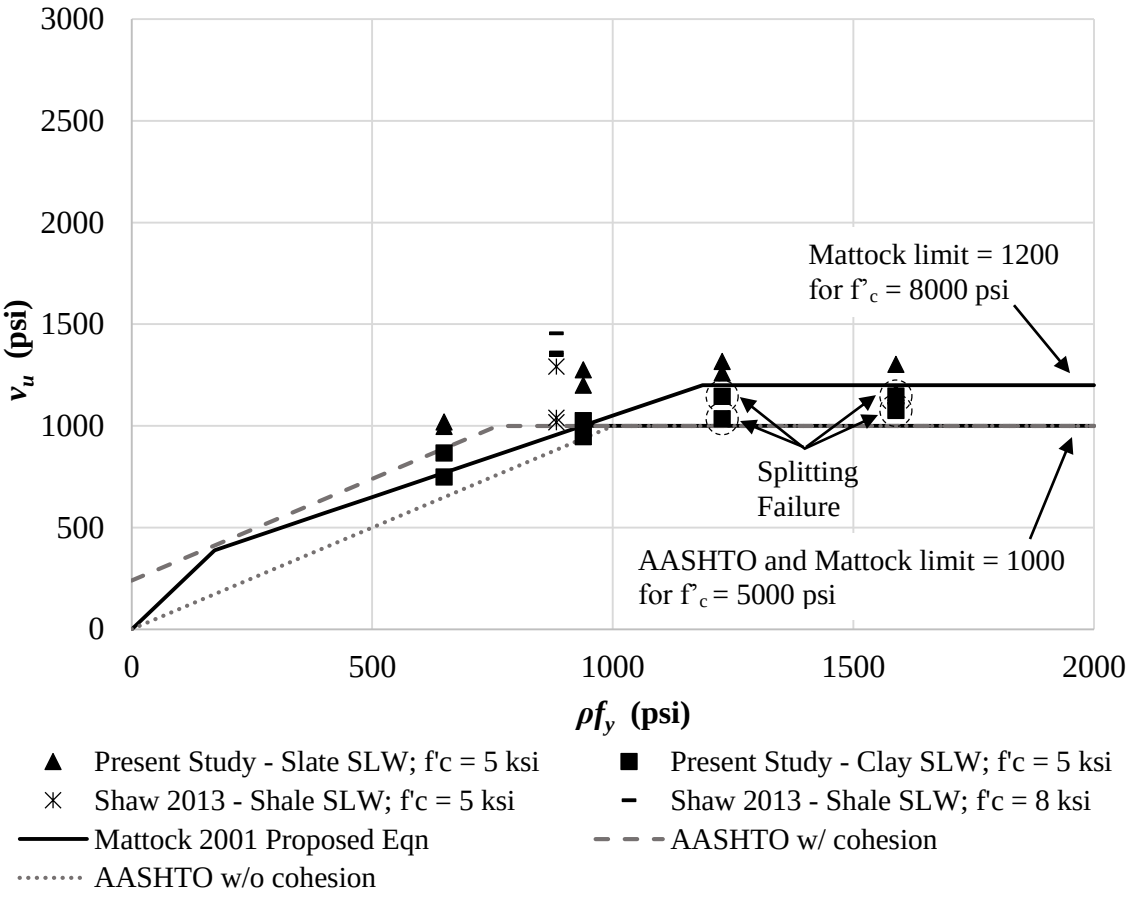

Figure 4.40. Comparison of Mattock (2001) proposed equation and AASHTO specification for sand-lightweight cold-joint specimens with a roughened interface

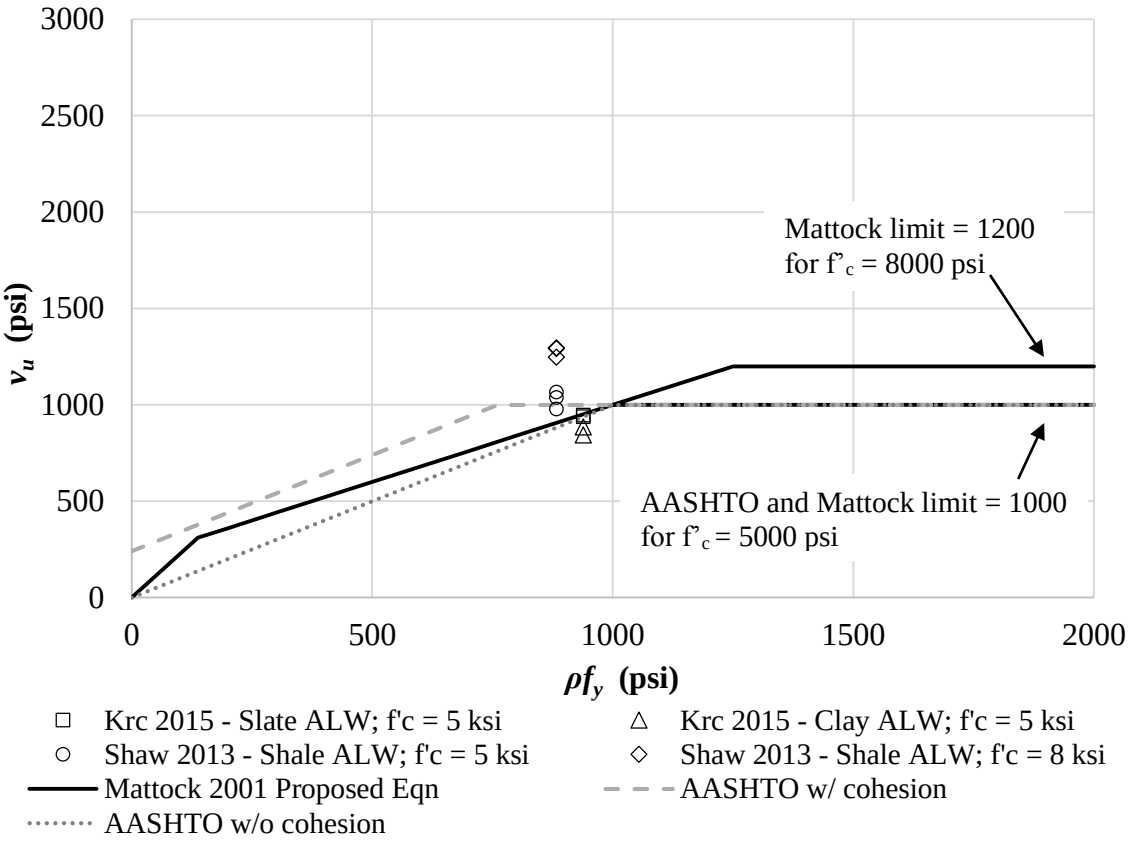

Figure 4.41. Comparison of Mattock (2001) proposed equation and AASHTO specification for all-lightweight cold-joint specimens with a roughened interface

As shown in Figures 4.40 through 4.42, the Mattock equations provide a more accurate prediction of shear strength of roughened specimens because the test data and predicted values are similar. However, the AASHTO equations are more conservative for most data points. For the smooth specimens constructed from lightweight concrete (Figures 4.43 and 4.44), the opposite is true: the AASHTO equations provide a closer fit to the test data, and the Mattock equation is more conservative. All three equations on these two figures are conservative for each data point. For the normalweight specimens (Figure 4.45), the AASHTO equations are again more aligned with the test data, but there are a few unconservative points for specimens with $f'_c \leq 4000$ psi. The Mattock proposed equation is conservative for all data points in Figure 4.45.

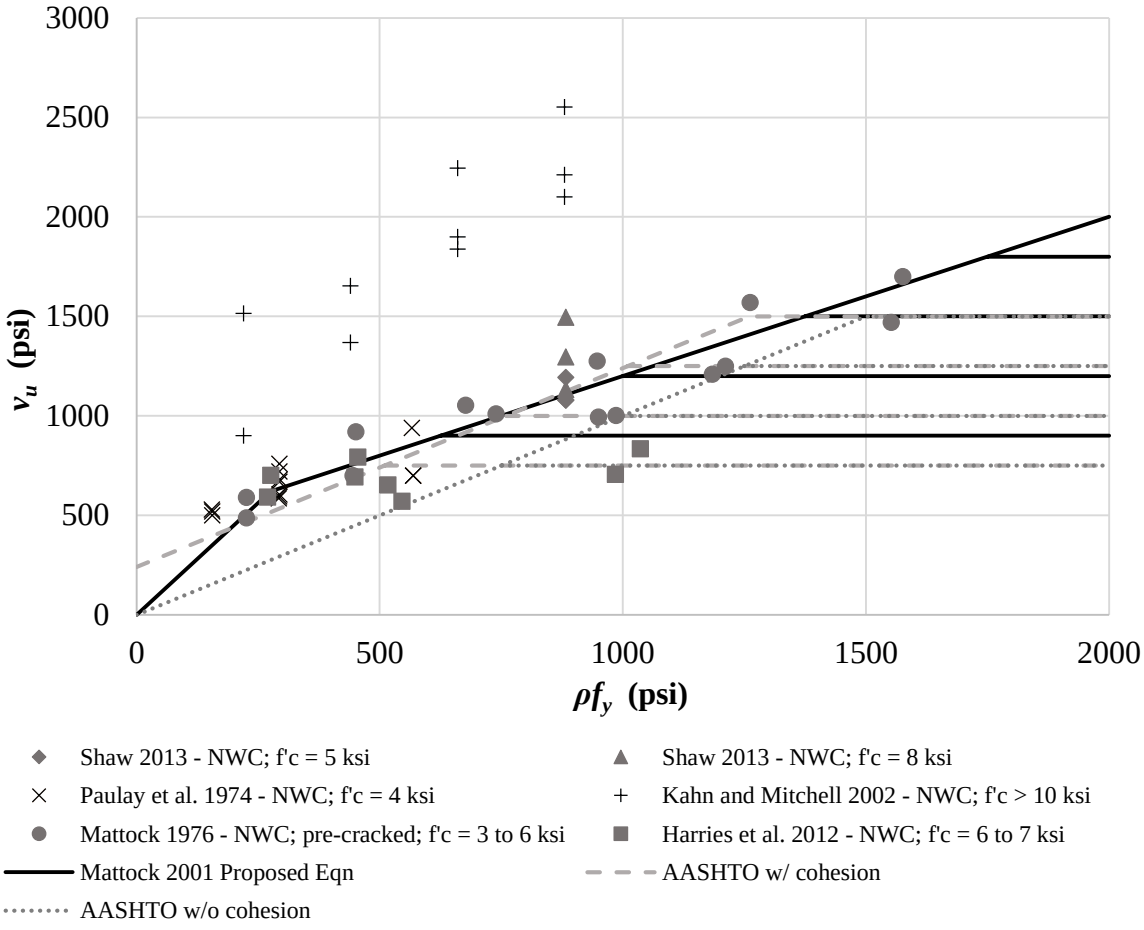

Figure 4.42. Comparison of Mattock (2001) proposed equation and AASHTO specification for normalweight cold-joint specimens with a roughened interface with limits as shown in Table 4.11

Table 4.11. Calculated Limits on Shear Strength for Normalweight Concrete Specimens in Figure 4.42

Concrete Compressive Strength (psi)	**Mattock Calculated Limit (psi)**	**AASHTO Calculated Limit (psi)**
3000	900	750
4000	1200	1000
5000	1500	1250
6000	1800	1500
8000	2400	1500
10,000	2400	1500

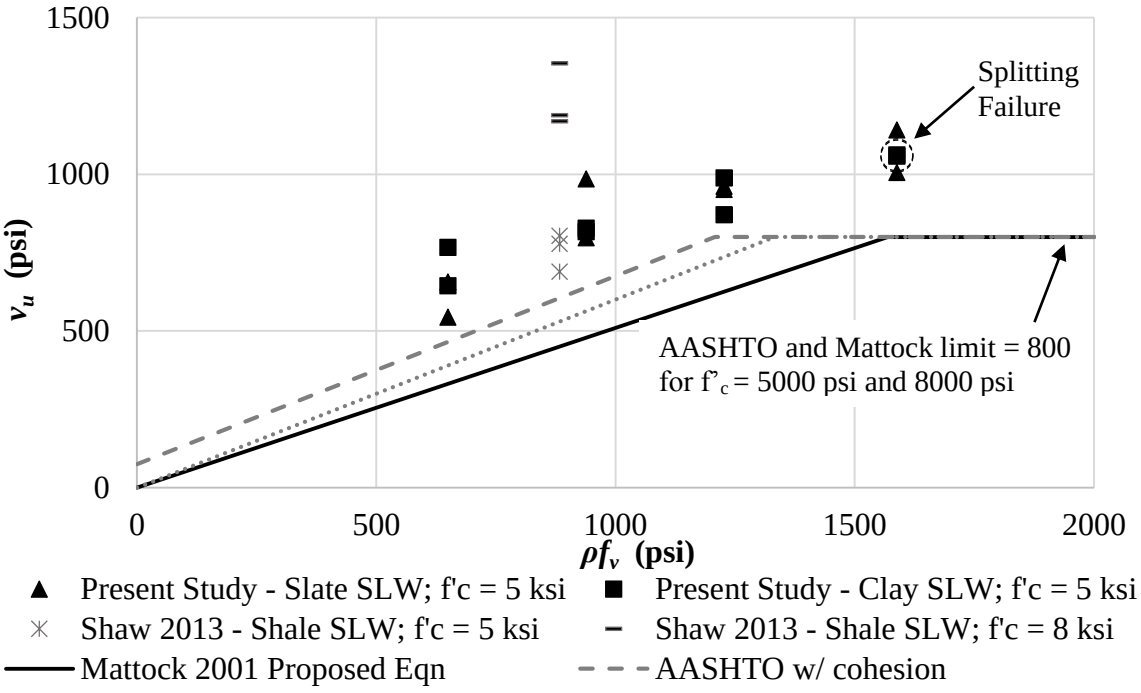

Figure 4.43. Comparison of Mattock (2001) proposed equation and AASHTO specification for sand-lightweight cold-joint specimens with a smooth interface

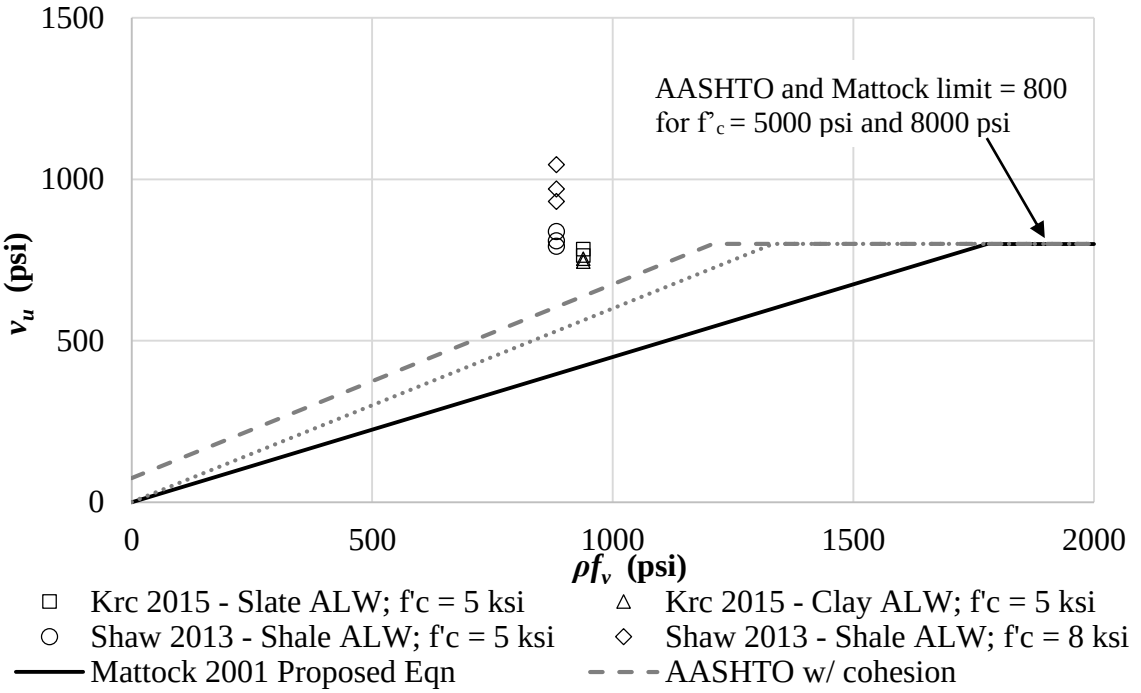

Figure 4.44. Comparison of Mattock (2001) proposed equation and AASHTO specification for all-lightweight cold-joint specimens with a smooth interface

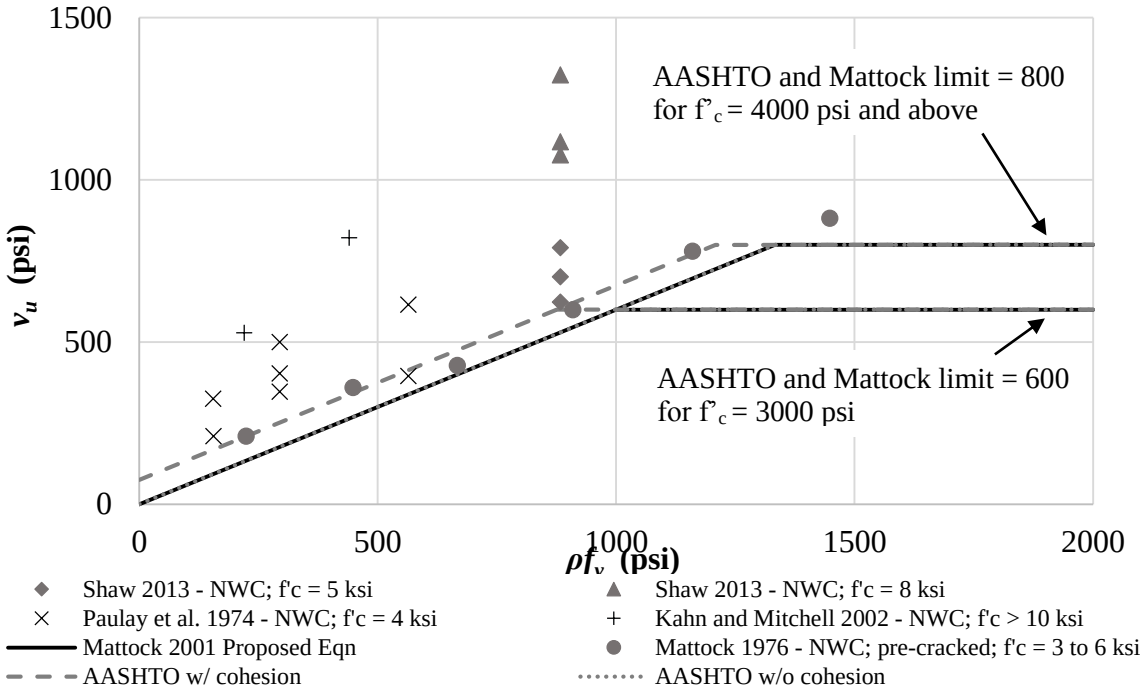

Figure 4.45. Comparison of Mattock (2001) proposed equation and AASHTO specification for normalweight cold-joint specimens with a smooth interface

5. SUMMARY, CONCLUSIONS, AND RECOMMENDATIONS

5.1. SUMMARY

This testing program studied the effects of aggregate type, interface condition, and reinforcement ratio on the shear strength of non-monolithic (cold-joint) lightweight concrete specimens. Cold-joints (or construction joints) are common at the connections to precast elements, and shear forces can be high in these areas. Shear-friction principles are often used for the design of reinforcement crossing a cold-joint. This study was intended to expand a previous study by Shaw (2013) and a concurrent study by Krc (2015) to include more types of lightweight aggregate and also to discover how shear strength is affected when the shear reinforcement ratio ρ is varied. The overall goal of this study was to determine if values for shear strength v_u and effective coefficient of friction μ_e were conservatively predicted by current ACI, PCI, and AASHTO shear-friction design provisions.

Thirty-two specimens were constructed with a cold-joint which was either troweled smooth or intentionally roughened to an amplitude of ¼ in. All specimens were considered sand-lightweight (λ = 0.85), since they were constructed from river sand and either expanded clay or expanded slate coarse aggregate. The shear specimens were reinforced with No. 3 double-legged steel stirrups in varying numbers to create reinforcement ratios of ρ = 0.009, ρ = 0.013, ρ = 0.017, or ρ = 0.022 across the shear interface. The target concrete compressive strength of all specimens was 5000 psi, with actual compressive strengths ranging from 4550 psi to 5570 psi. Each specimen was loaded monotonically at a constant platen displacement of 0.015 in. per minute until failure. Data was presented for all specimens in terms of the following relations: shear force vs. slip, shear force vs. dilation, shear force vs. interface steel strain, slip vs dilation, and slip vs. interface steel strain. General behaviors of the specimens were noted, and results were compared to current shear-friction design provisions from ACI 318, the PCI Design Handbook, and AASHTO Specifications as well as data from previous studies.

5.2. CONCLUSIONS

Based on the data from these 32 sand-lightweight specimens, the following conclusions can be made:

1. The global cracking behavior of specimens with higher reinforcement ratios was different than that of specimens with smaller amounts of reinforcement. The specimens with more reinforcement had splitting cracks and flexural cracks which accompanied the shear interface cracking, and in some specimens, (the CL-R-17, CL-R-22, and CL-S-22 series) concrete splitting was the principal failure mode. This is most likely due to the low tensile strength of the clay sand-lightweight concrete. To mitigate this type of failure in clay sand-lightweight concrete shear-friction specimens, more cover (at least 1.5 in.) is recommended if the value of ρf_y is high (ρf_y > 1000 psi).
2. Shear strength v_u was 5% to 68% higher for specimens with a roughened interface than a smooth interface (with similar aggregate type and reinforcement ratio). The slate aggregate specimens were more sensitive to interface condition than the corresponding clay aggregate specimens. Also, the influence of interface condition diminished as reinforcement ratio increased.
3. The roughened specimens behaved in a more quasi-brittle manner than the smooth specimens, with a sharper drop-off in applied shear force after the peak. Yet residual shear strength v_{ur} for roughened and smooth specimens was similar.
4. The average interface cracking stress v_{cr} (the point at which shear cracking first occurs) was higher for the roughened specimens than the smooth specimens of similar aggregate type and reinforcement ratio.
5. For specimens with a similar interface condition and reinforcement ratio, the average ultimate shear stress $v_{u,avg}$ was generally higher for the slate aggregate specimens than the clay aggregate specimens (with one outlier: for CL-S-9 series, $v_{u,avg}$ was greater than that of SL-S-9). The specimens with a roughened interface were much more sensitive to lightweight aggregate type than the smooth specimens. Also, the influence of lightweight aggregate type diminished as reinforcement ratio increased.

6. As a general trend, the shear transfer strength increased with increasing reinforcement ratio. However, for the CL-R series and the SL-R series, the shear strength leveled off at the higher reinforcement ratios. The clay, roughened series may have behaved this way due to the splitting failures of the CL-R-17 and CL-R-22 specimens. For the SL-R-22 specimens which failed along the shear plane, the influence of splitting and flexural cracking could have reduced the shear strength of these specimens, causing the trendline to flatten out at higher values of ρ.
7. Residual shear strength v_{ur} increased with increasing reinforcement ratio (with the exception of the clay aggregate, roughened series in which v_{ur} appeared to be unaffected by reinforcement ratio).
8. All shear strengths v_u from the smooth interface test specimens in this study were higher than the predicted shear strength from the current ACI, PCI, and AASHTO codes/specifications. This includes the μ_e approach from the 7th Edition of the PCI Design Handbook, which is not applicable in this version. All design methods were conservative for smooth specimens with the highest reinforcement ratio (ρ = 0.022). The AASHTO design provisions, with cohesion term cA_{cv} included, have the closest correlation to the test data for smooth specimens.
9. All shear strengths from the roughened interface test specimens in this study were higher than the predicted shear strengths from the current ACI, PCI, and AASHTO codes/provisions. When the cohesion term cA_{cv} is included in the AASHTO design provisions (using values of c from AASHTO 7th Ed. Section 5.8.4.3), predicted shear strengths are unconservative for most of the clay specimens. The closest correlation to test data for roughened interface specimens, while still being conservative, came from the AASHTO design equation with the cohesion factor c taken as 0.0 (which follows current AASHTO provisions for vertical shear interfaces).
10. Equation 5-33 from the 7th Edition of the PCI Design Handbook conservatively predicts values of μ_e for both roughened and smooth interface specimens, even though the μ_e approach is considered ‘not applicable’ for the design of smooth

specimens (Case 3). Also, PCI Handbook Equation 5-33 is more conservative for the slate specimens than the clay sand-lightweight specimens in this study (with one exception: SL-S-9 was less conservative than CL-S-9).

11. The use of the lightweight modification factor λ twice in the calculation for the effective coefficient of friction (once explicitly in the equation and again in the definition of μ) is conservative for the sand-lightweight concretes tested in this study.
12. The limits on shear strength of sand-lightweight connections for roughened interfaces in the PCI and ACI shear friction provisions could be raised to 1000 psi and still be conservative for the specimens in this study. Likewise, the limits on shear strength of sand-lightweight cold-joint connections with a smooth interface could be raised to 800 psi in the PCI shear friction provisions and still be conservative for the values in this study. This could be accomplished by directly changing the ACI limit of $v_u \leq 800$ psi to 1000 psi, and by eliminating λ from the PCI roughened and smooth limits of $v_u \leq 1000\lambda$ psi and $v_u \leq 800\lambda$ psi, respectively. These changes would bring the ACI and PCI limits for sand-lightweight concrete with ($f'_c \geq 5000$ psi) in line with the AASHTO shear strength limits which had the best fit to the experimental data in this study.

5.3. RECOMMENDATIONS FOR DESIGN EQUATIONS

As discussed in Section 5.2, using the effective coefficient of friction μ_e approach from the 7th Edition of the PCI Design Handbook produced conservative predictions of shear strength for specimens with a smooth interface. As noted in earlier sections, this approach is not considered applicable to smooth interfaces (Case 3). However, the results of this study support the use of the μ_e approach for a smooth interface. The value of $\mu_{e,max}$ from the 6th Edition of the PCI Design Handbook was also proven to be valid for this set of test data. Therefore, it is recommended that the μ_e approach used in the 7th Edition of the PCI Design Handbook be considered applicable for a smooth interface condition, and $\mu_{e,max}$ be set equal to 2.2, as designated in the 6th Edition of the PCI Design Handbook.

Predicted values for μ_e using Equation 5-33 from the 7th Edition of the PCI Design Handbook were conservative for all specimens in this study. The lightweight modification factor λ appears twice in Equation 5-33, once explicitly and again in the definition for μ which significantly reduces the μ_e values for lightweight concrete. Removing the explicit value of λ from Equation 5-33 (and leaving the λ which is included in the definition of μ alone) produces a much better correlation to the test data with the predicted values for μ_e still being conservative for all specimens from this study except one (as shown in Figures 4.36 and 4.37). This result is also supported by data from Shaw (2013) and suggests that one of the two instances of the lightweight modification factor λ may not be required in the equation for μ_e.

Also, as a simplification of shear friction design equations, the current design codes and specifications could allow design using the residual shear strength, which was found to be independent of interface condition, but dependent on reinforcement ratio. For the specimens in this study, conservative nominal shear strength values of v_n = 540 psi, v_n = 680 psi, v_n = 670 psi, and v_n = 730 psi (which correspond to reinforcement ratios of 0.009, 0.013, 0.017, and 0.022, respectively) could be used for shear friction design. These values represent the average residual shear strength $v_{ur,avg}$ of the specimens from this study within each reinforcement ratio, excluding those which failed due to concrete splitting.

5.4. RECOMMENDATIONS FOR FUTURE WORK

Other considerations in the study of shear-friction that are recommended to be incorporated in future work include the following:

1. The study by Shaw (2013) could be further expanded to study the effect of varying the reinforcement ratio for normalweight, shale sand-lightweight, and shale all-lightweight concrete.
2. To prevent concrete splitting from becoming the principal failure mode for specimens that have high reinforcement ratios and are constructed from concrete with a low tensile strength, the specimen could be redesigned. The geometry could be altered so that the shear plane is the same size, yet the flanges could be

increased in size, along with an associated increase in flange reinforcement as well.

3. A common industry practice is to make sand-lightweight concrete using lightweight coarse aggregate as a partial substitute for normalweight coarse aggregate. A study to determine the loss of shear strength with certain percentages of normalweight aggregate replaced would determine the validity of ACI 318-14 provision in Table 19.2.4.2. This provision states that λ may be linearly interpolated between 0.85 and 1.0 on the basis of volumetric fractions, for concrete containing a partial replacement of normalweight coarse aggregate with lightweight coarse aggregate.
4. Although it is outside the scope of shear friction, it would be interesting to study the effect of different lightweight aggregate types on the bond strength of reinforcing bars to lightweight aggregate concretes since inadequate bond strength caused several specimens in this study to fail due to concrete splitting.
5. More sand-lightweight and all-lightweight concrete test data is needed to verify whether or not the equation for the effective coefficient of friction μ_e needs to include two instances of the lightweight modification factor λ.
6. For completeness, future shear-friction push-off tests should not stop testing at 60% of peak load if slip has not yet reached 0.15 in. This way values for residual shear force V_{ur} can be recorded. This data could be useful for research of the post-peak residual capacity of a connection.
7. It would be useful study the individual contributions of concrete and reinforcing steel to the shear strength of an interface. Decoupling the concrete and steel components could be done in a similar manner as was done by Harries et al. (2012) and would further describe the fundamental mechanisms of shear friction.

Specimen ID		Concrete Properties		Shear Plane Geometry and Condition			Shear Plane Reinforcement			Testing Data	
		f'_c at Test (psi)	Density (pcf)	Interface Condition	Casting Procedure	A_{cr} (sq. in.)	A_{vf} (sq. in.)	f_y (ksi)	$\rho_{rf}f_y$ (psi)	V_n (kips)	v_n (psi)
Wermager, 2015	S-SL-CJ-R-9-1	5380	117	Cold Joint - Rough	Composite	49.5	0.44	72.2	533	49.3	997
	S-SL-CJ-R-9-2	5380	117	Cold Joint - Rough	Composite	49.5	0.44	72.2	533	50.5	1020
	S-SL-CJ-S-9-1	5380	117	Cold Joint - Smooth	Composite	49.5	0.44	72.2	533	26.9	544
	S-SL-CJ-S-9-2	5380	117	Cold Joint - Smooth	Composite	49.5	0.44	72.2	533	32.6	658
	S-SL-CJ-R-13-1	5570	117	Cold Joint - Rough	Composite	49.5	0.66	72.2	800	63.2	1276
	S-SL-CJ-R-13-2	5570	117	Cold Joint - Rough	Composite	49.5	0.66	72.2	800	59.4	1199
	S-SL-CJ-S-13-1	5570	117	Cold Joint - Smooth	Composite	49.5	0.66	72.2	800	39.5	798
	S-SL-CJ-S-13-2	5570	117	Cold Joint - Smooth	Composite	49.5	0.66	72.2	800	48.8	985
	S-SL-CJ-R-17-1	4950	117	Cold Joint - Rough	Composite	49.5	0.88	72.2	1067	62.4	1260
	S-SL-CJ-R-17-2	4950	117	Cold Joint - Rough	Composite	49.5	0.88	72.2	1067	65.2	1316
	S-SL-CJ-S-17-1	4950	117	Cold Joint - Smooth	Composite	49.5	0.88	72.2	1067	49.8	1006
	S-SL-CJ-S-17-2	4950	117	Cold Joint - Smooth	Composite	49.5	0.88	72.2	1067	56.5	1142
	S-SL-CJ-R-22-1	5000	118	Cold Joint - Rough	Composite	49.5	1.1	72.2	1333	64.5	1302
	S-SL-CJ-R-22-2	5000	118	Cold Joint - Rough	Composite	49.5	1.1	72.2	1333	57.6	1163
	S-SL-CJ-S-22-1	5000	118	Cold Joint - Smooth	Composite	49.5	1.1	72.2	1333	49.8	1006
	S-SL-CJ-S-22-2	5000	118	Cold Joint - Smooth	Composite	49.5	1.1	72.2	1333	56.5	1142

Specimen ID		Concrete Properties		Shear Plane Geometry and Condition			Shear Plane Reinforcement			Testing Data	
		f'_c at Test (psi)	Density (pcf)	Interface Condition	Casting Procedure	A_{cr} (sq. in.)	A_{vf} (sq. in.)	f_y (ksi)	$\rho_{rf}f_y$ (psi)	V_u (kips)	v_u (psi)
Wermager, 2015	S-CL-CJ-R-9-1	4770	105	Cold Joint - Rough	Composite	49.5	0.44	72.2	533	37.1	749
	S-CL-CJ-R-9-2	4770	105	Cold Joint - Rough	Composite	49.5	0.44	72.2	533	42.9	867
	S-CL-CJ-S-9-1	4770	105	Cold Joint - Smooth	Composite	49.5	0.44	72.2	533	31.9	644
	S-CL-CJ-S-9-2	4770	105	Cold Joint - Smooth	Composite	49.5	0.44	72.2	533	37.9	766
	S-CL-CJ-R-13-1	4640	105	Cold Joint - Rough	Composite	49.5	0.66	72.2	800	50.8	1026
	S-CL-CJ-R-13-2	4640	105	Cold Joint - Rough	Composite	49.5	0.66	72.2	800	46.9	947
	S-CL-CJ-S-13-1	4640	105	Cold Joint - Smooth	Composite	49.5	0.66	72.2	800	41.0	828
	S-CL-CJ-S-13-2	4640	105	Cold Joint - Smooth	Composite	49.5	0.66	72.2	800	40.4	816
	S-CL-CJ-R-17-1	4550	105	Cold Joint - Rough	Composite	49.5	0.88	72.2	1067	51.2	1034
	S-CL-CJ-R-17-2	4550	105	Cold Joint - Rough	Composite	49.5	0.88	72.2	1067	56.7	1145
	S-CL-CJ-S-17-1	4550	105	Cold Joint - Smooth	Composite	49.5	0.88	72.2	1067	43.1	871
	S-CL-CJ-S-17-2	4550	105	Cold Joint - Smooth	Composite	49.5	0.88	72.2	1067	48.9	988
	S-CL-CJ-R-22-1	4790	105	Cold Joint - Rough	Composite	49.5	1.1	72.2	1333	56.7	1145
	S-CL-CJ-R-22-2	4790	105	Cold Joint - Rough	Composite	49.5	1.1	72.2	1333	53.2	1075
	S-CL-CJ-S-22-1	4790	105	Cold Joint - Smooth	Composite	49.5	1.1	72.2	1333	52.4	1059
	S-CL-CJ-S-22-2	4790	105	Cold Joint - Smooth	Composite	49.5	1.1	72.2	1333	52.6	1063

Specimen ID		Concrete Properties		Shear Plane Geometry and Condition			Shear Plane Reinforcement			Testing Data	
		f'_c at Test (psi)	Density (pcf)	Interface Condition	Casting Procedure	A_{cr} (sq. in.)	A_{vf} (sq. in.)	f_y (ksi)	$\rho_{rf}f_y$ (psi)	V_n (kips)	v_n (psi)
Krc, 2015	N-MO-P-13-1	4840	147	Monolithic	Precracked	49.5	0.66	72.2	800	61.1	1234
	N-MO-P-13-2	4840	147	Monolithic	Precracked	49.5	0.66	72.2	800	57.0	1151
	N-MO-U-13-1	4840	147	Monolithic	Uncracked	49.5	0.66	72.2	800	63.4	1281
	N-MO-U-13-2	4840	147	Monolithic	Uncracked	49.5	0.66	72.2	800	62.2	1257
	S-SH-MO-P-13-1	4770	114	Monolithic	Precracked	49.5	0.66	72.2	800	50.6	1022
	S-SH-MO-P-13-2	4770	114	Monolithic	Precracked	49.5	0.66	72.2	800	51.9	1048
	S-SH-MO-U-13-1	4770	114	Monolithic	Uncracked	49.5	0.66	72.2	800	55.4	1120
	S-SH-MO-U-13-2	4770	114	Monolithic	Uncracked	49.5	0.66	72.2	800	56.6	1143
	A-SH-MO-P-13-1	4700	109	Monolithic	Precracked	49.5	0.66	72.2	800	46.1	932
	A-SH-MO-P-13-2	4700	109	Monolithic	Precracked	49.5	0.66	72.2	800	52.7	1064
	A-SH-MO-U-13-1	4700	109	Monolithic	Uncracked	49.5	0.66	72.2	800	52.0	1051
	A-SH-MO-U-13-2	4700	109	Monolithic	Uncracked	49.5	0.66	72.2	800	52.5	1062
	S-SL-CJ-R-13-1	5570	117	Cold Joint - Rough	Composite	49.5	0.66	72.2	800	63.2	1276
	S-SL-CJ-R-13-2	5570	117	Cold Joint - Rough	Composite	49.5	0.66	72.2	800	59.4	1199
	S-SL-CJ-S-13-1	5570	117	Cold Joint - Smooth	Composite	49.5	0.66	72.2	800	39.5	798
	S-SL-CJ-S-13-2	5570	117	Cold Joint - Smooth	Composite	49.5	0.66	72.2	800	48.8	985

Specimen ID		Concrete Properties		Shear Plane Geometry and Condition			Shear Plane Reinforcement			Testing Data	
		f'_c at Test (psi)	Density (pcf)	Interface Condition	Casting Procedure	A_{cr} (sq. in.)	A_{vf} (sq. in.)	f_y (ksi)	$\rho_{rf}f_y$ (psi)	V_n (kips)	v_n (psi)
Krc, 2015	A-SL-CJ-R-13-1	4380	106	Cold Joint - Rough	Composite	49.5	0.66	72.2	800	46.5	939
	A-SL-CJ-R-13-2	4380	106	Cold Joint - Rough	Composite	49.5	0.66	72.2	800	46.9	947
	A-SL-CJ-S-13-1	4380	106	Cold Joint - Smooth	Composite	49.5	0.66	72.2	800	37.8	764
	A-SL-CJ-S-13-2	4380	106	Cold Joint - Smooth	Composite	49.5	0.66	72.2	800	38.8	784
	S-CL-CJ-R-13-1	4640	105	Cold Joint - Rough	Composite	49.5	0.66	72.2	800	50.8	1026
	S-CL-CJ-R-13-2	4640	105	Cold Joint - Rough	Composite	49.5	0.66	72.2	800	46.9	947
	S-CL-CJ-S-13-1	4640	105	Cold Joint - Smooth	Composite	49.5	0.66	72.2	800	41.0	828
	S-CL-CJ-S-13-2	4640	105	Cold Joint - Smooth	Composite	49.5	0.66	72.2	800	40.4	816
	A-CL-CJ-R-13-1	4460	88	Cold Joint - Rough	Composite	49.5	0.66	72.2	800	41.8	844
	A-CL-CJ-R-13-2	4460	88	Cold Joint - Rough	Composite	49.5	0.66	72.2	800	43.8	885
	A-CL-CJ-S-13-1	4460	88	Cold Joint - Smooth	Composite	49.5	0.66	72.2	800	36.9	745
	A-CL-CJ-S-13-2	4460	88	Cold Joint - Smooth	Composite	49.5	0.66	72.2	800	37.3	754

Specimen ID		Concrete Properties		Shear Plane Geometry and Condition			Shear Plane Reinforcement			Testing Data	
		f'_c at Test (psi)	Density (pcf)	Interface Condition	Casting Procedure	A_{cr} (sq. in.)	A_{vf} (sq. in.)	f_y (ksi)	$\rho_{vf}f_y$ (psi)	V_u (kips)	v_u (psi)
Shaw 2013	N-5-R-4	4860	147	Cold Joint - Rough	Composite	49.5	0.66	66.2	883	59.1	1193
	N-5-R-5	4860	147	Cold Joint - Rough	Composite	49.5	0.66	66.2	883	53.4	1079
	N-5-R-6	4860	147	Cold Joint - Rough	Composite	49.5	0.66	66.2	883	53.4	1080
	N-5-S-4	4860	147	Cold Joint - Smooth	Composite	49.5	0.66	66.2	883	30.9	623
	N-5-S-5	4860	147	Cold Joint - Smooth	Composite	49.5	0.66	66.2	883	34.7	701
	N-5-S-6	4860	147	Cold Joint - Smooth	Composite	49.5	0.66	66.2	883	39.2	791
	S-5-R-1	4580	118	Cold Joint - Rough	Composite	49.5	0.66	66.2	883	51.4	1039
	S-5-R-2	4580	118	Cold Joint - Rough	Composite	49.5	0.66	66.2	883	50.4	1018
	S-5-R-3	4580	118	Cold Joint - Rough	Composite	49.5	0.66	66.2	883	63.9	1291
	S-5-S-1	4580	118	Cold Joint - Smooth	Composite	49.5	0.66	66.2	883	38.5	778
	S-5-S-2	4580	118	Cold Joint - Smooth	Composite	49.5	0.66	66.2	883	34.1	689
	S-5-S-3	4580	118	Cold Joint - Smooth	Composite	49.5	0.66	66.2	883	39.8	804
	A-5-R-1	6080	108	Cold Joint - Rough	Composite	49.5	0.66	66.2	883	48.4	979
	A-5-R-2	6080	108	Cold Joint - Rough	Composite	49.5	0.66	66.2	883	52.8	1067
	A-5-R-3	6080	108	Cold Joint - Rough	Composite	49.5	0.66	66.2	883	51.4	1039
	A-5-S-1	6080	108	Cold Joint - Smooth	Composite	49.5	0.66	66.2	883	41.5	838
	A-5-S-2	6080	108	Cold Joint - Smooth	Composite	49.5	0.66	66.2	883	40.1	810

Specimen ID		Concrete Properties		Shear Plane Geometry and Condition			Shear Plane Reinforcement			Testing Data	
		f'_c at Test (psi)	Density (pcf)	Interface Condition	Casting Procedure	A_{cr} (sq. in.)	A_{vf} (sq. in.)	f_y (ksi)	$\rho_{vf}f_y$ (psi)	V_{ti} (kips)	v_{ti} (psi)
Shaw 2013	A-5-S-3	6080	108	Cold Joint - Smooth	Composite	49.5	0.66	66.2	883	39.2	793
	N-8-R-1	7550	144	Cold Joint - Rough	Composite	49.5	0.66	66.2	883	74.0	1496
	N-8-R-2	7550	144	Cold Joint - Rough	Composite	49.5	0.66	66.2	883	56.1	1133
	N-8-R-3	7550	144	Cold Joint - Rough	Composite	49.5	0.66	66.2	883	64.1	1296
	N-8-S-1	7550	144	Cold Joint - Smooth	Composite	49.5	0.66	66.2	883	65.6	1324
	N-8-S-2	7550	144	Cold Joint - Smooth	Composite	49.5	0.66	66.2	883	53.3	1077
	N-8-S-3	7550	144	Cold Joint - Smooth	Composite	49.5	0.66	66.2	883	55.3	1118
	S-8-R-1	7200	118	Cold Joint - Rough	Composite	49.5	0.66	66.2	883	72.0	1455
	S-8-R-2	7200	118	Cold Joint - Rough	Composite	49.5	0.66	66.2	883	67.4	1361
	S-8-R-3	7200	118	Cold Joint - Rough	Composite	49.5	0.66	66.2	883	66.7	1348
	S-8-S-1	7200	118	Cold Joint - Smooth	Composite	49.5	0.66	66.2	883	67.0	1354
	S-8-S-2	7200	118	Cold Joint - Smooth	Composite	49.5	0.66	66.2	883	57.9	1169
	S-8-S-3	7200	118	Cold Joint - Smooth	Composite	49.5	0.66	66.2	883	58.9	1189
	A-8-R-1	7843	109	Cold Joint - Rough	Composite	49.5	0.66	66.2	883	61.8	1248
	A-8-R-2	7843	109	Cold Joint - Rough	Composite	49.5	0.66	66.2	883	63.9	1292
	A-8-R-3	7843	109	Cold Joint - Rough	Composite	49.5	0.66	66.2	883	64.1	1295
	A-8-S-1	7843	109	Cold Joint - Smooth	Composite	49.5	0.66	66.2	883	46.1	931
	A-8-S-2	7843	109	Cold Joint - Smooth	Composite	49.5	0.66	66.2	883	48.0	970
	A-8-S-3	7843	109	Cold Joint - Smooth	Composite	49.5	0.66	66.2	883	51.7	1045

Specimen ID		Concrete Properties		Shear Plane Geometry and Condition			Shear Plane Reinforcement			Testing Data	
		f'_c at Test (psi)	Density (pcf)	Interface Condition	Casting Procedure	A_{cr} (sq. in.)	A_{vf} (sq. in.)	f_y (ksi)	$\rho_{vf}f_y$ (psi)	V_u (kips)	v_u (psi)
Harries, et al. 2012	615-3A	5800	NWC, N/R	Cold Joint - Rough	Composite	160.4	0.66	67.3	276	112.5	701
	615-3B	5800	NWC, N/R	Cold Joint - Rough	Composite	163.2	0.66	67.3	269	96.5	591
	615-4A	5800	NWC, N/R	Cold Joint - Rough	Composite	165	1.20	61.5	449	114.5	694
	615-4B	5800	NWC, N/R	Cold Joint - Rough	Composite	162.5	1.20	61.5	455	129	794
	1035-3A	5800	NWC, N/R	Cold Joint - Rough	Composite	157.5	0.66	130.0	546	90	571
	1035-3B	5800	NWC, N/R	Cold Joint - Rough	Composite	160.7	0.66	126.0	517	105	653
	1035-4A	5800	NWC, N/R	Cold Joint - Rough	Composite	162.5	1.20	140.0	1036	135.7	835
	1035-4B	5800	NWC, N/R	Cold Joint - Rough	Composite	160.7	1.20	131.3	985	113.5	706
Kahn and Mitchell 2002	SF-7-1-CJ	11734	NWC, N/R	Cold Joint - Rough*	Composite	60	0.22	83.0	220	54.0	900
	SF-7-2-CJ	11734	NWC, N/R	Cold Joint - Rough*	Composite	60	0.44	83.0	440	82.1	1368
	SF-7-3-CJ	12471	NWC, N/R	Cold Joint - Rough*	Composite	60	0.66	83.0	660	110.3	1838
	SF-7-4-CJ	12471	NWC, N/R	Cold Joint - Rough*	Composite	60	0.88	83.0	880	132.7	2211
	SF-10-1-CJ	14326	NWC, N/R	Cold Joint - Smooth	Composite	60	0.22	83.0	220	31.7	529
	SF-10-2-CJ	12053	NWC, N/R	Cold Joint - Smooth	Composite	60	0.44	83.0	440	49.3	822
	SF-10-3-CJ	12953	NWC, N/R	Cold Joint - Rough*	Composite	60	0.66	83.0	660	113.9	1899
	SF-10-4-CJ	12953	NWC, N/R	Cold Joint - Rough*	Composite	60	0.88	83.0	880	126.0	2101
	SF-14-1-CJ	14756	NWC, N/R	Cold Joint - Rough*	Composite	60	0.22	83.0	220	90.9	1515
	SF-14-2-CJ	14756	NWC, N/R	Cold Joint - Rough*	Composite	60	0.44	83.0	440	99.2	1653
	SF-14-3-CJ	15218	NWC, N/R	Cold Joint - Rough*	Composite	60	0.66	83.0	660	134.7	2245
	SF-14-4-CJ	15218	NWC, N/R	Cold Joint - Rough*	Composite	60	0.88	83.0	880	153.1	2552
	*Not intentionally roughened; left as cast, but interface was rough with amplitude approximately 1/4 in.										

Specimen ID		Concrete Properties		Shear Plane Geometry and Condition			Shear Plane Reinforcement			Testing Data	
		f'_c at Test (psi)	Density (pcf)	Interface Condition	Casting Procedure	A_{cr} (sq. in.)	A_{vf} (sq. in.)	f_y (ksi)	$\rho_{vf}f_y$ (psi)	V_u (kips)	v_u (psi)
Mattock 1976	B1	5840	NWC, N/R	Cold Joint - Rough*	Composite	50.0	0.22	51.3	226	24.4	487
	B2	5840	NWC, N/R	Cold Joint - Rough*	Composite	50.0	0.44	50.6	445	35.0	700
	B3	6055	NWC, N/R	Cold Joint - Rough*	Composite	50.0	0.66	51.3	677	52.7	1054
	B4	6055	NWC, N/R	Cold Joint - Rough*	Composite	50.0	0.88	53.8	947	63.8	1276
	B5	5895	NWC, N/R	Cold Joint - Rough*	Composite	50.0	1.24	49.3	1262	78.5	1570
	B6	5895	NWC, N/R	Cold Joint - Rough*	Composite	50.0	1.60	49.3	1576	85.0	1700
	C1	5870	NWC, N/R	Cold Joint - Smooth*	Composite	50.0	0.22	50.9	224	10.5	210
	C2	5870	NWC, N/R	Cold Joint - Smooth*	Composite	50.0	0.44	50.9	448	18.0	360
	C3	5980	NWC, N/R	Cold Joint - Smooth*	Composite	50.0	0.66	50.6	667	21.4	428
	C4	5980	NWC, N/R	Cold Joint - Smooth*	Composite	50.0	0.88	51.6	909	30.0	600
	C5	6165	NWC, N/R	Cold Joint - Smooth*	Composite	50.0	1.10	52.7	1160	39.0	780
	C6	6165	NWC, N/R	Cold Joint - Smooth*	Composite	50.0	1.60	45.3	1448	44.1	882
	D1	3770	NWC, N/R	Cold Joint - Rough*	Composite	50.0	0.22	51.3	226	29.5	590
	D2	3770	NWC, N/R	Cold Joint - Rough*	Composite	50.0	0.44	51.3	451	46.0	920
	D3	2940	NWC, N/R	Cold Joint - Rough*	Composite	50.0	0.66	56.0	739	50.5	1010
	D4	2940	NWC, N/R	Cold Joint - Rough*	Composite	50.0	0.88	56.0	986	50.1	1002
	D4A	2495	NWC, N/R	Cold Joint - Rough*	Composite	50.0	0.88	54.0	950	49.7	994
	D5	2955	NWC, N/R	Cold Joint - Rough*	Composite	50.0	1.24	47.7	1184	60.5	1210
	D5A	2795	NWC, N/R	Cold Joint - Rough*	Composite	50.0	1.24	48.8	1211	62.5	1250
	D6	2955	NWC, N/R	Cold Joint - Rough*	Composite	50.0	1.60	48.5	1552	73.5	1470
	*Specimens were pre-cracked prior to loading.										

Specimen ID		Concrete Properties		Shear Plane Geometry and Condition			Shear Plane Reinforcement			Testing Data	
		f'_c at Test (psi)	Density (pcf)	Interface Condition	Casting Procedure	A_{cr} (sq. in.)	A_{vf} (sq. in.)	f_y (ksi)	$\rho_{vf}f_y$ (psi)	V_u (kips)	v_u (psi)
Paulay, et al. 1974	TBO1	3930	NWC, N/R	Cold Joint - Smooth	Composite	96.0	0.66	42.6	294	33.3	347
	TAO2	3930	NWC, N/R	Cold Joint - Smooth	Composite	96.0	0.30	50.2	156	20.2	210
	TBO2	3930	NWC, N/R	Cold Joint - Smooth	Composite	96.0	0.66	42.6	294	38.7	403
	TCO2	3930	NWC, N/R	Cold Joint - Smooth	Composite	96.0	1.18	45.9	564	59.0	615
	TAM1	2920	NWC, N/R	Cold Joint - Smooth	Composite	96.0	0.30	49.9	155	31.2	325
	TBM1	2920	NWC, N/R	Cold Joint - Smooth	Composite	96.0	0.66	42.6	294	48.0	500
	TCM1	2920	NWC, N/R	Cold Joint - Smooth	Composite	96.0	1.18	45.9	564	37.9	395
	ZBO1	3930	NWC, N/R	Cold Joint - Rough*	Composite	96.0	0.66	42.6	294	58.1	605
	RBO1	3930	NWC, N/R	Cold Joint - Rough*	Composite	96.0	0.66	42.4	293	56.2	585
	WBO1	3930	NWC, N/R	Cold Joint - Rough*	Composite	96.0	0.66	42.6	294	69.1	720
	SBO1	3930	NWC, N/R	Cold Joint - Rough*	Composite	96.0	0.66	42.5	293	73.0	760
	RAO1	3930	NWC, N/R	Cold Joint - Rough*	Composite	96.0	0.30	50.1	155	49.9	520
	RAO2	3930	NWC, N/R	Cold Joint - Rough*	Composite	96.0	0.30	50.0	155	50.9	530
	RBO2	3930	NWC, N/R	Cold Joint - Rough*	Composite	96.0	0.66	42.5	293	57.1	595
	RCO2	3930	NWC, N/R	Cold Joint - Rough*	Composite	96.0	1.18	46.0	566	90.2	940
	RAM1	3480	NWC, N/R	Cold Joint - Rough*	Composite	96.0	0.30	50.1	155	48.0	500
	RBM1	3480	NWC, N/R	Cold Joint - Rough*	Composite	96.0	0.66	42.7	294	65.3	680
	RBM2	3480	NWC, N/R	Cold Joint - Rough*	Composite	96.0	0.66	42.6	294	64.3	670
	RCM1	3480	NWC, N/R	Cold Joint - Rough*	Composite	96.0	1.18	46.3	569	67.2	700
	RCM2	3480	NWC, N/R	Cold Joint - Rough*	Composite	96.0	1.18	46.3	569	67.2	700
	*Intentionally roughened, but actual amplitudes for some specimens reached as high as 0.75 in. and others may have been below 0.25 in.										

REFERENCES

AASHTO (2014). "AASHTO LRFD Bridge Design Specifications," Seventh edition, American Association of State Highway and Transportation Officials (AASHTO), Washington, DC.

ACI Committee 318 (2014). "Building Code Requirements for Structural Concrete and Commentary (ACI 318R-14)," Farmington Hills, MI: American Concrete Institute.

ACI Committee 318 (2011). "Building Code Requirements for Structural Concrete and Commentary (ACI 318-11)," Farmington Hills, MI: American Concrete Institute.

ACI Committee 211 (1998). "Standard Practice for Selecting Proportions for Structural Lightweight Concrete. (ACI 211.2-98)," Farmington Hills, MI: American Concrete Institute.

Anderson, A. R., "Composite Designs in Precast and Cast-in-Place Concrete," *Progressive Architecture, Vol.* 41, No. 9, September 1960, pp. 172-179.

ASTM A370 (2012a). "Standard Test Methods and Definitions for Mechanical Testing of Steel Products." Annual book of ASTM standards, ASTM, West Conshohocken, Pennsylvania.

ASTM A615 (2012). "Standard Specification for Deformed and Plain Carbon-Steel Bars for Concrete Reinforcement." Annual book of ASTM standards, ASTM, West Conshohocken, Pennsylvania.

ASTM C29 (2009). "Standard Test Method for Bulk Density (Unit Weight) and Voids in Aggregate." Annual book of ASTM standards, ASTM, West Conshohocken, Pennsylvania.

ASTM C127 (2012). "Standard Test Method for Density, Relative Density (Specific Gravity), and Absorption of Coarse Aggregate." Annual book of ASTM standards, ASTM, West Conshohocken, Pennsylvania.

ASTM C128 (2012). "Standard Test Method for Density, Relative Density (Specific Gravity), and Absorption of Fine Aggregate." Annual book of ASTM standards, ASTM, West Conshohocken, Pennsylvania.

ASTM C136 (2006). “Standard Test Method for Sieve Analysis of Fine and Coarse Aggregates.” Annual book of ASTM standards, ASTM, West Conshohocken, Pennsylvania.

ASTM C138 (2012). “Standard Test Method for Density (Unit Weight), Yield, and Air Content (Gravimetric) of Concrete.” Annual book of ASTM standards, ASTM, West Conshohocken, Pennsylvania.

ASTM Cl43 (2012). “Standard Test Method for Slump of Hydraulic-Cement Concrete.” Annual book of ASTM standards, ASTM, West Conshohocken, Pennsylvania.

ASTM Cl73 (2012). “Standard Test Method for Air Content of Freshly Mixed Concrete by the Volumetric Method.” Annual book of ASTM standards, ASTM, West Conshohocken, Pennsylvania.

ASTM C192 (2012). “Standard Practice for Making and Curing Concrete Test Specimens in the Laboratory.” Annual book of ASTM standards, ASTM, West Conshohocken, Pennsylvania.

ASTM C231 (2010). “Standard Test Method for Air Content of Freshly Mixed Concrete by the Pressure Method.” Annual book of ASTM standards, ASTM, West Conshohocken, Pennsylvania.

ASTM C 330 (ASTM C330 (2009). “Standard Specification for Lightweight Aggregates for Structural Concrete.” Annual book of ASTM standards, ASTM, West Conshohocken, Pennsylvania.

ASTM C469 (2010). “Standard Test Method for Static Modulus of Elasticity and Poisson's Ratio of Concrete in Compression.” Annual book of ASTM standards, ASTM, West Conshohocken, Pennsylvania.

ASTM C494 (2012). “Standard Specification for Chemical Admixtures for Concrete.” Annual book of ASTM standards, ASTM, West Conshohocken, Pennsylvania.

ASTM C496 (2011). “Standard Test Method for Splitting Tensile Strength of Cylindrical Concrete Specimens.” Annual book of ASTM standards, ASTM, West Conshohocken, Pennsylvania.

ASTM C1231 (2012). “Standard Practice for Use of Unbonded Caps in Determination of Compressive Strength of Concrete Cylinders.” Annual book of ASTM standards, ASTM, West Conshohocken, Pennsylvania.

Baldwin, J. W., (1965). "Bond of Reinforcement in Lightweight Aggregate Concrete," *Preliminary Report*, University of Missouri, Mar., 10.

Bass, R.A., Carrasquillo, R.L. , and J.O. Jirsa. (1989). "Shear Transfer Across New and Existing Concrete Interfaces," *ACI Structural Journal*, Vol. 84, No. 4, pp. 383-393.

Birkeland, H.W. (1969), Class Notes for Course on "Precast and Prestressed Concrete," University of British Columbia, Spring 1968.

Birkeland, P.W. and Birkeland, H.W. (1966). "Connections in Precast Concrete Construction," ACI Journal, *Proceedings*, Vol. 63, No. 3, pp. 345-368.

Hanson, N.W., (1960). "Precast-Prestressed Concrete Bridges 2: Horizontal Shear Connections," *PCA – Journal of the Research and Development Division*, Vol. 2, No. 2, pp. 38-58.

Harries, Kent A., Zeno, and Shahrooz. (2012). "Toward an Improved Understanding of Shear-Friction Behavior," *ACI Structural Journal*, Vol. 109, No. 6, pp. 835-844.

Hofbeck, J. A.; Ibrahim, I. O.; and Mattock, A. H. (1969). "Shear Transfer in Reinforced Concrete," ACI Journal, *Proceedings*, V. 66, No. 2, pp. 119-128.

Hoff, G.C. (1992). "High Strength Lightweight Aggregate Concrete for Arctic Applications--Part 3: Structural Parameters," *American Concrete Institute Special Publication*, SP-136, pp. 175-246.

Hsu, Thomas T.C., S.T. Mau, and Bin Chen. (1987). "Theory of Shear Transfer Strength of Reinforced Concrete," *ACI Structural Journal*, Vol. 84, No. 2, pp. 149-160.

Ivey and Buth. (1967) "Shear Capacity of Lightweight Concrete Beams." ACI Journal, *Proceedings*, Vol. 64, No. 10. pp. 634-43.

Kahn, L.F. and A.D. Mitchell. (2002). "Shear-friction Tests with High-Strength Concrete," *ACI Structural Journal*, Vol. 99, No. 1, pp. 98-103.

Krc, Kristian. (2015). "An Investigation of Shear-Friction of Lightweight Aggregate Concretes." MS Thesis. Missouri University of Science and Technology.

Loov, R.E. and A.K. Patnaik. (1994). "Horizontal Shear Strength of Composite Beams with a Rough Interface," *PCI Journal*, Vol. 39, No. 1, pp. 48-58.

Mansur, M.T., T. Vinayagam, and Kiang-Hwee Tan. (2008). "Shear Transfer Across a Crack in Reinforced High-Strength Concrete," *ASCE Journal of Materials in Civil Engineering*, Vol. 20, No. 4, pp. 294-302.

Mast, R.F. (1968). "Auxiliary Reinforcement in Concrete Connections," *ASCE Journal of the Structural Division Proceedings*, Vol. 94, No. ST6, pp. 1485-1504.

Mattock, A.H. (1974). "Shear Transfer in Concrete Having Reinforcement at an Angle to the Shear Plane," American Concrete Institute Publication SP-42, *Shear in Reinforced Concrete*, pp. 17-42.

Mattock, A. H., W. K. Li, and T. C. Wang. (1976). "Shear Transfer in Lightweight Reinforced Concrete." *PCI Journal*, Vol. 21, No. 1, pp. 20-39.

Mattock, A.H. (1976). "Shear Transfer Under Monotonic Loading Across and Interface Between Concretes Cast at Different Times," *University of Washington Department of Civil Engineering Report SM 76-3*.

Mattock, A.H. (2001). "Shear-friction and High-Strength Concrete," *ACI Structural Journal*, Vol. 98, No. 1, pp. 50-59.

Mattock, A. H., Johal, L, and Chow, C. H. (1975). "Shear transfer in reinforced concrete with moment or tension acting across the shear plane." *PCI Journal*, Vol. 20, No. 4, pp. 76-93.

Mattock, A.H. and N.M. Hawkins. (1972). "Shear Transfer in Reinforced Concrete – Recent Research," *PCI Journal*, Vol. 17, No. 2, pp. 55-75.

Nagle, T.J. and D.A. Kuchma. (2007). "Nontraditional Limitations on the Shear Capacity of Prestressed Concrete Girders," *University of Illinois at Urbana-Champaign NSEL Report-003*.

Paulay, T., R. Park, and M.H. Phillips. (1974). "Horizontal Construction Joints In Cast-In-Place Reinforced Concrete," *American Concrete Institute Special Publications*, SP-42, pp. 599-616.

PCI Committee on Connection Details (1973), *PCI Manual on Design of Connections for Precast Prestressed Concrete*, Prestressed Concrete Institute (PCI), Chicago, IL.

Precast/Prestressed Concrete Institute (1992). *PCI Design Handbook: Precast and Prestressed Concrete Institute*. 4th ed. Chicago: Precast/Prestressed Concrete Institute.

Precast/Prestressed Concrete Institute (1999). *PCI Design Handbook: Precast and Prestressed Concrete Institute*. 5th ed. Chicago: Precast/Prestressed Concrete Institute.

Precast/Prestressed Concrete Institute (2004). *PCI Design Handbook: Precast and Prestressed Concrete Institute*. 6th ed. Chicago: Precast/Prestressed Concrete Institute.

Precast/Prestressed Concrete Institute (2010). *PCI Design Handbook: Precast and Prestressed Concrete Institute*. 7th ed. Chicago: Precast/Prestressed Concrete Institute.

Rahal, Khaldoun N. (2010). "Shear Transfer Strength of Reinforced Concrete." *ACI Structural Journal*, Vol. 107, No.4, pp.419-426.

Raths, C. H. (1977). "Reader Comments: Design Proposals for Reinforced Concrete Corbels." *PCI Journal*, Vol. 21, No. 3, pp 93–98.

Robins, P. J., and Standish, I. G. (1982). "Effect of Lateral Pressure on Bond of Reinforcing Bars in Concrete," *Bond in Concrete—Proceedings of the International Conference on Bond in Concrete*, Paisley, Applied Science Publishers, London, pp. 262-272.

Saemann, J. and G.W. Washa. (1964). "Horizontal Shear Connections Between Precast Beams and Cast-In Place Slabs," ACI Journal, *Proceedings*, Vol 61, No. 11, pp. 1383-1408.

Scott, Jana. (2010) "Interface Shear Strength in Lightweight Concrete Bridge Girders." MS Thesis. Virginia Polytechnic Institute.

Shaikh, Fattah A. (1978). "Proposed Revisions to Shear-friction Provisions." *PCI Journal*, Vol. 23, No. 2, pp. 12-21.

Shaw, Dane. (2013). "Direct Shear Transfer of Lightweight Aggregate Concretes with Non-Monolithic Interface Conditions." MS Thesis. Missouri University of Science and Technology.

Shaw, D. and Sneed, L. (2014). "Interface Shear Transfer of Lightweight Aggregate Concretes Cast at Different Times," *PCI Journal*, V. 59, No. 3, pp. 130-144.

Tanner, John A. (2008). "Calculating Shear-friction Using Effective Coefficient of Friction." *PCI Journal*, Vol. 53, No. 3, pp. 114-20.

Walraven, J. C.; Frenay, J.; and Pruijssers, A. (1987). "Influence of Concrete Strength and Load History on the Shear-friction Capacity of Concrete Members," *PCI Journal*, Vol. 32, No. 1, pp. 66-84.

Walraven, J. and Stroband. J. (1994). "Shear-friction in High-Strength Concrete," *American Concrete Institute Special Publication*, SP-42, pp. 311-330.

Wermager, S. and Baur, S. (2013). "Energy Analysis of a Student-Designed Solar House," *Energies*, Vol. 6. No. 12, pp. 6373-6390.

Zia, P. (1961). "Torsional Strength of Prestressed Concrete Members," *ACI Journal*, Vol. 57, No. 10, pp. 1337-1360.

VITA

Samantha L. Wermager was born May 10, 1991 to parents Anthony and Connie Wermager of Hokah, Minnesota. She graduated in May 2014 with a Bachelor of Science in Civil Engineering (Structural Emphasis) from Missouri University of Science and Technology in Rolla, MO. She also minored in Sustainability. During her undergraduate career, Samantha researched energy modeling of a student-designed solar house under Dr. Stuart Baur. The summary of this research was published in *Energies* in December 2013, and is documented in the References section of this thesis.

As a recipient of the Chancellor's Fellowship, she was able to stay in Rolla to pursue her Master's Degree in Civil Engineering, Structural Emphasis. Samantha graduated in December 2015 and began her career as a structural (bridge) engineer with Burns & McDonnell in Kansas City, Missouri.